LASER SURFACE ALLOYING OF ALUMINUM AND SURFACE MELTING OF Al-12Si-4Cu-1.2Mn ALLOY

A Thesis Submitted in Partial Fulfillment of the Requirements

for the Degree of

DOCTOR OF PHILOSOPHY

by

Woldetinsay Gutu Jiru

(Roll No. 136103029)

Department of Mechanical Engineering

Indian Institute of Technology Guwahati

Guwahati–781039

INDIA

December **2018**

Department of Mechanical Engineering

Indian Institute of Technology Guwahati

Guwahati–781039

INDIA

CERTIFICATE

It is certified that the work contained in the thesis entitled **"Laser Surface Alloying of Aluminum and Surface Melting of Al-12Si-4Cu-1.2Mn alloy"** submitted by **Mr. Woldetinsay Gutu Jiru** to the Indian Institute of Technology Guwahati for the award of the degree of Doctor of Philosophy has been carried out under our supervision in the Department of Mechanical Engineering, Indian Institute of Technology Guwahati. This work has not been submitted elsewhere for the award of any other degree or diploma.

(Dr. Uday S. Dixit)
Professor
Department of Mechanical Engineering,
Indian Institute of Technology Guwahati,
Guwahati–781039, INDIA

(Dr. Ravi M. Sankar)
Assistant Professor
Department of Mechanical Engineering,
Indian Institute of Technology Guwahati,
Guwahati–781039, INDIA

December 2018

Dedicated to

My Mother ***Shashitu Galata***

It is my prayer that I will get you in the heaven!

DECLARATION

I declare that,

a. The work contained in this thesis is original and has been done by me under the guidance of my supervisors.
b. The work have not been submitted to any other institute for any degree or diploma.
c. I have followed the guidelines provided by the institute in preparing this thesis.
d. I have confirmed to the norms and guidelines given in the ethical code of conduct of the institute.
e. Whenever I used materials (data, theoretical analysis, figures and text) from other sources, I have given their detail in references.

Signature of Student

(Woldetinsay Gutu Jiru)

Acknowledgement

First of all, I give heartfelt thanks to my savior Jesus Christ for being with me through tough and hard times in my life. Without God's help, it would have been impossible to achieve my goals. I would like to acknowledge Adama Science and Technology University for providing me this chance to study Ph.D. Thanks to Government of Ethiopia for funding a full-time scholarship for my research in IIT Guwahati, India. I also thank DST-FIST (2009–2014) scheme of Government of India for providing CO_2 laser facility. My appreciation to Centeral of Instruments Facility of IIT Guwahati for providing different instruments for characterization.

I would like to express my sincere gratitude and heartfelt thanks to my supervisor Professor Uday Shanker Dixit for his continuous guidance, support and encouragement in my thesis from the beginning to completion. He helped me tremendously for editing my journal publications and thesis. If without him, I could not achieve my research work. Many thanks to Dr. Mamilla Ravi Sankar for guiding, motivating as well as providing some metal powders for my experimentations. May I take this chance to thank Professor Hengcheng Liao, who helped me to get aluminum alloy for my experimental work.

Thanks to the doctoral committee, Prof. Arun Chattopadhyay, Dr. Ganesh Narayanan and Dr. Pankaj Biswas for their continuous evaluation, suggestions and motivations. May I take this chance to thank Prof. S.K. Dwivedy who is present head of the Department of Mechanical Engineering, Prof. A.K. Dass and Prof. P. Mahanta, former heads of the Department for facilitating various types of equipment and machines I had used for research work.

I express my sincere thanks to all Mechanical Engineering workshop staffs, in IIT Guwahati. Thanks to technical staffs— Mr. Jiten Basumatary, Mr. Saiffuddin Ahmed and Mr. Mrinal Sarma. Thanks to all my friends— Dr. Vinod Yadav, Dr. V. Satheeshkumar, Dr. Muthuraja A, Mr. Ketema Bobe, Mr. Getu Tilahun, Dr. Besufekad Feten, Dr. Dawit

Gudeta, Mr. Kishor Kumar, Mr.Vikash Vanik, Mr. Rajkumar Sufen, Dr. Ashish Rajak, Mr. Rasmi Ranjan, Mr. Vignesh Babu, Mr.Amit Raj and Mr. Faladrum Sharma.

I express my deep gratitude and love to my wife Kebebush Kitessa for her immense support, love and motivation for my career in life. Especially she has been taking care of my children Dursanwaq and Mooti. Her love and motivation helped me for this achievement. Thanks to my father Gutu Jiru, my brothers and sisters and deep love to my mother whom I missed. Thanks to those people who prayed for me, encouraged me and supported me.

God bless all!

December 2018

Woldetinsay Gutu Jiru
IIT Guwahati

Abstract

Aluminum alloys are groups of nonferrous metals finding a wide range of applications. They have appreciable properties such as high strength to weight ratio, high thermal conductivity, excellent corrosion resistance and workability. This favors their high demand in many industries. Aluminum is used in many applications—automobile parts, aircraft parts, nuclear plant material and shipbuilding materials. They are also used to fabricate various domestic items like kitchen utensil and packaging. Due to its high conductivity, pure aluminum is used for electrical transmission lines and protective coating on the surface of other metals. Alloying aluminum with different metals enhances its mechanical properties and makes it suitable for structural applications. However, mechanical alloying of aluminum by casting and other techniques may not be cost-effective, when only the properties at the surface need to be changed.

In this thesis, the motivation is implementing the cost-effective method of surface modification of commercially pure aluminum. For this, a continuous wave CO_2 laser was used. Laser surface alloying (LSA) was conducted by adding additional metal and ceramic materials to the aluminum substrate and high energy laser beam was used to melt pre-placed material as well as a portion of substrate aluminum. For LSA, powders of copper, magnesium, manganese, titanium and zinc were used. The average particle size of each powder was about 10 μm. In order to investigate the effect of the material combination on the alloy formed, copper, magnesium and manganese were mixed by a ratio of 2:1:1 and alloyed with aluminum substrate. Ceramic materials of SiC and TiO_2 were also used for laser surface alloying of aluminum. Alloying powders were pre-placed uniformly on substrate material after mixing with Fevigum binder, which is a cost-effective method due to high laser beam absorptivity and material utilization. The formation of metallurgical bonding of added materials with aluminum substrate played a great role in improving surface properties such as microhardness, wear, and corrosion resistance. Alloy depth and alloy width are highly affected by laser beam parameters such as laser power, laser scan speed and beam diameter. For example, alloy depth increased when laser beam power was increased from 1.7 to 1.9 kW power. Similarly, when laser scan speed was increased from 300 to 500 mm/min, both alloy depth and alloy width got decreased. The effect of beam diameter was also observed; there is an optimum beam diameter for the best performance.

Wear is a major cause of the failure of engineering parts. In this work, after laser surface alloying, a pin on disc wear testing in dry condition was conducted for 20 minutes for AlCu, AlMg, AlMn and Al-CuMgMn alloys. The result was promising since wear resistance after alloying with different metals was achieved. For example, an improvement of 30–50 % was achieved for different alloy. The highest wear resistance was observed for AlCu and Al-CuMgMn alloys. The effect of normal load, sliding speed and sliding time on wear mass loss were investigated. In general, for different alloys, a two-fold increase in normal load had wear mass loss by 1.4–3.2 times.

Both acid and salt immersion tests were conducted for corrosion evaluation for 200 hours at room temperature. Very attractive results were obtained. For example in acid (2.5% H_2SO_4) corrosion immersion test, highest corrosion improvement was achieved for AlTi alloy and AlMg alloys and other materials as well. For different alloys, corrosion resistance was improved by 22% to 55%, where AlTi and AlMg alloy got first and second ranks in improving the acid corrosion resistance. The corrosion attack in the form of pitting that grows faster in the material and microcracks were the major causes of corrosion. Corrosion affects the hardness of the material as confirmed in the experiment. After corrosion about 50% hardness reduction in hardness was observed for AlTi alloy.

The second study for surface modification was laser surface melting (LSM) on Al-12Si-4Cu-1.2Mn alloy. Due to LSM, microhardness increased by about 2.5 and 2.6 times for heat treated and as-cast samples, respectively. There was a considerable improvement in mechanical properties of as-cast samples at low laser specific energy. Although the heat treated samples also showed the improvement in mechanical properties, yet they could not surpass the as-cast samples. The ultimate tensile strength increased by 23% and 70% for heat treated and as-cast samples, respectively. Surface scratch resistances after LSM also increases. The coefficient of friction reduced after LSM.

Overall, this research work established the feasibility of surface modification by alloying and remelting of aluminum on a CO_2 laser machine. There is a scope to model and optimize the process. Surface modification of exotic materials may also be studied.

Contents

List of Figures

List of Tables

Acronyms

AA	Aluminum association
CAD	Computer aided design
CIF	Central instruments facility
CW	Continuous wave
DMLS	Direct metal laser sintering
EDM	Electric discharge machining
EDS	Electron dispersive X-ray spectroscopy
EIS	Electrochemical impendence spectroscopy
FESEM	Field emission scanning electron microscopy
HPDL	High power diode laser
LSA	Laser surface alloying
LSM	Laser surface melting
LUDT	Linear variable differential traducer
Nd: YAG	Niobium yttrium aluminum garnet
SCC	Stress corrosion cracking
SLM	Selective laser melting
SLS	Selective laser sintering
SEM	Scanning electron microscopy
UTS	Ultimate tensile strength
XRD	X-ray diffraction

Notations

C	Concentration of alloying elements
C_p	Specific heat
C_t	Concentration of alloying element at top
d	Laser beam diameter
D	Average crystal size
E	Laser specify energy
E_t	Total energy irradiating
F	Laser energy density
g	Hardness
F_n	Normal load
H	Standoff distance
h	Alloy height
I_o	Incident intensity
I	Laser beam intensity
k	Thermal conductivity
K	Wear coefficient
M^2	Laser beam quality factor
m	Wear mass loss
P	Laser power

Q	power density
R	Refractivity coefficient
R^2	Coefficient of determination
s	Sliding distance
T	Temperature
ΔT	Temperature variation
v	Laser scan speed
V	Wear volume loss
w	Alloy width
w_0	Laser beam waist
$wt.\%$	Weight percent
×	Magnification
Z	Distance
α	Absorption coefficient
β	Full width at half maximum
η	Lattice strain
Θ	Beam divergence
λ	Wave length
ν	Poisson's ratio
ρ	Density

Chapter 1

Background, Motivation and Scope

1.1 Introduction

Aluminum is the first most abundant metallic element on the Earth and the third most common element comprising about 8% of the Earth's crust. Aluminum alloys are used widely next to steel due to their resourcefulness. Aluminum never occurs as a free element in nature; it is present in the form of compounds in ores like bauxite, kaolinite, nepheline and cryolite. The demand and production of aluminum is continuously increasing. In year 2016, the world demand for aluminum was about 112 million metric tons, whilst 115 million metric tons was supplied (Aluminum Association, 2017).

After the end of service life, the aluminum products can be easily remanufactured to form a component for the same or different purpose. The cost of energy consumption for recycling aluminum product is about 5–10% than that for primary aluminum production (Bergsdal *et al*., 2004). Pure aluminum is soft and corrosion resistant with good electrical and thermal conductivity. Alloying aluminum with different metals enhances its mechanical properties and makes it suitable for structural applications. Aluminum alloys can usually have the strength to weight ratio more than that of steel. The main attractive properties of aluminum alloys are high formability, lightweight, good corrosion-resistance, high thermal as well as electrical conductivity and recyclability (Hatch, 1984). Due to its high chemical affinity to oxygen, aluminum exists in ore form. Extracting it from the ores consumes a lot of energy.

Aluminum alloys are used to make components in automobile, aircraft and ship building industry mainly due to their light weight. They are also used to fabricate various domestic items like kitchen utensils and packaging. They are also used as electrical

transmission lines because of their lightweight and good electrical conductivity. They are deposited on the surface of other metals for protective coating.

1.2 Production of Aluminum

The demand for aluminum is increasing day by day due to its availability, cost and recyclability (Bergsdal *et al*., 2004). Aluminum production started by dry electrolysis, after its invention by Paul Louis Héroult in France and Charles Martin Hall in America (Davis, 1993). A production process for converting the mineral bauxite to alumina was developed by Karl Josef Bayer in Austria in 1888, which is named as Bayer process. Bayer process is very popular nowadays.

In Bayer process Al_2O_3, Fe_2O_3 and SiO_2 are formed from bauxite ore (Luo and Soria, 2007). The final product is made by Hall-Heroult process when aluminum is reduced via electrolysis process. The main reactions in the aluminum extraction are as follows:

$$Al_2O_3 + 3H_2O + 2NaOH + heat \rightarrow 2NaAl(OH)_4, \quad (1.1)$$

$$NaAl(OH)_4 + H_2O \rightarrow Al(OH)_3 \bullet H_2O + NaOH, \quad (1.2)$$

$$2Al(OH)_3 \bullet H_2O + Heat \rightarrow Al_2O_3 + 5H_2O, \quad (1.3)$$

$$2Al_2O_3 + 3C \rightarrow 4Al + 3CO_2. \quad (1.4)$$

Parts made from aluminum and its alloys are recycled using casting process. A suitable metal forming process, e.g., rolling or extrusion, is employed to make parts from the casting. Kaufman and Rooy (2004) reported different types of casting processes used to produce aluminum components for different purposes. The life cycle of typical aluminum products considering sustainable manufacturing is schematically depicted in Figure 1.1. The recycling process is cost-effective as well as environmentally friendly, thus making it sustainable.

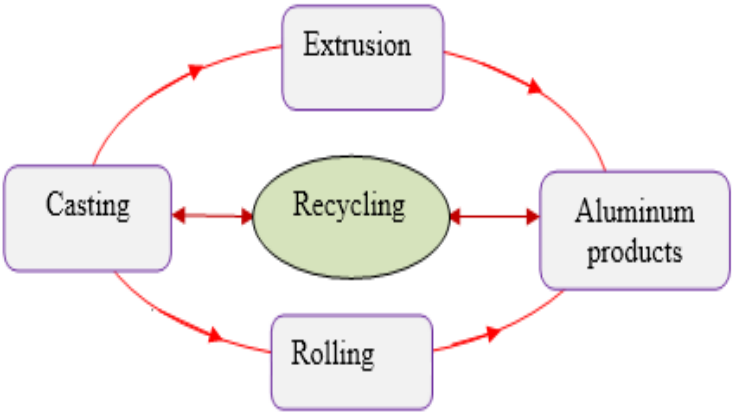

Figure 1.1 Production and recycling of aluminum products

1.3 Designation of Aluminum Alloys and their Applications

Aluminum alloys are classified into two major groups as cast and wrought alloys. Aluminum Association (AA) developed nomenclatures of cast and wrought alloys. For wrought alloys, a four-digit system is used to produce a list of different alloy compositions. Aluminum cast compositions are described by a three-digit system followed by a decimal number. A number 0 after a decimal digit indicates the final casting, 1 indicates standard commercial ingot and 2 indicates an ingot having narrower composition ranges but within those of standard ingots (Kaufman and Rooy, 2004).

Cast alloys are usually produced by pressure-die, permanent mold, green sand, dry sand, investment or plaster mold casting processes. Aluminum is mostly sold in the form of plate, wire, rod or bar, which are produced from a casting by extrusion, rolling, forging, wire drawing or a combination of these processes. Different components of aluminum can be produced by sheet metal forming. Aluminum alloys are also classified as heat treatable and non-heat treatable alloys (Davis, 2001). The heat treatment can be done by solution heat treatment, quenching, precipitation and hardening methods. Heat treatable alloys are 2xxx, 6xxx and 7xxx series, which can be hardened or strengthened by controlling a cycle of heating and cooling. The cold working process strain hardens the non-heat treatable aluminum alloys by deformation. The non-heat treatable alloys are 1xxx, 3xxx, 4xxx and 5xxx aluminum alloy series. Application of each wrought alloy and properties are given in Table 1.1

Table 1.1 Properties and applications of wrought aluminum alloys (Aluminum Association, 1998)

Series	Properties	Applications
1xxx (no major alloying)	Ultimate tensile strength (UTS) of 69–186 MPa, strain hardening, high thermal and electrical conductivity, high corrosion resistance	Electrical conductors, electric bus bar (1350), food packaging (1100)
2xxx (Al-Cu)	UTS 186–427 MPa, good high temperature creep strength, high toughness even at cryogenic temperatures, good machinability	Welding wires, fuel tanks and rocket parts (2219), aircraft body (2024, 2124, 2618)
3xxx (Al-Mn)	UTS 110–283 MPa, high ductility, excellent corrosion resistance	Foils, roofing sheets, packaging, beverage cans (3004, 3104), radiator (3002), heat exchanger (3003)
4xxx (Al-Si)	UTS 172–379 MPa, excellent weldability, moderate strength, heat and non-heat treatable, excellent corrosion resistance	Filler materials, welding wire (4043) and brazing wires, forged engine pistons (4032), complex shape forging, architectural application
5xxx (Al-Mg)	UTS 124–352 MPa, high rate of work hardening, high corrosion resistance	Transportation structures, tanks for petrol, milk and grains, pressure vessels, architectural applications, marine structures and cryogenic applications
6xxx (Al-Mg-Si)	UTS 124–400 MPa, medium tensile strength 245 MPa, higher strength on ageing, corrosion resistance	Roof structures (6063, 6061), transportation, pressure vessels, constructions, automotive parts, marine application (6061, 6063, 6111)
7xxx (Al-Zn)	UTS 221–607 MPa, stress corrosion cracking resistance	Light weight military bridge, aircraft construction (7075-T73), automotive applications
8xxx (Al-other elements)	UTS 117–241 MPa, high corrosion resistance, high temperature &pressure vessels, good formability	Nuclear energy installations: Al-1.1Ni-0.6Fr (8001), bottle caps: Al-0.75Fe-0.7Si (8011), soft bearings: Al-Sn with Sn up to 7%, aerospace: Al-Li

1.4 Laser Application in Manufacturing

The laser is an acronym for light amplification by stimulated emission of radiation. The laser is a coherent, convergent and monochromatic beam of electromagnetic radiation. The wavelength of the lasers can range from 180 nm to 1 mm covering ultraviolet, visible and infra-red regions of the spectrum. Laser works on the principle of quantum theory and was first envisaged by the famous physicist Albert Einstein (Einstein, 1917). At Hughes research laboratory, Theodor Mailman carried out the invention of the first actual laser based on a pink ruby crystal in 1960 (Maiman, 1960). Gordon Gould first used the term LASER in 1959 and claimed to be the first inventor of laser.

The laser can be created when excited atoms and molecules are stimulated by electromagnetic waves to emit photons, which are packets of light. According to quantum theory, every atom has energies only in certain energy levels. The atoms at the lowest energy level are at the ground state. When light from a power source like a flash lamp or mercury arc falls on a substance, the atoms in ground state can be excited to go to the higher levels. This process is called absorption. After staying at the level for a very short duration (about 10^{-8} s), they return to the initial ground state, after emitting a photon; this process is called spontaneous emission. The two processes of absorption and spontaneous emission take place in a conventional light source. However, if the atom in its excited state is impacted by an outside photon having the energy necessary for spontaneous emission, two photons are released from the same excited state in the same phase, which is called stimulated emission (Zinth *et al.*, 2011). A schematic of laser production highlighting the distinct feature of its beam is shown in Fig. 1.2. The laser produced by stimulated emission has following unique characteristics (Ion, 2005):

i. Monochromatic

The light produced has a single wavelength while the ordinary light sources such as sunshine and lamplights are composed of different wavelengths.

ii. Coherent

The photons have the same phase and polarization so that the laser has a very high intensity of power. The ordinary light sources have a random phase and polarization, due to which its power intensity is low.

iii. Sharply Focused

A very narrow and collimated source of light has a very high-intensity power. The narrow beam divergence (θ) of a laser is shown in Figure 1.2 (d). The beam divergence is proportional to beam wavelength and inversely proportional to diameter of a laser beam.

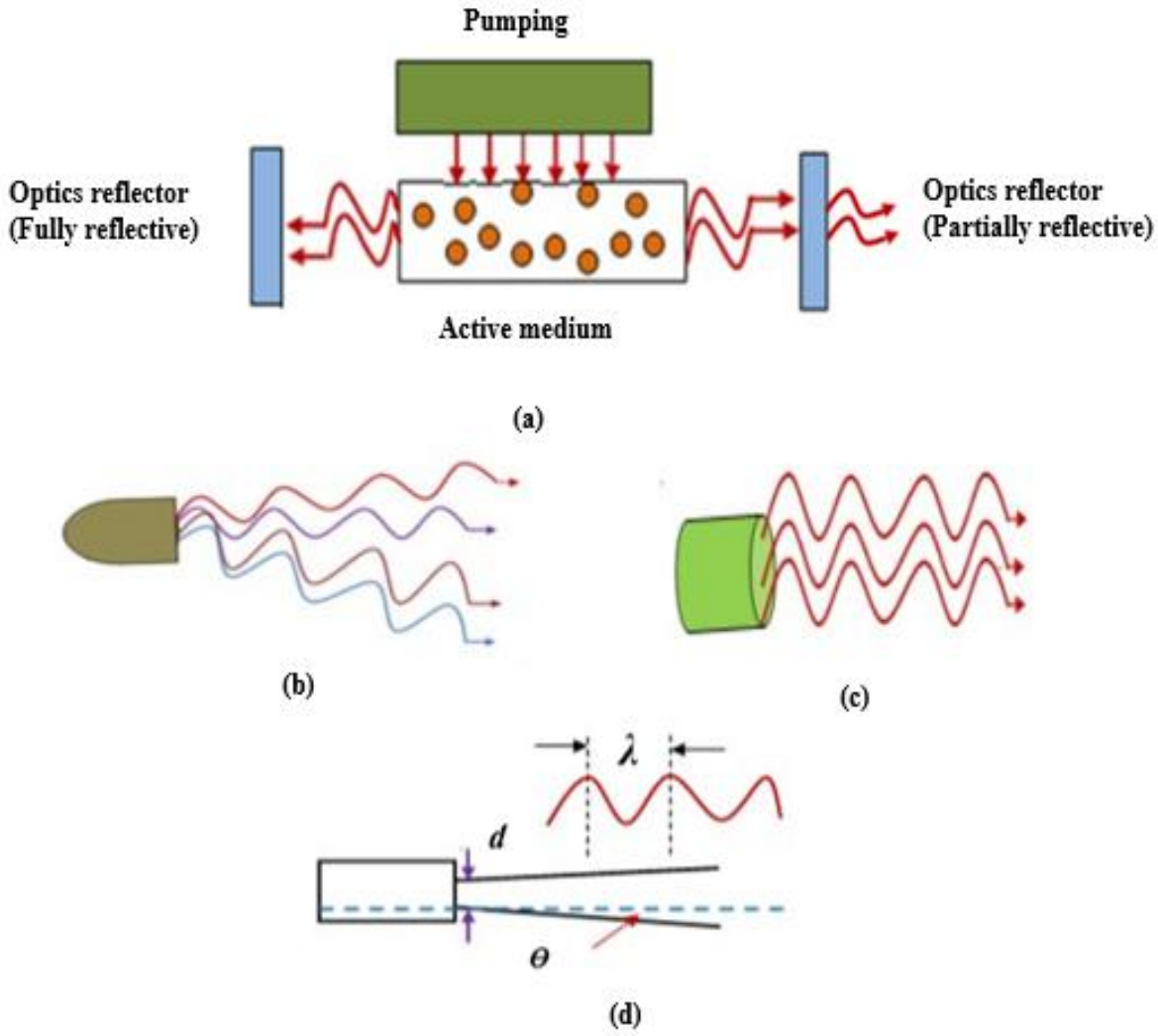

Figure 1.2 Schematic diagram of (a) laser production (b) ordinary light source and (c) laser beam light source and (d) laser diffraction angle

iv. Highly Directional

A laser gives high directional and a narrow convergent light source as shown in Fig. 1.2 (c). Conventional light sources emit light in all directions and are highly divergent as shown in Figure 1.2(b). The three main components of laser production are as follows as schematically shown in Fig. 1.2 (a):

1. Gain medium or active medium that amplifies the light source,
2. Resonator i.e., reflecting mirrors, providing a suitable optical feedback and
3. Excitation source or pumping source to cause the population inversion process.

Due to population inversion, more number of electrons will exist at the higher energy level than at the lower.

1.4.1 Types of lasers

There are different kinds of practical lasers. The major classification is based on the mode of operation and type of lasing medium. Based on the mode of operation, laser can be divided into two, viz., continuous and pulsed mode. The major types of a laser based on active medium are solid state, gas, semiconductor and liquid lasers.

Solid-state lasers have active ions in a crystal or a glass host material, which are optically pumped to form population inversion. In ruby laser, the first practical laser invented by Maiman (1960), the active ions are distributed in a solid matrix of ruby rod (chromium-doped aluminum oxide). The pumping source may be a helical xenon (or krypton) flash lamp to supply energy to the crystal rod. However, nowadays instead of helical, linear flash lamps are used. A solid-state laser works both in continuous wave (CW) and pulsed modes; however, the pulsed mode is more common. The majority of popular solid-state lasers use neodymium (Nd) doped materials e.g., Nd:YVO_4, Nd:Glass and Nd:YAG. YAG stands for yttrium aluminum garnet with a chemical formula of $Y_3Al_{15}O_{12}$.

The gas lasers utilize a gas or mixtures of gases as the active medium; operate in both CW and pulsed modes. The types of gases used are neutral atom gases such as He-Ne, ionized gases such as argon, krypton and He-Cd and molecular gases such as CO_2 and CO. The excitation of a gas laser is achieved by applying high voltage across the gas. The

most popular gas laser for materials processing is CO_2 laser. Some worth-noting facts about this laser are as follows**:**

- The wavelength of CO_2 laser is 10.64 μm.
- Lasers providing the output power more than 30 kW have been developed.
- The efficiency of CO_2 lasers can be as high 20% compared to single digit efficiency of several solid-state lasers.

Semiconductor or diode lasers are electrically pumped, compact and small power lasers (Li, 2000). They are widely used in laser printers and compact disc players. The properties of semiconductor lasers are wide spectrum bands 2–20 nm, large beam divergence (up to 40° half- angle), non-symmetrical beam distribution and lower energy intensity per unit area. The diode lasers use microscopic chips of gallium arsenide or other exotic semiconductors to generate coherent laser in a very small packaging. The maximum output power of semiconductor lasers used in CD players is 3–5 mW. Typical efficiency of diode lasers is 20–30%. Diode lasers with CW power more than 0.5 W are called high power diode lasers (HPDLs). HPDLs have been used for soldering, hardening, cladding, welding, scribing, machining etc. HPDLs up to 4 kW power are commercially available.

The liquid dye lasers use a liquid lasing medium. The output laser beam of liquid lasers possesses wide range of wavelengths. They have efficiency of about 25% and find application in medical and research fields.

1.4.2 Laser interaction with solid surface

The output energy from laser interacts with a solid surface that creates an electronic excitation and de-excitation of the solid surface in a short period of time. The heating and cooling time when laser beam interacts with the solid surface is about 10^3–10^{10} K/s and incident energy can be 0.1–10 J/cm^2. This energy only affects the near surface region without causing any effect on the bulk material property. The solid surface first absorbs laser beam, which creates an electronic excitation and de-excitation at the solid surface. The effect can create electronic energy from a beam of incident photons to heat energy, which is used for surface modification. The spatial profile of deposited energy from the

laser beam is dependent on reflectivity and absorption coefficients of the solid surface. The laser beam intensity decreases with depth as

$$I(z,t) = I_o(t)(1-R)\exp(-\alpha z), \tag{1.5}$$

where I is the laser beam intensity at a given depth (z) and time (t), I_o is the incident intensity, R is the reflectivity coefficient and α is the absorption coefficient.

Heating due to laser irradiation is heavily dependent on the thermal diffusivity given by

$$D = \frac{k}{\rho c_p}, \tag{1.6}$$

where k is the thermal conductivity, c_p is the specific heat and ρ is the density. For one dimensional heat flow condition, heat balance equation is given as

$$\rho c_p \frac{\partial T(z,t)}{\partial T} = Q(z,t) + \frac{\partial}{\partial z}\left(k \frac{\partial T(z,t)}{\partial z}\right), \tag{1.7}$$

where T is the temperature and Q is the power density at a given vertical distance z and time t. Depending on the power, density of the laser and temperature created near the surface, processes like heating, melting and evaporation take place.

1.5 Lasers in Material Processing

The use of a laser for material processing is increasing rapidly. Some advantages include high productivity, good process capability, contact-free processing, near net-shape manufacturing, improved product quality and minimum wastage of material. Figure 1.3 shows the classification of laser material processing. Surface modification is the main focus of this thesis. Surface modification is used to change either the surface topography or microstructure or both. Some processes are briefly described in the following subsections.

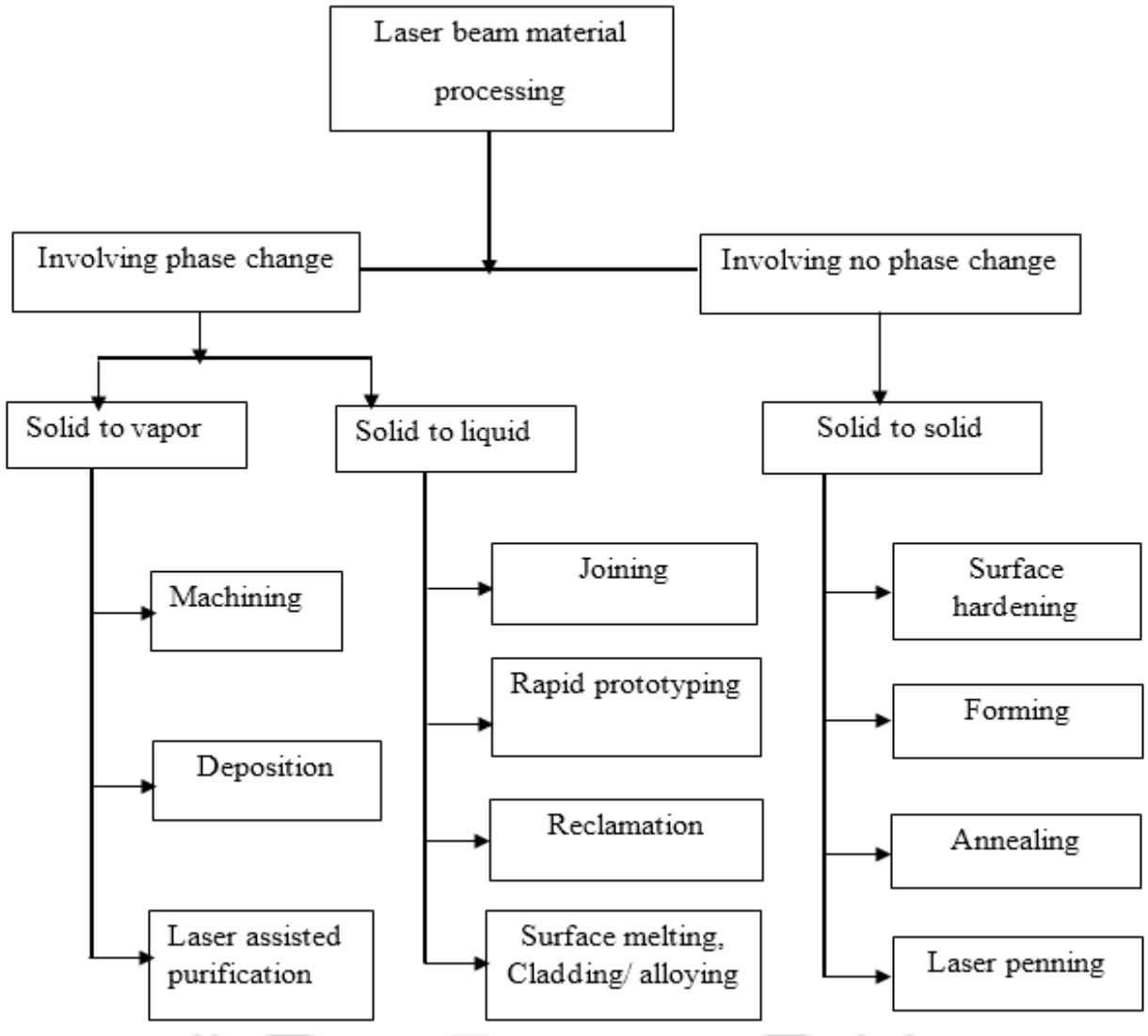

Figure 1.3 Classification of laser material processing (Majumdar and Manna, 2003)

1.5.1 Laser Forming

Manufacturing involves making a finished product from raw material to correct design, shape and geometrical dimension. Laser forming deforms a sheet metal into the desired shape by applying the thermal load from a laser beam source without external load. Laser assisted forming makes use of external mechanical load along with laser irradiation. To get the desired bend angle of a sheet, the parameters that affect the process are laser power, laser scan speed, beam diameter and worksheet properties **(**Eideh *et al*., 2015; Shichn and Jinson, 2001). The laser can also be used for straightening of thin sheets by heating with

laser beam. Generally, laser bending is an easy, flexible and productive method for various materials and applications.

1.5.2 Laser Rapid Prototyping

Laser rapid prototyping, more popularly known as 3D printing, is an additive manufacturing process. In this process, a computer aided design (CAD) model of the product is sliced in layers. After slicing the data is transferred to a 3D printer, which fabricates the component layer by layer (Das, 2003). One of the most common 3D printers employ selective laser melting (SLM) or selective laser sintering (SLS) also known as direct metal laser sintering (DMLS). In both the processes, metallic processes are heated by laser beam layer by layer in the desired location. In SLM powder material is scanned to melt it, whilst in SLS it is only sintered. Selective laser sintering has been used for manufacturing of hard tools from metallic powders (Abe *et al.*, 2001, Agarwala *et al*., 1995). During SLM of aluminum components made from powdered aluminum the formation of oxides was indicated as the major challenge (Bartkowiak *et al*., 2011; Louvis *et al.*, 2011). Dahotre and Harimkar (2008) has presented an excellent review on laser based rapid prototyping processes.

1.5.3 Laser Joining

Joining of similar or dissimilar metallic sheets using a laser heat source is called laser welding. The quality of joining is based on the selection of appropriate laser power, laser beam diameter and laser travel speed. It is also based on the type of sheet metals to be joined together and physical properties like thermal conductivity. The laser beam joining of lightweight structures for application in automobile and aerospace industries has got a lot of potential (Schubert *et al*., 2001; Yunlian *et al*., 2000).

1.5.4 Laser Machining

Laser machining refers to the removal of material by laser beam heating. It also includes laser cutting and drilling of metallic parts. The removal of material from the surface at a certain depth is achieved by melting and vaporization, since laser generates high power intensity focused on a narrow area. Laser machining is very much suitable for machining the hard materials like diamond (Chryssolouris *et al*., 2013). Small channels for

microfluidics application can be made by laser. There are a number of excellent review papers on laser beam machining (Meijer, 2004; Dubey and Yadava, 2008). The ceramic material can also be well machined using a laser beam (Forget et al., 1988; Samant *et al*., 2009).

1.5.5 Laser Surface Modification

Laser surface modification is carried out by melting the surface of a material using laser beam or by adding additional material followed by laser beam melting. The former process is called laser surface melting while the latter process can be either laser cladding or laser surface alloying. In laser surface melting, a laser beam irradiates a thin layer on the surface of a material. The heat deposited on the surface of a material is soon conducted away through the bulk material enabling a rapid cooling. As a result, the melted region undergoes transformational hardening and grain refinement processes. The depth of melted layer depends on laser beam processing parameters such as the beam power, scan speed and beam focusing distance. The major advantages of laser surface melting are improvement of hardness and wear resistance as well as corrosion resistance of material (Bergmann and Mordike, 1986; Serbiński *et al*., 2002; Liu *et.al*., 2006; Susnik *et al*., 2012; Pariona *et al*., 2013).

Laser surface modification by adding other material to the substrate material can be achieved by laser cladding and laser surface alloying. In laser cladding, the added material is built on top of substrate material and forms less depth along the substrate surface. The built-up material has a very small combination of substrate material portion so that the cladded material dominates the major surface properties. Laser cladding has many advantages; it improves surface hardness, wear as well as corrosion resistance of a material (Serlin and Richard, 1980; Shepeleva *et al.*, 2000; Sexton *et al.*, 2002; Toyserkani *et al.*, 2004).

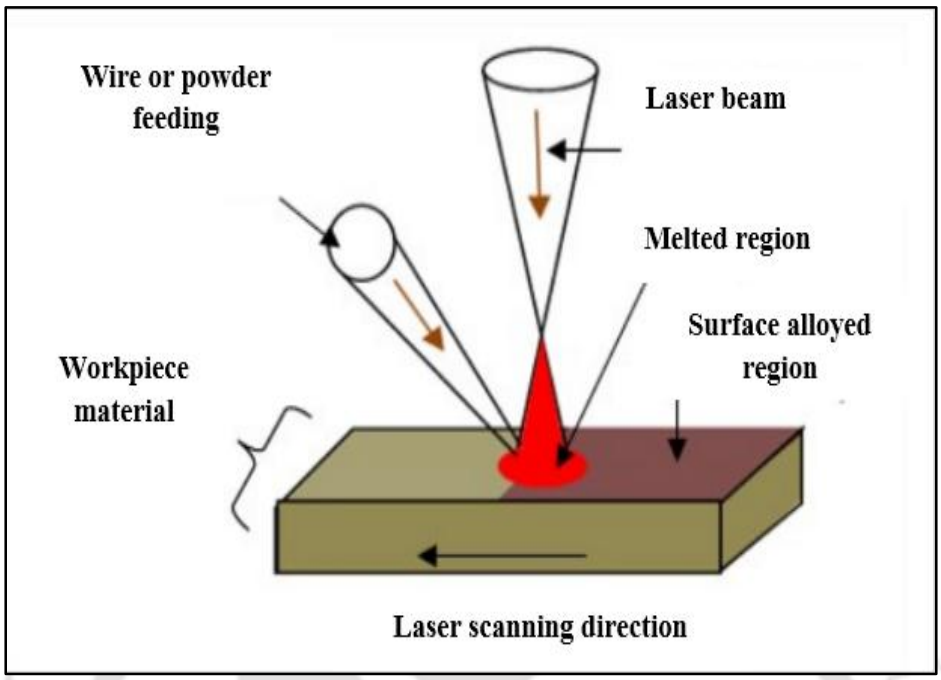

Figure 1.4 Schematic diagram of wire or powder feeding method

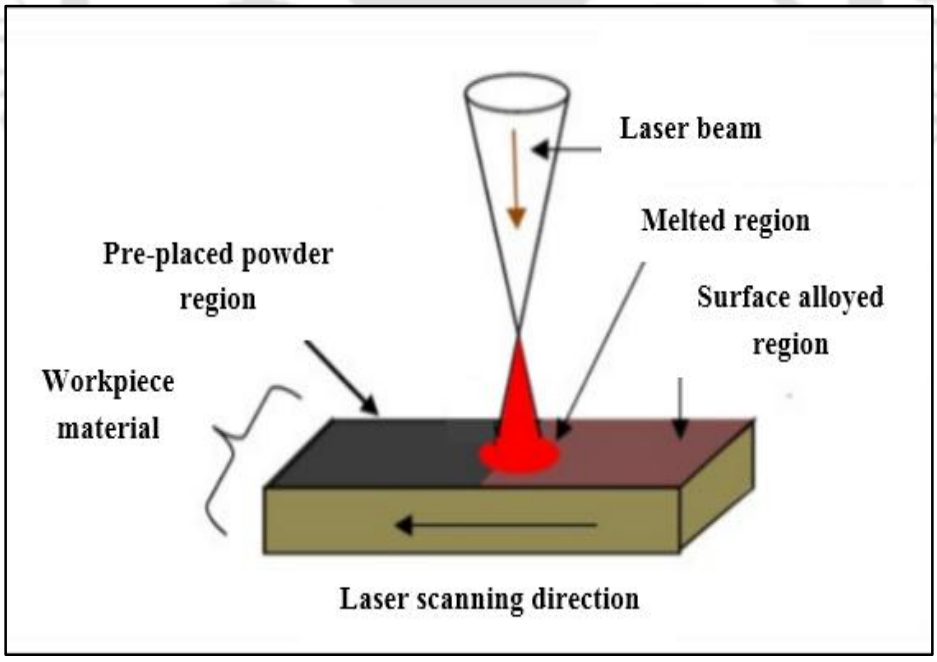

Figure 1.5 Schematic diagram of powder pre-placing method

Laser surface alloying can improve the surface of a material due to formation of new intermetallics, refined microstructure and reduced porosity during alloying. Alloying materials can be added during laser beam melting by wire or powder feeding directly from the side of the laser beam (Singh and Harimkar, 2012; Obadele *et al*., 2014). The alloying material can be pre-placed on the substrate material before laser beam melting (Kadolkar and Dahotre, 2003; Sahoo *et al*., 2015). Farnia *et al*. (2013) reported that a powder pre-placing method has an advantage of controlling coating thickness; a less amount of powder is required resulting in a high utilization of material.

In this thesis, the powder pre-placing method was used for adding alloying material during laser surface alloying process. This method is cost-effective because no accessories are required unlike in wire and powder feeding methods. Moreover, the pre-placed powder can be easily melted since laser beam absorbability is high due to coating. The other advantage of pre-placing method is a high utilization of alloying material, which a challenge during wire or powder feeding method where due to high reflection of the laser beam, some amount of powder does not melt. Figures 1.4 and 1.5 depict wire or powder feeding and powder pre-placing methods, respectively.

1.6 Motivation and Scope

The use of laser beam in manufacturing is getting more attention in research and industry because of the advantages that can be maintained only by laser beam properties. Two main features are easy controllability of heat input to the material during processing and easy focusing of the laser beam at a small area during machining, welding and surface modifications. There is minimal distortion of the material being processed by laser beam. In this thesis, the motivation of using a high power CO_2 laser for surface modification of aluminum and its alloy is due to the fact that a laser beam helps to achieve improved microhardness, improved wear and corrosion resistances of aluminum easily and economically. In addition to this, laser surface modification by alloying and melting is cost effective and environmentally friendly.

The scope of this thesis is limited to surface modification by two methods—laser surface alloying of commercially pure aluminum and surface melting of Al-12Si-4Cu-

1.2Mn alloy. Laser surface alloying was conducted on commercial aluminum as substrate material and different metallic and ceramic materials were alloyed using a laser beam to improve its property. Commercially pure aluminum was selected since the cost of this material is less compared to its alloys. Beside this the properties like hardness and wear resistance of pure aluminum is less than its alloys and it needs surface improvement. The corrosion resistance of pure aluminum is higher than that of many aluminum alloys. Hence, corrosion improvement by laser surface alloying with different metals is also investigated. Al-12Si-4Cu-1.2Mn alloy has good high temperature strength and finds application as cylinder blocks of internal combustion engines.

1.7 Organization of the Thesis

This thesis comprises ten chapters. This chapter gives a brief introduction of aluminum alloys. Introduction of laser and its application for surface modification are explained. The remaining chapters in the thesis are organized as follows:

- In Chapter 2, a review of literature on laser surface alloying and surface melting of aluminum and its alloys are discussed.
- Chapter 3 presents the details of experimentations used in the thesis.
- Chapter 4 presents results of pilot experiments on surface alloying of copper in aluminum using CO_2 laser.
- Chapter 5 presents laser surface alloying of copper, magnesium and manganese in aluminum: microstructure and mechanical properties.
- Chapter 6 presents wear behavior after laser surface alloying of aluminum with copper, magnesium, manganese and their combination.
- In Chapter 7, corrosion behavior after laser surface alloying aluminum with different metals are discussed.
- Chapter 8 presents laser surface alloying of aluminum with TiO_2 and SiC powders.
- Chapter 9 presents laser Surface Melting of Al-12Si-4Cu-1.2Mn Alloy.
- In the last Chapter 10, the conclusion and scope of future work are discussed

Indian Institute of Technology Guwahati

Chapter 2

Literature Review on Laser Surface Modification of Aluminum and its Alloys

2.1 Introduction

Aluminum alloys are groups of nonferrous metals finding a wide range of applications. They have appreciable properties such as high strength to weight ratio, high thermal conductivity, excellent corrosion resistance and workability. This favors their high demand. Aluminum alloys find applications in automotive, aircraft and shipbuilding structures. Often laser finds application during fabrication of these structures. It also finds application in improving the mechanical properties of aluminum alloys. Laser surface modification is a method for improving the surface properties. Often it is economical to alloy some material around the surface instead of bulk alloying. Laser surface alloying can create a novel microstructure at the surface that boosts its mechanical properties including hardness, fatigue and wear resistance. Laser surface modification improves the microstructure, hardness, wear resistance as well as corrosion resistance of the metal.

Gnanamuthu (1980) investigated laser surface treatment of two ceramic powders, silicon and alumina, for surfaces melting and surface cladding of two aluminum substrate materials (AA390 and AA219 alloys). For cladding AA390 aluminum alloy, 44 μm particle-size silicon powder was used. For cladding AA2219 aluminum alloy, 0.3 μm particle-size alumina powder was used. Before laser cladding, the samples were pre-heated at 20 ºC. A CO_2 laser was used for surface treatment purposes with 4.3 kW laser power for silicon cladding and 12.5 kW laser power for alumina cladding. The hardness of laser cladded material by Si particle was 400 kg/mm^2 whereas substrate hardness was 125 kg/mm^2. After alumina cladding, the hardness improved in the ranges of 2000 to 2300

kg/mm^2. Rapid solidification process of laser surface alloying refines its grain structure, reduces micro-segregation and extends solid solubility (Dubourg *et al*., 2002a/2002b; Kannatey *et al.*, 2009).

The alloying material is added to the melt pool during laser cladding or alloying process by different methods. In one method, they can be injected co-axially from the side in powder forms (Almeida *et al.*, 2001; Ignat *et al.*, 2004; Zhong *et al*., 2010). In another method, the alloying material can be added as a wire feeding from a side as reported by Syed *et al*. (2005) and Kim *et al*. (2000). The alloying materials can be pre-placed on the substrate material by making a slurry of alloying material and binder together as reported by Tomida *et al. (*2001/2003) and Rajamure *et al*. (2014).

In this chapter, relevant research works on aluminum laser surface alloying and melting are presented. Review on laser surface coating is presented in Section 2.2. Review on laser cladding is presented in Section 2.3. Laser alloying is reviewed in Section 2.4. Laser surface melting is reviewed in Section 2.5. Finally, after literature review, the research gaps are discussed in Section 2.6. The objectives of the thesis are stated in Section 2.7.

2.2 Laser Surface Coating

Surface modification of aluminum alloys is done by laser surface coating with metals and ceramics to improve its hardness, wear and corrosion resistance. The newly developed surface has new surface properties because of added materials due to phase transformation during melting. The formation of metallurgical bonding between coated and substrate material plays a great role in improving the surface properties. The uniformity of the coating can be controlled by controlling laser parameters such as power, scan speed and beam diameter. The thickness of laser coating is very small. During laser surface cladding higher thickness of the material is deposited on the surface. Laser surface coating is different from laser surface alloying since the coated material has less depth of fusion. However, in laser surface coating, a stronger metallurgical bonding is formed with the substrate material than that in conventional coatings (thermal spraying, vacuum vapor

deposition and electroplating). A schematic diagram of laser surface coating is shown in Figure 2.1.

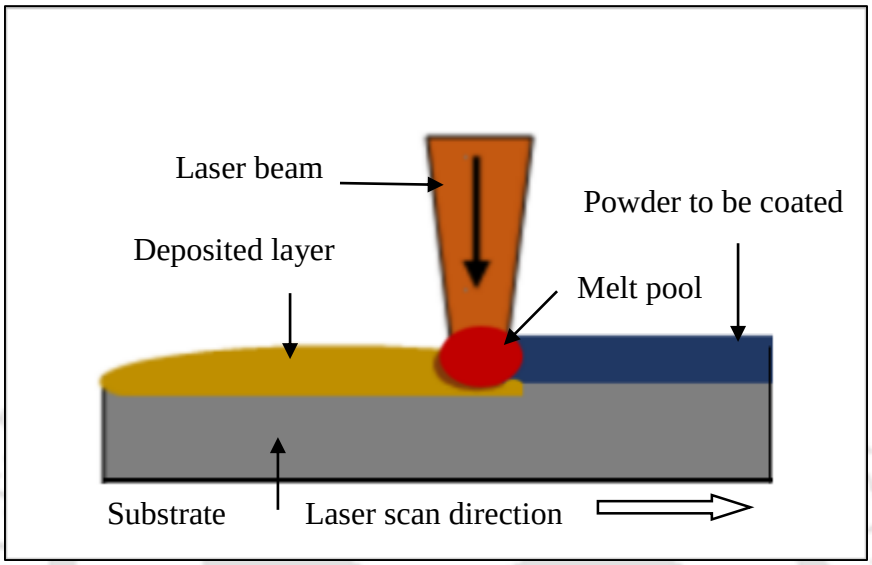

Figure 2.1 Schematic of laser surface coating by powder pre-placing method

Kadolkar *et al*. (2007) and Ravnikar *et al*. (2013) studied the thermal residual stress developed during laser beam melting. The method is applicable only when the coating and substrate materials have the same temperature as well as there is no deformation of the substrate. The residual stress was calculated as

$$\sigma_T = \frac{E_c E_s t_s \left(\alpha_c - \alpha_s\right)\Delta T}{\left(1-\nu\right)\left(E_s t_s + E_c t_c\right)}, \tag{2.1}$$

where σ_T is thermal residual stress, ΔT is the difference between the processing temperature and room temperature, α coefficient of thermal expansion, E is Young's modulus, t is the thickness of coating and ν is Poisson's ratio. The subscripts c and s refer to coating and substrate materials, respectively.

Liang *et al.* (2000) compared a plasma-sprayed Ni-Cr-B+WC coating and Ni-Cr-B-Si laser coating on a cast aluminum alloy (Al-8.23 wt.% Si-0.056 wt.% Mg-1.35 wt.% Cu).

Laser surface coating was done using a continuous wave CO_2 laser with 36 W/mm^2 power density and 10 mm/s laser beam scanning velocity. Wear resistance of laser coated samples with Ni-Cr-B-Si coating was higher than that of plasma sprayed Ni-Cr-B+WC coating. Loosening and granular peeling of the coating from the surface resulted in higher wear of the plasma sprayed samples than that of the laser coated samples. Katipelli *et al.* (2000) reported laser surface coating of aluminum alloy using TiC powder by Nd: YAG laser in continuous wave mode. Laser processing parameters were 1.8 kW laser power and 1200 mm/min laser scanning speed. Authors observed intermetallic compounds like $TiSi_2$ and $TiAl_3$ using X-ray diffraction method. The wear resistance of laser coated sample was improved due to intermetallic and modified microstructure. Tomida *et al.* (2001) improved the hardness of Al-Mg alloy up to 500 HV by laser coating with TiC powder. A study of residual stress developed in laser deposited TiC ceramic coating on 2024 and 6061 aluminum alloys were reported by Kadolkar *et al.* (2007). Laser deposition was conducted using Nd:YAG laser. Laser processing parameters were 2 kW laser power and 1500–2000 mm/min laser scanning speed for 2024 alloy. For 6061 aluminum alloy, 1000–1500 mm/min laser scanning speed was used. The micro stresses after TiC coating got reduced compared to the uncoated substrate. Increase in the laser scanning speed resulted in the increase of the micro stress developed during laser coating. The surface residual stresses developed in laser coated samples were of compressive type. Ravnikar *et al.* (2013) studied laser coating on 6082-T651 aluminum alloy with two ceramics of TiB_2 and TiC. Laser coating was achieved by melting the ceramics with substrate material using 3 kW diode pumped Ytterbium fiber laser. The coating thickness was 110 µm and the average coating hardness was improved by 40% over the substrate material. The flexural strength of the coating improved due to the high content of TiB_2 compound that delayed the occurrence of the micro-crack in the coating. The compressive residual stresses present in the coating were measured by relaxation method.

Kooi *et al.* (2003) noted that the addition of titanium helped to increase the fracture toughness during TiB-Ti composite coating made by laser melting. Sahoo *et al.* (2015) also reported the TiC coating on a pure aluminum substrate using a pulsed Nd:YAG laser using 1–2 kW laser powers. Hardness of 2200 $HV_{0.05}$ was achieved for samples processed by 1

kW laser power. For samples processed by 1.5 kW laser power, hardness of 2500 $HV_{0.05}$ was achieved. However, it was also observed that the hardness reduced to 2250 $HV_{0.05}$ when 2 kW laser power (with 70% pulse overlapping) was used for processing. However, 2 kW laser power with 80% pulse overlapping provided very low hardness (< 250 $HV_{0.05}$). In all the cases, the hardness was higher near the top surface and reduced towards the substrate.

2.3 Laser Surface Cladding

Laser cladding is a process of surface modification of engineering parts by depositing additional material on another material by laser beam melting. A lot of work has been done on the significance of and applications of laser surface modification. Agarwal and Dahotre (1999) deposited TiB_2 and Ti ceramic powders on steel AISI 1010 using continuous wave Nd:YAG laser; as a result the hardness was enhanced up to about 12 times. Agarwal and Dahotre (2001) also reported flexural study to confirm interfacial strength of laser surface engineered TiB_2 coating on AISI 1010 steel. Their results show strong bonding between coated region and substrate material with no delamination of the coating at the interface. Laser cladding takes less production time and produces less distortion due to properly controlled heat input. It is used for repairing failed components. The most significant advantage of laser cladding is manufacturing of complicated parts and functionally graded parts of different materials as a single component. Figure 2.2 shows a schematic diagram of laser surface cladding using powder pre-placing method.

Nowotny *et al.* (1999) reported laser cladding of ceramic materials to improve mechanical properties of aluminum alloy. They used two different ceramic oxides, Al_2O_3 and ZrO_2, for laser cladding of Al-Si10Mg substrate using 6 kW laser power by CO_2 laser. Laser cladding was done by using 0.5–2 kW laser powers and 150–600 mm/min laser scan speeds. The track overlapping was in the range of 15%–50%. The thickness of cladding layer was made minimum from 0.1–1 mm. Their results show that zirconia and alumina cladding formed unstable bonding, which resulted in the formation of micro-crack. However, the hardness of cladding region increased in the range of 1800–2000 $HV_{0.1}$. Ouyang *et al.* (2001) also reported laser cladding of yttria partially stabilized ZrO_2 ceramic without and with doping of 2.5 wt.% TiO_2 on $AlSi_9Cu_3$ aluminum alloy by melting using a

continuous wave CO_2 laser. The laser power used for melting was in range of 1.1–2 kW. The cladded height was up to 1 mm with overlapping of 30–50%. The results show increased hardness, ranging from 1415 $HV_{0.1}$ to 1575 $HV_{0.1}$.

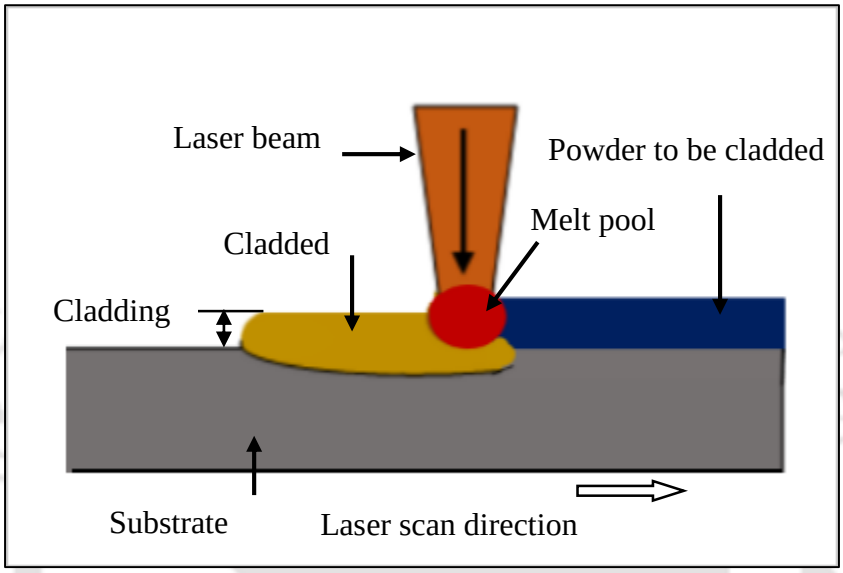

Figure 2.2 Schematic of laser surface cladding by powder pre-placing method

Laser cladding improves the wear resistance of aluminum alloy. Chong *et al.* (2001) studied wear resistance of AA6061 aluminum alloy after laser cladding with MoWC powders. A continuous wave Nd: YAG laser of 2 kW laser power was used. Abrasive wear resistance was improved because of MoWC cladding due to improved hardness. Yunshan *et al.* (2003) reported that laser cladding for re-fabrication of expensive components had a number of advantages compared with traditional repairing techniques such as flame or plasma spraying and welding. Dong *et al.* (2008) reviewed the application of laser cladding for repairing of engineering components and highlighted that laser cladding was an easy and economical method for repairing expensive components by reducing manufacturing cost of making new product.

Yevko *et al.* (1998) pointed out the influence of laser process parameters on the cladded height and width. They conducted two-dimensional finite difference analysis as well as experiments. Their results show that cladded height decreased with an increase in

laser scanning speed. When the laser power was less, cladded material did not properly bond to substrate material. Chryssolouris *et al.* (2002) studied the effect of laser process parameters on clad quality. They observed that as laser scan speed was increased, the clad height decreased. The clad depth slightly increased when the powder feed rate was increased. Lalas *et al.* (2007) conducted analytical modeling supported by experimental work during laser cladding and predicted clad depth and width dimensions. Increasing laser scan speed and powder mass flow rate resulted in the formation of smaller clad width. Song *et al.* (2012) developed a hybrid controller to control temperature and deposition during laser cladding for complex part like turbine blade. Li *et al*. (2018) reported laser cladding of 7075 aluminum alloy using Ti/TiBCN coating using semiconductor laser of 4 kW power. The laser cladding system was connected to a six-axis robot and the cladding powder was projected coaxially with a laser beam. When TiBCN content was 15 wt.%, the microstructure of coating zone was mainly composed of equiaxed grains and white lath like crystals, while the transition zone contained dendrite grains. The average hardness of the cladded zone increased by five times that of substrate material hardness of 127 $HV_{0.2}$. Wear and corrosion resistance after laser cladding improved.

2.4 Laser Surface Alloying

Laser surface alloying is the process of imparting an existing surface with new properties by adding additional materials to the substrate material by laser beam melting. Laser surface alloying of aluminum with different metals and ceramics has been conducted for years. Recently, Chi *et al.* (2018) presented a good review on laser surface alloying of aluminum. Mechanical properties such as hardness and wear resistance as well as corrosion resistance of aluminum alloys can be easily improved by laser surface alloying. Figure 2.3 shows a schematic diagram of laser surface alloying using powder pre-placing method.

Abboud *et al.* (1990) carried out laser surface alloying of titanium by blowing 99.97% purity aluminum powder. A continuous wave CO_2 laser was used for melting with 1.8 kW power and 7 mm/s laser scan speed. At 30% aluminum composition, a columnar microstructure was formed. The growth direction of columnar structure was from the interface to the top region. At 50% aluminum composition, a region of planar growth was

formed at the interface and the dendrite structures at the top region. Anthony and Cline (1977) discussed heat flow and diffusion of alloying particles due to temperature penetration into the material during laser surface alloying. The surface of the material during laser melting ripples because of surface-tension gradients. Rippling decreases as the scanning speed increases.

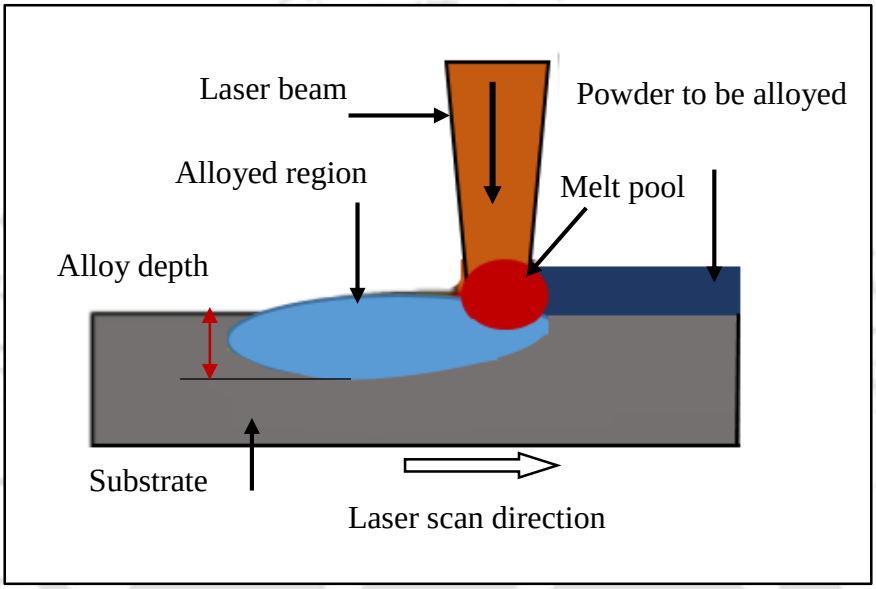

Figure 2.3 Schematic of laser surface alloying by powder pre-placing method

Ghosh *et al*. (1999) investigated wear resistance of Al-356 alloy after silicon and molybdenum powders were deposited in the ratio of 1:2 as a precursor coating using 3 kW CO_2 laser. The deposited layer got higher hardness because of intermetallics formed with high molybdenum content. Almedia *et al.* (2001) reported a powder blowing technique of laser surface alloying of Al-Nb powders on a pure aluminum substrate using a 2 kW power CO_2 laser. The laser beam diameter was 1.2 mm and corresponding laser power density was 1.8×10^3 W/mm^2. After alloying with 25 wt.% Nb powder, its hardness increased from 480–650 HV due to the formation of Al_3Nb intermetallic compound. The depth of alloy formed increased from 320 µm to 550 µm due to the decreased laser scan speed. Sarkar *et al.* (2002) conducted a three-dimensional computational modeling of momentum, heat, mass transfer and fluid flow in laser surface alloying of aluminum. High temperature caused high dilution depth by forcing dispersion of alloying elements in the melt pool.

Bhat and Majumdar (2003) proposed a mathematical model to calculate fluid flow in the melt pool during high energy laser beam melting of Ni powder alloyed with Al-4.5 wt.% Cu alloy as a substrate material. Ni distribution in the melt pool was caused by diffusion process. The particle penetration was due to the laser beam and Marangoni effect (a mass transfer of particles along the interface between two fluids due to a gradient of surface tension). In this case, the two fluids in the melt pool were nickel and aluminum.

Pinto *et al*. (2003) investigated laser surface alloying of copper with Al-15 wt.% Cu alloy using 1 kW power of CO_2 laser. The laser scan speeds were 500 mm/min and 800 mm/min. Their results show the formation of different microstructures including cellular structure, dendritically perpendicular and dendritically parallel to the direction of laser beam scanning. The thickness of microstructure was controlled by laser scan speed since the higher laser scan speed created wider cellular structure zone. The mean hardness in the unmelted region was 75 HV, while after laser alloying the hardness increased to 160 HV. The maximum hardness measured in the dendritic structure at the top alloy region was 210 HV. The alloying by adding low melting point metals like lead, bismuth and tin have been reported in papers by Lepper *et al.* (1997). Metals alloyed with low melting point metals reduce the coefficient of friction of the alloy and enhances its tribological performance. They can be used as a bearing material due to their lubricating property.

Phanikumar *et al.* (2004) carried out mathematical modeling of heat and fluid flows in laser surface alloying. Their results predicted bismuth particle distribution in aluminum by laser beam melting using a continuous wave of CO_2 laser at 10 kW power. The size distribution of bismuth particles was less affected by the initial composition of bismuth. The micro-cracks developed in the alloyed zone was due to Al_3Ni intermetallic bonds formed in the alloy without complete dispersion. Later, Balla *et al.* (2009) conducted laser surface alloying to improve the thermal conductivity of Al-4Cu-1Mg aluminum alloys. Laser surface alloying was conducted by Nd:YAG laser with 250–500 W laser power and different laser scan speed from 5–20 mm/s. Alloying powders of 60% Cu-25% graphite, 75% Ni-25% graphite, and 80% Cu–20% Mo were blown at 15–40 g/min feed rates. Laser surface alloying with 80% Cu–20% Mo coating on 2024 aluminum alloying increased the average thermal conductivity of aluminum from 121 W/mK to 225 W/mK.

Vaziri *et al.* (2009) reported the effect of laser parameters on properties of laser surface alloyed with nickel on aluminum. Nickel powders were coated by electroplating up to 30 μm thickness on the substrate. The alloying was achieved by melting with a pulsed Nd:YAG laser with a peak power 400 W. The hardness of the alloy increased by 10–15 times. The nickel concentration in the melt pool increased with increased laser power from 200–260 W. However, nickel concentration increased at a higher laser beam diameter. The thickness of the alloyed layer was decreased when laser beam diameter was increased. Selvan *et al.* (2000) reported an improved hardness when intermetallic phase precipitates due to nickel in aluminum melt pool during alloying. Later, Das (1994) reported that nickel concentration in the aluminum melt pool was more when laser defocusing was higher since it created a temperature variation due to surface tension gradient.

Almeida and Vilar (2010) reported the formation of Al_7Cr eutectic compound of AlCr alloys synthesized by laser alloying. The surface alloying was prepared by injecting Cr powder into the melt pool generated by CO_2 laser beam. The microstructure of laser alloyed region had equiaxed cells comprised of an extremely fine Al_7Cr intermetallic compound. Alwafi *et al.* (2011) reported laser surface alloying of pure aluminum with iron and copper. A thin layer of Fe-Cu alloy was developed on pure aluminum using Nd: YAG laser with a pulse duration of a nanosecond. On the substrate surface, 0.8 mm alloying thickness was formed. The intermetallic compound of $Cu_{9.9}Fe_{0.1}$was identified using an X-ray diffraction analysis. The presence of metastable phases— $Cu_{9.9}Fe_{0.1}$ and AlFe, $Al_{13}Fe_4$, in the alloy zone improved its hardness.

A computational modeling was demonstrated to predict the dilution of molybdenum on aluminum substrate (Vora *et al.*, 2013) in laser surface alloying. The model was used to predict the melt pool geometry (depth and width). The results show that dilution increases when the laser power is more while it decreased when laser scan speed increased. The presence of Al_5Mo, Al_8Mo_3 and $AlMo_3$ and Al_2O_3 intermetallic compounds were identified by an X-ray diffraction analysis to validate computational model.

2.4.1 Studies on Wear Resistance

Laser surface alloying with metals and ceramics are very important to improve the wear resistance of parts made from aluminum. The erosion cavitation of laser surface alloyed coatings on Al-12%Si aluminum alloy was improved by laser surface alloying as reported by Tomlinson and Bransden (1995). The main reason for improved cavitation erosion resistance was due to the formation of densely packed intermetallic compounds. Iron and nickel alloying resulted a fiber-reinforced composite that restricted the size of the cracks formed during erosion. The presence of iron and nickel in the alloy improved the cavitation erosion resistance. Without alloying, the erosion rate was 27.6 mg/h. After alloying with iron erosion rate decreased to 7.2–3.8 mg/h and after nickel alloying, the erosion rate was 2.47–0.71 mg/h.

Fu and Batchelor (1998) reported laser alloying of AA 6061 aluminum alloy with 70 %Ni and 30% Cr by melting using Nd:YAG laser in a pulsed mode. The alloy was formed by melting using 30 J/mm^2 laser power density. After alloying, the hardness increased to 100–425 HV due to Ni_3Al intermetallic compound formation. The presence of micro-crack was a challenge when a laser power increased from 200 to 300 W. The thickness of alloyed layer was in the range 50–80 μm. The fretting wear resistance increased by three times due to alloying. The adhesive and abrasive type of wears were also investigated. The coefficient of friction for laser alloyed sample was less than an unalloyed substrate. Staia *et al*. (2000) studied the tribological property of A-356 aluminum alloy after laser surface alloying with 96 wt.% WC, 2 wt.% Ti and 2 wt.% Mg metallic powders by melting using Nd:YAG laser. The powders were applied by a pre-deposition method on the substrate during the experiment. As a result, intermetallic compounds of WC, W_2C, and $W_6C_{2.56}$ were formed in the alloy region. Additionally, oxides of Al_2O_3, SiO_2 and Al_4C_3 were also observed. The load applied during the wear test was 5 N. The average coefficient of friction varied with the change in sliding speed. Wear resistance of laser surface alloyed samples was promising. Chuang *et al.* (2006) reported laser surface alloying of Ni-Cr-B-Si on Al-MgSi substrate. The particle sizes of alloying elements were in the range 70–200 μm. A continuous wave CO_2 laser was used at 5 kW laser power and 10 mm/s laser scan speed. The wear performance of laser surface alloyed samples

improved due to the formation of Al_3Ni and Al_3Ni_2 intermetallics. The friction coefficient of laser surface alloyed samples was less than unalloyed substrate material. However, when the temperature increased, both wear rate and friction coefficient increased. The hardness of the alloy was 1100 HV that showed improvement of laser surface alloyed samples.

Rajamure *et al.* (2014) reported laser surface alloying of molybdenum on Al 100 aluminum. The alloying powder was coated by spraying up to 175 µm thicknesses. A diode pumped Ytterbium laser with 3 kW laser power was used for alloying. The wear resistance of laser surface alloyed sample increased by six times. The formation of intermetallic compounds like Al_8Mo_3 and Al_5Mo contributed for the improved wear resistance. Popoola *et al.* (2011) studied laser surface alloying of AA1200 aluminum alloy by alloying with 50% Cu+50% Mo metals. Alloying was achieved by melting using Nd:YAG laser using 4 kW power and 1.4–1.8 m/min laser scanning speed. Hardness of the alloy formed increased to 148 $HV_{0.1}$ because of Al_2Zr_4 and MoO_3 intermetallic compounds. The wear resistance of the laser surface alloyed sample increased due to the formation of fine microstructure.

2.4.2 Studies on Corrosion Resistance

Aluminum and its alloys are good corrosion resistant materials in the presence of low aqueous and acidic environments. However, when exposed to aggressive environments, aluminum alloys suffer corrosion damage. In a normal condition, a protective oxide layer prevents corrosion by acting as a barrier between the metal and its environment. When the environment is more aggressive, the oxide layer gets broken down by chloride ions (Sato, 1990). The oxide layer may repair itself in most cases as reported by Davis (1999). However, in aggressive corrosive condition, aluminum and its alloys can be damaged in the form of localized attacks of pitting corrosion. Szklarska *et al.* (1999) pointed out that four stages of pitting corrosion of aluminum alloys are (1) formation of pit on passive film or at the boundary, (2) processes occurring within the passive film devoid of visible microscopic changes, (3) growth and re-passivation of pits and (4) stable growth of pits. Aluminum-zinc alloys are known for their corrosion resistance. Shah and Dahotre (2002) improved corrosion attack by molten aluminum after laser deposition of vanadium carbide

on AISI H13 steel using Nd:YAG laser. Laser surface modification also reduces corrosion degradation of biometallic materials (Singh and Dahotre, 2007).

A study made by Abolikhina and Molyar (2003) shows the corrosion of aircraft structures made from aluminum alloys was due to corrosion attacks. The failure of aircraft-material was due to different reasons like fatigue failure, stress corrosion cracking and high temperature corrosion. Pitting and exfoliation corrosion of the aluminum are the most common kinds of corrosion in structural elements made from aluminum alloys. Almeida *et al.* (1995) reported laser surface alloyed 7175 aluminum alloy with a mixture of Al-25 wt. % Cr powders. The powder was blown to the laser melt pool. Laser power density used was 1.1–2.6 W/cm^2 and interaction time of laser was 0.04–0.3 s. There was 50% track overlapping during alloying. The corrosion evaluation was made by anodic polarization test in 3% NaCl solution. The hardness after laser alloying was increased to 300 HV while unalloyed base material hardness was 155 HV. The corrosion resistance improved due to the formation of passive film chromium oxide. Watkins *et al.* (1998) reported laser surface melting and alloying of 2014 aluminum alloy by melting Cr, W, and Ni with aluminum powder in different combinations. Laser surface alloying was accomplished by melting with 1.45 kW laser power and 2 mm/s laser scanning speed with 50% track overlapping. The formation of pitting corrosion along a planar front and in cellular zones was observed. With Al-Cr alloying, the improvement in corrosion resistance was due to high anodic potential. Pitting corrosion reduced to preheating effect and track overlapping. During alloying with tungsten, pitting potential was formed in heat affected zone (HAZ), but during zirconium alloying, deep corrosion pits were formed in the overlapped region. In Al-Ti-Ni alloying, pitting polarization increased. The formation of micro-segregation in the planar region and coarse structures in the heat affected zone reduced its corrosion resistance. The micro-segregation formed in track overlapped area was a reason for pitting corrosion.

Chan *et al*. (2002) reported the advantage of laser surface treatment to improve the corrosion behavior of 6013-T651 aluminum alloy. After corrosion test in electrochemical polarization and immersion tests, the pitting potential of the alloy was increased due to the intergranular corrosion resistance of the alloy. The reduction in corrosion current density

was about three orders of magnitude. There was no formation of intermetallic compounds and the absence of precipitate free zones were a reason for improved corrosion resistance. The formation of needle-like precipitates in the grain boundaries caused corrosion. The superior corrosion resistance of laser treated zone was due to chemically stable AlN compound phase. Almedia and Villar *et al*. (2008) studied laser surface alloying of aluminum alloy by melting using CO_2 laser and alloyed transition metals like Cr, Mo, and Nb to improve its corrosion resistance. In the alloyed zone intermetallic compounds of Al-Cr and Al-Mo were formed. The microhardness in re-melting zones was higher than in non-melted areas. The hardness improved to 110–120 HV for Al-Cr, 65–350 HV for Al-Mo and 500–650 HV for Al-Nb alloying.

Ares *et al.* (2008) reported corrosion resistance of Zn-Al alloys in 3% NaCl solution at room temperature and indicated that the columnar morphology had a higher value of charge transfer resistance than equiaxed morphology. Thus, corrosion resistance was more of Zn-Al alloy. El-Sherbini *et al*. (2003) reported weight loss method and potentiodynamic polarization tests in 1 M HCl and 1 M H_2SO_4 solutions at different temperatures from 25–55 °C. For both the solutions, the corrosion protection efficiency decreased as the temperature raised. Hinton (1995) investigated corrosion of aluminum and magnesium alloy, mostly in the formation of pitting and white powdery deposits on the surface of the metal. Kamoutsi *et al*. (2006) studied the causes of pitting corrosion due to attack of chloride ions on the metal. Bardal (2007) reported three main categories of corrosion – (i) wet corrosion when the corrosive medium is water with dissolved species, (ii) corrosion in fluids such as salts and molten metal and (iii) dry corrosion where dry gases exist. As the corrosion proceeds, the metal dissociates and transferred to the corrosive medium in the form of ions.

2.5 Laser Surface Melting

Laser surface melting (LSM) is a method of modifying aluminum and its alloys without adding any alloying materials. A schematic diagram of laser surface melting is shown in Figure 2.4. Laser beam melting creates new phase transformation in a melted layer that refines microstructure and avoids porosity by forming a homogeneous melted layer. The

depth of melting is controlled by controlling the heat from a laser beam. Zimmermann *et al.* (1989) reported a surface modification of A1-32.7 wt.% Cu aluminum alloy by melting using CO_2 laser. The solidification rate of 500 mm/s resulted in the formation of lamellar spacing of 40 nm. At a solidification rate of 200 mm/s, the spacing was 17 nm. These observations were confirmed by the authors through mathematical modeling, which showed a continuous decrease in lamellar spacing when solidification rate increased.

Chen and Huang (1990) reported a finite difference method to study heat and fluid flow during laser melting. Their result shows that the size of the melt pool reduced due to the latent heat of fusion and melt depth was less at high laser scanning velocity. The density variation in the melt pool was due to surface tension and temperature of the melt pool. Noordhuis and Hosson (1993) investigated laser treatment of Al 2024-T3 alloy (4.4% Cu, 1.5% Mg, and 0.6% Mn) by melting using continuous wave of CO_2 laser.

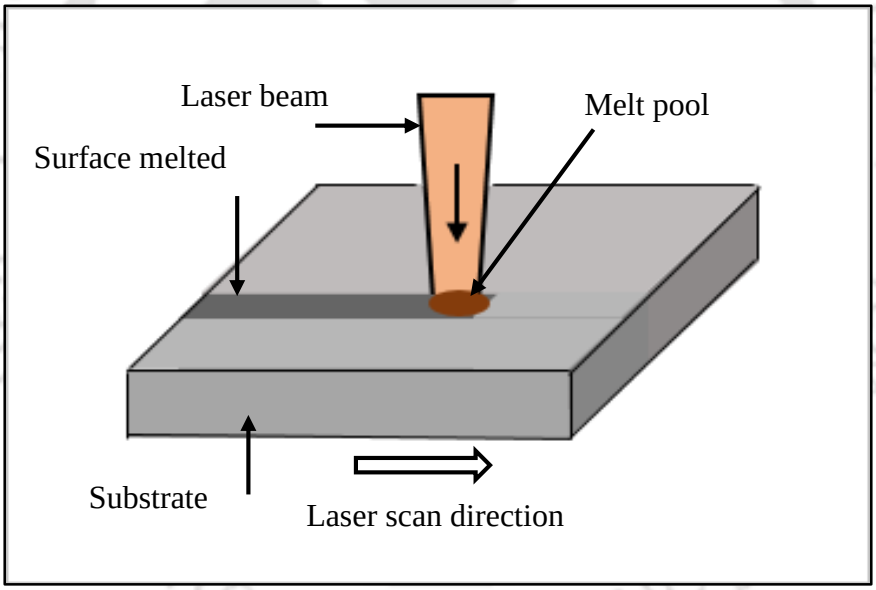

Figure 2.4 Schematic of laser surface melting process

Laser power was1.3 kW and laser beam diameter was 0.75 mm. Their results show the formation of cracks at low and high laser scan velocity because of reduced ductility. The X-ray diffraction study showed intermetallic compounds like $CuAl_2$ and $CuMgAl_2$ formed in the alloy zone. The cellular structure developed during solidification decreased in size when laser scanning speed was increased. Further, the hardness of laser treated

sample increased but was less affected by laser scan velocity. The hardness in low scanning velocity regime was due to homogenization and helical dislocation created.

2.5.1 Studies on Wear Resistance of LSM

Van Otterloo *et al.* (1995) reported on enhanced mechanical property and microstructure of aluminum-copper alloy by laser melting using a continuous wave CO_2 laser. The processing laser power was 1.3 kW and beam diameter was 0.175 mm. The laser scanning velocity was in the range 1.25–125 mm/s. The depth of remelting was 0.5 mm and 0.3 mm for lowest and highest scan velocities, respectively. The Al_2Cu intermetallic phase was formed. More copper presented in the microstructure led to the formation of a lamellae structure. The interface microstructure had plate-like cellular but changed to networks of lamellae structure as Cu content was increased. The maximum hardness was 212 HV, achieved at 40 wt.% Cu. The amount of Cu quenched in solid solution increased its solidification hardening.

Serbinsiki *et al.* (2003) reported the tribological property of laser modified surface of the AlSi-13Mg-1CuNi cast aluminum alloy by melting using CO_2 laser. Laser melted region had a smooth surface having a dense and pore-free cast structure. The hardness increased from 110 $HV_{0.05}$ to 260 $HV_{0.05}$ due to the decrease in grain size. The wear resistance of laser modified sample also improved and its coefficient of friction reduced. When the sliding distance increased, more wear formed. Tomida *et al.* (2003) reported improvement in wear resistance of Al-Si cast alloy by laser surface melting using a continuous wave CO_2 laser. The wear resistance improved because of improved microhardness up to 140 HV. The wear resistance was more for Al-30 wt.% Si than Al-20 wt.% Si. Wang *et al.* (2014) reported ZrO_2-7 wt.% Y_2O_3 thermal barrier coating on AlTi alloy followed by laser remelting using 2 kW CO_2 laser. Laser scanning velocity was 400 mm/min and beam output power 550 W. Microhardness of sprayed coating was 1050 HV while laser remelted sample hardness was 1900 HV. The hardness was gradually decreasing in the depth direction. The original hardness of substrate was in the range 240–260 HV. The erosion resistance of laser remelted sample was better than thermal barrier coated samples.

2.5.2 Studies on Corrosion Resistance of LSM

Some work has been conducted on the effectiveness of laser surface melting for corrosion resistance. Even, there are reports showing the disadvantages of laser surface melting with regards to corrosion protection. Li *et al.* (1996) reported anodic polarization of localized corrosion in 3% NaCl de-aerated solution after laser treatment of aluminum alloy. The substrate material at attacked by intergranular region and pitting corrosion occurred in a distributed manner. Laser surface melted region had less pitting corrosion. Chong *et al.* (2003) also reported laser surface treatment of 2014-T6 aluminum alloy. They reported that beam overlapping had an effect on pitting corrosion protection. Nd:YAG laser was used with 3 kW laser power at different beam traverse speeds from 0.25 to 6 m/min for laser surface melting. Single tracks with overlap of 25%, 50%, and 75% were developed by laser melting under argon gas shielding with flow of 20 l/min. Both as received and laser treated samples were tested using corrosion polarization study in de-aerated 1 M NaCl solution at 30 °C. The results show an improvement in pitting potential of laser treated sample due to redistribution of second phase particles of Al_2Cu and Mg_2Si. However, laser track overlapping had no significant effect.

Yue *et al.* (2004) carried out laser surface melting of AA775-T651 aluminum alloy and improved its corrosion resistance. Excimer laser with 103 J/mm^2 energy density was used with a laser scan velocity of 2 mm/s. Laser melting was carried out with 70% track overlapping. The oxide layer formed due to melting reduced the corrosion current by six times. The untreated surface suffered a wide spread of pitting corrosion, while laser treated samples was less affected by corrosion. Electrochemical impendence data showed that the polarization resistance of laser treated specimen was one order magnitude higher than that of untreated sample, thus confirming the improvement in corrosion resistance by laser melting.

Liu *et al.* (2005) studied corrosion mechanisms of laser melted AA2014 and AA2024 aluminum alloys. A 2 kW continuous wave CO_2 laser was used. The results showed the formation of a finer intermetallic compound. For AA2014-T6 alloy, cathodic nature of Al_2Cu increased corrosion potential in α-aluminum solution and reduced galvanic corrosion. For AA2024-T351 alloy, anodic nature of Al_2CuMg phase relative to α-Al

solution enhanced the driving force for pit initiation resulting in a pitting corrosion. Liu *et al.* (2006) reported the fundamental understanding of corrosion performance of laser treated metallic alloys. They reasoned that the corrosion resistance of laser treated metallic alloys was mainly dependent on refined microstructure, phase transformation of new intermetallic compounds and cooling rates.

Osorio *et al.* (2008) reported the laser surface melting of Al-9 wt.% Si casting alloys. Samples were remelted using a continuous CO_2 laser using 1 kW. The corrosion evaluation of samples was conducted by electrochemical impedance spectroscopy (EIS) technique and polarization curves in both 0.5 M NaCl and 0.5 M H_2SO_4 solutions at 25 °C. Their conclusion shows no significant improvement in LSM for corrosion resistance but an improvement in microstructure after laser surface melting was achieved. Yilbass *et al.* (2009) reported laser surface melting of 8022 aluminum alloy using CO_2 laser by melting using 2 kW pulsed mode. Their results did not show any improvement in corrosion resistance as tested in 0.7 M NaCl solution; the surface morphology of laser treated samples resulted in raising its pitting corrosion. The irregular surface morphology enhanced crevice corrosion at the surface. The potentiodynamic curve shows the corrosion potential of laser treated sample is reduced. The corrosion current and corrosion rates increased by a factor of ten due to rise in irregularity in laser treated sample. Laser treated surface had no cracks and pore cavities.

2.6 Research Gaps

Following observations are worth noting:

- Laser surface alloying of aluminum using powder pre-placing method has been initiated in 1990s. Due to immense importance of aluminum and its alloys in automobile and aerospace sector, there is a need of continuous research in this area.
- The effect of different laser parameters like laser power, scanning speed and beam spot diameter on laser surface alloying and melting needs further investigation. Optimization to reduce the energy consumption is the need of hour for present day sustainable manufacturing.

- Many laser surface alloying processes use shielding gas, while sometimes open air alloying is also carried out. A comparison of these two types of process will be of interest to industry.
- Corrosion tests have been carried out for a number of substrate-alloying element combinations. However, there are several different combinations and hence the need for this type of study remains.
- Laser surface melting of aluminum alloys is an interesting area that needs to be further explored.
- Mathematical modelling of laser surface alloying is also an interesting research area.

2.7 Objectives and Research Plan

The main objective of the thesis is to investigate the effectiveness of the powder pre-placing method of laser surface alloying of aluminum with metallic and ceramic powders to improve mechanical as well as corrosion performances. In addition to this, the significance of laser surface modification by surface melting Al-12Si-4Cu-1.2Mn aluminum alloy is carried out to improve mechanical properties such as hardness and tensile strength. There has been a lot of work of the surface alloying of aluminum and its alloys. The novelty of this work stems by using different combinations of alloying elements. In that sense, the work presented in this work is evolutionary rather than revolutionary. However, it is important in the present context. Here, different additives (alloying elements) were selected based on cost, availability as well as desired property after alloying. In conventional aluminum alloys, copper is a principal alloying element in 2xxx series, magnesium in 5xxx series, manganese in 3xxx series, and zinc in 7xxx series (Davis, 2001). Copper addition increases hardness and wear resistance property (Dubourg *et al*., 2002). The addition of magnesium increases hardness and corrosion resistance. Titanium alloying improves corrosion resistance (Abboud *et al*., 1990). Instead of using aluminum alloys with these metals, laser surface alloying may be more economical in several situations. Table 2.1 lists the prices of some powders. Usually, the aluminum is cheaper compared to alloying metals like copper. Hence, instead of using Al-Cu alloy for a big structure, it may be prudent to alloy the surface with Cu. The alloying metals used in this research work are easily

available and are usually alloyed by a casting route. From a scientific point of view, this research can reveal the difference between laser alloying and other methods of alloy preparations.

Table 2.1 Prices of some powders

Metal	Price/kg (in Indian Rupees)	Specification
Cu	590	99.7%
Al	100	-
Mn	225	-
Ti	2500	99%
Zn	285	-
SiC	12	60-600 mesh
TiO_2	200	-

Source: https://dir.indiamart.com/impcat/metal-powder.html (accessed on September 26, 2018)

The specific objectives of the thesis are explained as follows:

i. Studying the effect of laser surface alloying of aluminum with different metals and ceramics
ii. Studying the effect of laser process parameters on the quality of laser surface alloying
iii. Understanding microstructure, surface topology, and mechanical properties of laser surface alloying
iv. Investigation of wear performance of laser surface alloying of aluminum with different metals using pin on disc sliding wear testing in dry condition at room temperature.
v. Investigation on corrosion performance after laser surface alloying of aluminum with different metals in acid and salt concentrations
vi. Investigating the use of surface melting of Al-12.5Si-4Cu-1.2Mn alloy to improve mechanical properties.

The overall plan of the thesis is given in flowchart shown in Figure 2.5.

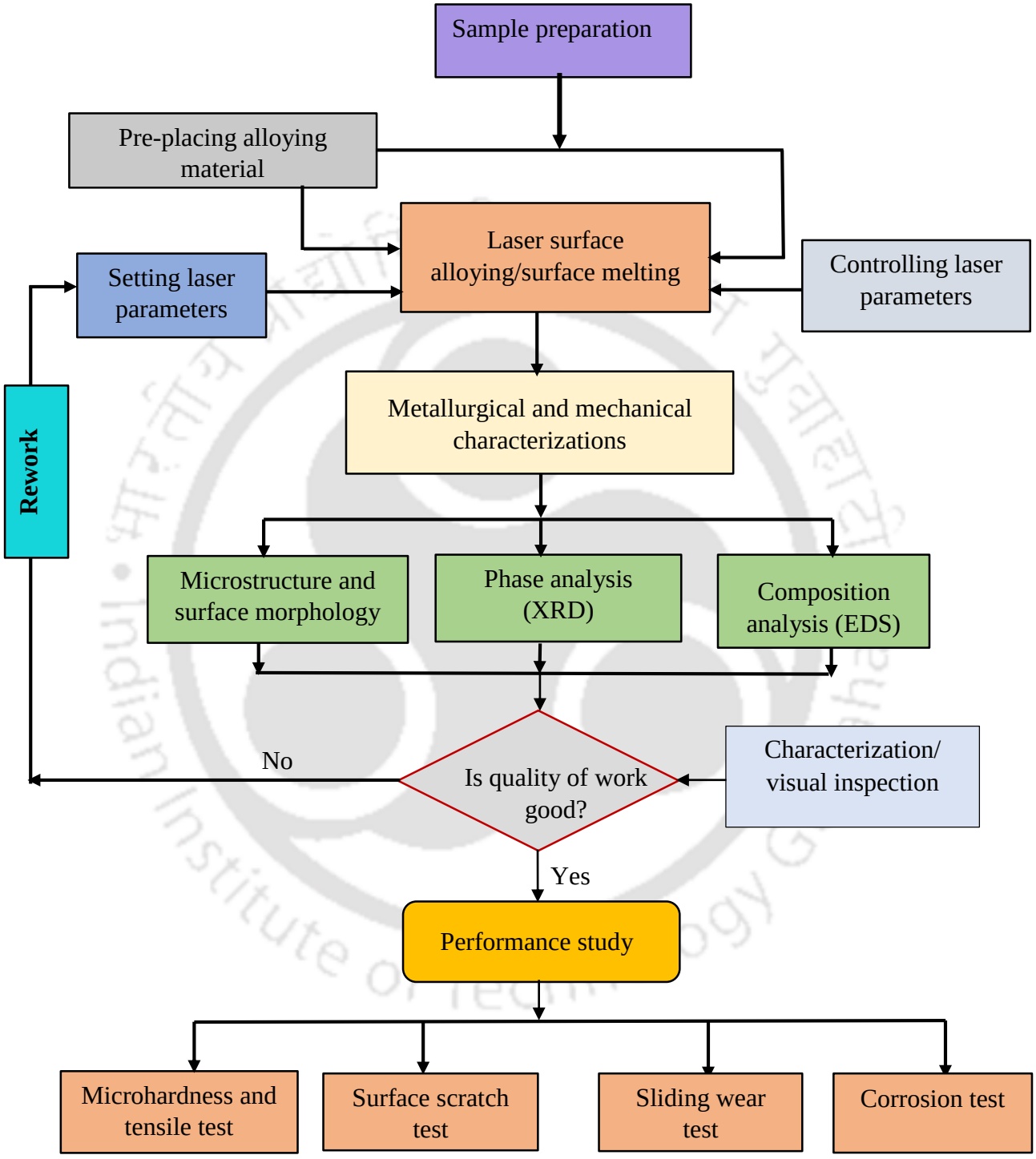

Figure 2.5 Flowchart of experimental plan

Indian Institute of Technology Guwahati

Chapter 3

Details of Experimentation

3.1 Introduction

In this thesis, laser surface modification of aluminum by alloying and surface melting is conducted. Laser surface alloying of commercially pure aluminum with different metals and ceramic powders using a powder pre-placing method is studied. Laser surface melting was conducted on Al-12Si-4Cu-1.2Mn alloy. The details of experimentations are presented in this chapter. All machines and instruments are discussed with supporting photographs and schematic diagrams. Some of those machines are CO_2 laser cutting machine, Vickers hardness tester, universal testing machine (UTM), wire-cut electric discharge machine (EDM), X-ray diffraction machine, field emission scanning electron microscopy (FESEM), non-contact optical profilometer, pin-on-disc wear testing machine and surface scratch testing machine. For laser surface alloying, a commercially pure aluminum was selected as the substrate material because of its low cost and availability. The surface of the aluminum plate was mechanically cleaned by wire brushing to avoid any oxides. Metal powders used for surface alloying were copper, magnesium, manganese, titanium, zinc and combinations of these metals. Additionally, two ceramic powders–SiC and TiO_2–were also used for alloying commercially pure aluminum. The average particle size of SiC powders was 10 µm and TiO_2 powder was 45 µm.

Laser surface melting was conducted on Al-12Si-4Cu-1.2Mn cast aluminum alloy after solutionizing heat treatment in an electric furnace at 510 ºC for 5 hours and cooling in a furnace at 165 ºC for 6 hours. Al-12Si-4Cu-1.2Mn alloy has good high-temperature strength and finds application as cylinder blocks of internal combustion engines.

3.2 Sample Preparation

Figure 3.1 shows the flow chart of laser surface modification processes by laser surface alloying and surface melting. Aluminum plate was cut into different sizes and was cleaned by wire brushing to avoid any surface oxides. The composition of aluminum substrate analyzed using EDS test was 0.1wt.% Cu, 0.9 wt.% Si, 0.4wt.% Fe and the balance aluminum. The selection of alloying materials depends on the mechanical properties required to improve hardness and wear resistances. For example, laser surface alloying with copper, magnesium and manganese enhances its mechanical properties like hardness, tensile strength and wear resistance. Figure 3.1 illustrates a flowchart of laser surface modification. Figure 3.2 (a) shows copper powder and Figure 3.2 (b) shows copper powder mixed with Fevigum binder in a slurry form. Fevigum binder does not affect the property of the alloy, formed during laser alloying. The alloying material after preparing in slurry form is pre-placed uniformly on the substrate. For drying purpose, samples were kept in room for 2–3 days. Figure 3.3 (a) shows sample with pre-placed copper powder slurry. Figure 3.3(b) shows cross-sectional view of alloyed sample. Figure 3.4 illustrates the photographs of laser surface alloyed samples. On the surfaces of the samples, a single laser track is shown as a rectangle mark.

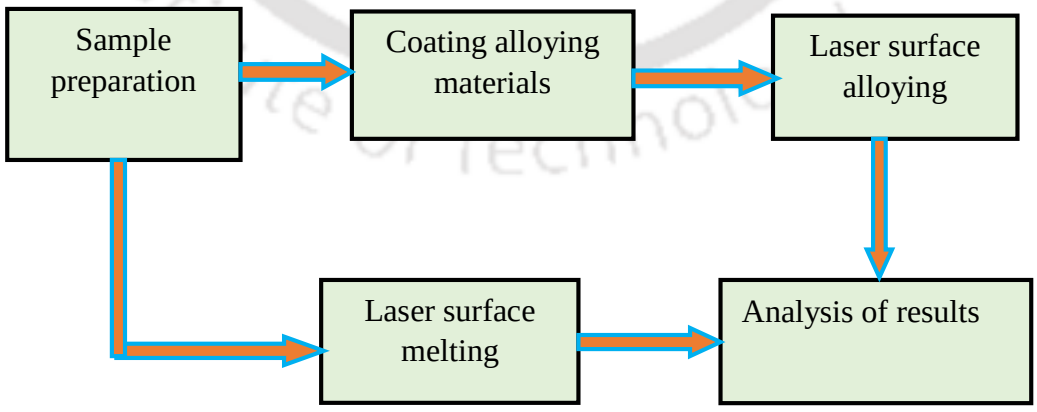

Figure 3.1 A flowchart of laser surface modification

Laser surface melting was conducted on Al-12Si-4Cu-1.2Mn cast aluminum alloy. The cast samples were prepared in a graphite crucible of 3 kg capacity using a melting/vacuum holding furnace. Aluminum plate thickness was 5mm. For the comparison, a cast alloy and heat treated samples were used. Heat treatment was conducted in a furnace at 510 ^{o}C for 5 hours then it was cooled in the furnace at 162 ^{o}C for 6 hours.

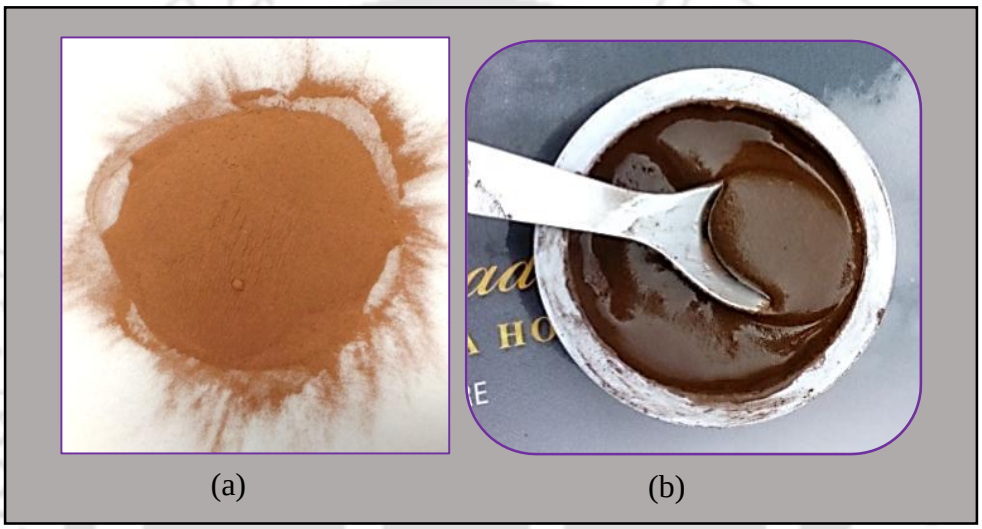

Figure 3.2 Preparation of alloying material: (a) Cu powder and (b) Cu powder slurry

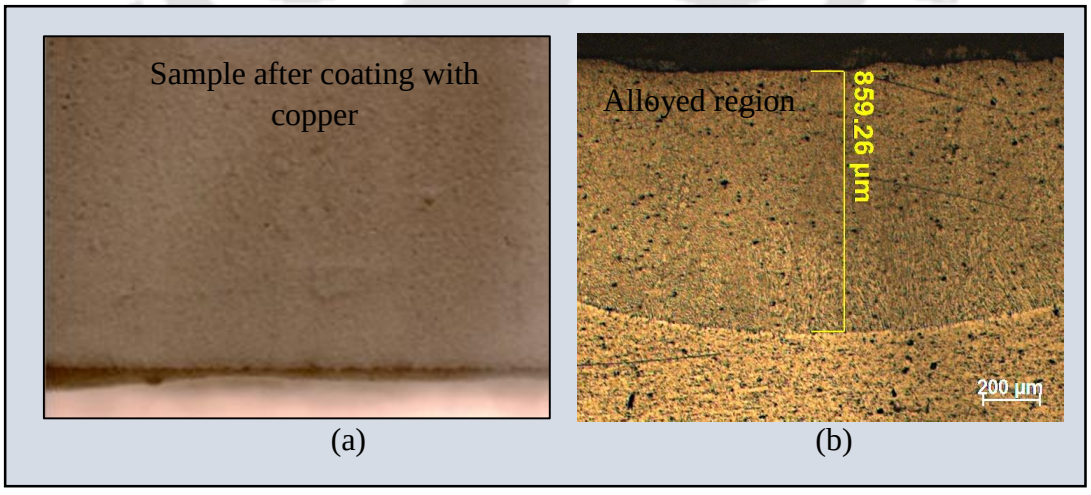

Figure 3.3 Photographs of laser surface alloying processes: (a) sample after coating and (b) cross-section of sample after laser surface alloying

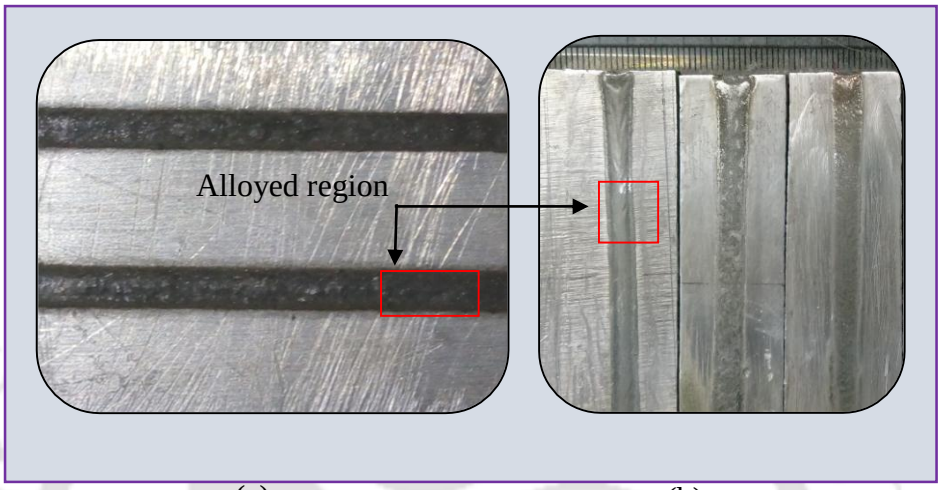

Figure 3.4 Photographs of laser surface alloyed samples

3.3 Laser Surface Alloying

Laser surface alloying was made using a continuous mode of CO_2 laser machine (Model: Orion 3015, Make: LVD, Belgium). The laser head moves in two directions: along Z-vertical and Y-horizontal. The movable table where the workpiece was fixed, moves in the x-horizontal direction. Laser nozzle and workpiece do not make any contact with each other. The CO_2 laser cutting machine is shown in Figure 3.5.

The following widely used formula for calculating the laser beam diameter $d = 2R$ was employed (Sun,1998):

$$R = w_0 \left[1 + \left(\frac{M^2 \lambda H}{\pi w_0^2} \right)^2 \right]^{1/2} \tag{3.1}$$

where $w_0 = 0.05$ mm is laser beam waist, which is the minimum beam diameter at the focal point of the lens, λ=10.6 µm is CO_2 laser beam wavelength; H is the standoff distance,

M^2 is the beam quality factor. Here, M^2 was taken as equal to 1 considering the beam as perfect Gaussian, although in practice it is always greater than 1. For example, Kant et al. (2015) took it as 1.4.

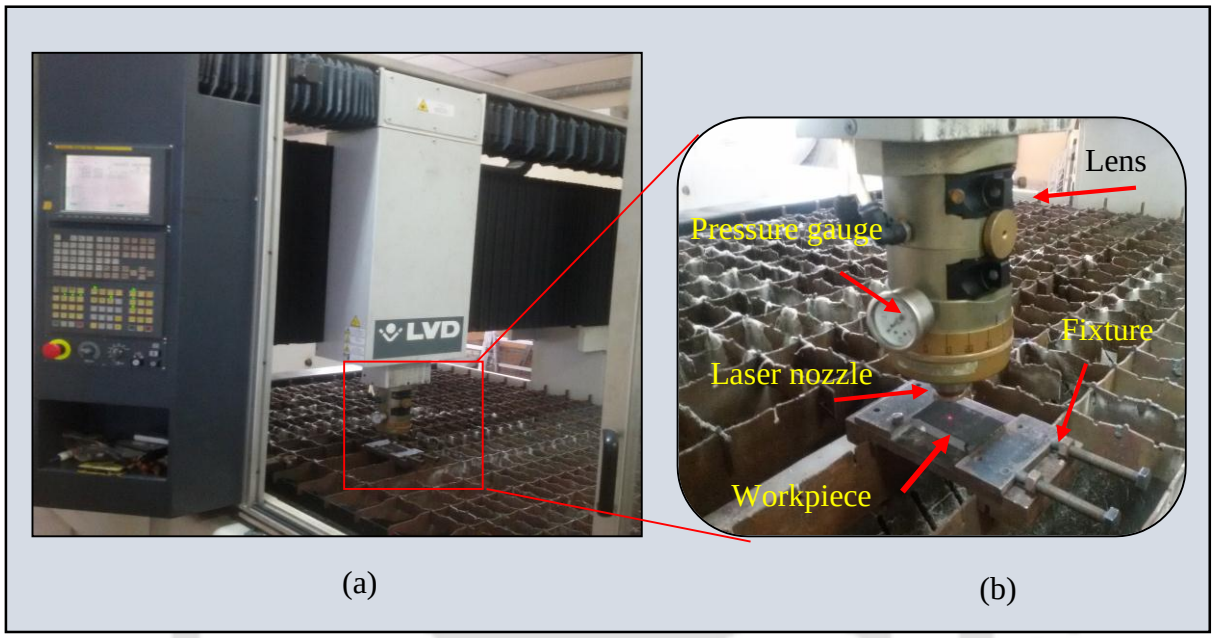

Figure 3.5 Experiment setup of CO_2 laser cutting machine

3.4 Studying Microstructure

For metallographic study, the samples are cut into small sizes and are mounted on molding machine with the help of phenolic polymer. Mounted samples are easy for handling and fixing into the automatic polishing machine, which can polish six samples at a time. Different grades of grit sheets were used starting from rough to fine grades like 120, 240, 360, 600, 800, 1200, 1500 and finally fine grade 2000 grit size was used systematically until a smooth surface was achieved. Then the final mirror polishing was done using a wool cloth by applying chemical Silvo. After drying the samples, etching was done using standard Keller's reagent comprising 2 ml HF, 3 ml HCl, 5ml HNO_3 and 190 ml H_2O (distilled water). Etching for 6–8 seconds at room temperature. The process was done by brushing with the cotton wool after immersing the cotton in the reagent. Dipping the sample in the reagent did not give good result. After etching, the optical microscopy was used to

study the size of the grain and the microstructure of laser surface alloyed region. Figure 3.6 illustrates the procedures used for studying microstructure after laser surface alloying. Figures 3.7 (a-c) show the photographs of precision cutting machine, sample mounting machine and automatic polishing machine.

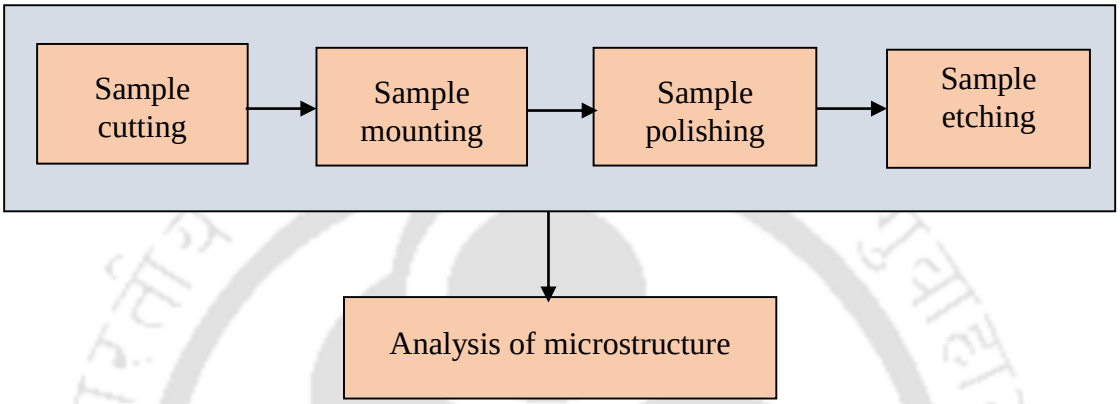

Figure 3.6 A flowchart for studying microstructure

Figure 3.7 Photographs of machines: (a) precision cutting, (b) sample molding and (c) automatic polishing

3.5 Chemical Composition and Phase Analysis

The chemical composition of aluminum base material was tested using electron dispersive X-ray spectroscopy (EDS) machine, which is available in the Central Instruments Facility

(CIF) of Indian Institute of Technology Guwahati. In addition to this, high resolution and high magnification microscopes were used to study surface morphology. Figure 3.8(a) shows Field Emission Scanning Electron Microscopy (FESEM) machine with EDS attachment. The analysis of laser surface alloyed and surface melted samples and X-ray diffraction study were carried out on solid samples using PANalyticalX'pert powder machine. The X-ray diffraction (XRD) was conducted after polishing the solid samples. The XRD was used with filtered Cu-Kα1 radiation (λ = 0.154056 Å) at 40 kV and 20 mA. Figure 3.8(b) shows a photograph of XRD machine.

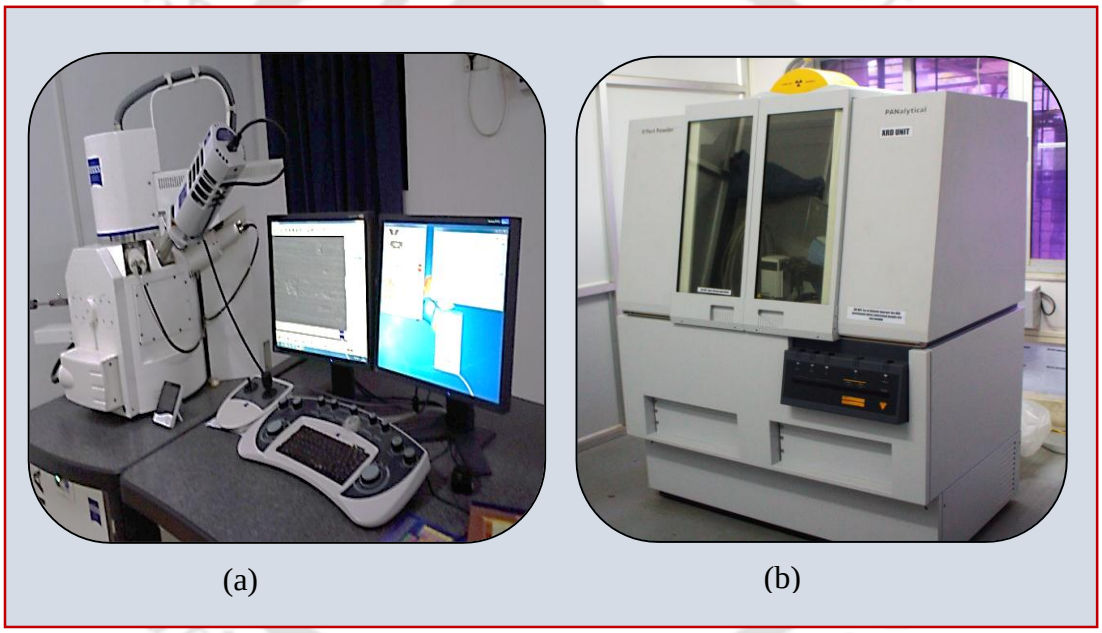

(a) (b)

Figure 3.8 Photographs of machines used for characterization: (a) field emission scanning electron microscopy and (b) X-ray diffraction

3.6 Study of Surface Roughness

The quality of the surface made using conventional and non-conventional machining is important because a smooth surface reduces the chances of surface damage caused by wear and corrosion. Likewise, quality of a part made by laser surface alloying and surface melting can affect the performance of the surface for wear and corrosion protection. In this

research, after laser surface alloying, centerline average surface roughness was measured using non-contact optical profilometer. It also helps to measure corrosion surface damages. Figure 3.9 shows optical surface profilometer used in the experiment to measure different parameters such as corrosion surface damages, wear scar profile and scratch grooves.

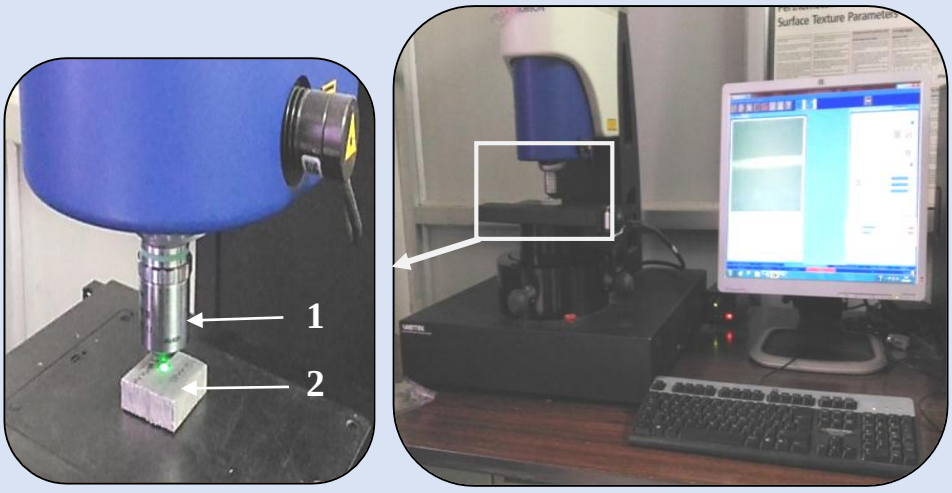

1 light source 2 sample workpiece

Figure 3.9 Photographs of non-contact optical profilometer

3.7 Hardness and Tensile Testing

The important mechanical properties of metallic material are hardness and tensile strength. In this research, both surface hardness and tensile strength analysis are carried out after laser surface melting and alloying.

3.7.1 Surface Hardness Testing

Surface hardness test is conducted using Vickers hardness testing machine, which has 0.1, 0.2, 0.3 and 0.5 kg of loading capacity. A diamond indenter tip is pressed on the surface of the sample to make indentation mark. The hardness of the sample was measured from the dimension of indenter mark observed on the surface. Figure 3.10 illustrates a schematic diagram of Vickers hardness testing. The value of Vickers hardness is displayed on the machine after an operator measures the distance of two diagonals 'd_1' and 'd_2'. The applied

load is the direct influential parameter of hardness as well as average dimension values of the diagonals measured. The smaller the indention mark formed on the surface confirms the harder the material when compared to bigger indentation mark under the same load and surface condition. Figure 3.11 shows Vickers hardness testing machine. Vickers hardness is evaluated using the following expressions:

$$HV = \frac{2F \sin\frac{136^{o}}{2}}{d^{2}}, \tag{3.2}$$

or,

$$HV = 1.854\frac{F}{d^{2}} \tag{3.3}$$

where F is load and d arithmetic mean of two diagonals d_1 and d_2.

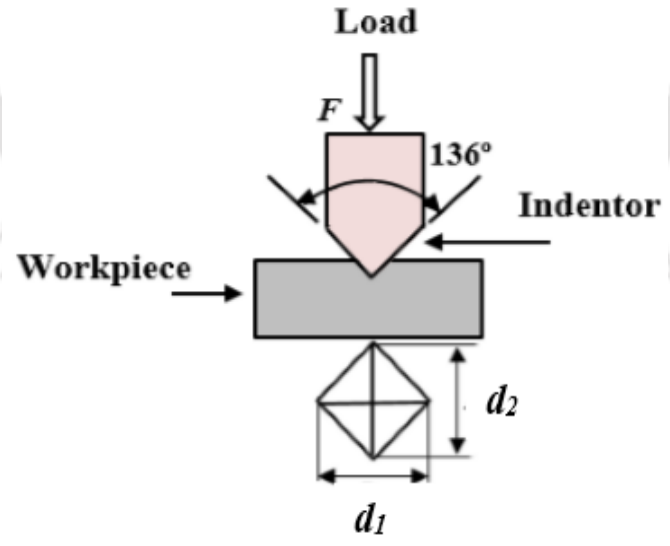

Figure 3.10 A schematic of Vickers hardness testing machine

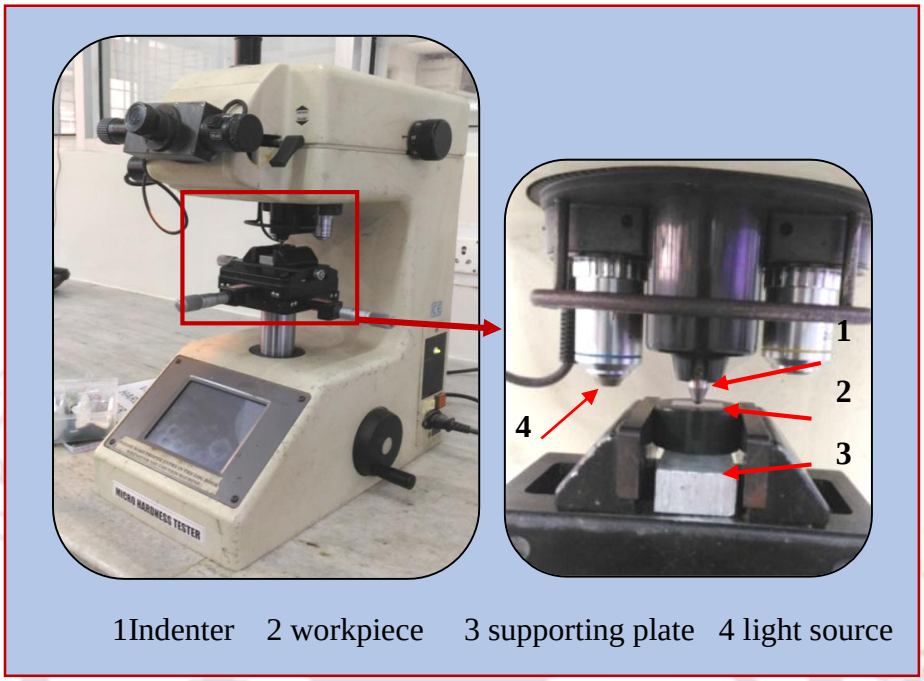

Figure 3.11 Vickers hardness-testing machine for measuring hardness

3.7.2 Tensile Testing

Tensile test was conducted using universal hydraulic tensile testing machine (model 881J4051 make INSTRON) with a capacity of 100 kN. Extensometer of gauge length 50 mm is used to measure elongation and strain. The specimen was prepared according to ASTM standard. The gauge length, width and radius of fillet were 50 mm, 30 mm and12.5 mm, respectively, and overall length was 260 mm. Laser surface alloyed tensile samples were prepared by multiple remelting laser tracks without overlapping. Tensile specimens were prepared by cutting laser surface alloyed region using a wire electrical discharge machine. For laser surface melting, the tensile sample thickness was 5 mm and gauge length was 25 mm. The width of the gauge length portion was 6 mm and the total length of the sample was 100 mm. Figure 3.12 shows tensile samples used after cutting using wire

EDM machine. Finally, laser surface melting was conducted. The complete setup of the tensile testing machine is shown in Figure 3.13.

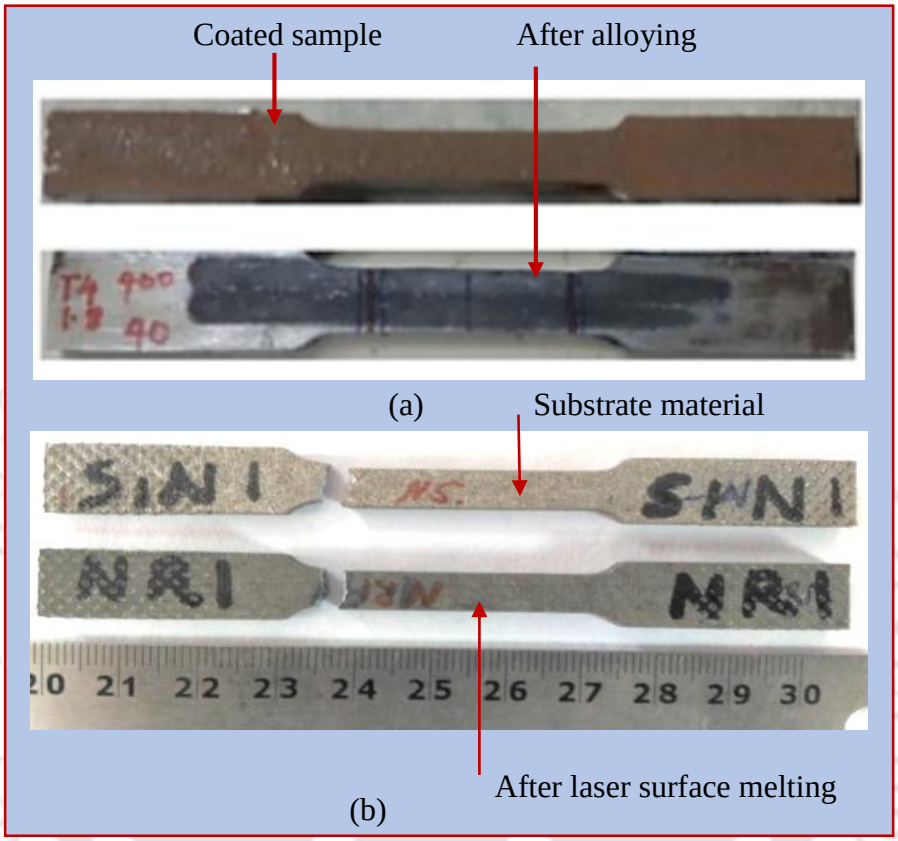

Figure 3.12 Photograph of tensile specimens: (a) laser surface alloyed (b) laser surface melted

3.8 Wear and Surface Scratch Testing

Wear is a material removed from the surface of solid material by physical separation due to plastic deformation and micro-fracture when the surfaces are in contact with each other. The parameters that highly affect the wear of parts include operating parameters, types of material and surface condition. The operating parameters are load, speed and temperature. The wire-cut EDM machine setup is shown in Figure 3.14 (a). The square pin samples were cut from laser surface alloyed region using wire EDM machine as shown in Figure 3.14

(b). The top circle mark on the top of the pin sample shown in Figure 3.14 (b) represents the laser surface alloyed region

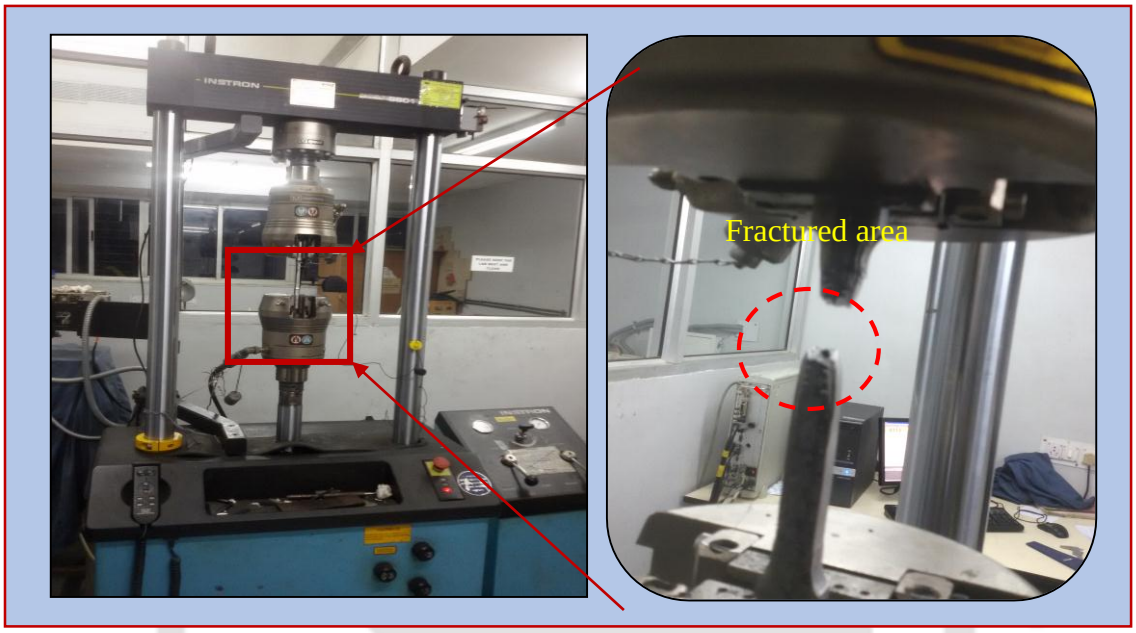

Figure 3.13 Tensile testing machine with sample at elongation and final breakage

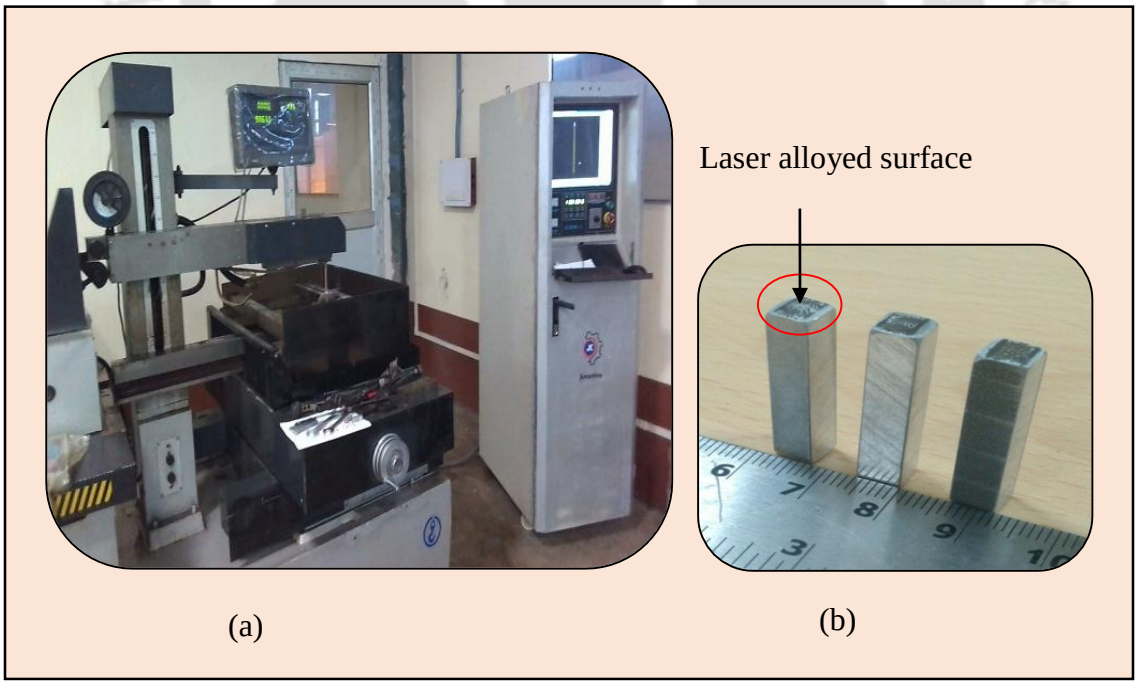

Figure 3.14 (a) Photograph of wire EDM machine and (b) square pin specimens

3.8.1 Studying Friction and Wear

Friction and wear study was conducted using a pin-on-disc machine (DUCOM TR 201 make). The sliding occurred between the stationary pin specimen and a rotating disc. The normal load, rotational speed and wear track diameters were fixed according to the need. The frictional force and wear were measured using sensors. The machine loading capacity was up to 100 N and the speed from 100–1000 rpm. The machine is applicable for sliding wear test in a dry condition. The minimum and maximum wear track diameters were 10 and 80 mm, respectively. The specimen samples were prepared in a square geometry and placed inside the specimen holder.

The linear variable differential transducer (LVDT) measures the wear between pin specimen and hardened disc. The friction between pin and disc is also measured by a load cell. A beam type load cell has a capacity of 5 kg, which measures frictional force up to 100 N. The load cell was fixed on sliding plate and moves with it for fixing the wear track diameter. Figure 3.15(a) shows a schematic of pin specimen on disc material. Figure 3.16(c) shows a photograph of wear testing machine.

3.8.2 Studying Surface Scratch

The scratch test was conducted by scratch tester machine (TR-101). This machine works for the load range from 20–200 N and accuracy of $1\pm1\%$. A compound transducer is fixed on the machine to measure both normal load and traction force. The indenter of the machine is a standard Rockwell 'C' type and the tip of the indenter is a hard diamond with nose radius (conical angle is 120^{o} and hemispherical tip radius of 200 microns). Figure 3.16 shows photograph of the scratch testing machine.

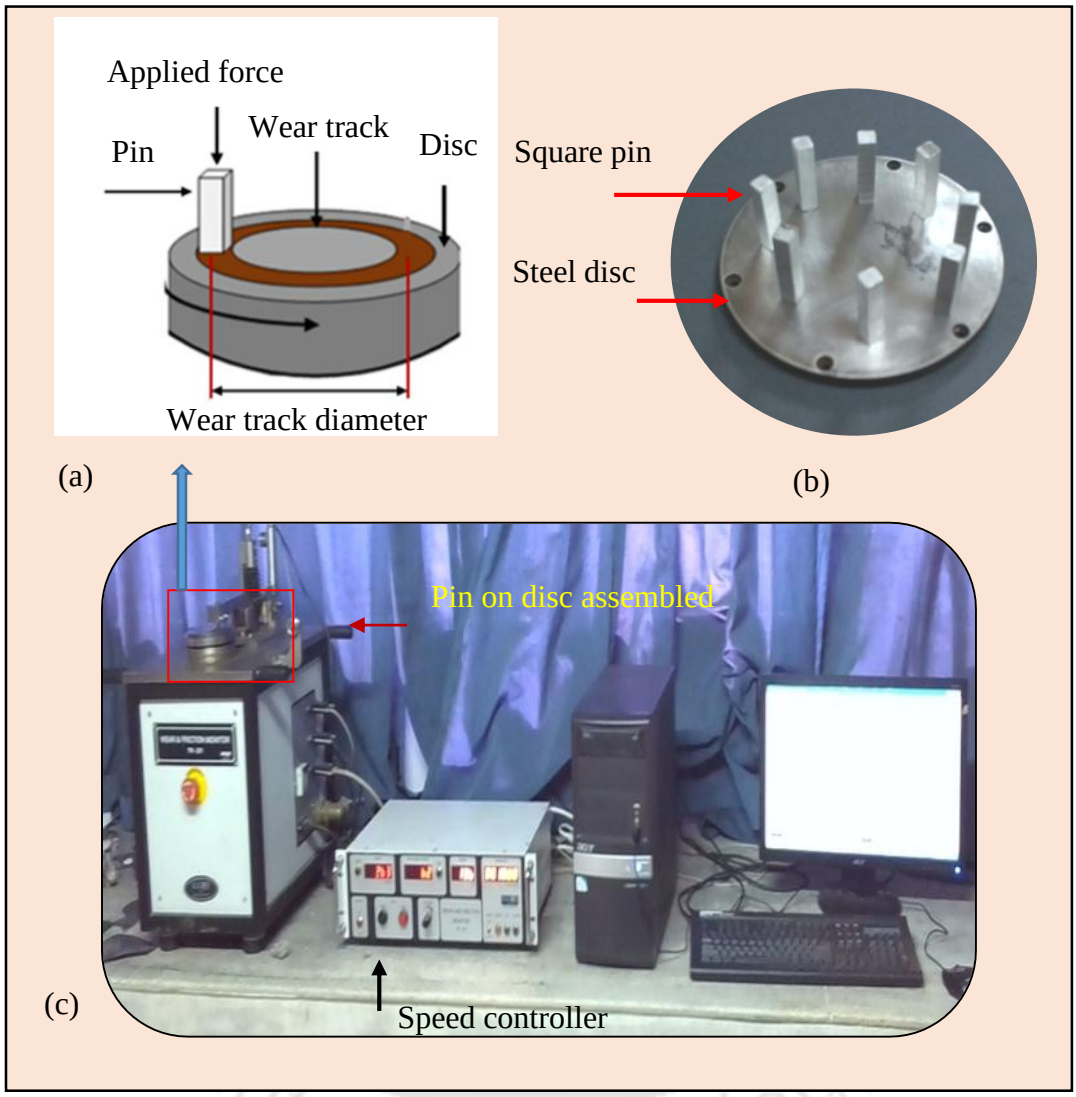

Figure 3.15 Setup photo for wear study: (a) schematic diagram, (b) photographs of disc and square pin samples and (c) wear testing machine

.

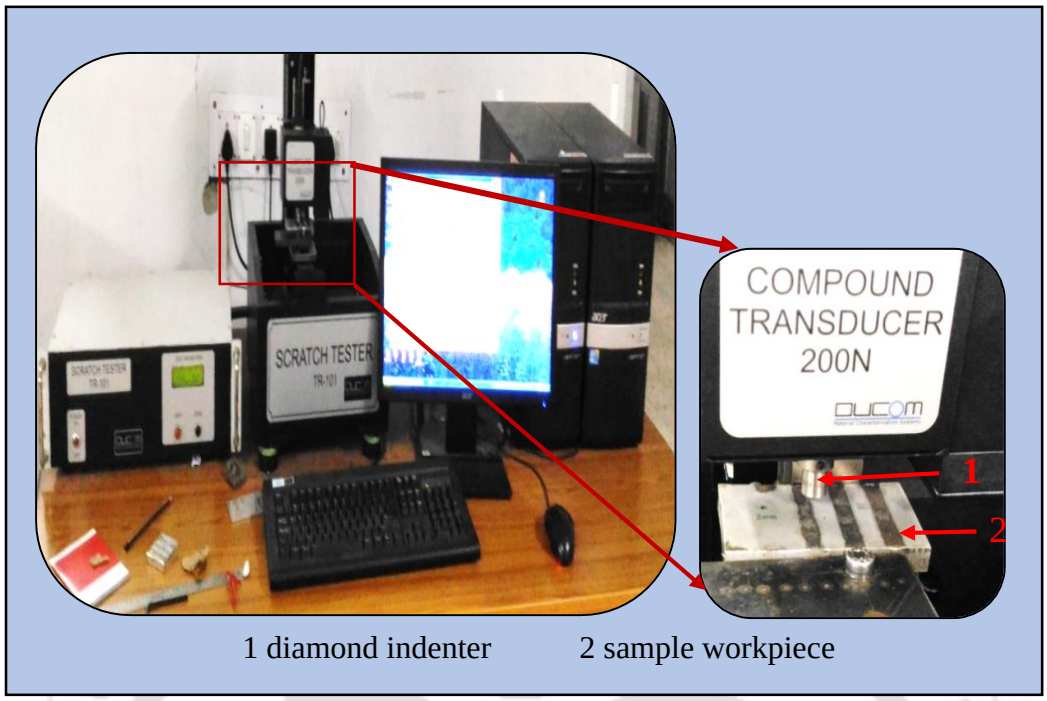

Figure 3.16 Surface scratch testing machine

3.9 Corrosion Testing

The study of corrosion is conducted for laser surface alloyed samples. Corrosion is the electrochemical effect on the metallic surface from an external environment. Surface corrosion of metal parts is one of the biggest challenges that causes failure of important engineering parts. After laser surface alloying of aluminum substrate with Mg, Mn, Ti, Zn and combination of Cu, Mg and Mn in a ratio of 2:1:1, corrosion immersion test was studied. First, samples were cut from laser surface alloyed portion in the form of square dimensions: 10 mm × 10 mm and 5 mm. Then the samples were mounted with phenol resin that resisted corrosion caused due to salt and acidic solutions. The portion of the surface to be tested for corrosion was exposed to corrosive media. The pH of the solution was measured before corrosion test by a pH meter (Eutech Singapore, make), model: pH 2700, electrode: 93X218819. The calibration of pH was conducted using the standard solution of precisely known pH that was purchased from Oakton (USA). Accordingly, acidic corrosive media had 0.074 pH value and salt corrosive media had 9.08 pH value. After corrosion test, samples were cleaned using acetone and were dried. The weight of the samples was measured using weight measuring machine with 0.1 mg accuracy. The weight loss due to

corrosion damage was measured before and after corrosion test. The corrosion pit depth and corrosion pit width were also measured by non-contact optical profilometer. The surface damage was analyzed by FESEM machine. Figures 3.17 (a–d) show the setup used for corrosion testing.

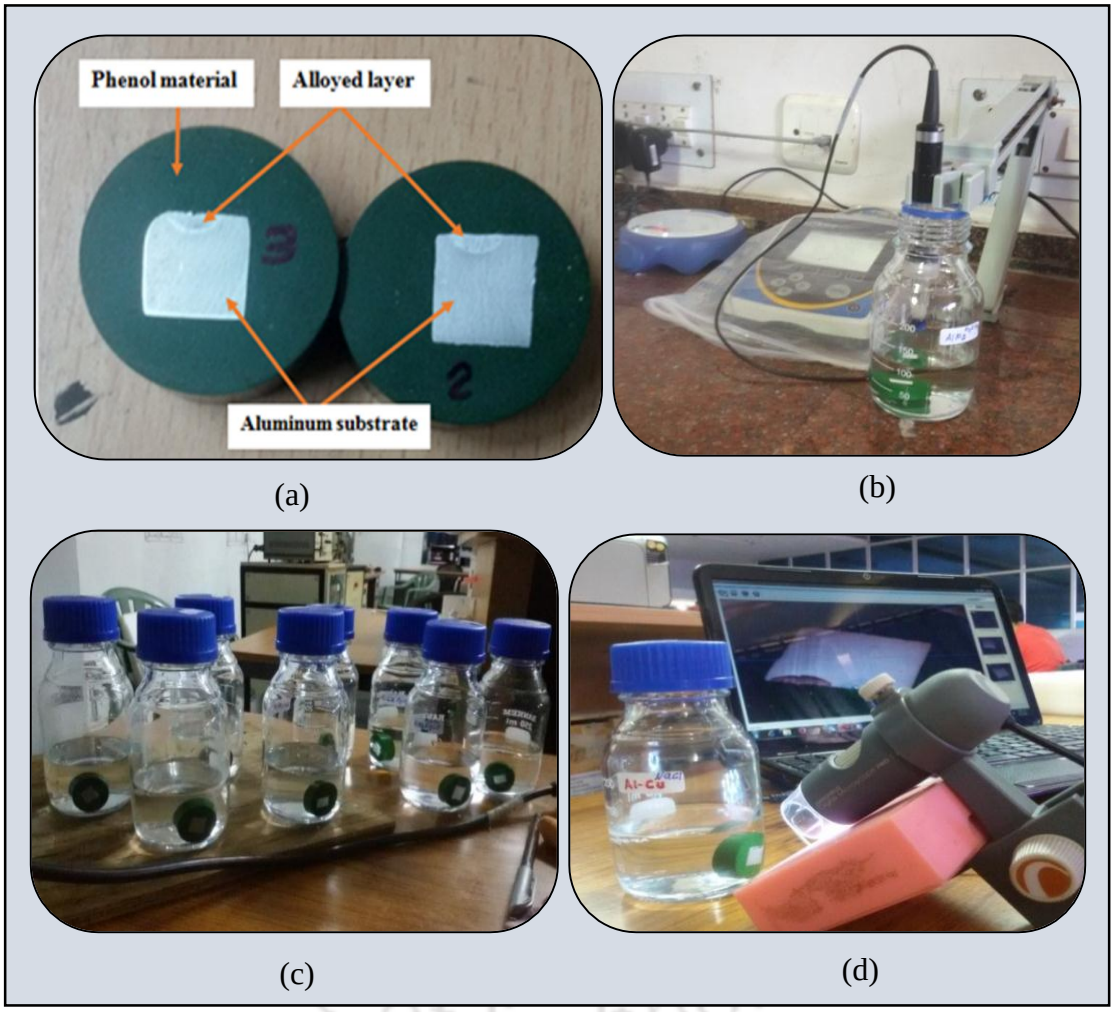

Figure 3.17 Corrosion experiment setup: (a) mounted samples, (b) pH measuring meter (c) samples in closed glass and (d) digital camera connected to the computer for capturing images

3.10 Conclusion

In this chapter, details of experimentations used in the research of aluminum laser surface alloying and surface melting using CO_2 laser are presented. For every experiment, procedures are discussed with a schematic diagram. Photographs of the machines have been used to present the experiment. The substrate material and alloying materials used for each experiment are also discussed accordingly. All the machines are available at Indian Institute of Technology Guwahati. Workpiece fixture used for holding samples was prepared in workshop. The setup for corrosion test was prepared in the tribology laboratory. Other instruments are also available in Central Instruments Facility (CIF), IIT Guwahati.

Indian Institute of Technology Guwahati

Chapter 4

Pilot Experiments on Surface Alloying of Copper in Aluminum Using CO_2 Laser

4.1 Introduction

Failure of engineering parts are caused by mechanical loading and chemical interaction at their surface. Most applications in the real world require components, which have a good hardness, wear resistance and corrosion resistance. However, it is not easy to get metallic alloys with such properties. Investigations have been carried out to improve the properties of metals by laser surface modification through melting and alloying. Laser surface melting has been implemented to improve surface properties of metallic parts as reported by Pagano *et al*. (2016) and Read *et al*. (2015). Metallic surfaces have also been by laser surface cladding (Chong *et al*., 2001; Iwatan *et al*., 2005).

Laser surface alloying is a cost-effective technique to improve the surface properties of materials using a laser beam heat source (Wendt *et al*., 2003; Hecht, 2011; Nath *et al*., 2012). Laser surface alloying utilizes a high power density of laser beam to melt the metal alloying elements and the surface of the substrate material (Dahotre, 1998; Zhao *et al*., 2012). Melting takes place in a very short period of time while the bulk material remains cold and acts as a heat sink for self-quenching with fast solidification. The intimate contact between the laser melted region and the solid substrate causes a very fast heat extraction during solidification resulting in very high cooling rates of 10^5–10^8 K/s. Soon the solidification begins from the liquid-solid interface to the entire alloyed region. The benefits of rapid solidification by laser power for surface modification are as follows: fine grain structure due to fast solidification (Kannatey, 2009), reduced micro-segregation and extended solubility of alloying elements. Adding alloying elements into the melted pool makes them inter-diffuse into the substrate material. The high cooling rates result in the

formation of different microstructures leading to improved properties of the alloyed region (Dubourg *et al*., 2002; Rajamure *et al*., 2014). The structure of alloyed zone depends on properties of the alloying material and laser parameters like laser power and scan speed. The alloyed region changes chemical composition and microstructure to give it certain desired properties (Man *et al*., 2001; Mabhali *et al*., 2012).

This chapter presents a pilot study of laser surface alloying of commercially pure aluminum with 95 wt. % copper powder mixed with 5wt. % aluminum powder. After laser surface alloying microstructure and microhardness of alloyed samples were investigated. The use of copper as a binary alloying element in aluminum is crucial due to many advantages. It increases ductility, thermal conductivity, hardness and strength. It is a primary alloying element of 2xxx series alloy used in aerospace wing structure material (Dursun and Soutis, 2014, Eswara *et al*., 2014). Some worth noting studies yet conducted on laser surface alloying on pure aluminum as a substrate material are as follows: (1) iron and nickel using CO_2 laser (Salim *et al*., 2017), (2) Al_2O_3 ceramic alloying (Huang et al., 2008), (3) WC+Co+NiCr alloying (Nath *et al*., 2014) alloying, (4) chromium alloying (Almeida *et al*., 1995), (5) nickel alloying (Das,1994), (6) Al-Nb alloying using CO_2 laser (Almeida *et al*., 2001), (7) tungsten coating using 3 kW fiber optics delivery diode pumped Ytterbium fiber laser for enhanced corrosion resistance (Rajamure *et al*., 2015) and (8) molybdenum alloying (Vora *et al*., 2013). Some work has been conducted on copper alloying in pure aluminum substrate material (Dubourg *et al*., 2002). Dubourg *et al*. (2002) alloyed the copper in an inert atmosphere with preheating. Owing to the advantages of alloying copper with aluminum, a lot of work needs to be done in this area. This thesis explores the copper alloying in aluminum in an ambient environment. Moreover, remelting has been also employed to enhance the mechanical properties. Industrial importance of the work is that in some cases, particularly for large structure required hard surface, surface alloying is preferable to whole structure of AlCu alloy.

The use of Fevicol as chemical binder to pre-place copper powder before laser surface alloying was decided to check out the viability of the process. After conducting the pilot study, there was an enhancement in microhardness, but the quality of microstructure is not good and some porosity was founded. Fevicol binder gets stuck in the melting.

Subsequently, this problem was resolved by using Fevigum binder. Therefore, the results included in this chapter is not much attractive, but pave the way for the subsequent work.

4.2 Materials and Method

In the present work, commercially pure aluminum plate size of 110 mm × 50 mm × 6 mm was prepared. Copper powder of 10 μm particle size and aluminum powder of 10 μm particle size were mixed with Fevicol binder (make Hira Industry, India) in three different methods. First, 95 wt.% copper powder and 5 wt.% aluminum powder were mixed together. Afterwards, three methods were used for pre-placing alloying powders. The three methods are as follows:

i. Stirring metal powders with Fevicol and then painting on aluminum substrate up to 0.5 mm coating thickness for samples designated with Sample numbers 12, 13, 14 and 15

ii. First painting Fevicol on aluminum substrate, then applying alloying powders uniformly and finally compacting it to achieve a coating thickness of 1 mm for Samples 4, 5, 6, and 9

iii. First painting Fevicol on the aluminum substrate, then applying alloying powders and blowing out excess powders to achieve a coating thickness of 0.5 mm for Samples 1, 2, 3, 7, 8, 10 and 11.

After the samples were dried at room temperature for 2-3 days, laser alloying was conducted. A continuous wave CO_2 laser was used at different laser parameters as shown in Table 4.1. The selection of laser beam parameters was done after conducting many experiments. It was observed that laser power beyond 2 kW damaged the surface. The minimum value below 1.6 kW did not provide good melting for alloying. During alloying, 50 % laser track overlapping was provided between adjacent tracks. After air cooling, for a while, re-melting was carried out in an orthogonal direction to laser melted direction for same samples. After laser surface alloying, microstructure was tested using scanning electron microscopy (SEM) and surface roughness was measured using a non-contact optical profilometer. The hardness of laser alloyed region was measured using Vickers hardness testing machine.

Table 4.1 Laser parameters used for alloying of copper in aluminum

Sample No.	Process parameters for alloying				Process parameters for re-melting			Re-melting
	P (kW)	*H* (mm)	*v* (mm/min)	*d* (mm)	*P* (kW)	*v* (mm/min)	*d* (mm)	
1	1.7	30	600	4.05	1.6	600	4.05	Yes
2	1.7	30	500	4.05	1.6	600	4.05	
3	1.7	30	500	4.05	1.6	800	5.39	
4	1.7	40	500	5.39	1.6	800	5.39	
5	1.7	30	400	4.05	-	-	-	No
6	1.6	30	500	4.05	1.6	800	5.39	Yes
7	2.0	40	400	5.39	-	-	-	No
8	1.6	30	400	4.05	1.7	500	4.05	Yes
9	1.8	30	400	4.05	1.6	800	5.39	
10	1.7	30	600	4.05	1.7	500	4.05	
11	1.8	30	500	4.05	1.5	400	5.39	
12	1.7	40	600	5.39	-	-	-	No
13	1.8	40	600	5.39	1.5	800	5.39	Yes
14	1.6	30	600	4.05	1.6	800	5.39	
15	1.7	30	400	4.05	1.7	500	4.05	

Note: *P* is laser power, *H* is standoff distance, *v* is laser scan speed and *d* is laser beam diameter

4.3 Results and Discussion

In this section, results of the experiment are discussed. XRD phase analysis, surface roughness, microstructure of laser alloyed region and microhardness are presented. Problem of porosity during laser surface alloying is discussed.

4.3.1 Crystal Size and Lattice Strain

The crystal size and lattice strain developed due to thermal effect were examined for Sample 4 using a X-ray diffraction analysis. Figure 4.1 shows the pattern of XRD result. Thermal strain developed in the alloyed region due to laser beam melting was calculated

based on the formula developed by Williamson and Hall (1953). The strain in the sample was measured as 0.002 as shown in the inset of Figure 4.1. The average crystallite size was 152.06 nm. The crystal has cubic structure as justified by the International Centre for Diffraction Data (ICDD) with card number 02-1254, which confirmed that formation of Al_4Cu_9 compound phase. The formation of this compound improved mechanical property of the alloy. Strain was calculated using

$$\beta\cos\theta = \frac{K\lambda}{D} + 4\eta\sin\theta \tag{4.1}$$

where β is the full width at half maximum, K is a constant, λ is the X-ray wave length of CuK_α radiation (λ = 1.5418 *Å*), D is the average crystal size and η is the lattice strain.

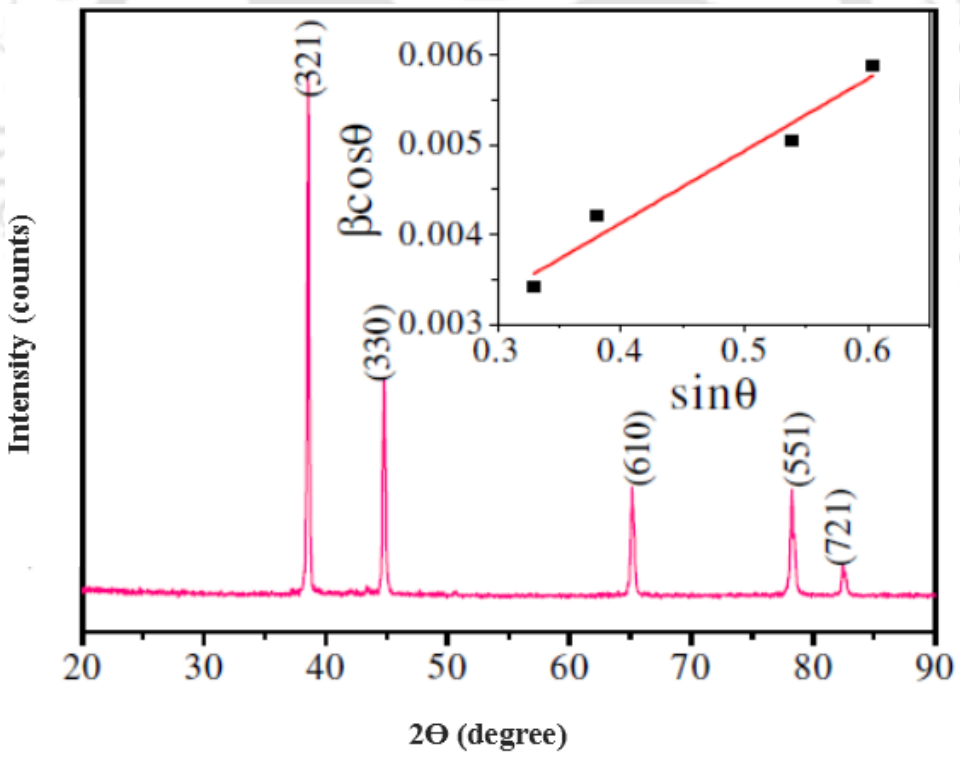

Figure 4.1 X-ray diffraction pattern of Al_4Cu_9

4.3.2 Surface Roughness

The surface roughness of metallic part plays an important role in determining how the surface interacts with its environment. Metal parts which have more roughness on their surfaces usually wear more quickly than those parts with a smooth surface. On the other hand, when a rough surface is in contact motion with other bodies, higher ploughing friction resistance is created. As a result more material will be removed due to wearing. The performance of metallic parts to resist wear when in contact with other surfaces, highly depends on the condition of their surface finish. The irregularities on the surface act as initiation sites for wear and corrosion to be formed. On the other hand, when a smooth surface is in contact with other surfaces, less ploughing frictional resistance is created due to which less material is removed due to wear. In the present work, the surfaces of the laser surface alloyed samples were tested without polishing their surface. Figure 4.2(a) shows Sample 2 where the area of non-uniform alloying resulted in more voids on the surface. The center line average surface roughness of Sample 2 was 2.5 µm. This indicates alloying was not uniformly done. Figure_4.2(b) shows Sample 9 where uniform laser alloying was achieved. The center line average surface roughness value of 1.9 µm was measured. Therefore, a good surface alloying was achieved with a good uniformity. This will improve mechanical properties of the alloy.

4.3.3 Microhardness Analysis

Micro-hardness test was conducted on thickness side of the samples for laser surface alloyed samples. Vickers hardness test was conducted using a 0.5 kg load. Figure 4.3 shows microhardness results of laser surface alloyed samples at different laser processing parameters. The maximum hardness achieved was 156 $HV_{0.5}$ for Sample 4 which was processed by 1.7 kW laser power and 5.39 mm laser beam diameter. Laser beam re-melting was done in an orthogonal direction to the alloyed track direction at 1.6 kW laser power and 800 mm/min laser scan speed. The hardness of aluminum substrate was on an average 60 $HV_{0.5}$. After laser alloying, all the samples show improved microhardness values. The hardness was the maximum at the top and minimum at the bottom. Dubourg *et al*. (2002)

reported that hardness decreased when alloy depth was more during Al-Cu laser surface alloying. As the concentration of copper decreases, the hardness also decreases.

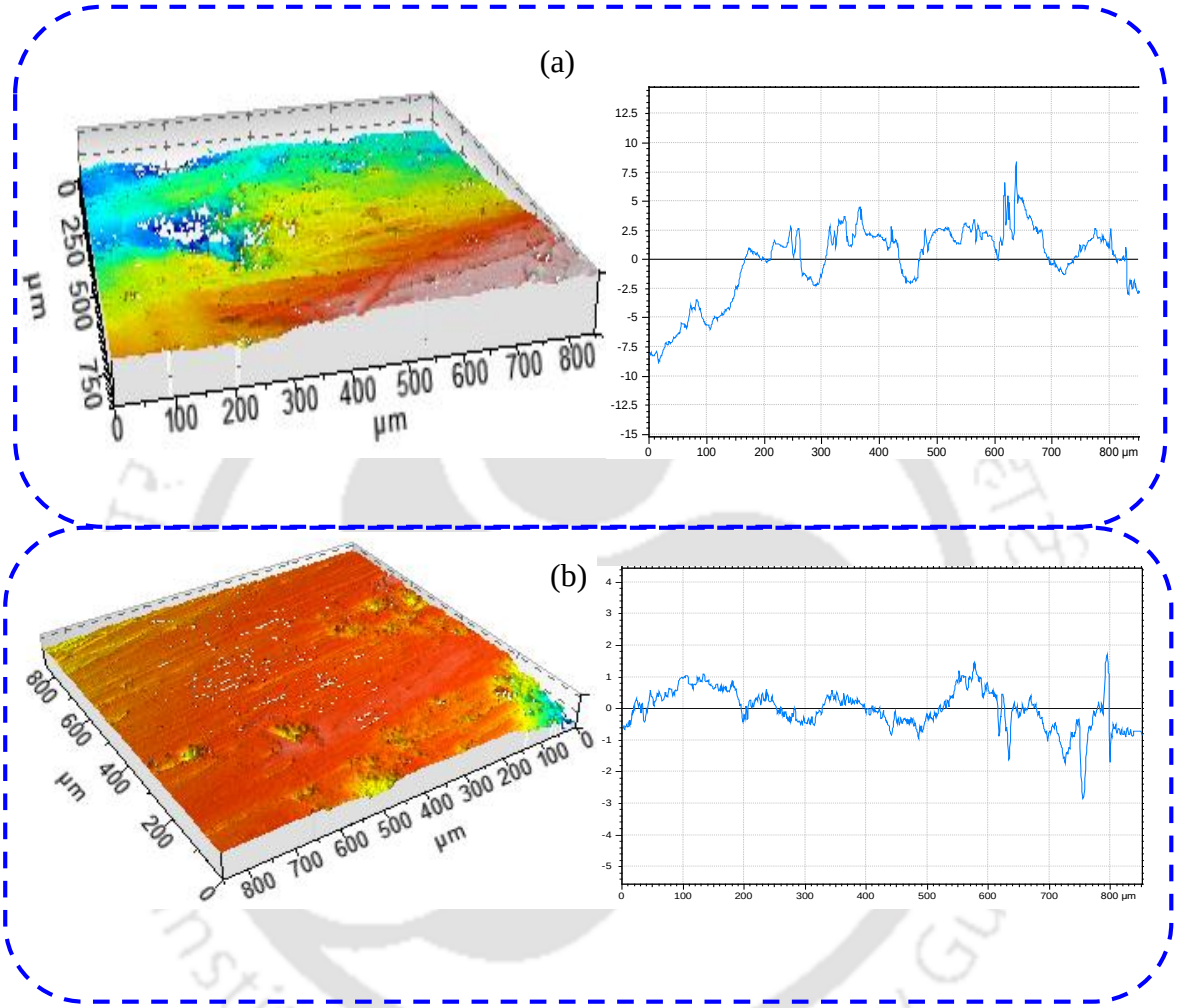

Figure 4.2 3D surface roughness and their 2D graph for laser alloyed samples: (a) non-uniform alloyed surface and (b) uniformly alloyed surface

It is stated that the variation of microhardness values for different samples was due to laser power, laser scan speed and laser beam diameter remelting of laser tracks. The effect of pre-placing alloying material was also observed. Those samples, processed by first painting Fevicol on aluminum substrate, then applying uniformly alloying powders and then compacting got more of microhardness. Samples 4 and 9, which first coated with 1 mm

alloying element, got more hardness when compared to other samples. Re-melting had smoothened the surface and reduced porosity. Thus remelting had improved microhardness. The effect of re-melting was reported by Pinto *et al*. (2000), during microstructural and hardness investigation of an aluminum–copper using laser alloying. Their results show re-melting had improved micro-hardness after laser surface alloying. In this work, when laser power was more, more melting created on the surface which further pushed the alloying material deep into the substrate portion because of which the microhardness got reduced.

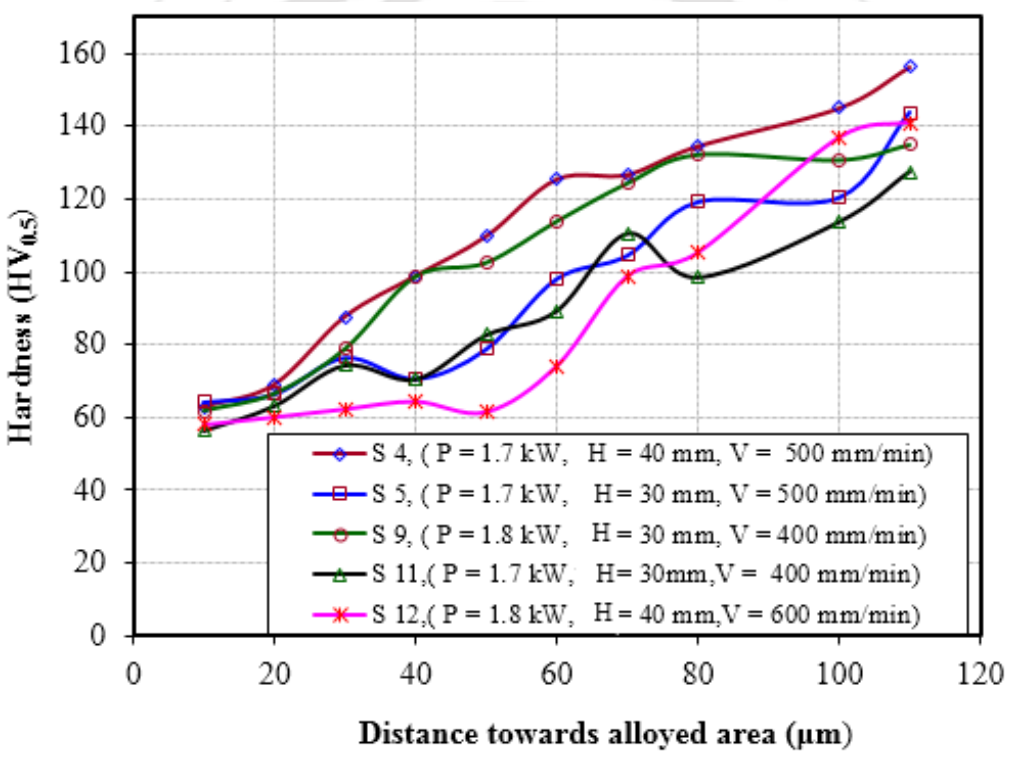

Figure 4.3 Vickers hardness result of laser surface alloyed samples at different laser processing parametrs

4.3.4 Microstructure and Surface Morphology

Figure 4.4 (a) shows an optical image of laser alloyed sample 4 and Figure 4.4(b) shows sample 9. The morphology of alloyed region was uniform without defects. During laser alloying, copper powder was bonded with aluminum forming an Al_4Cu_9 intermetallic

compound phase. Uniform alloying was created without porosity and defect. Dubourg *et al*. (2002) reported mechanical characterization of laser surface alloyed aluminium with copper after laser alloying. They observed that microstructure was initially cellular at the bottom of the molten pool. After solidification, homogeneous structure was created in the alloyed.

Figure 4.5(a) shows SEM image of Sample 9 showing the uniformity of copper growth into aluminum primary grains and dark eutectic, well distributed in the alloy. The formation of Al_4Cu_9 inter-metallic compound phase was revealed. Figure 4.5(b) shows the grain boundary formed which have a micro-crack due to more copper concentration at a point. The micro-crack was formed at grain boundary. This may be due to high cooling rate causing insufficient precipitation on grain boundaries. The micro-crack may be susceptible to stress corrosion cracking (SCC) as reported by Van Otterloo *et al*. (1995).

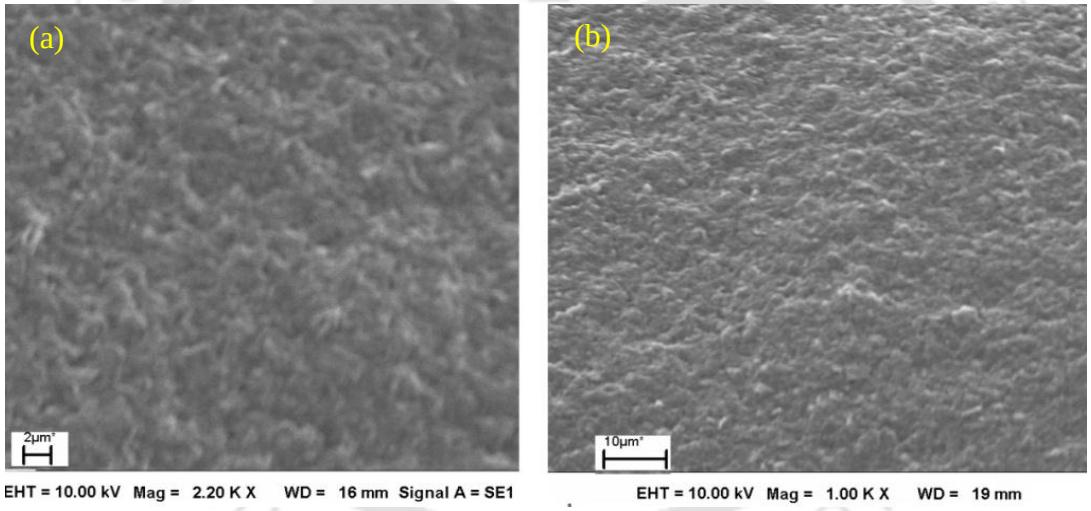

Figure 4.4 SEM images morphology of (a) Sample 4 and (b) Sample 9

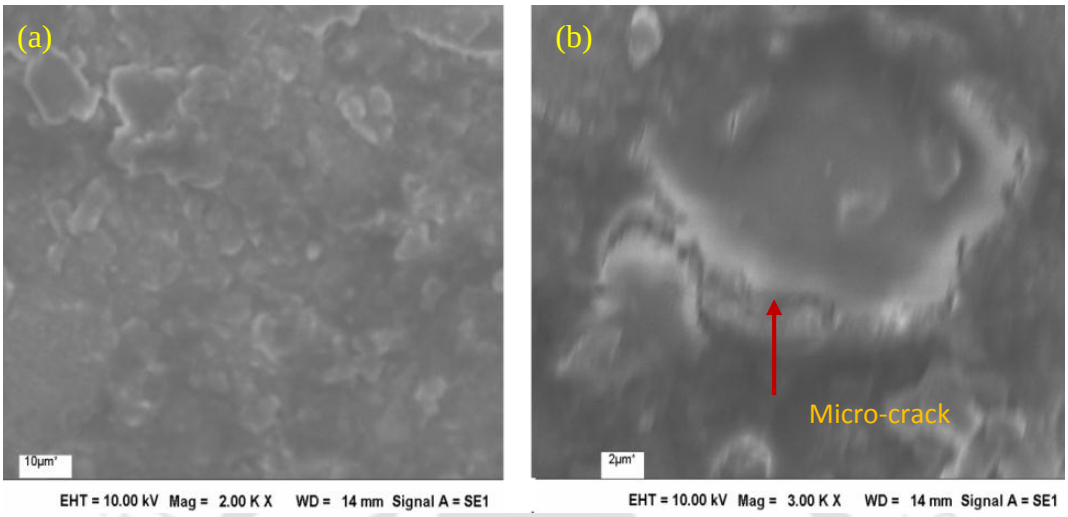

Figure 4.5 SEM image of Sample 9: (a) morphology and (b) micro-crack at grain boundary

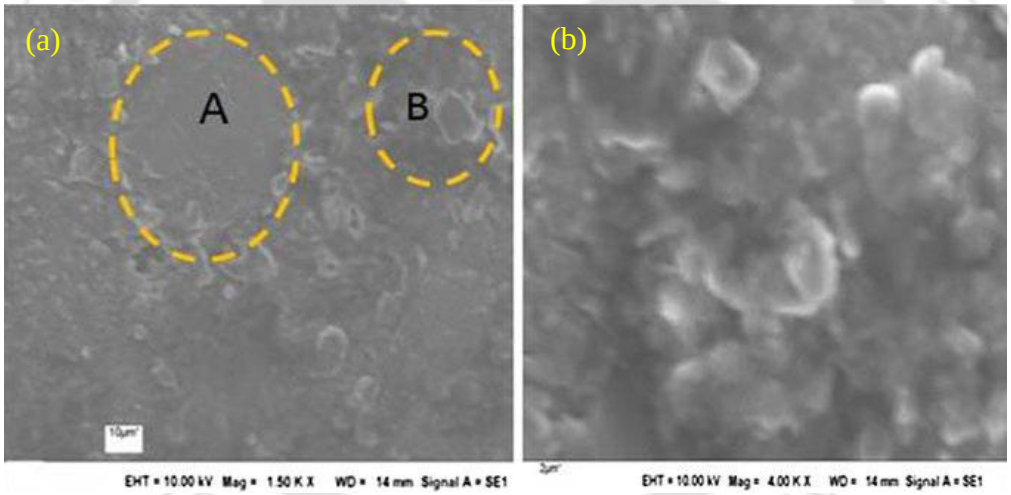

Figure 4.6 SEM image of Sample 5: (a) normal view (b) magnified view of region B

Figure 4.6(a) shows the morphology of Sample 5 at a lower magnification where region 'A' mark shows un-melted region. Almedia and Vilar (2008) reported that un-dissolved and partially dissolved particles were created at the bottom of the melt pool during laser surface alloying of aluminum with transition metals. This may be due to lower free energy of copper when it migrates to lattice defects such as grain boundaries, phase boundaries and dislocation. Segregation to grain boundaries affects the mobility of the boundary and has pronounced effects on re-crystallization and grain growth. Figure 4.6(b)

shows a magnified view of region 'B'. When Al_4Cu_9 compound got fast cooling time, it resulted in the formation of fine microstructure as shown in Figure 4.6(b) at higher magnification.

4.3.5 Porosity Problems in Surface Alloying

Figures 4.7 (a–b) show photograph and SEM image morphology of Sample 11. The porosity was observed on the surface as well as in the morphology. The voids were formed due to gas entrapment during solidification which is likely to occur when the rate of solidification is fast and there is no adequate time for the evolved gases to be removed. Formation of porosity in the alloy region may cause failure of the material during service life. Porosity is created due to the presence of gas pores or pockets within the fusion zone due to gas entrapment during the solidification process. It occurs when gases such as oxygen, nitrogen and hydrogen are absorbed from the atmosphere or developed when the chemical reactions occur during alloying. The sources of these gases may be due to contaminated substrate material or wetting conditions. For example, the present experiment shows the existence of gas pores or pockets within the alloyed area for samples first painted by adhesive followed by copper powder deposition.

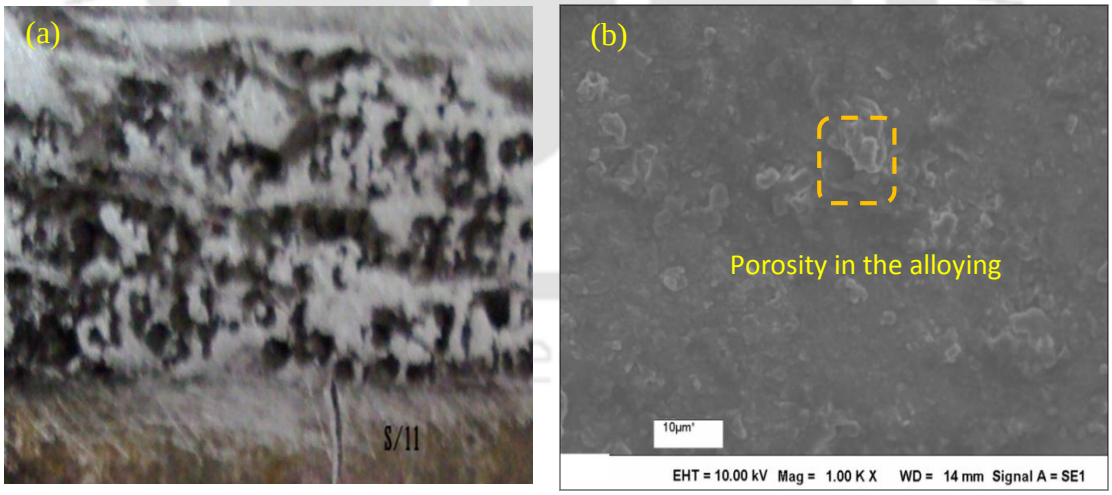

Figure 4.7 Images of Sample 11: (a) photograph and (b) SEM image morphology

Fracture surface morphology shows whether the alloyed region is ductile or brittle as well as the presence of surface defects formed in the alloy. The fracture surface of Samples 4 and 9 are shown in Figure 4.8 (a–b). Small chips were removed from the alloyed region and tested for fracture study using field effect scanning electron microscopy. The quality of laser surface alloyed samples confirmed that there no cracks and other defects in the alloy region. Laser alloying and re-melting resulted in good metallurgical alloying. Figures 4.8 (a-b) show fracture test of laser alloyed regions. As observed from the morphology images, no defect occurred in the alloyed region. The material is ductile and small dimple marks are observed on the surface (Figure 4.8a). The formation of micro-dimples shows material got harder after alloying.

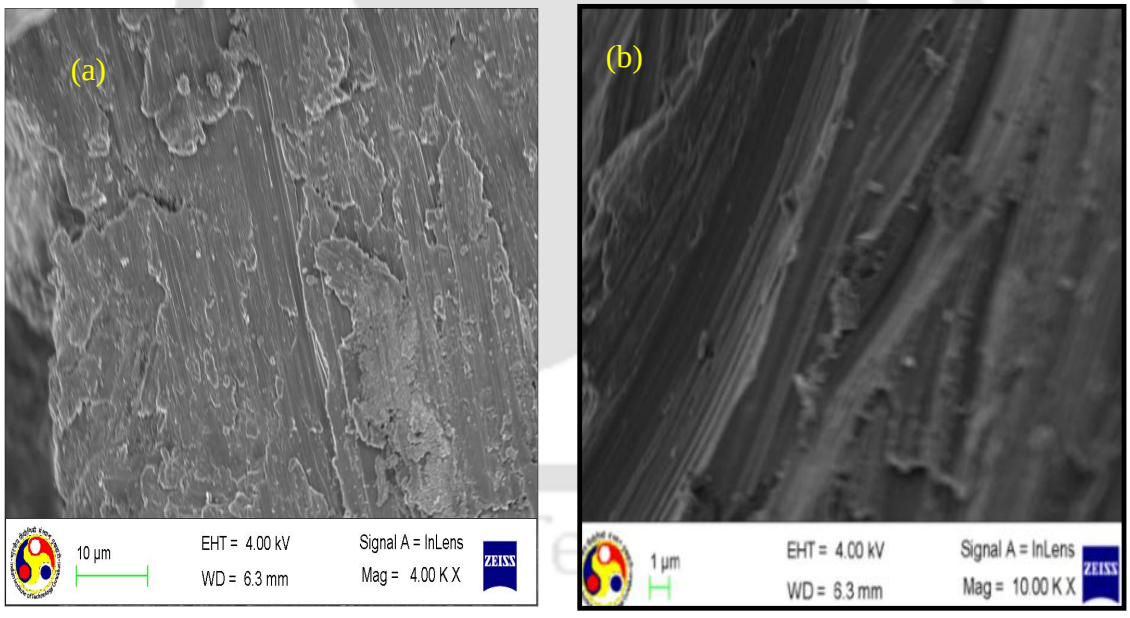

Figure 4.8 FESEM image of fractography tests from powder of alloyed region for: (a) Sample 4 and (b) Sample 9

4.4 Conclusion

Laser surface alloying of commercially pure aluminium with copper was achieved. The following are the main observations:

- Uniformly deposited Cu powder by compacting method resulted in good surface alloyed layer with average surface roughness of 1.9 µm.
- Laser surface alloying improved the microhardness from 60 $HV_{0.5}$ to 156 $HV_{0.5}$. Hardness was the maximum at the surface and the minimum at the bottom of substrate portion.
- The optimized laser parameter was 1.7 kW, 500 mm/min laser scan speed and 5.39 mm laser beam diameter. The effect of laser processing parameters on microhardness was observed. The hardness and uniformity of laser alloyed region varies with laser power, laser scan speed, laser beam diameter and re-melting. Laser remelting has improved microhardness of laser alloyed region. Porosity was formed in the alloyed region when substrate surface was first painted with chemical binder and the gases are enclosed in the solidification process.

Chapter 5

Surface Alloying of Copper, Magnesium and Manganese in Aluminum: Microstructure and Mechanical Properties

5.1 Introduction

The behavior of metallic parts is mainly affected by their mechanical properties such as hardness, ductility and strength. When an external load is applied on a part, the material must have sufficient strength in order to overcome the load. The strength of metal parts also depends on its interatomic bonding in grain structure where grain structure depends on the type of manufacturing methods such as casting, rolling, forging and heat treatment processes (Chryssolouris, 2013). Interatomic forces must overcome externally applied load in order to resist failure or fracture. The hardness of a material correlates directly with its strength (Pelleg, 2012). The attractiveness of aluminum metal is its relatively low cost, lightweight, heat treatability and refabricability. Commercially pure aluminum sheet metal with up to 1.5 wt.% impurities usually find applications in chemical equipment, truck bodies and packaging (Epstein *et al*., 1994). However, it has poor surface hardness and wear resistance. Aluminum alloys have many applications in engineering, most likely in automobile parts and airframe materials since the year 1920 (Campbell, 2011).

Laser surface alloying is a method of improving metal surface by adding other materials of any metal and ceramic to the substrate material. Laser surface alloying improves surface hardness, wear resistance and corrosion resistance of metal. For example, Kwok and Wong (2010) studied laser surface alloying of four substrate materials—aluminum alloy A97075, mild steel G10500, stainless steel S30400 and brass C2600. Powder of FeCrMoMnWCB having 15–53 μm particle size was used for alloying. Alloying powder was pre-placed on the substrate materials using flame spraying up to 0.2 mm thickness and a continuous wave CO_2 laser was used at 1.2 kW power, 25 mm/s scan

speed and 4 mm laser beam diameter for melting in the presence of argon shielding gas at 20 l/min. In laser surfaced alloyed A97075, G10500 and S30400, uniform alloyed layer was created except some cracks in A97075. However, due to high reflectivity, non-uniform alloying was observed in C2600. Microhardness was increased from 220 to 250 HV for G10500 and S30400 alloys and 450 HV for A97075 material due to iron aluminides formed in the alloy. The sliding wear resistance was improved after laser alloying. Except for C2600 material, corrosion resistance of all materials got deteriorated. Gordani *et al.* (2008) investigated microstructure, microhardness and corrosion behavior of laser surface alloyed Ni-P (92 mass % Ni and 8 mass % P) electro-less plating on Al-356 substrate material. Laser alloying was carried out using 1 kW pulsed Nd:YAG laser. Maximum laser energy of 600 mJ, beam diameter of 1 mm and beam scanning speed of 180 mm/min was used for alloying in argon shielding gas at 5 l/min. Laser beam track of 50% overlapping from previous track was reported. Results show low concentration of Ni, microhardness was 550 HV in the alloyed region of 100 μm. The hardness was the maximum (in the range of 900–940 HV) in intermediate thickness of Ni-P coating but hardness was reduced (in the range of 750–850 HV) in high thickness of coating achieved at high laser power density. After LSA, the corrosion resistance was good for Ni-P coating when compared with (as received) substrate material.

Fu and Batchelor (1998) reported laser surface alloying of AA6061aluminum with 70% Ni and 30% Cr metallic powder. First, alloying powder was plasma sprayed on aluminum substrate up to 50–80 μm thickness. Afterwards, Nd:YG laser at 30 J/mm^2 laser power density, 360 mm/min scan speed and 2 mm laser beam diameter was used for alloying. An alloyed depth of 300 μm could be achieved. In the alloyed zone, the maximum microhardness was about 325 HV while the substrate hardness was 60–70 HV. The fretting wear resistance after LSA got increased. Almeida *et al*. (2001) carried out laser surface alloying of commercial purity aluminum with Al-25 wt.% Nb powder using CO_2 laser at 2 kW beam power. The hardness got increased from 480–650 HV depending on the volume fraction of dendrite spacing formed in the alloy zone. Microhardness was decreasing in the alloy depth when laser scan speed was increasing. Dubourg *et al*. (2002) reported mechanical characterization of laser surface alloyed aluminum-copper system using CO_2

laser. Metal powders of 90 wt.% Cu and 10 wt.% Al and 99.5wt.% Al were alloyed in commercial purity aluminum. By increasing copper ratio from 11 to 40 wt.%, the micro-hardness improved from 90 $\pm$ 10 to 250 $\pm$ 10 $HV_{0.2}$. After annealing at 480 °C for 24 h, the micro-hardness evolved according to Cu ratio. At 11, 19 and 28 wt.% copper, micro-hardness decreased to a value of 50–100 $HV_{0.2}$. However, at 40 wt.% copper, micro-hardness achieved before annealing was retained.

Vaziri *et al*. (2009) reported laser surface alloying of Ni with aluminum substrate using Nd:YAG laser. Ni concentration was varying with depth of alloying. When depth of alloying was more, Ni concentration got reduced and its hardness was less. But at the surface where alloyed depth was less, the hardness was higher. Yang and Wu (2012) reported laser surface alloying of Ni in commercially pure aluminum. First, Ni was coated up to 25 μm on aluminum substrate in different acid bath of 5 pH value at 70 ^{o}C temperature. After that, Nd:YAG laser was used at 5.36 $\times 10^9$ W/m^2 power density and 180 mm/min scan speed for 4 ms duration. Using a single laser track, alloy depth was 125 μm. Laser treated samples were tempered in vacuum furnace at 300, 400 and 500 °C temperature for 2.5 h. The alloyed layer had Al_3Ni, Ni_3Al and little amount of non-equilibrium phases and Ni-P amorphous phases. When heat treatment temperature was increased, the amount of NiAl, Ni and Ni_3P phases also increased. Uniform microstructure of tempered layer was obtained at 400 °C. Authors reported surface microhardness values of 106, 124 and 156 $HV_{0.1}$ for heat treated samples at 300, 400, 500 °C temperatures, respectively while untreated samples microhardness was 56 $HV_{0.1}$. The highest micro-hardness of 430 $HV_{0.1}$ was reported for samples tempered at 400 °C at approximately 75 μm depth from surface, against untreated alloyed layer micro-hardness of 220 $HV_{0.1}$ formed at 5.39 W/m^2 laser power density.

Selvan *et al*. (2000) studied laser alloying of commercially pure aluminum after electrodepositing nickel and optimized the process parameters. The thickness of electroplated Ni was 12, 24 and 35 μm. An alloyed depth of 650 μm was formed by melting with a continuous mode CO_2 laser. The optimized parameters were 1.5 kW, 1100 mm/min laser scan speed and 1 mm laser beam diameter that gave uniform alloying with increased microhardness (600–950 $HV_{0.1}$), 20–27 times the base material hardness. The hardness

decreased when depth of alloying was increased. The homogeneity of the coating as well as hardness enhanced as the laser power increased from 1.1 to 1.5 kW. Tomida *et al*. (2001) reported formation of metal matrix composite by laser surface alloying of Cu and TiC on A50383 Al-Mg alloy. The particle size of Cu and TiC were 20 μm and 40 μm, respectively. The alloying powders were pre-placed on substrate material using acrylic binder and dried on hot plate. A continuous mode CO_2 laser at a beam power of 2100 W and laser scan speed between 80 to 1000 mm/min was used for alloying in argon shielding at 20 l/min. The microstructure of laser alloyed region had smooth, rough and flaking surface. A good smooth layer was obtained at 200–400 mm/min laser traveling speed with Cu content from 50 to 60 wt.%. The rough surface was obtained approximately at less than 200 mm/min when Cu content was more than 30 wt. %. The microstructure contains hypo-eutectic, lamellar eutectic and hyper-eutectic structures which contained hardened primary $CuAl_2$ phase. The hardness of MMC layer at laser travelling speed of 400 mm/min was 550–750 $HV_{0.2}$ due to lump like Cu_9Al_4 compound and the hardness in hyper-eutectic structure was 400 $HV_{0.2}$ at 50 wt.% Cu. The hardness increased to 600 $HV_{0.2}$ with 60 wt.% of copper due to Cu_9Al_4 structure. When the hardness reached up to 500 $HV_{0.2}$, crack was formed.

Tomida and Nakata (2003) reported laser surface alloying of a mixture of Al and Fe on A5052 Al-Mg alloy using a continuous wave CO_2 laser. The alloying powders of Al (99.9 wt.%, diameter less than 177 μm) and Fe (99.9 wt.%, diameter less than 149 μm) was mixed in ratios of 20, 50, 70 and 100 wt. % of Fe powder. Hardness increased with Fe content (45 wt.%) and reached approximately 800–1000 $HV_{0.1}$. It was reported that when microhardness exceeded 600 $HV_{0.1}$, crack was created due to brittle lump-like Fe_2Al_3 compound formed in the alloy. As a result of increased hardness, wear resistance after laser surface alloying was also improved. Salim *et al*. (2017) investigated evolution of structure and mechanical property of pure aluminum after laser surface alloying with Fe (150 μm particle size) and Ni (10 μm particle size) powders using low power CO_2 laser. A low power of 27 W, at optimum Fe-Ni ratio of 1:2, the amount of Ni in the melt pool increased due to its large absorptivity. The hardness of alloyed region was from 27 to 53.9 $HV_{0.1}$ processed at 30–50 s laser exposure. The maximum hardness was achieved at 50 s exposure time but beyond that the intense energy on the surface caused more damage.

In this chapter, individual and combined metal powders of Cu, Mg and Mn are alloyed with commercially pure aluminum substrate. The main feature of this work is that alloying was achieved in a CO_2 laser setup by a simple pre-placing technique. The procedure used here is easy to implement in industries. The results of the experiment are presented. Microstructure, microhardness, chemical composition and tensile strength are studied. The effect of laser parameters on alloyed geometry is also discussed.

A literature survey shows only a few attempts on laser surface alloying of commercially pure aluminum with copper additive discussed in Chapter 4. As a new combination, in this work copper, magnesium and manganese are alloyed in aluminum substrate in a 2:1:1 ratio. Experimental study was conducted for wear resistance study using pin on disc dry sliding test at different loads and sliding speeds. Al-Mg alloys are often used in automobile sector for getting high specific strength. Manganese provides a good corrosion resistance. Due to distinctive advantages of all these alloys, it was decided to explore the properties of their combination.

5.2 Materials and Method

The substrate material was 98.6% pure aluminum plate with dimension 55 mm × 30 mm ×10 mm. In this work, in the first set of experiments, copper, manganese and magnesium powders were mixed in the ratio of 2:1:1 by weight. In the additive, share of copper was 50% as it helps in strengthening the aluminum by forming intermetallics. Copper is a major alloying element in aluminum 2xxxx series which is used in aerospace application (Li et al., 2005 and Smith, 2003). Tomida *et al*. (2001) reported an increase in hardness of laser surface alloyed layer due to copper content. Regarding the wear resistance of Al-Cu alloy, Dubourg *et al*., (2002) observed that wear mass loss decreased when copper content was higher in laser surface alloyed AlCu system. Here, the intention of having more copper was aimed at maintaining more hardness as well as high wear resistance after laser surface alloying. Magnesium and manganese help in improving corrosion resistance. Each of them formed 25% share of additives. However, magnesium is much lighter than manganese. Hardness achieved after combining Cu, Mg and Mn by 2:1:1 ratio was compared with other

alloys (AlCu, AlMg and AlMn). This study explores if the mixed alloying is beneficial over the individual alloying. In future, researchers can investigate optimum composition. The particle size of each metal powder was about 10 μm. In this experiment, Fevigum binder was used instead of using Fevicol binder that was used in a pilot study in Chapter 4. Fevigum binder gives good result because it easily evaporates from the surface during drying time. In this case, there is no need to apply compacting after pre-placing alloying powders on the substrate. A slurry of alloying powder was prepared by mixing with Fevigum and uniformly coated on aluminum substrate up to 1.5 mm thickness for a material combination. A continuous wave of CO_2 laser machine (Model: Orion 3015, Make: LVD, Belgium) was used. Table 5.1 presents laser input parameters used for alloying material combinations.

The second set of experiments was carried out for individual alloying of copper, magnesium, manganese in commercially pure aluminum. The combination of Cu, Mg and Mn was also used for comparing the results with individual alloying. In this case, three laser powers—1.7, 1.8 and 1.9 kW were used. Laser scan speed of 500 mm/min and laser beam diameter of 5.8 mm are same for all materials. Laser specific energy was calculated using (Kadhim *et al*., 2013);

$$E = \frac{P}{vd}, \tag{5.1}$$

where P is laser power, v is scan speed and d is laser beam diameter.

Table 5.1 Laser 1.7 kW laser power for material combination of Cu, Mg and Mn

Samples number	**Scanning speed (mm/min)**	**Laser beam diameter (mm)**	**Laser specific Energy (J/mm^2)**
1	300	5.80	58.62
2	300	7.40	45.94
3	300	9.80	34.49
4	400	7.40	34.28
5	500	7.40	27.57

5.3 Results and Discussion

In this section results of experiments of laser surface alloying are explained in details. The effect of laser parameters such as laser power, laser scan speed and laser beam diameter on the alloyed geometry such as depth '*D'*, height '*h'*, width 'w' and area of heat affected zone '*d'* are investigated.

5.3.1 Surface Topology Study

Figures 5.1 (a–e) show micrographs at 50 magnification for Samples: 1, 2, 3, 4 and 5, respectively. The surface topology was studied without polishing the surface. A good metallurgical bonding and uniformity of laser alloyed layer were observed. The alloyed surface had no crack, porosity and discontinuity that confirmed the formation of metallurgical bonding of added elements with substrate material. The uniformity of the alloyed surface was visible as shown in Figures 5.1(a–e).

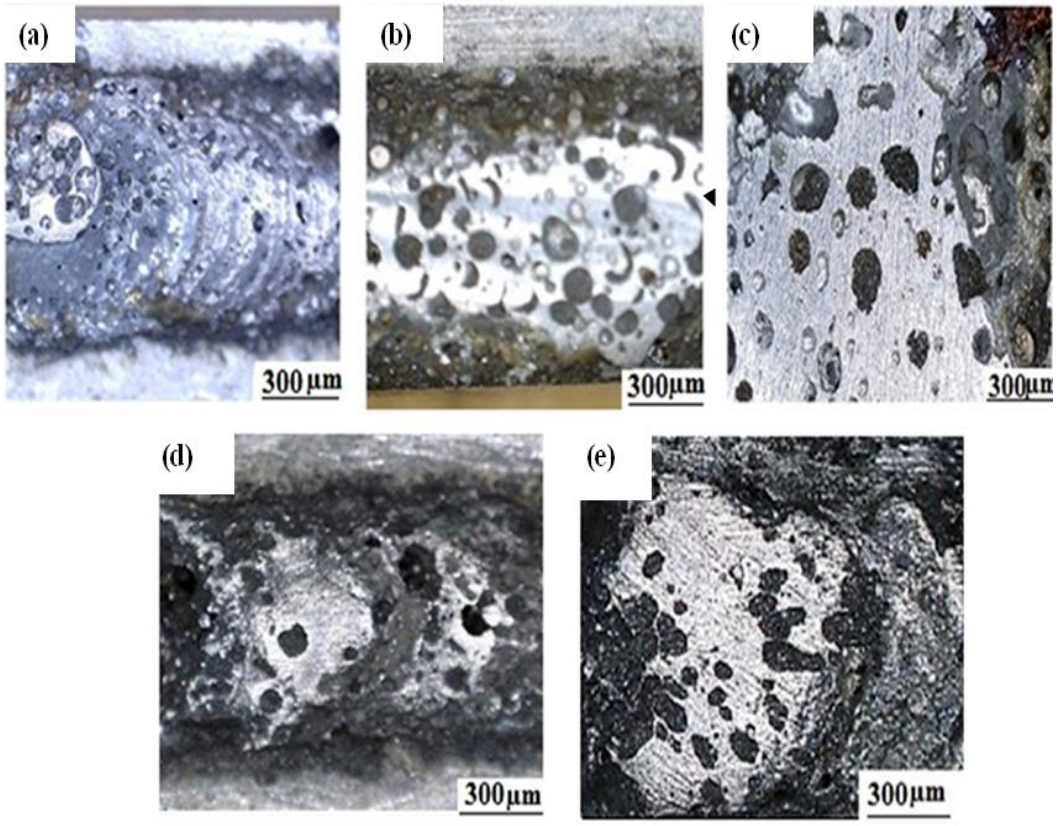

Figure 5.1 Surface topology of alloyed region (×50) processed by 1.7 kW laser power: (a) Sample 1, (b) Sample 2, (c) Sample 3, (d) Sample 4 and (e) Sample 5

The surface topology of laser alloyed region was somewhat irregular since different shapes of round and elliptical forms were observed (Fig.5.1b). The aluminum substrate was seen on the top of the surface as white color. This is advantageous for improving corrosion resistance of the alloy. The porosity observed on micrographs shown in Figures 5.1(d) and 5.1(e), was due to insufficient use of laser specific energy (Table 5.1), which caused poor fusion. There was insufficient melting but the top surface underwent rapid cooling, which caused cracks due to thermal stresses. These cracks were limited to only top surface due to sudden quenching, but got eliminated after polishing. With high laser specific energy, sufficient liquefaction is achieved and high thermal stresses are not generated.

5.3.2 Effect of Laser parameters on Alloy Geometry

Figures 5.2 (a–e) represent a cross-sectional images of Samples 1, 2, 3, 4 and 5, respectively. As clearly observed from the images, the depth, height and width of the alloys vary due to the change in laser scan speed and laser beam diameter. Figure 5.3(a) shows the effect of laser beam diameter on alloyed geometry. Samples—1, 2 and 3 were processed by 1.7 kW laser power and 300 mm/min scan speed. The depth of alloying increased from 0.5 to 2 mm as laser beam diameter increased from 5.8 to 9.8 mm. The geometric dimension of alloyed width was highly sensitive to laser beam diameter. It increased from 3 to 7 mm when laser beam diameter was increased from 5.8 to 9.8 mm. The depth of heat affected zone was also changed from 0 to 1mm. The height of alloyed layer was 1 mm for smaller laser beam diameter of 5.8 mm. For larger laser beam diameter of 9.8 mm, the alloyed height was 0.3 mm. From this, it is clear that Sample 2 provides optimum alloying at 300 mm/min laser scan speed. The height of the alloyed region and HAZ region was very small.

Figure 5.3 (b) shows the effect laser scan speed on the dimension of alloyed geometry. When laser scan speed was varied from 300 to 500 mm/min, different alloy geometries were observed for the same 1.7 kW laser power and 7.4 mm laser beam diameter, for Samples 2, 4 and 5. The depths of alloyed region were 1.5, 1.3 and 0.3 mm when laser scan speeds were 300, 400 and 500 mm/min, respectively. The height of alloyed region was increased from 0.7 mm to 1 mm as the laser scan speed was increased from 300

to 500 mm/min. However, width of alloyed layer was decreasing from 3 to 1.4 mm when laser scan speed was increased.

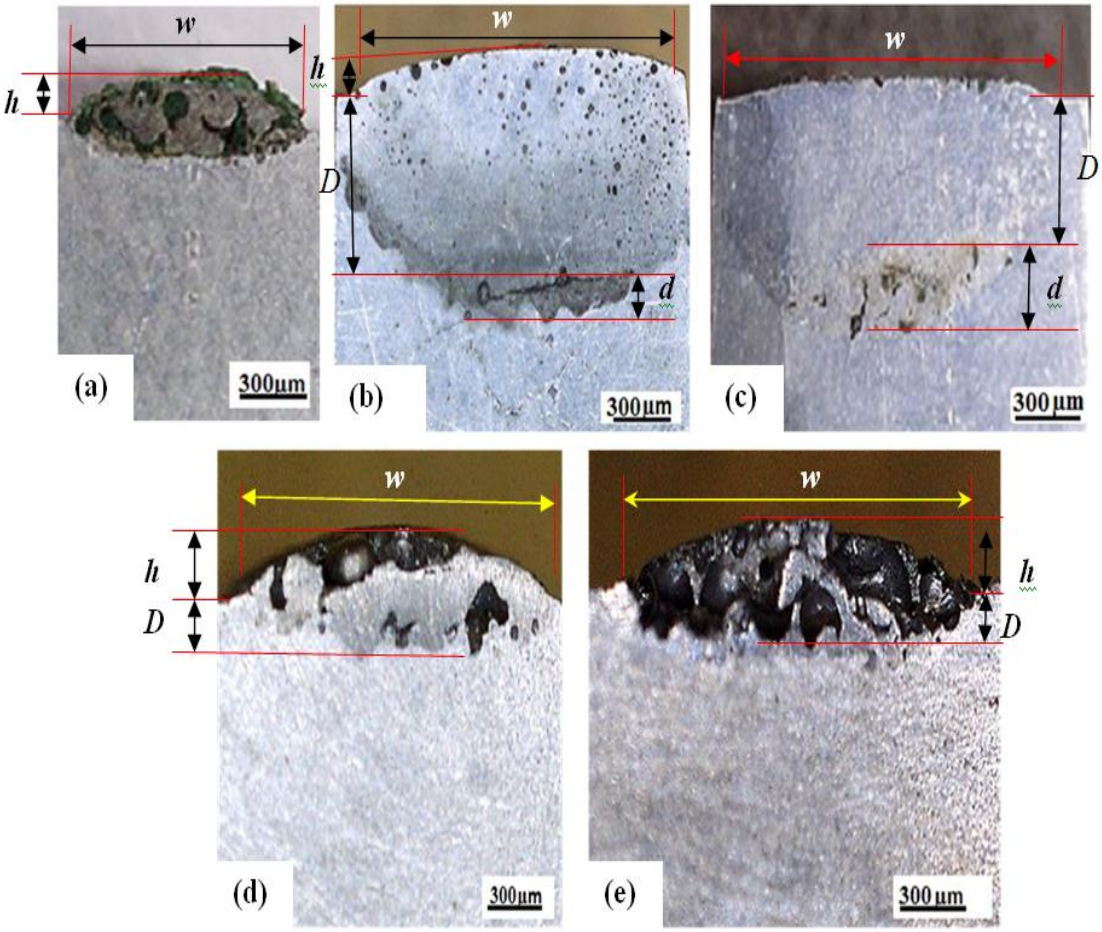

Figure 5.2 Photographs of Al-CuMgMn alloy cross-sections (×50): (a) Sample 1, (b) Sample 2, (c) Sample 3, (d) Sample 4 and (e) Sample 5

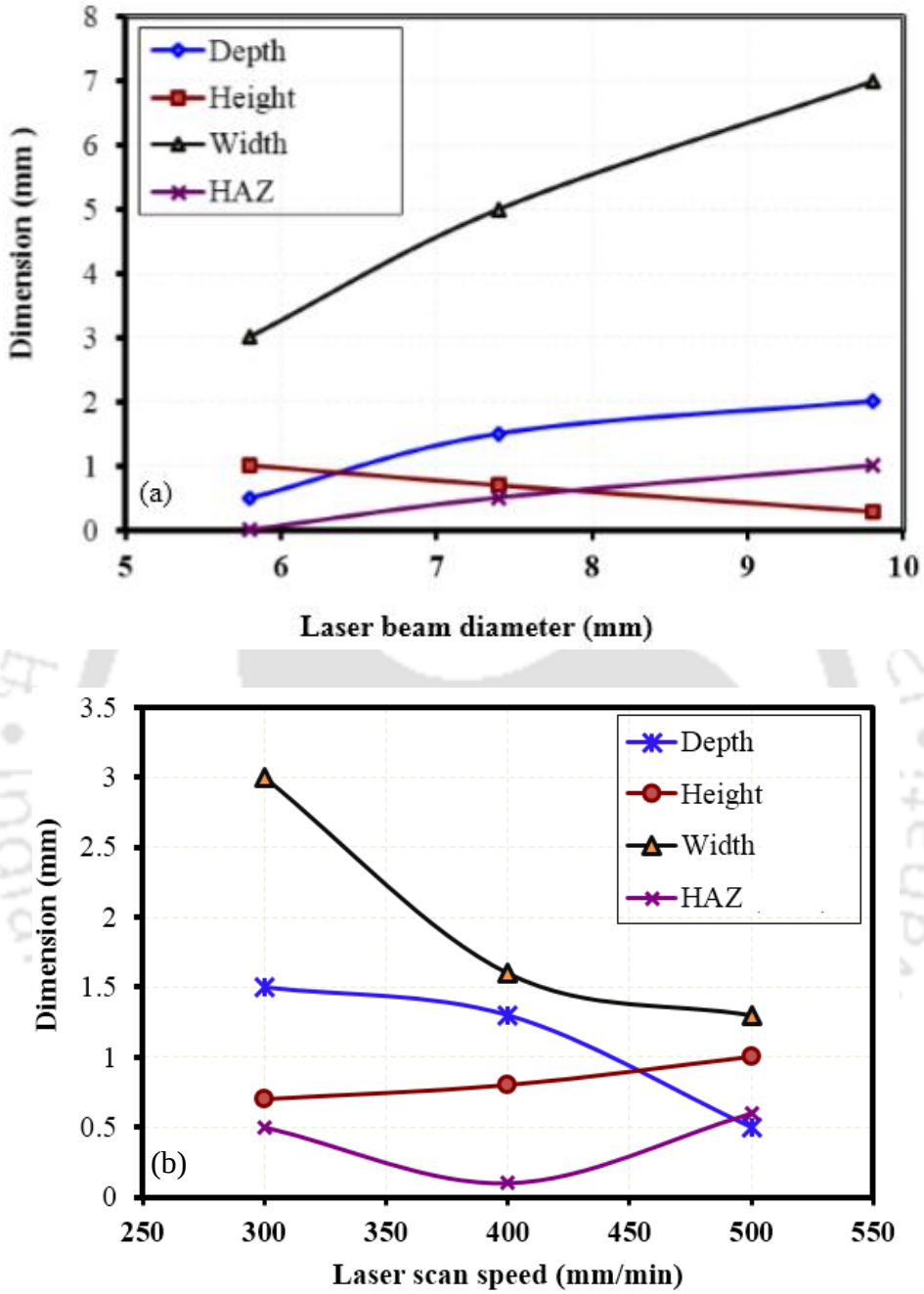

Figure 5.3 Effect of laser parameters on the alloy geometry for Al-CuMgMn alloy processed by 1.7 kW laser power and 7.4 mm laser beam diameter: (a) effect of laser beam diameter (b) effect of laser scan speed

The depth of the heat affected zone depends on the laser scan speed. The depth of heat affected zone fluctuates with the change of laser scan speed. Tomida *et al*. (2001) reported the thickness formed as a metal matrix composite layer was decreasing when laser scan speed was increased during laser surface alloying aluminum with TiC and Cu. Almeida *et al*. (2001) reported the depth of remelting was decreasing when laser scan speed was increasing during laser surface alloying commercially pure aluminum with Al-25 wt.% Nb alloying.

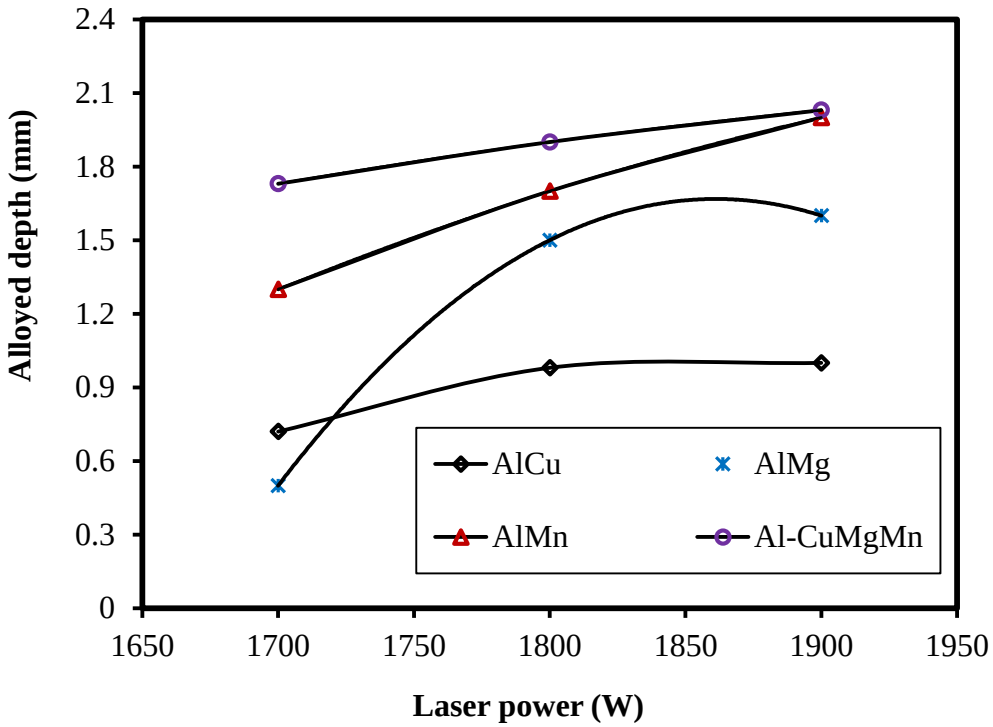

Figure 5.4 The variation of the laser surface alloyed depth with laser power when processed by 500 mm/min laser scan speed and 5.8 mm laser beam diameter for different alloys

Figure 5.4 shows the effect of laser power on alloyed depth for four materials—AlCu, AlMg, AlMn and Al-CuMgMn. For same laser scan speed of 300 mm/min and laser beam diameter of 5.8 mm, the depth of the alloy formed varies at different laser powers—1.7, 1.8 and 1.9 kW. After laser surface alloying was done, 5.5 mm alloyed width was formed. For different materials such as copper, magnesium,

manganese and their combination, the depth of alloy was varying. This is because of the varying diffusion rate of copper, magnesium and manganese in aluminum during laser melting. The minimum depth of alloy was observed for samples processed at 1.7 kW laser power. At the constant laser power of 1.9 kW, the alloy depths for different materials were 2, 1.9, 1.6 and 1 mm for Al-CuMgMn, AlMn, AlMg and AlCu, respectively. From this, it can be stated that increasing laser power creates more melting by pushing alloying elements to move into the substrate material. As a result, for all materials, the depth of alloying was maximum for 1.9 kW laser power. For 12% increase in laser power from 1.7 to 1.9 kW, the depth of alloying was increased at least by 15.6% for Al-CuMgMn alloy and 68.75% for AlMg alloy. It was also increased for AlMn and AlCu alloys. Gordani *et al.* (2008) reported laser alloyed depth increased with an increase in laser energy density during laser surface alloying Ni-P on Al-356 aluminum alloy. Vora *et al*. (2013) reported dilution depth of alloying was mainly affected by laser energy density during laser surface alloying aluminum substrate with molybdenum.

5.3.3 X-ray Diffraction Analysis

Figure 5.5 shows the X-ray diffraction pattern of Al-CuMgMn alloy for three samples 1, 2, and 3 given in Table 5.1. The diffraction pattern with corresponding peaks and diffraction angle was observed from the X-ray pattern. The formation of two intermetallics phases of Al_2Cu and $Al_7Cu_3Mg_6$ were identified with the existing JCPDS database with entry cards 96-901-2197 and 00-007-0258, respectively. As a result, the Al_2Cu compound had tetragonal structure while $Al_7Cu_3Mg_6$ compound had a cubic structure.

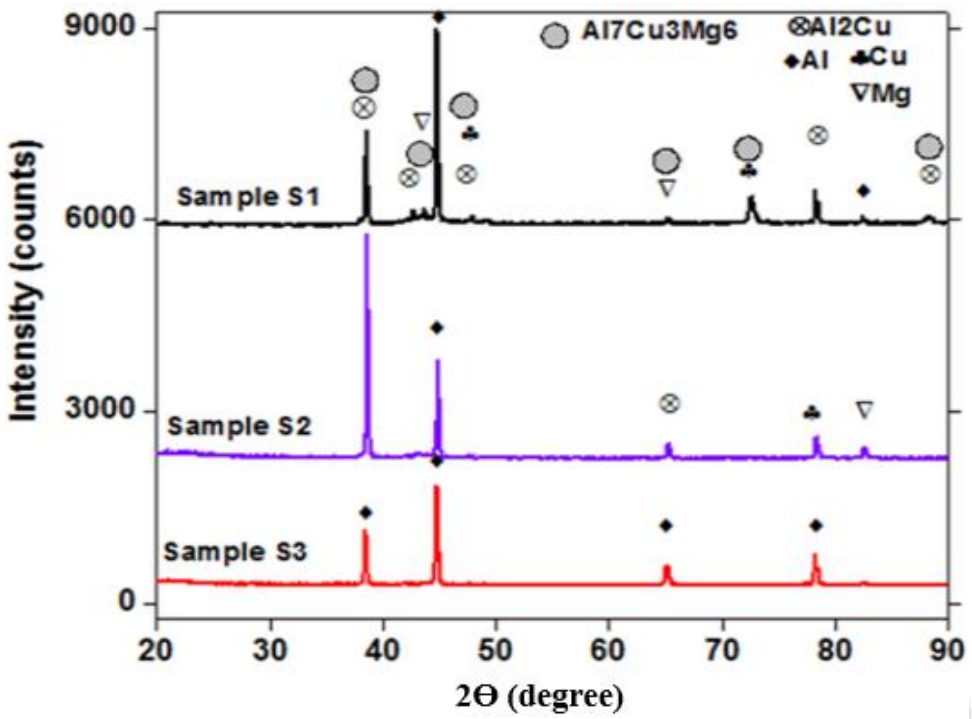

Figure 5.5 XRD pattern of laser surface alloyed samples for Al-CuMgMn alloy for selected samples

5.3.4 Microstructure and Surface Morphology

Figures 5.6 (a–b) show micrograph of alloyed region for Sample 1. Different microstructures formed in the alloy region, the re-melted region and the heat affected zone. Figure 5.6(a) shows the depth of alloy layer formed was 0.5 mm. The boundary of alloyed layer and aluminum substrate is free from cracks as well as porosity. The re-melted region has dendrite structure with very dense alloying elements at the interface zone and small heat affected zone as shown in (Fig. 5.6b). The circle mark in (Fig.5.6b) shows the area of heat affected zone (HAZ) with no alloying elements were observed. However, due to laser heating the structure was re-arranged by forming dendrite structure. The alloyed region and HAZ can be easily recognized along with alloy surface formation with different microstructures. In the re-melted region, no surface defects were formed even when the composition was changed. The distribution of alloying elements was as follows— 26.1 wt.% Cu, 11 wt.% Mn, 0.2 wt.% Mg and aluminum substrate composition is 56.7 wt.%. It

was observed that alloying was successfully done with fine microstructure and very less heat affected zone.

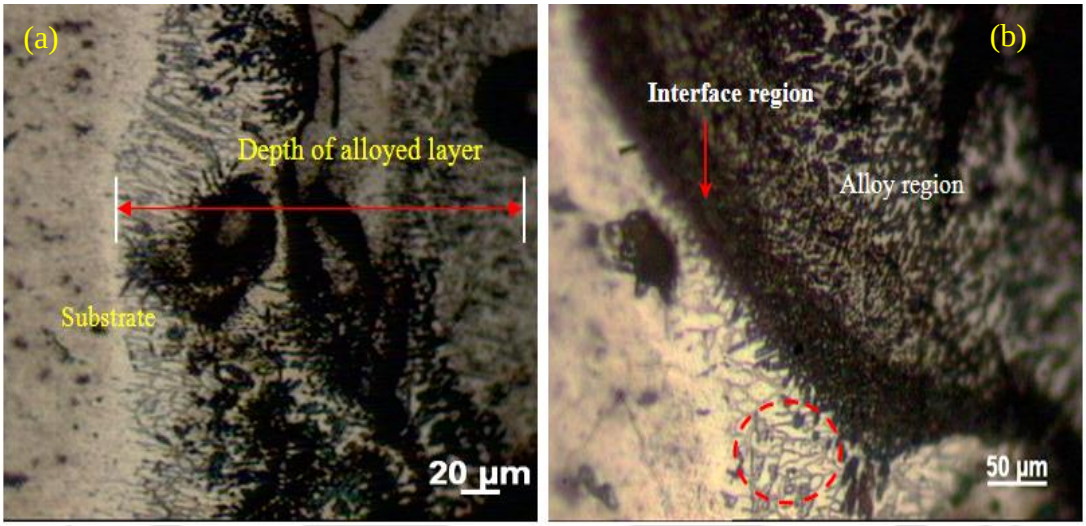

Figure 5.6 Optical images of Sample 1 (×50), processed by 1.7 kW laser power, 300 mm/min laser scan speed and 5.8 mm beam diameter: (a) micrograph showing thickness of alloy layer, (b) micrograph showing different layers

Figure 5.7 shows the EDS micrograph and the corresponding spectrum depicting composition of alloying elements and aluminum substrate. Figure 5.7(a) shows the micrograph where both area and point spectrum tests were conducted. The concentration of major alloying elements decreased from top alloyed layer to aluminum substrate material. The concentration decreased because of diffusion of atoms of alloying elements. First row of Table 5.2 and Figure 5.6(b) shows spectrum 14 that was on top of the alloyed zone with maximum concentration of 32.1 wt.% Cu, 13.1 wt.% Mn, 2.0 wt.% Si, 0.3 wt.% Mg and 0.2 wt.% Fe. The alloying elements were decreased in order from spectra 14 to 18 as shown in Figure.5.6 (b) and 5.6(c). This confirms that diffusion takes place during melting process down the substrate. Silicon concentration in alloy layer reached 4 wt.% which may be added from SiC emery sheet used during the polishing of the samples.

Table 5.2 Chemical composition (in wt. %) of Sample 1

Spectrum	Al	Cu	Mn	Si	Mg	Fe
14	52.30	32.10	13.10	2.00	0.30	0.20
15	56.70	26.10	11.00	5.80	0.20	0.10
17	71.10	17.30	4.10	4.90	0.20	0.40
18	98.69	0.10	-	0.90	-	0.40

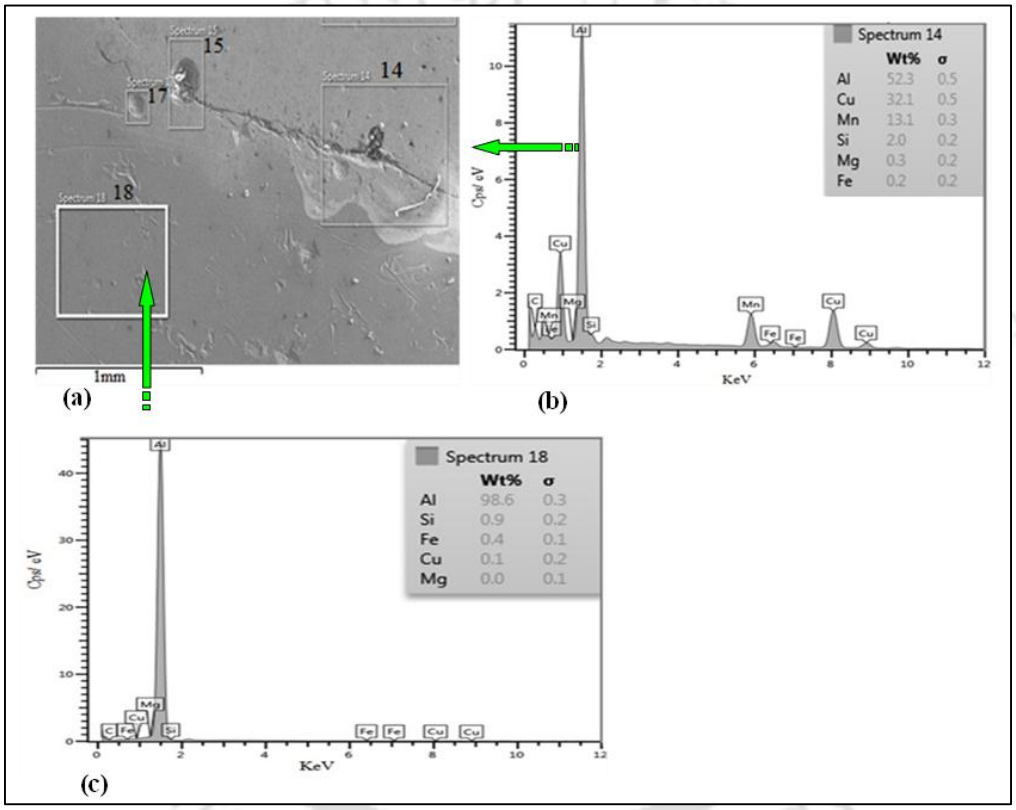

Figure 5.7 EDS spectra of Sample 1: (a) micrograph, (b) composition of spectrum 14 (alloyed region) and (c) composition of spectrum 18 (substrate region)

Figures 5.8 (a–b) show an optical image of Sample 2 at different magnification to reveal segregated particles in solidified regions. The structure looks cellular in the shape of needle structure as shown in a circle at the bottom right part as shown in Figure 5.8(a). There is a structural growth in the direction towards partially melted zone. The change in the structure from primary phase to dendrites of eutectic aluminum solid solution as shown

by rectangular mark at the bottom left is shown in Figure 5.8(a). Phase identification in the composition of transition zone quantified by EDS shows 29.9 wt.% Cu, 1.6 wt.% Si, 1.5 wt.% Fe and 0.1 wt.% Mg and 66.9 wt.% aluminum substrate. The maximum solid solubility of copper in aluminum at the eutectic temperature (548 °C) is 5.65%.

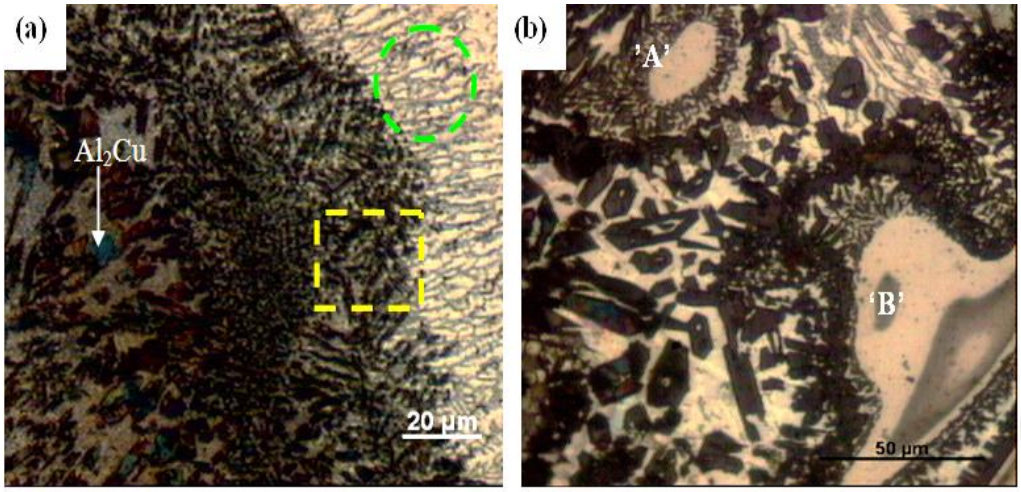

Figure 5.8 Optical images of Sample 2, processed by 1.7 kW laser power, 300 mm/min laser scan speed and 7.4 mm laser beam diameter: (a) microstructure zones (×20) and (b) micrograph of undisolved element (×50)

The areas shown as ‘A’ and ‘B’ regions in Figure 5.8(b) indicate un-dissolved manganese formed as micro-segregates. Micro-segregation formed due to insufficient temperature to melt manganese. There is lack of liquid homogenization in the melt pool, which is due to high melting temperature of manganese (1244 °C), higher than that of copper (1084 °C) and magnesium (650 °C). The concentration was identified by EDS at point spectrum 11 as shown in Figure 5.9 (a). The point marked ‘A’ had concentration of 30.8 wt.% Mn and 60 wt.% Cu and other impurity elements less than 1wt.% as shown in Figure 5.9(b). Higher concentration of these elements resulted in the formation of micro-crack at grain boundary as observed using optical image shown in Figure 5.9(a).

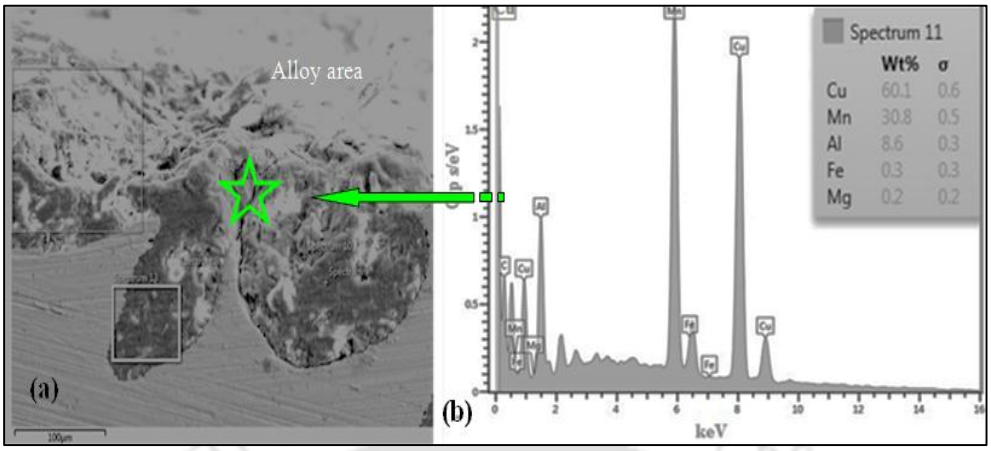

Figure 5.9 EDS micrograph for Sample 2, processed by 1.7 kW laser power, 300 mm/min scan speed and 7.4 mm laser beam diameter: (a) micrograph image and (b) spectrum image

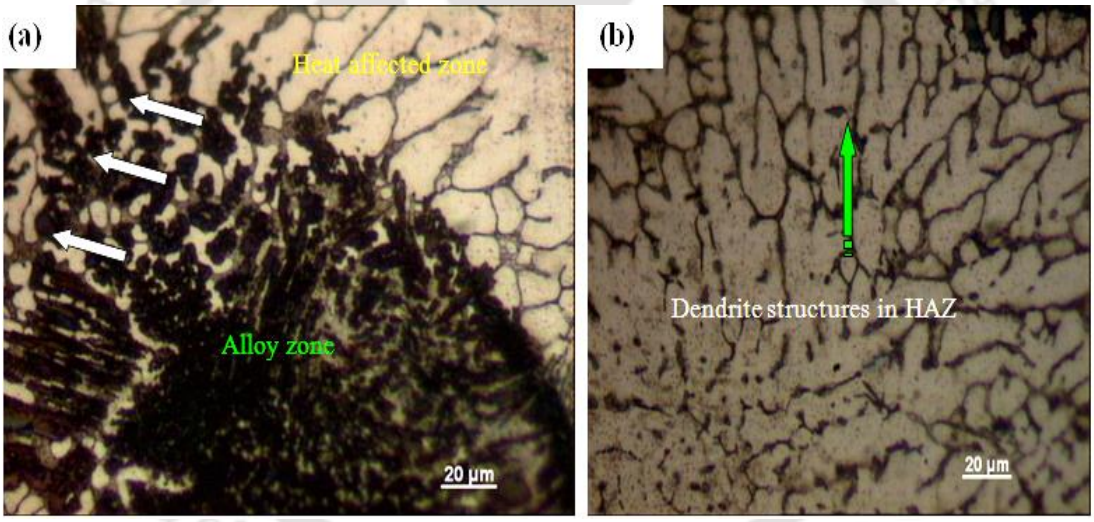

Figure 5.10 Optical images of Sample 3 (×50), processed by 1.7 kW laser power, 300 mm/min scan speed and 9.8 mm laser beam diameter: (a) alloyed region and (b) heat affected region

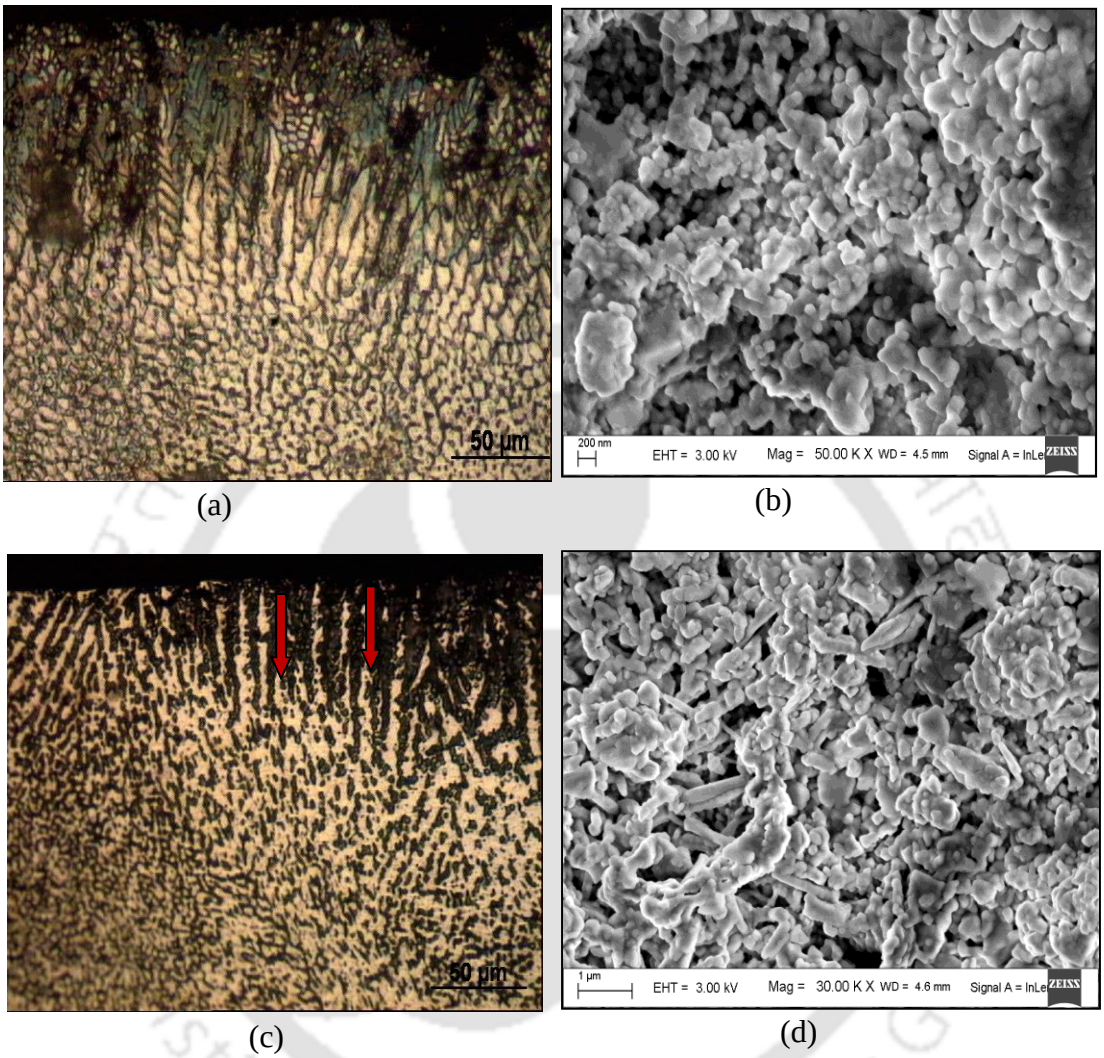

Figure 5.11 Optical image (×20) and FESEM images for laser surface alloyed Samples, processed by 1.7 kW laser power, 500 mm/min laser scan speed and 5.8 mm laser beam diameter: (a–b) AlCu alloy and (c–d) AlMg alloy

Figures 5.10 (a–b) show the microstructure of Sample 3. Alloying elements diffused down inside the substrate as shown by arrows in Figure 5.10(a). During laser surface alloying, temperature gradient decreased continuously and solidification velocity increased gradually from bottom of melt pool to the top. Figure 5.10(b) shows the heat affected zone where no alloying elements were visible. The alloying elements were melted and deposited directly on solid substrate. The structural orientation of the base material grains at the melt

zone interface continued into fusion zone. As a result, nucleation stage was bypassed at the interface of substrate and alloy zone. The microstructure of heat affected zone was fully dendrite structure.

Figures 5.11(a–b) show an optical image and FESEM image of AlCu sample. The concentration of copper added to the material created dendrite structure in the upper alloyed portion. The dendrite grain structure had a directional growth towards substrate material and the interface had a columnar grain structure. The morphology had a good metallurgical alloy formed because the grains were closely bonded together as shown in Figure 5.11(b). Figure 5.11(c) shows microstructure of AlMg alloy, where laser irradiation caused the particles of magnesium to diffuse down into the substrate portion. During laser surface alloying, there is high atomic vibration which creates every atom of the material to bond with next atoms as shown in Figure 5.11(d). In the alloyed morphology, the structure of bonding had lateral growth and small rounded shapes. The morphology of AlMg alloy is shown in Figure 5.11(d). The maximum copper concentration in the alloy was 23.3 wt.% Cu and other elements were given in Table 5.3. The minimum concentration was 11.2 wt.% Cu with other impurity elements. The composition of major alloying element, magnesium, in laser surface alloyed AlMg sample was the maximum at 36.3 wt.% Mg as observed from Table 5.4.

During laser surface alloying, the concentration of alloying elements is not uniform throughout the alloyed region. This is because of fast solidification effect causing the formation of metastable and intermetallic compounds. In slow cooling process during casting and welding processes, phase diagram states an equilibrium condition of the alloy. Stefanescu and Ruxanda (2004) studied solidification and microstructure of different aluminum alloys during casting process. They discussed eutectic composition and dendritic structure of AlCu alloy. However, there is a shortage of literature explaining non equilibrium phase diagram formed during fast cooling processes such as electron beam and laser beam surface modifications. For example, in laser beam surface alloying, the cooling rate is about 10^5—10^8 K/s. Rapid solidification limits time available for melting to form equilibrium phases thus favors the nucleation of non-equilibrium phase to be created. Brochu *et al*. (2011) studied two different metastable phases formed during rapid solidification. The one was formed by change of chemical composition as a solid solubility extension forming chemical composition of the alloy outside the range of equilibrium condition. Rapid solidification alloys also formed from different phases in which the alloy had different crystal

structure non-existent in an equilibrium phase diagram. The authors concluded that rapid solidification process restricts chemical diffusion and consequently deviation from chemical equilibrium. Campbell, (2012) pointed out that phase diagrams do not give information about size, shape and distribution of phases that are very important for mechanical properties. The solid solubility of copper in aluminum is 5.65 wt.% at 548 °C and eutectic composition is 33.2 wt.% (Davis 1994, Sigworth, 2014, Rambabu *et al*. 2017). Zimmermann *et al*. (1989) reported that eutectic composition of Al-32.7 wt.% Cu was created by laser remelting by CO_2 laser forming of different structures like lamellar eutectic.

Table 5.3 Chemical composition (in wt. %) of AlCu alloy

Spectrum	Cu	Mg	Fe	Si	Al
1	11.2	0.4	26.2	2.0	60.3
2	11.6	6.1	5.2	14.6	62.5
3	14.6	0.8	16.8	1.7	66.2
4	15.6	1.3	4.6	4.9	73.6
5	23.3	0.1	0.7	1.0	74.8

Pelletier *et al*. (1991) reported solidification and microstructure for different alloys including aluminum alloys using CO_2 laser. For aluminum based alloys dendrite structure was randomly oriented when the quenching rate was 10^4 K/s. The solidification occurs in dendritic regime. Composition evolution and interfacial segregation of Al-Cu precipitate was reported by Biswas *et al*. (2011). The authors reported their results after using pulsed laser beam and electron beam aging on pure aluminum (99.99%). At higher aging temperature of 463 to 533 K, thickness of copper precipitate is higher in the range 8 to 50 nm. The precipitate formed at 463 K and the concentration shifted out of equilibrium composition of Al_2Cu. Moreno *et al*. (1999) reported rapid characterization of intermetallics and interfaces of AlCu, Al_2Cu and Al_9Cu_4 compounds. Guo *et al*. (2011) also studied intermetallic phases of different AlCu system formed in diffusion bonded Cu/Al laminates prepared by plasma activated sintering at a temperature range 673–773 K for 10–30 min. Authors reported calculated values of activation energy for different intermetallics of AlCu (84.6 kJ/mol), Al_2Cu (71.1 kJ/mol) and Al_9Cu_4 (89.8 kJ/mol) compounds. Different solidification curves of AlCu, AlMg and AlCuMg aluminum alloys were reported by Chen and Huang (1996).

In the present work, the composition was not uniform and the maximum percentage of copper was 23.3%. It is lesser than eutectic composition. Dubourg *et al*. (2000) has presented a

non-equilibrium phase diagram obtained after laser surface alloying. Eutectic (Al + Al_2Cu) composition was at 17.1% wt. Cu. A hypoeutectic microstructure was obtained until 24 wt. % Cu.

Table 5.4 Chemical composition (in wt. %) of AlMg alloy

Spectrum	Mg	Cu	Fe	C	Si	O	Al
1	36.3	0.1	0.1	13.7	0.2	17.7	31.9
2	13.0	-	0.2	56.5	0.2	9.3	20.8
3	22.6	0.1	0.3	19.0	0.1	-	57.9
4	16.8	0.1	0.7	37.4	0.2	-	45.0
5	23.4	0.2	1.1	15.9	0.3	-	59.2
6	22.8	0.2	0.8	28.2	0.	-	48.0

Magnesium is a major alloying element in 5xxx series alloy which is applicable in automotive industry. A simple information about the composition of this alloy (AlMg) produced by laser surface alloying is given in Table 5.4. The concentration of magnesium was different at different spectrum. In the alloyed region, magnesium concentration was in the range 36.3 wt.% to 13 wt.% Singh *et al*. (1991) illustrated that below 18 wt.% Mg in AlMg system, there is no chemical ordering in the liquid and the distribution of the atoms in the alloy is random. A detailed study of phase diagram and thermodynamic calculations were reported for AlMg system during mechanical alloying by different researchers—Zuo *et al*. (1993); Zhang *et al*. (1994); Chartrand *et al*. (1994); Su *et al*. (1997) and Li *et al*. (2012). Further information can be obtained from well written review article by Islam *et al*. (2014) on AlMg binary phase diagram. A study of thermal stability of phases in Mg-Al phases was conducted by Czeppe *et al*. (2003). They reported that phase stability reached at 450 ^{o}C, having the composition 61 at.% Al which was in good agreement with Su *et al*. (1997) and Liang *et al*. (1998). In this work, the base metal is at a lower temperature than molten pool; solidification of molten metal begins with the formation of solid nuclei at the interface region.

Figure 5.12(a) shows the microstructure of AlMn alloy. The grain structure had columnar grains at the left side of the rectangular mark and small round grains towards the right side. The portion of the rectangular zone showed a high concentration of manganese due to micro-segregation. The formation of micro-segregation was due to variation in melting temperatures (1246 °C for manganese and 650 °C for aluminum). Further study was conducted using FESEM analysis where the grain structure is shown in Figure 5.12(b).

The small ball like grains were observed in the morphology, which was visible at high magnification of 150 k. No metallurgical defect formed in the alloyed region since uniform alloying was achieved.

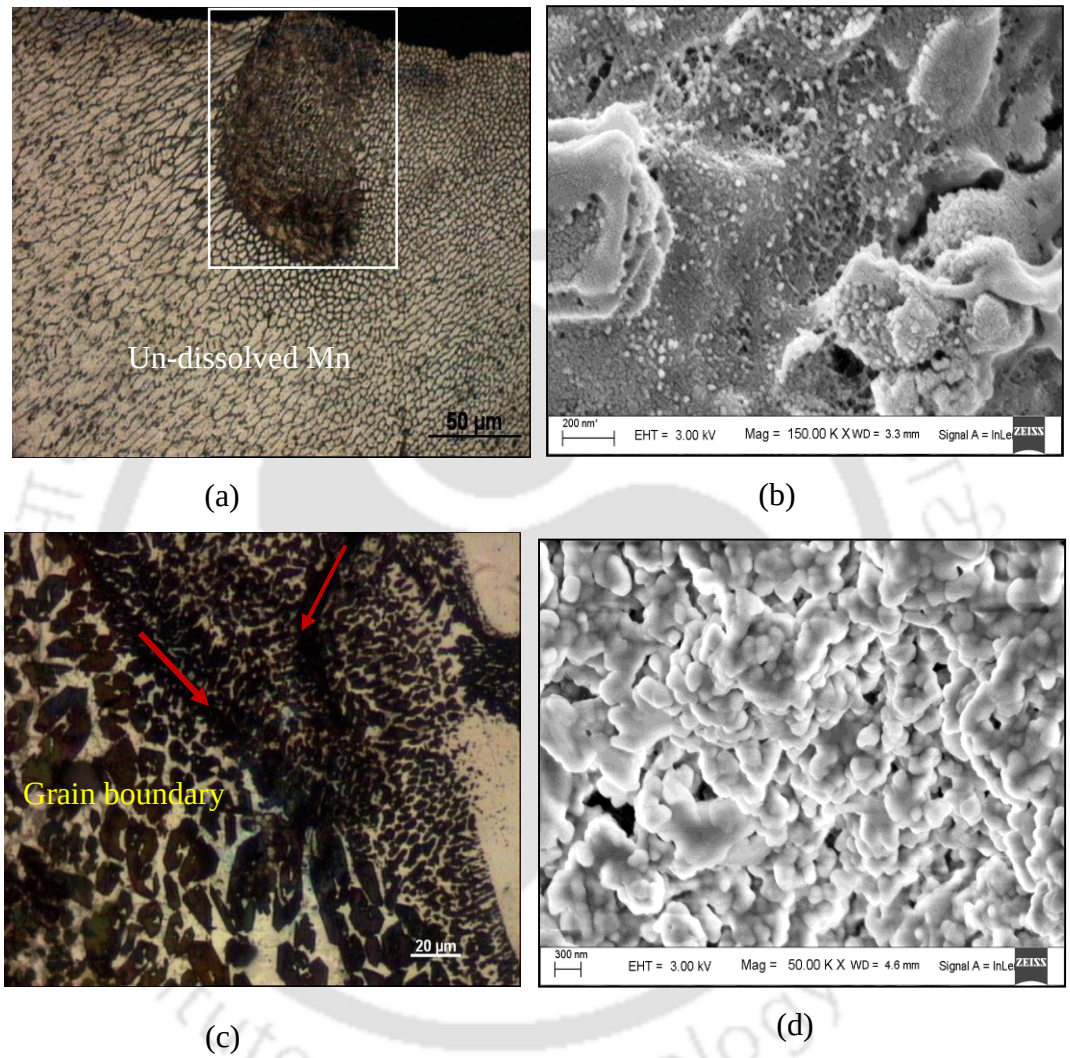

Figure 5.12 Optical image (×20) and FESEM image for laser surface alloyed samples, processed by 1.7 kW laser power, 500 mm/min laser scan speed and 5.8 mm laser beam diameter: (a–b) AlMn alloy and (c–d) AlCuMgMn alloy

Figure 5.12(c) shows the microstructure of Al-CuMgMn alloy where the formation of grain boundaries with different types of dendrite structures was observed. Because of the diffusion process of alloying elements and high temperature created by laser beam, alloying was formed. The temperature was highest at the center of the melting pool during

alloying. The surface tension force pulled the alloying elements into the substrate portion to create a good alloying. The substrate portion enhanced the solidification process by conducting heat from the melting pool. The formation of grain boundary in the alloy region increased its strength by acting as an obstacle to the movement of dislocation defects. Figure 5.12(d) shows that high magnification was conducted using FESEM image analysis. It confirmed that the formation of good alloying was achieved without defect. The composition of Al-CuMgMn alloy is given in Table 5.6. From EDS study, a composition with 32.1 wt.% Cu and 13.1 wt.% Mn was observed. The good metallurgical bonding within the substrate aluminum was free from micro-cracks and porosity.

The EDS result shown in Table 5.5 indicates higher concentration of manganese up to 84.9 wt.%, the minmum concentration was 29.6 wt.%. The composition is supersaturated solid solution due to shorter melting time. Microsegregation was formed due to variations of composition from top alloyed region towards the substrate region. The cooling and solidification effects are other factors, since diffusion process is difficult. In Figure 5.12(a), the rectangle portion indicates the microsegregated manganese. There are studies showing the reason for this. Thermodynamic calculation of AlMn phase diagram was carried out by different researchers—Liu *et al*.(1999) reported formation of stable phases like Al_8Mn_5 and aluminum rich phase 10 at.% Mn, 30 at.% Mn and 100 at.% Mn phases at different temperatures. Janotová *et al*. (2017) presented phase analysis and structure of rapid quenched Al-Mn system made by planar flow casting. The diffusion coefficent of different elements including Mn in aluminum was also reported by Du *et al*. (2003).

Table 5.5 Chemical composition (in wt. %) of AlMn alloy

Spectrum	Mn	Mg	Cu	C	Fe	Si	Zn	Al
1	84.9	1.2	0.2	-	-	0.1	3.8	0.3
3	29.6	10.7	0.9	-	2.5	30.2	11.1	15.1
4	69.1	0.5	-	29.2	-	-	0.4	0.4
5	72.7	13.5	0.4	-	-	0.4	12.2	0.9
6	37.9	14.5	0.5	-	0.5	8.7	30.6	7.3

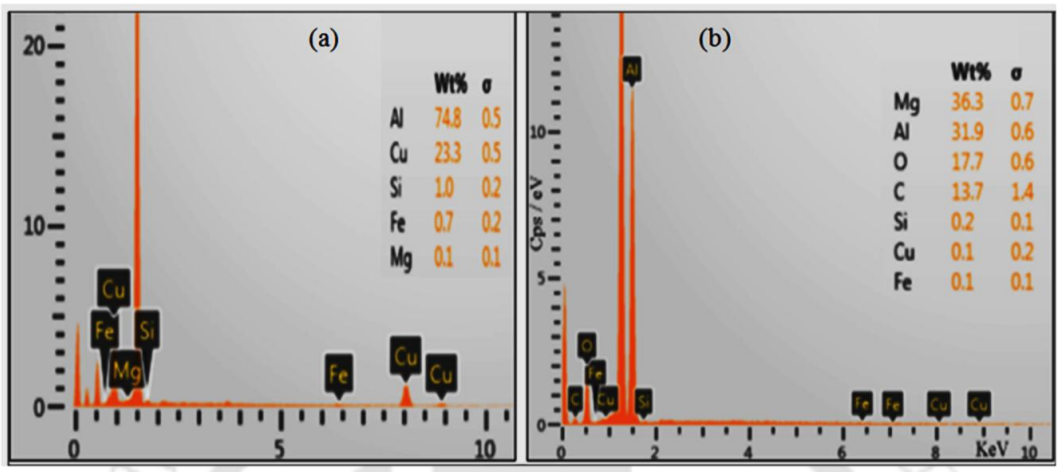

Figure 5.13 Typical EDS spectrum of: (a) AlCu sample and (b) AlMg alloy

Table 5.6 Chemical composition (in wt. %) of Al-CuMgMn alloy

Spectrum	Cu	Mn	Mg	Fe	Si	Al
1	32.1	13.1	0.3	0.2	2.0	52.3
2	26.1	11.0	0.2	0.1	5.8	56.7
3	14.6	8.1	0.3	-	0.4	76.6
4	19.3	4.1	0.2	0.4	4.9	71.1

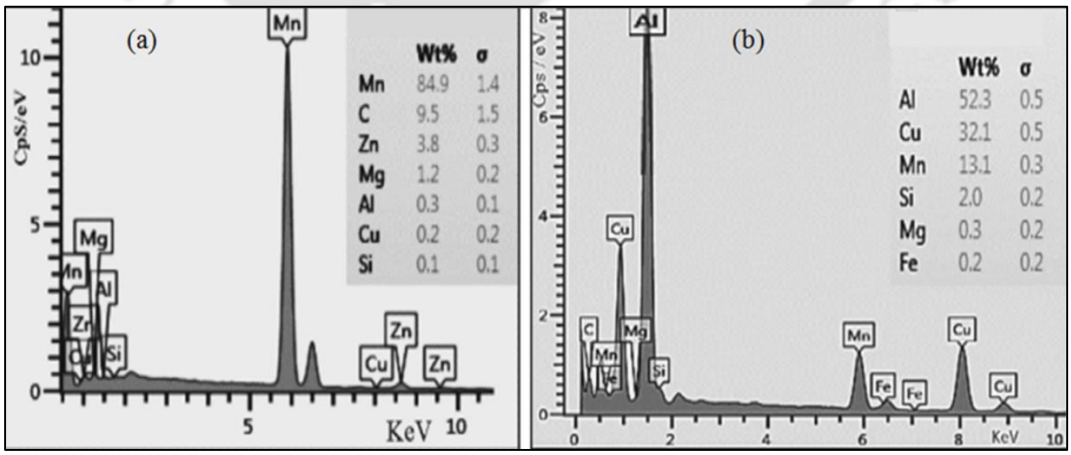

Figure 5.14 Typical EDS spectrum of: (a) AlMn alloy and (b) Al-CuMgMn alloy

5.3.5 Microhardness Analysis

Figure 5.15 shows the hardness result of three samples—1, 2 and 3. These samples were processed by laser parameters given in Table 5.1. The comparison of micro-hardness for the Samples 1, 2 and 3 was done. Addition of alloying elements and formation of intermetallic compounds enhanced its hardness. The maximum hardness achieved in the alloy zone was 430 $HV_{0.5}$ for Sample 1 and 375 $HV_{0.5}$ for Sample 2. The variation in hardness resulted due to the change in laser parameters. The lowest hardness value of 60 $HV_{0.5}$ was formed in the heat affected zone. It can be stated that the hardness decreased from the top alloy region towards the substrate region. This is because of the variation in the concentration of alloying elements, decreasing from top alloy layer towards substrate region. Figure 5.16 shows micrograph of Vickers hardness indentation in alloyed and heat affected areas. The smaller indentation shape as shown in Figure 5.16(a) indicates the alloyed zone with superior hardness. The bigger indentation shape shown in Figure 5.16 (b) indicates that the hardness of heat affected region is much lower than that of alloyed region. The indentation shape is free of edge tearing which shows crack resistance of surface alloyed layer.

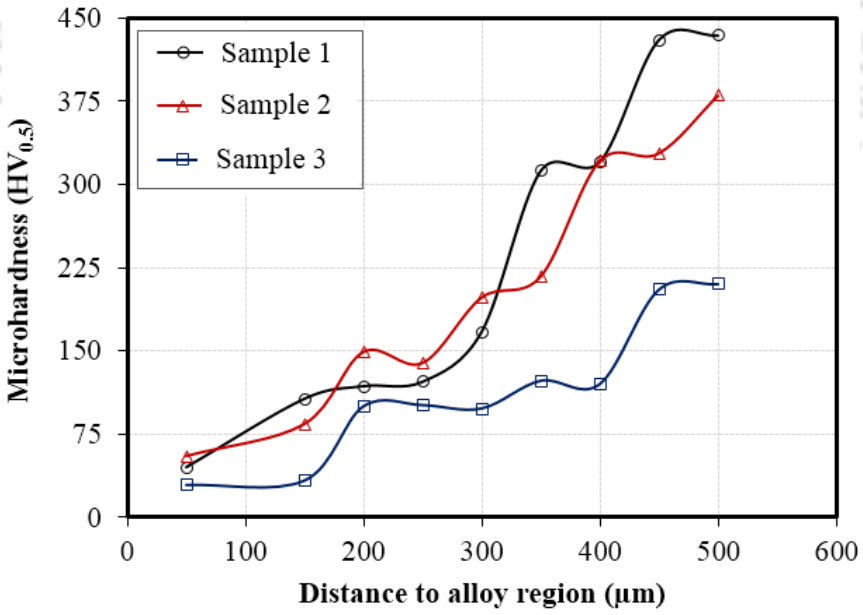

Figure 5.15 Microhardness graph of Al-CuMgMn alloy conducted at 1.7 kW laser power while different laser scan speed and laser beam diameter

The maximum micro-hardness for Sample 1 was due to the deposition of alloying elements on the top surface. In this case, the alloyed height above the surface of the substrate was 1 mm, whilst the alloyed depth was only 0.5 mm. This type of surface alloying may be undesirable due to high alloying height and low dilution depth. Good alloying was obtained with Sample 2 with alloyed depth of 1.4 mm, alloyed width of 3 mm and alloyed height of 0.4 mm. The minimum hardness was obtained for Sample 3 with alloying width of 7 mm and alloyed depth of 2 mm. As seen from Table 5.1, laser specific energy was lesser than the first two samples. Hence, the low hardness obtained in this case was not surprising. Here the alloying elements were scattered on both sides of laser path. Considering Sample 2 as the best, the optimized laser parameters are laser power of 1.7 kW, laser scan speed of 300 mm/min and laser beam diameter of 7.4 mm.

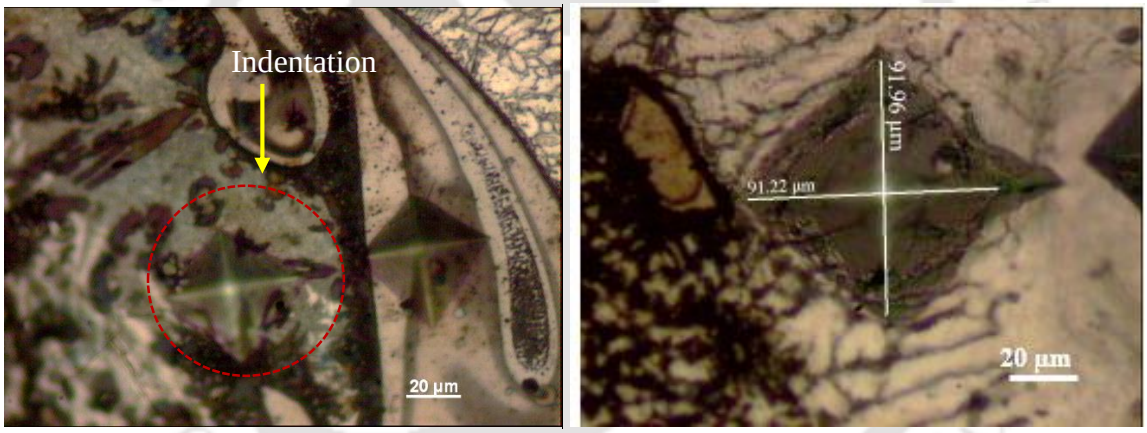

(a) (b)

Figure 5.16 Optical images showing hardness indention (×50): (a) alloyed region and (b) heat affected region

Figure 5.17 shows the micro-hardness value of laser surface alloyed samples for four materials. Micro-hardness of commercially pure aluminum was in the range of 32–33 $HV_{0.5}$. The hardness of all laser surface alloyed samples processed at lower 1.7 kW laser power was higher than the hardness of the samples processed at higher 1.9 kW laser power. The hardness of AlCu alloy was 215 $HV_{0.5}$ for the alloying carried out at a laser power of 1.7 kW. But at higher 1.9 kW laser power, its hardness was reduced to 139 $HV_{0.5}$. For Al-

CuMgMn alloy, maximum hardness of 189 $HV_{0.5}$ was achieved when the laser power was reduced. On the other hand, when the laser power was increased to 1.9 kW, then 118 $HV_{0.5}$ minimum hardness was achieved. It is also observed that for AlMn alloy samples, the hardnesses was 121 $HV_{0.5}$ at low laser power and 78 $HV_{0.5}$ at high laser powers. When compared with other materials, AlMg alloyed sample had least micro-hardness of 97 $HV_{0.5}$ at low laser power and 63 $HV_{0.5}$ at high laser powers.

For 12% increase in the laser power, hardness was reduced by 35% for Al-Cu alloy, 38% for Al-CuMgMn alloy, 36% for AlMn alloy and 35% for Al-Mg alloy. In general, the improvement of hardness for all materials was due to refined grain structure and good metallurgical bonding between alloyed metals with aluminum substrate. In addition to this, fast solidification process of laser beam alloyed created dendrite microstructure. The maximum depth of alloying for all samples was observed for 1.9 kW laser power. However, the hardness at this power is lower than that of 1.7 kW laser power. When the depth of alloying is more, concentration of alloying elements is less, providing low hardness. The order of alloys with decreasing hardness is AlCu, Al-CuMgMn, AlMn and AlMg alloy. In general, surface alloying increased the micro-hardness by 2 to 7 times when laser processing was carried out at 1.7 kW laser power. The effect of laser energy density on microhardness was observed for all materials. For each laser powers of 1.7, 1.8 and 1.9 kW, calculated laser energy density was 357.74, 372.42 and 393 J/mm^2, respectively. From the hardness graphs, as laser energy density increased microhardness for laser surface, alloyed materials were decreasing. Rajamure *et al*. (2014) reported that cumulative weight loss due to wear was minimum when laser specific density was less during laser surface alloying of molybdenum on aluminum. More laser specific energy causes surface damage and deep melting. In this case the alloying material get dispersed reducing the hardness of material. The other factor for reduced hardness with alloy depth was due to coarsening of microstructure with depth of alloying (Nath *et al*., 2012). The present study also found similar broad observations.

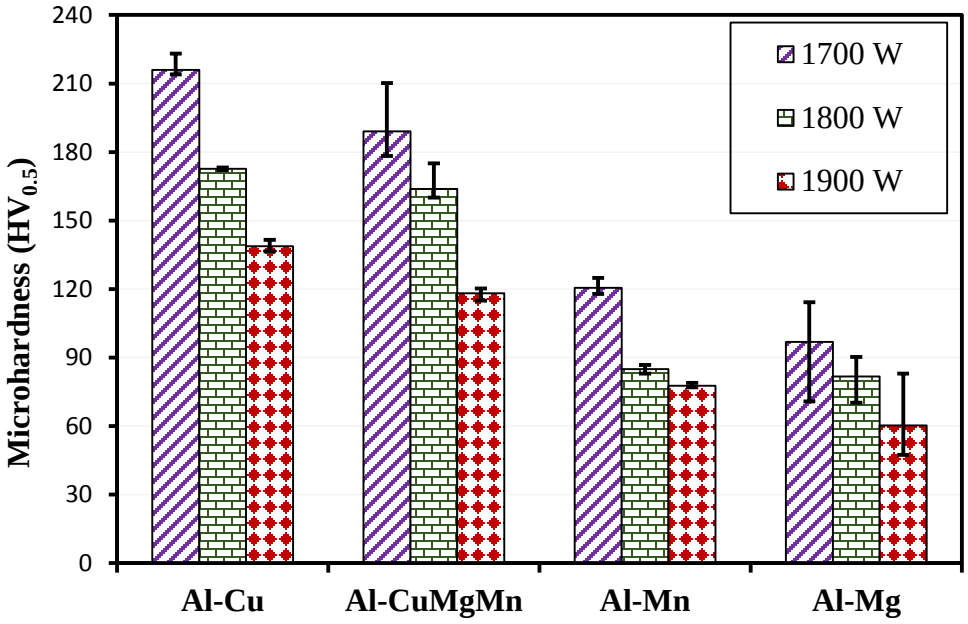

Figure 5.17 Effect of laser power on micro-hardness for different materials at same 500 mm/min laser scan speed and 5.8 mm laser beam diameter. The error bar indicates range

5.3.6 Tensile Strength

Figure 5.18 shows the stress-strain graph of aluminum substrate and laser surface alloyed Al-CuMgMn specimen. The proof stress at 0.2% strain is about 60 MPa and 30 MPa for unalloyed and alloyed specimens, respectively. The ultimate tensile strength is 85 MPa and 83 MPa for unalloyed and alloyed specimens, respectively. No significant change was observed in the ultimate tensile strength, although the hardness was improved as a result of alloying. The improved hardness is good for wear resistance of the alloy formed. The total elongation for aluminum substrate was 35% while it was 23% after laser surface alloyed. Laser surface alloying caused a decrease in total elongation due to its surface hardened effect after alloying aluminum with Cu, Mg and manganese metals. The ductility of a metal is a measure of the plastic deformation that has been sustained at fracture point. Since the alloyed region is a thin layer on the surface, hardness and grain structure got improved but tensile strength did not improve. The reason is that tensile strength is a bulk property and is more or less independent of surface hardness.

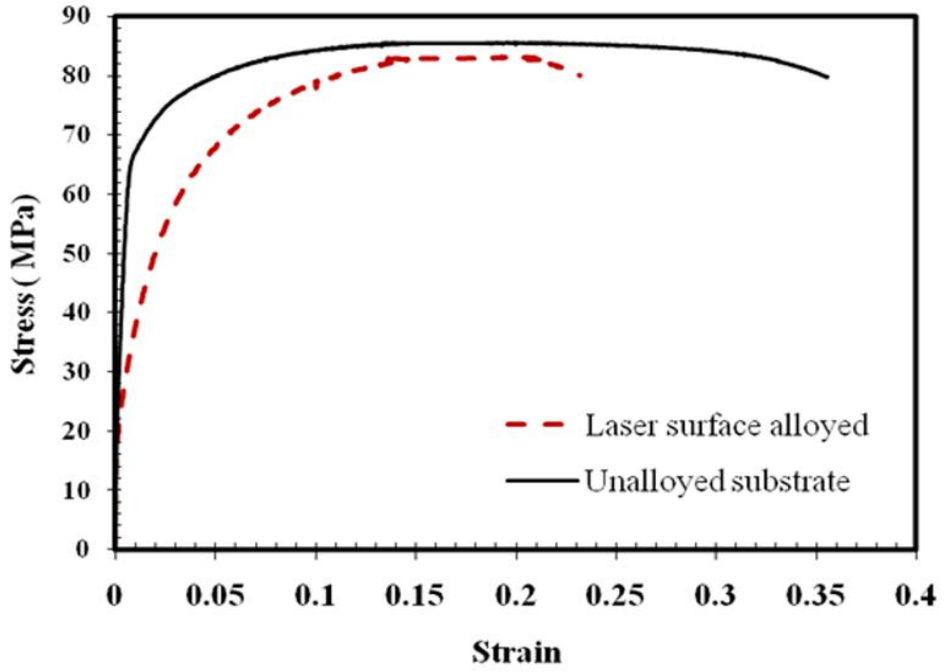

Figure 5.18 Stress-strain graph of laser surface alloyed and unalloyed aluminum substrate processed by 1.7 kW laser power, 300 mm/min laser scan speed and 7.4 mm laser beam diameter

5.4 Conclusion

Microstructure, micro-hardness and tensile strength of laser surface alloyed aluminum substrate with Cu, Mg, Mn and their combination by 2:1:1 ratio was successfully achieved with good results. The following are the major findings:

- The microstructure was very refined dendrite structure, uniform alloying, smooth surface and free from defects.
- Laser power, laser scan speed and laser beam diameter had profound effect on alloy geometry (height, depth and width of alloying).
- The hardness was the maximum at the top and kept decreasing along the depth of alloying.
- At 12% increase in laser power from 1.7 to 1.9 kW, the depth of alloying increased atleast by 15.6% for Al-CuMgMn alloy and 68.75% for AlMg alloy.

- Hardness depended on laser power. For 12% increase in the laser power beyond 1.7 kW, hardness reduced by 35% for Al-Cu alloy, 38% for Al-CuMgMn alloy, 36% for AlMn alloy and 35% for Al-Mg alloy.
- Laser surface alloying had no significant effect on ultimate tensile strength. The yield strength and the total elongation of laser surface alloyed specimens reduced significantly, because of increased hardness due to laser alloying.

Chapter 6

Wear Behavior after Laser Surface Alloying of Aluminum with Copper, Magnesium, Manganese and their Combination

6.1 Introduction

Aluminium is a non-ferrous metal with a wide range of applications in transport vehicles, construction, packaging industry, electronic products and household appliances. The demand of this metal is highly increasing, according to the research presented by Luo and Soria (2007). Whenever two surfaces move over each other, wear will occur by causing damage to one or both surfaces by involving progressive loss of material. Wear is a progressive loss of materials from the surfaces which are in relative motion under load (Suh, 1986). Wear causes an increased clearance between moving components, unwanted freedom of movement and loss of precision. It often leads to vibration that increases mechanical loading and fatigue failure. There are also cases where high wear rate is desirable e,g., in grinding, polishing and other manufacturing processes. Low friction is desirable in some operations e.g., in joints, hinges on doors, bridges and gears in machines (Hutchings and Shipway, 2017). The key solution to control friction and wear involves the use of proper lubrication, design, selection of material and surface modification of engineering parts by different coating processes (Bhushan and Gupta, 1991).

Laser surface alloying is used to improve surface hardness and wear by adding other materials to the existing surface. Mabhali *et al*. (2012) reported laser surface alloying of AA 1200 aluminum with different combinations of Ni, Ti and SiC powders by melting using Nd:YAG laser at 4 kW power. For different ratios of nickel, titanium and SiC, the hardness of laser alloyed region was in the range of 143.69 to 318.64 HV_1, while untreated

aluminum hardness was 24.03 HV_1. A maximum wear improvement of 82% was achieved when 40 wt.% Ni and 20 wt.% Ti and 40 wt.% SiC particles were used. Nath *et al.* (2012) reported laser surface alloying of aluminum with a powder of WC, Co and NiCr in the ratio of 70, 15 and 15. Laser processing was done using Nd-YAG laser of 3–3.5 kW power. The dispersion of metallic carbides increased substrate hardness from 22 to 650 HV that improved the wear resistance and reduced the coefficient of friction. Ravnikar *et al*. (2013) studied ceramic coating of TiB_2-TiC-Al on ENAW6082-T651 aluminium alloy by 3 kW diode pumped Yttrbium fiber laser using laser powers of 1 and 1.2 kW, which increased the surface hardness up to 40%. Labisz (2014) reported laser alloying of Al-Si-Cu cast aluminum with WC ceramic powder using high power diode laser (HPDL), which refined its microstructure and improved hardness properties. Majumdar *et al*. (2006) reported laser surface alloying aluminum by forming hard SiC dispersed composite layer on aluminum substrate. A continuous CO_2 laser was used for melting the pre-deposited (100 μm thickness) of SiC on aluminum that created composite layer. After composite layer was created, the surface hardness reached up to 700–800 HV due to its ceramic nature but the average hardness was about 250 HV and the hardness was decreasing along the depth. The wear resistance also improved after composite layer was formed by laser melting SiC. The improved wear resistance was due to increased microhardness and refined microstructure in laser composite layer.

In this chapter, the focus is on improving the wear performance of commercially pure aluminum by laser surface alloying with Cu, Mg, Mn and their combination. In Chapter 5, the advantages of alloying these metals with aluminum were discussed. In this chapter, the results of wear resistance, coefficient of friction and wear morphology are studied. The effect of load, sliding distance and speed are also investigated.

6.2 Materials and Method

Commercially pure aluminum blocks of dimension 120 mm × 30 mm × 10 mm were prepared. Copper, magnesium and manganese metal powders (each of 99.7% purity) were used as alloying elements. The average particle size of each metal powders was about 10

μm. Each metal powder was separately mixed with a low temperature polymer based Fevigum binder and was pre-placed on aluminum plate surface (area 120 mm × 10 mm) up to 0.3 mm thickness. In the similar way, copper, magnesium and manganese metal powders were mixed in ratio of 2:1:1 to make the fourth sample. The composition of aluminum substrate is 0.1 wt.% Cu, 0.9 wt.% Si, 0.4 wt.% Fe and balance aluminum. A continuous wave CO_2 laser machine was used at three laser powers, *viz.*, 1.7, 1.8and 1.9. Laser scan speed was 500 mm/min and laser beam diameter of 5.8 mm are same in all cases.

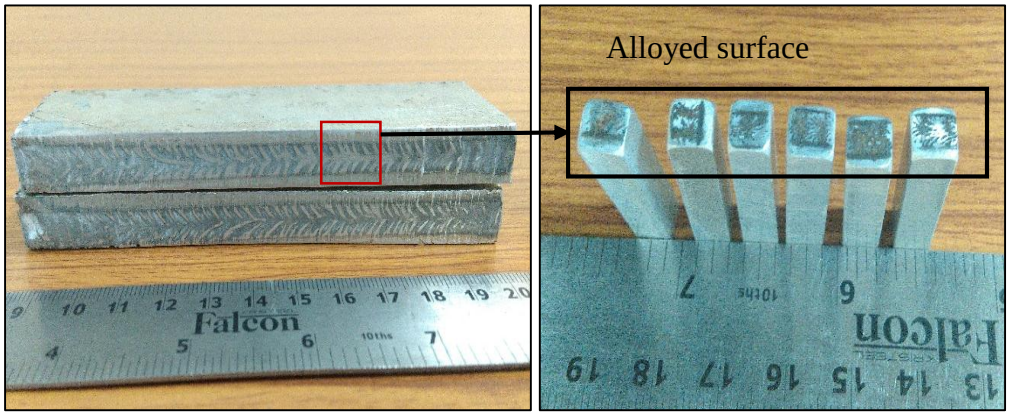

(a) (b)

Figure 6.1 Photograph of: (a) laser surface alloyed sample and (b) square pins samples

Wear test was conducted using pin-on-disc sliding in dry condition for 20 minutes at room temperature, following the ASTM G99/95 standard. Table 6.1 shows test parameters used during wear test. The friction and wear analysis were conducted using pin-on-disc tribometer (Wear and Friction Monitor TR-201, make DUCOM Instruments, India). The pin samples of size 6 mm × 6 mm × 30 mm were prepared from laser surface alloyed region as shown in Figure6.1. As already mentioned, the laser spot diameter was 5.8 mm. Hence, in the pin, the entire surface of 6 mm × 6 mm had good and almost uniform concentration of alloying elements. However, along the 30 mm direction, the concentration gradually dwindled from top surface and became zero after the alloying depth was completed.

After the pin samples were cut according to the size, wear test was carried out with a mating hardened steel disc (84 HRB) of 100 mm diameter and 10 mm thickness. The track was at 70 mm mean diameter. This implies that the relative sliding velocity varied up to the maximum of ±4% with respect to mean sliding velocity. Treating it as a small variation, only average sliding velocity based on the mean diameter was recorded. Friction force and wear was monitored continuously by computer based data system connected with the machine. After the test was completed, the specimen was removed, cleaned by acetone, dried and weighted by a digital machine (Model: BSA224S-CW, Make: Sartorius, Germany) with 0.1 mg accuracy.

Table 6.1 Experimental condition for pin-on-disc wear testing

Parameters	Operating conditions
Normal loads	10 N and 20 N
Sliding speeds	0.5, 1, 1.5 and 2 m/s
Testing time	20 minutes
Relative humidity and temperature	72 % and 24 °C
Wear track diameter	70 mm
Initial roughness of steel disc (R_a)	0.28─0.41 µm
Hardness of steel disc	80 ─ 85 HRB/170 HV
Initial roughness of pin (R_a)	1.05─1.43 µm

6.3 Modified Lancaster Wear Coefficient

Most of the researchers use a measure of sliding wear rate based on a pin-on-disc test. Lancaster, (1967) used the following formula to estimate a wear coefficient *k*:

$$k = \frac{V}{F_n s}, \tag{6.1}$$

where V is the volume of material removed, F_n the normal load and s the sliding distance. He called it wear rate. However, in literature (Pirso *et al*., 2004/2009), it is known as a

wear coefficient. For the case, where the wear volume does not linearly vary with sliding distance, a modified Lancaster wear coefficient can be expressed as follows:

$$k = \frac{1}{F_n}\frac{dV}{ds}. \tag{6.2}$$

In a pin-on-disc test, instead of wear volume, wear mass is measured, which is divided by the density to get the wear volume. In the laser alloyed sample, density keeps changing with the depth. This implies that it changes with the sliding distance. A simple way to estimate the density is explained as follows.

A typical schematic of surfaced alloyed sample is shown in Figure 6.2. It was observed, through EDS (discussed in Chapter 5), that concentration of alloying element changed almost linearly form top towards bottom. At the same time, the alloyed width also keeps on reducing with depth. As an approximation, the concentration C at a given wear depth d can be estimated as

$$C = C_t\left(1-\frac{d^2}{h^2}\right), \tag{6.3}$$

where C_t is the concentration of alloying element at top surface and h is the alloying depth. Knowing the concentration, the density ρ of the alloyed zone can be calculated as

$$\frac{1}{\rho} = \frac{C}{\rho_a} + \frac{1-C}{\rho_b}, \tag{6.4}$$

where ρ_a is the density of the added element and ρ_b is the density of substrate material.

As the wear depth is very small, instead of a variable density over the sliding distance, an average density ρ_{av} can be used. This is obtained by calculating the initial and final densities using Equation 6.4. In that case, the modified Lancaster wear coefficient is given by

$$k = \frac{1}{F_n}\frac{\mathrm{d}}{\mathrm{d}s}\left(\frac{m(s)}{\rho_{av}}\right), \tag{6.5}$$

where $m(s)$ is the wear mass as a function of sliding distance. In the present work, $m(s)$ was obtained by curve fitting of the data.

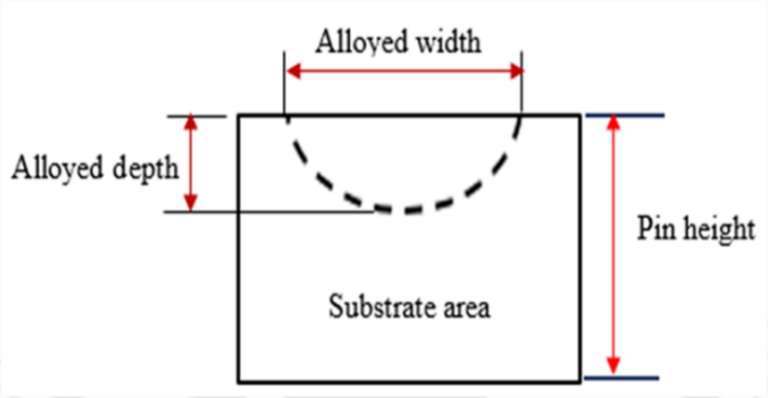

Figure 6.2 Schematic of pin showing the profile of the alloyed zone

6.4 Results and Discussion

This section comprises results of pin on disc wear testing for four materials—AlCu, AlMg, AlMn and Al-CuMgMn alloys. Wear mass loss, wear coefficient and coefficient of friction were studied after laser surface alloying. The wear surface morphology was also investigated.

6.4.1 Wear Analysis

Study of wear was carried out for the samples having high hardness. Hence, the samples processed at a laser power of 1.7 kW, scan speed of 500 mm/min and laser beam diameter of 5.8 mm were selected for the study of wear behavior. Figures 6.3(a–b) depict the wear mass loss for different materials. The effect of normal load and sliding distance were observed on wear values. The corresponding nominal pressures were 0.28 MPa and 0.56 MPa for 10 N and 20 N loads, respectively. These values were far less than the yield strength of aluminum. It was observed that the mass loss due to wear, increased in an exponential manner as the sliding distance was increased from 600 m to 2400 m. Curve fittings were done for different cases. In most of the cases, the coefficient of determination (R^2) was close to 1, indicating a good fitting. Fitted equations providing the loss of mass

with sliding distance, *m(s)*, were used to determine the modified Lancaster wear coefficient in Equation 6.5. As *m*(*s*) is of exponential form, the wear coefficient *k* also increases exponentially with the sliding distance. Interestingly, Rajmure *et al*. (2014) did not observe an exponential increase in the wear mass with sliding distance. However, the sliding distance in their experiments was limited to 160 m. In the present case, the sliding distance was up to 2400 m. As the sliding distance increased, the concentration of the alloying element decreased, reducing the hardness. Hence, the wear kept on increasing rapidly with the sliding distance.

The maximum mass loss at 10 N load for pure aluminum was 0.05 g. The highest improvement in mass loss due to wear was achieved for AlCu alloy, followed by for Al-CuMgMn alloy. At the maximum sliding distance, AlCu alloy showed 50% less wear as compared to Al substrate. For Al-CuMgMn alloy, wear resistance improved by 30%. Al-CuMgMn alloy developed an excellent wear resistance due to the presence of copper. Both AlMn and AlMg alloys had also improved the wear resistance since mass loss due to wear for these alloys were less than un-alloyed aluminum. When the normal load was doubled, wear volume loss for pure aluminum got increased by 39%. For all materials, as the normal load was doubled, wear weight loss increased by 1.4–3.2 times.

It is interesting to observe that on an average doubling, the normal load increased the wear by two times. In this load range, an asperity based model predicts almost linear increase of the contact area with increasing normal load (Mao *et al*., 2016). Doubling the normal load, doubles the contact area, keeping the same pressure, due to which the wear doubles. However, there are a number of noise factors present, such as varying adhesion behavior of material, variation in the surface topography and variation in the micro-hardness. Hence, the asperity based model is able to predict only the average behavior. The ranking of the laser surface alloyed materials in the order of decreasing wear resistance is AlCu alloy, Al-CuMgMn alloy, AlMn alloy and AlMg alloy. For each graph, the corresponding equation is shown in Figure 6.3. The upper one is for pure aluminum and the lower one is for AlCu alloy. Rajamure *et al.* (2014) investigated wear cumulative weight loss increased when sliding distance was increased during laser surface alloying molybdenum on aluminum.

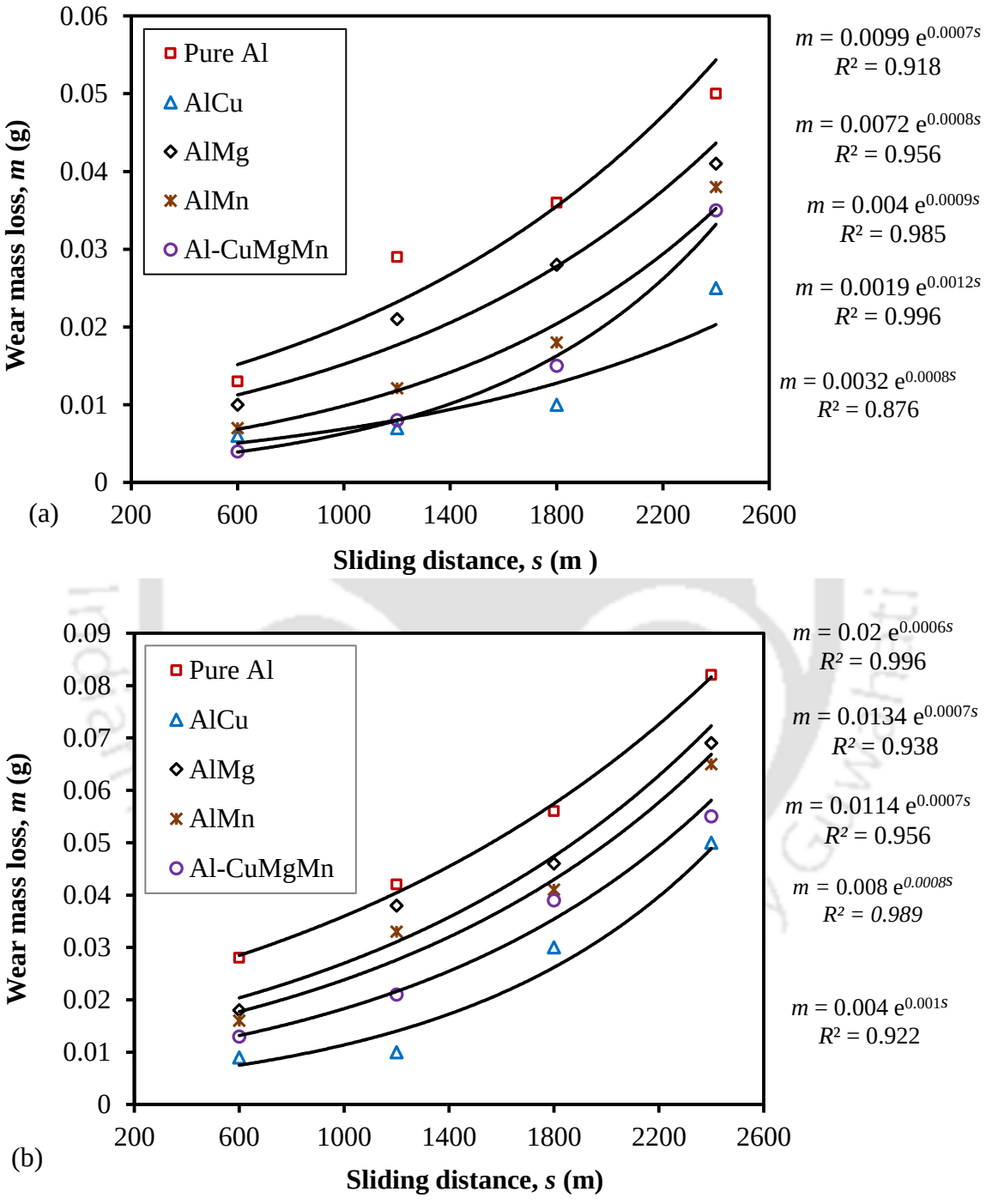

Figure 6.3 Effect of sliding distance on wear mass loss, 1.7 kW laser power, 500 mm/min laser scan speed and 5.8 mm laser beam diameter: (a) 10N load and (b) 20N load

Wear of material depends on many properties, like load, sliding distance, working temperature, surface condition and material property like hardness. The relation of hardness and wear resistance of materials can be explained as follows:

$$V_w = k_1 \frac{F_n L}{H} \tag{6.6}$$

where V_w is wear volume loss, k_1 is Archard's wear coefficient, F_n is normal load, L is sliding distance and H is material hardness. From adhesive wear model and abrasive wear, the volume of worn material removed V_w as a result of tribological interaction is directly proportional to the load F_n and sliding distance L. less wear is formed when the hardness of a soft material is increased, showing wear is inversely proportional to material hardness. Although this was first proposed by Holm, Archard first obtained it using simplified model of contact interaction (Archard and Hirst, 1956). The work of Luyckx and Love, (2004) shows an increase in wear resistance with an increase in the hardness of the material. Other study shows a decrease in the specific wear with an increase in hardness (Tomida *et al*., 2001). Moore (1974) reported an increase in wear resistance of material with an increase in bulk hardness.

Wear volume loss is calculated from experimental measured wear mass loss as a function of sliding distance from curve fitting shown in Figures 6.3(a) and 6.3(b) divided by modified density after alloying (ρ_{av}). The calculated Archard wear coefficient is given in Table 6.2. It is seen that this coefficient is dependent on the type of material and load. In general, the coefficient is lesser for higher load.

Table 6.2 Archard wear coefficient k_1 (10^{-3} mm^3s^2/kg) for different materials

Distance (m)	**Pure Al**		**AlCu**		**AlMg**		**AlMn**		**AlCuMgMn**	
	10 N	20 N	10 N	20 N	10 N	20 N	10 N	20 N	10 N	20 N
600	31.2	29.6	57.7	81.3	82.5	72.3	23.8	30.1	40.5	67.0
1200	23.7	21.2	46.6	74.1	66.7	55.0	20.4	22.9	41.6	54.2
1800	24.1	20.3	50.2	90.0	71.8	55.8	23.4	23.2	57.0	58.4
2400	27.5	21.8	60.9	123.0	87.1	63.7	30.1	26.5	87.8	70.7

Table 6.3 shows the calculated modified Lancaster wear coefficient for different laser surface alloyed materials at 10 N and 20 N loads. The wear coefficient of those materials increased when sliding distance was increased. However, when the normal load was doubled, the wear coefficient was reduced. For pure aluminum, the wear coefficient was increased from 3.59×10^{-4} to 12.66×10^{-4} $mm^3/N.m$ for 10 N load and the sliding distance was increased from 600 to 2400 m. When load was doubled, wear coefficient was increased from 3.19×10^{-4} to 9.38×10^{-4} $mm^3/N.m$. For AlCu, the wear coefficient was 1.29×10^{-4} and 5.44×10^{-4} $mm^3/N.m$ and for 10 N load, the sliding distances were 600 m and 2400 m respectively. Except for AlMg alloy, other laser surface alloyed materials reduced wear coefficient than pure aluminum material. AlMg alloy had less wear mass loss than pure aluminum, but its density was smaller than aluminum that resulted in high wear volume. All other materials had less values of wear coefficient than aluminum substrate. Tomida *et al.* (2001) reported a decrease in specific wear as an increase in surface hardness during laser surface alloying TiC and Cu in aluminum substrate. Man *et al*. (2007) also reported that wear volume loss increased when wear time increased during laser surface alloying AA 6061 aluminum alloy with NiTi metals.

Table 6.3 The modified Lancaster wear coefficient k (10^{-4} $mm^3/N.m$) for different materials

Distance (m)	**Pure Al**		**AlCu**		**AlMg**		**AlMn**		**AlCuMgMn**	
	10 N	20 N	10 N	20 N	10 N	20 N	10 N	20 N	10 N	20 N
600	3.59	3.19	1.29	1.14	4.08	3.12	1.06	1.05	1.54	1.70
1200	5.46	4.57	2.08	2.07	6.60	4.75	1.82	1.60	3.19	2.75
1800	8.32	6.54	3.36	3.77	10.66	7.22	3.13	2.43	6.51	4.45
2400	12.66	9.38	5.44	6.87	17.23	10.99	5.39	3.70	13.37	7.19

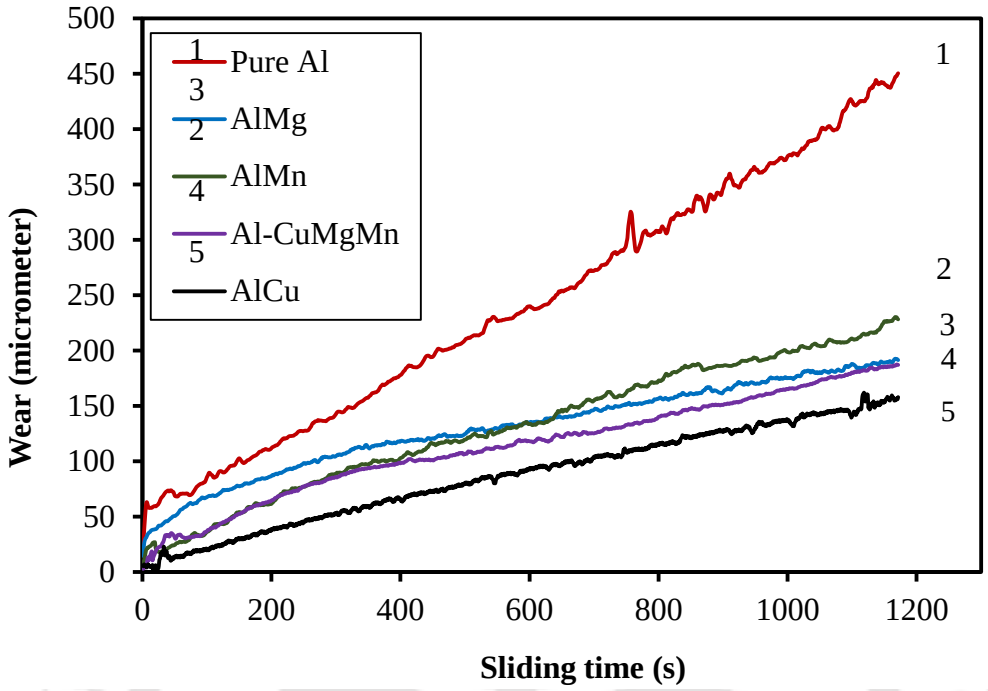

Figure 6.4 Online wear values of laser surface alloyed samples and aluminum for 20 N normal load and 2 m/s sliding speed

Figure 6.4 shows the plot of online wear measured by a linear variable differential transducer in micrometer as a function of sliding time when 20 N load and 2 m/s sliding speed were used. The maximum wear observed for pure aluminum was 450 µm. After laser surface alloying with different materials the wear got reduced. For all materials, wear resistance improved after individually alloying aluminum with copper, magnesium and manganese. It is also true that after alloying with Cu, Mg and Mn by ratio of 2:1:1, the wear resistance improved. For all materials, the effect of sliding distance on wear value was observed. The wear increased linearly with sliding distance. The abrasive wear rate of AA1200 aluminum was maximum when compared with laser surface alloyed samples with nickel, titanium and SiC material (Mabhali *et al.*, 2012).

6.4.2 Study on Coefficient of Friction

The average coefficient of friction for laser surface alloyed samples and aluminum substrate is shown in Table 6.3. It was evident that laser surface alloying reduced the frictional resistance of the surface. In some cases, the coefficient of friction got reduced

when the sliding speed was increased. However, it was not always same for some materials. As the sliding speed was increased, the interface temperature got increased and the material got softened. Softening of the material helps in reducing the coefficient of friction because the lubricating oxide film was not removed. In most cases, the coefficient of friction reduces with the normal load. This is consistent with the asperity based model of friction (Mao *et al*., 2016). The roughening of the surface during wear was due to the removal of soft aluminum and hard carbides in the microstructure. In the present case, as the hardness difference between alloying and alloyed element was not high, wear debris of these alloying elements provided better lubrication as compared to hard carbides. It also reduced coefficient friction.

Figure 6.5 shows the effect of the processing laser power on the coefficient of friction for Al-CuMgMn alloy. At 0.5 m/s sliding speed, the coefficient of friction was significantly less for 1.9 kW processing laser power than that for 1.7 kW processing laser power. This was because the material alloyed at 1.9 kW laser power was softer than that of laser alloyed at 1.7 kW laser power. The asperity based model also shows that softer materials have less frictional resistance. As the hardness decreases, the plasticity index increases causing a decrease in the coefficient of friction (Mao *et al*., 2016). However, at 1 m/s sliding speed, the coefficient of friction was the highest for the material processed at 1.9 kW power. This anomalous behavior may be due to considerably more wear at this speed, producing more debris that get entrapped in the softer pin and make it harder. At the same time, lubricating oxide layers also get broken down, which contributes to the increase in friction. The asperity based model predicts slight reduction in the coefficient of friction with increasing normal load (Mao *et al*., 2016). This may cause the reduction in wear coefficient too; however, at the range of applied loads, the reduction should be much smaller than what is observed.

Table 6.4 Calculated value of average coefficient of friction at 1.7 kW laser power, 500 mm/min scans speed and 5.8 mm laser beam diameter

Sliding speed (m/s)	AlCu		AlMg		AlMn		Al-CuMgMn		Pure Al	
	10N	20N	10N	20N	10N	20N	10N	20N	10N	20N
0.5	0.50	0.49	0.44	0.26	0.38	0.55	0.53	0.49	0.62	0.56
1.0	0.35	0.31	0.50	0.32	0.58	0.51	0.50	0.41	0.60	0.46
1.5	0.40	0.40	0.28	0.42	0.45	0.39	0.38	0.36	0.60	0.57
2.0	0.25	0.33	0.45	0.50	0.34	0.44	0.25	0.35	0.59	0.58

In the case, 1.5 m/s and 2 m/s sliding speeds, the coefficient of friction does not depend significantly on the processing laser power. It is envisaged that there were two contradicting mechanisms under operation. When the processing laser power was increased, the material got softened and reduced the coefficient of friction. On the other hand, due to wear, the lubricating layers got removed, which tended to reduce the coefficient of friction. As a result, the coefficient of friction remained almost constant for all the samples processed at different laser powers. Staia *et al*. (2000) reported that higher sliding speed has relatively lower coefficient of friction than lower sliding speed during laser surface alloying of A-356 aluminum with WC, Ti and Mg metals. The online coefficient of friction at 20 N normal load and 2 m/s sliding speed is plotted in Figure 6.6. The plot shows initial peaks followed by stable zones. This is an indication of static coefficient of friction being more than the dynamic coefficient of friction. The wavy nature of the coefficient of friction was an indication of the stick-slip phenomenon as well as the role played by the debris due to wear action.

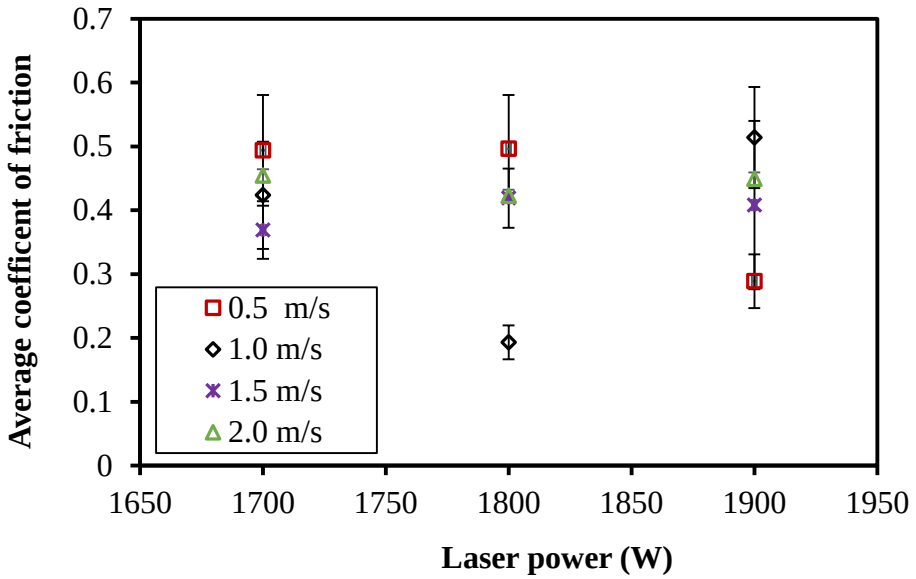

Figure 6.5 Effect of laser power and sliding speed on coefficient of friction for Al-CuMgMn alloy when 20 N loads was used, 500 mm/min laser scan speed and 5.8 mm laser beam diameter The error bar indicates standard deviation

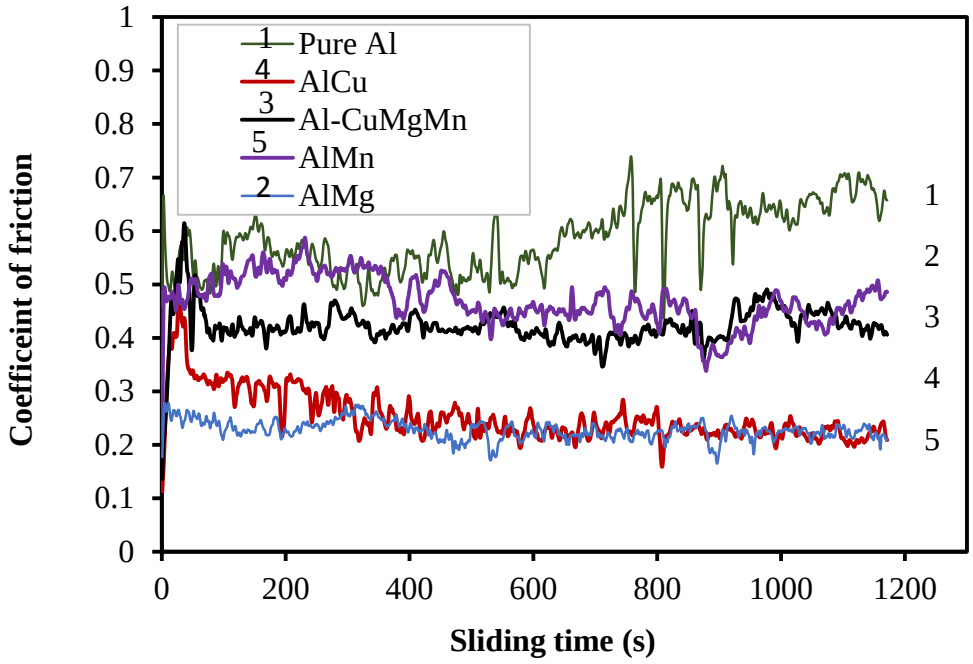

Figure 6.6 Comparison of coefficient of friction for aluminum substrate and laser surface alloyed samples at 20 N load and 2 m/s sliding speed

6.4.3 Worn Surface Morphology

Figures 6.7 (a–d) show the worn out surface and its corresponding EDS composition analysis. The wear testing was conducted at 20 N load and 2 m/s sliding speeds for 20 minutes. Figure 6.7 (a) shows AlCu alloy where 3.9 wt.% Cu was observed after wear testing. For AlMg alloy, 0.2 wt.% Mg was present as shown in Figure 6.7 (b). For AlMn alloy, worn surface morphology was 5.6 wt.% Mn composition. For Al-CuMgMn alloy, the worn surface composition was 1.6 wt.% Cu, 1.6 wt.% Mn and 0.8 wt.% Mg after wear test. In all cases, laser surface alloying had improved wear resistance. Wear mechanism was observed from worn surface morphology. More materials were removed from the softer materials than the harder materials which were formed by alloying. The material removal process during wear action was formed in the form of scuffing, galling and shearing. In harder materials like AlCu alloy and Al-CuMgMn alloy, micro-cutting was formed. Abrasive wear and adhesive wear were observed. It was also observed that plastic deformation was created for softer materials like AlMg alloy and AlMn alloy.

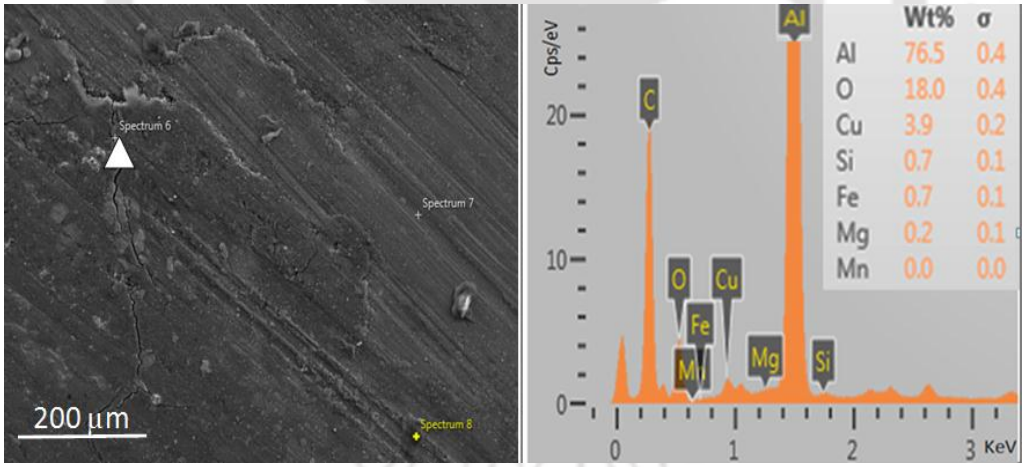

(a)

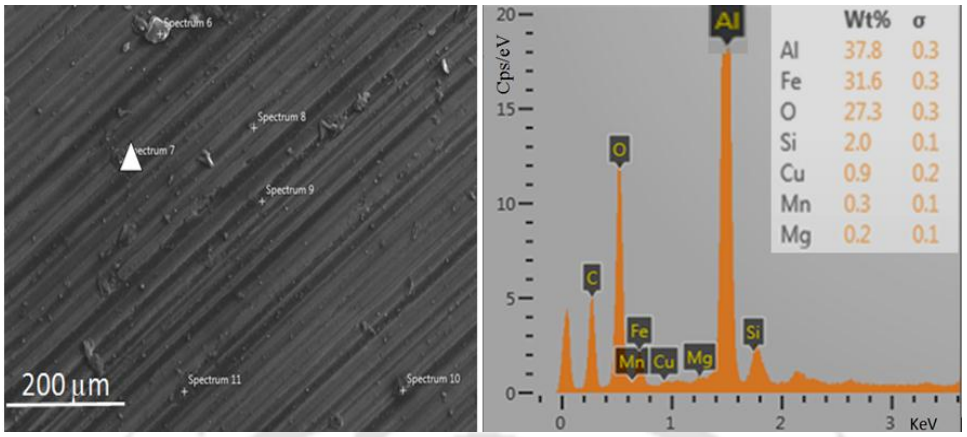

(b)

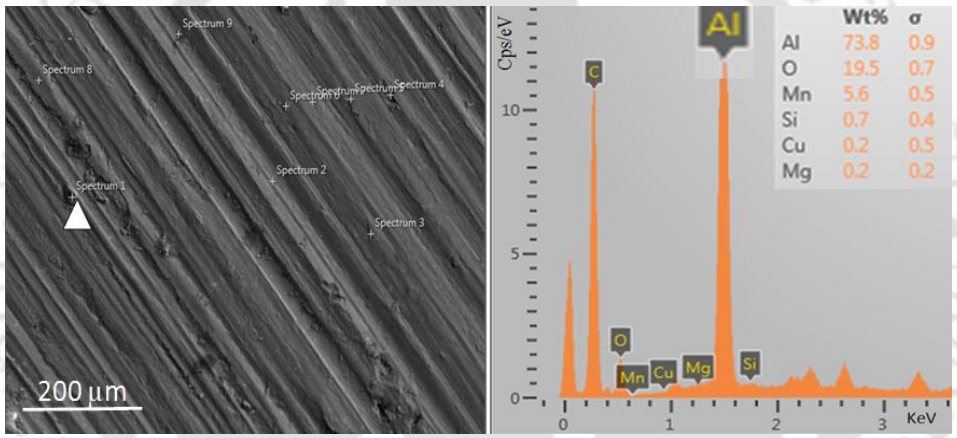

(c)

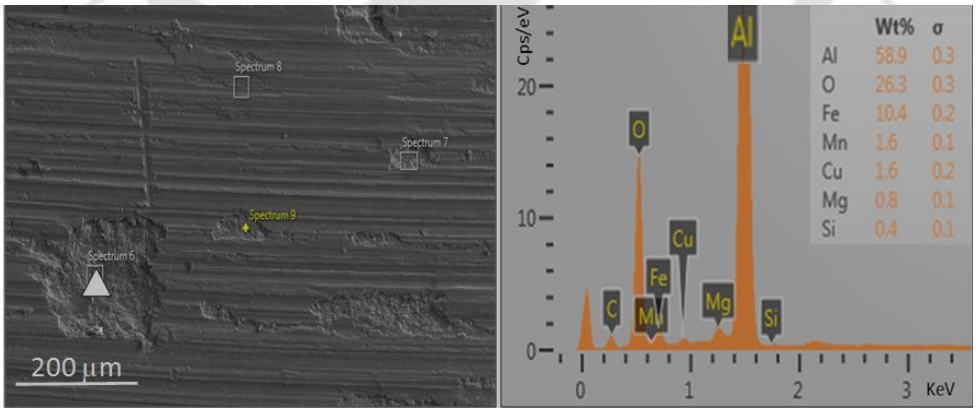

(d)

Figure 6.7 EDS composition of worn surface morphology: (a) AlCu alloy, (b) AlMg alloy, (c) AlMn alloy and (d) Al-CuMgMn alloy at 20 N load and 2 m/s sliding speed

6.5 Conclusion

Laser surface alloying of commercial pure aluminum with copper, magnesium, manganese and their combination was successfully achieved. The following are the major findings of the work:

- Laser surface alloying increased the wear resistance after alloying with different metals.
- For all samples processed by 1.7 kW laser power, 500 mm/min scan speed and 5.8 mm laser beam diameter, wear mass loss was reduced by 30–50 % for 10 N normal load at 2 m/s sliding speed.
- For all materials, a twofold increase in the normal load had increased wear mass loss by 1.4–3.2 times. This affirms that in a statistical sense, the wear is proportional to normal load.
- The ranking of laser surface alloyed samples in the order of decreasing wear resistance is AlCu, Al-CuMgMn, AlMn and AlMg samples.
- In some cases, as the processing laser power increases, the coefficient of friction reduces due to the reduction in the hardness as evident from an asperity based model.
- The generation of debris and break down of lubricating oxide layer splay their role.
- Study of wear scar morphology shows different types of wear such as adhesive wear, abrasive wear and delamination wear were formed.

Indian Institute of Technology Guwahati

Chapter 7

Corrosion Behavior After Laser Surface Alloying Aluminum with Different Metals

7.1 Introduction

Aluminum alloys are corrosion resistant due to passivation behavior of oxide, formed on their surfaces. When the material interacts with the aggressive working environment like strong acid and base, the protective oxide layer breaks and corrosion starts. According to Bardal, (2007) three main categories of corrosion are as follows—(i) wet corrosion where the corrosive medium is water with dissolved species, (ii) corrosion in fluids such as fused salts and molten metals and (iii) dry corrosion where dry gases exist. As the corrosion proceeds, the metal dissociates and is transferred to the corrosive medium as ions. The released electrons from the metal are consumed in cathodic reaction. The surrounding medium is the conducting liquid electrolyte forming a closed electrical circuit (Rosliza *et al*., 2008; Kaesche, 2012). The most corrosive working environments include petrochemical industries, offshore wells and oceans. Examples of critical engineering components requiring protection from corrosion are gas turbine, components of aircraft, structural components, heat exchangers and water tanks containing pollutants. The aqueous chloride salts and acid solutions are aggressive working environments for corrosion of metal structures. The chemicals like hydrochloric acid solutions cause huge damage to metals and alloys like copper and stainless steel. The corrosion behaviors of copper 90° elbow in an acidified dichromate solution and stainless steel 90° elbow in hydrochloric acid of 6 molar solution were studied (Fouad *et al*., 2017). The corrosion rate was higher for copper and relatively lower for stainless steel.

El-Sherbini *et al.* (2003) reported the corrosion of aluminum by weight loss and potentiodynamic polarization test in 1.0 M HCl and 1.0 M H_2SO_4 solutions in the temperature range of 25–55 °C. For both the solutions, the corrosion protection decreased as the temperature increased from 25 to 55 °C. Branzoi *et al.* (2002) reported the effect of organic inhibitors in pure aluminum acid solution of 0.5 M HCl. The use of organic inhibitor enhances the corrosion resistance of pure aluminum. Popoola *et al.* (2011) reported laser surface alloying of AA 1200 aluminum with 50% Cu + 50% Mo metals by Nd:YAG laser. Pitting corrosion resistance of the laser surface alloyed sample was more than that of the aluminum substrate. Laser surface alloying was often employed for protecting the surface from wear and corrosion (kwok and Wong, 2010). Moorthy and Srinivas, (2016) reported corrosion weight loss of different metals like copper, aluminum, mild steel and brass due to automotive base coolants. The automotive coolants cause corrosion to important engine components. A weight loss in the range of 21–367 mg was observed in aluminium due to corrosion attack with different base coolants. Hinton, (1995) reported the corrosion in aluminum and magnesium alloys in the form of pitting and white powdery deposits on their surface. Kamoutsi *et al.* (2006) reported that pitting corrosion of aluminum is caused when chloride ions attack the metal. The corrosion immersion test and weight loss method were the simplest and most direct measurement of corrosion of any kind. Titanium and its alloys are known for its high strength and corrosion resistance properties. Laser surface alloying of titanium with Si, Al and mixture of silicon with aluminum was reported by Majumdar *et al*. (1999). The results show that laser surface alloying with Si or Si + Al has a good effect on improving oxidation resistance of titanium. This enhanced oxidation resistance is due to the presence of thin adherent Al_2O_3/SiO_2 oxide layer on the surface. Abboud and West (1990) reported that laser surface alloying of titanium with aluminum resulted in the formation of columnar grain at the interface and martensite plate in the solid state within the grain.

Aluminum-zinc alloys with high amount of aluminum (designated as ZA alloys) were used in a material of die castings alloys. Zinc is known for corrosion protection of steel structures in the form of galvanized coating. Ares and Gassa, (2012) reported

corrosion resistance of Zn-Al alloys in 3% NaCl solution at room temperature and indicated that the columnar morphology has a higher value of charge transfer resistance than equiaxed grains. Thus corrosion resistance is more for Zn-Al alloy. Yang *et al.* (2012) studied the influence of Al content on the corrosion behavior of extruded superplastic Zn–Al alloys in the simulated acid rain. It was observed that with increasing Al content corrosion rate decreased.

In this chapter, improving the corrosion resistance of aluminum was achieved by laser surface alloying with magnesium (Mg), manganese (Mn), titanium (Ti) and zinc (Zn) metal powders using a continuous wave of 2.5 kW CO_2 laser cutting machine.

7.2 Materials and Method

The processes of sample preparation and coating with alloying elements, laser surface alloying and study of the microstructure/morphology are discussed. The procedure of corrosion immersion test in 2.5 % H_2SO_4 solution is discussed in details. Aluminum blocks with a dimension of 100 × 50 × 10 mm^3 were initially prepared. The composition of aluminum substrate was 0.1 wt.% Cu, 0.9 wt.% Si, 0.4 wt.% Fe obtained using EDS test. Magnesium, manganese, titanium and zinc powders were separately coated on the base material after making a slurry of metal powders with adhesive Fevigum (make: Hira Industries, India). Both Mg and Mn had average particle size of 10 μm. Titanium had an average particle size of 47 μm and zinc had an average particle of 10 μm. The coating thickness was 0.3 mm as measured using optical profilometer and Vernier caliper. Pre-placed samples were cured for two days at room temperature. In order to get the wider alloy region, two parallel laser passes were made using 1.6 kW laser power for Mg alloying and 1.8 kW laser power for others. Laser interaction time, beam spot diameter and laser scan speed were 7.5 s, 7.4 mm and 400 mm/min, respectively. The hardness test of laser surface alloyed samples before and after corrosion test was conducted using Vickers hardness testing machine.

The weighted samples of laser surface alloyed AlMg, AlMn, AlTi and AlZn, as well as pure aluminum, were separately tested in 2.5% H_2SO_4 acid, having a pH of 0.074. After mounting the samples with a high corrosion resistant phenolic polymer, laser surface alloyed samples with top surface area of 100 mm^2 were exposed to corrosive medium for

200 hours at room temperature. The cross-section of the sample that revealed both alloyed area and substrate area was also exposed for corrosion test in order to analyze the interface region after corrosion. Later the samples were removed and cleaned with acetone and weighted by electronic weighing machine with 0.1 mg accuracy in order to find out the weight loss due to corrosion. The depth and width of the corrosion pit were measured by a non-contact optical surface profilometer. The corroded surface morphology was examined by high-resolution FESEM test. Before the corrosion test, pH of the solution was measured using pH meter (pH 2700, make: Eutech, Singapore).

7.3 Results and Discussion

Under the following subsections, metallurgy of laser surface alloying, corrosion surface evaluation and mechanism of corrosion are discussed. The effect of corrosion on the microhardness of laser surface alloyed sample is also discussed. A comparison of 4 alloying elements is made.

7.3.1 Microstructure and XRD Phase Analysis

Phase analysis was conducted using XRD machine on the samples of laser alloyed surface. The XRD patterns of laser surface alloyed samples are shown in Figure 7.1. The formation of different phases were confirmed from standard JCPDS data. For AlMg sample, a cubic crystal of Al_2Mg phase was formed during laser surface alloying (card number 96-900-2072). For AlMn alloying, there was a formation of new phase of Al_3Mn_2 having orthorhombic crystal structure (card number 96-434-3336). For titanium alloying with aluminum, a new phase of Al_2Ti was identified by XRD analysis (card number 961528044). The crystal had an orthorhombic structure. For zinc alloying, there was no phase difference and hence a new phase was not observed from XRD pattern; only aluminum peaks were dominating.

Figures 7.2 (a–b) depict optical images of AlMg alloy, where columnar grains were formed near the bottom interface and the networks of dendrite grains were formed near the top and center of the alloyed region (right of the arrow). The dendrite microstructure were

formed near the top region of the alloyed area. The formation of dendritic structure improved the mechanical properties such as the hardness.

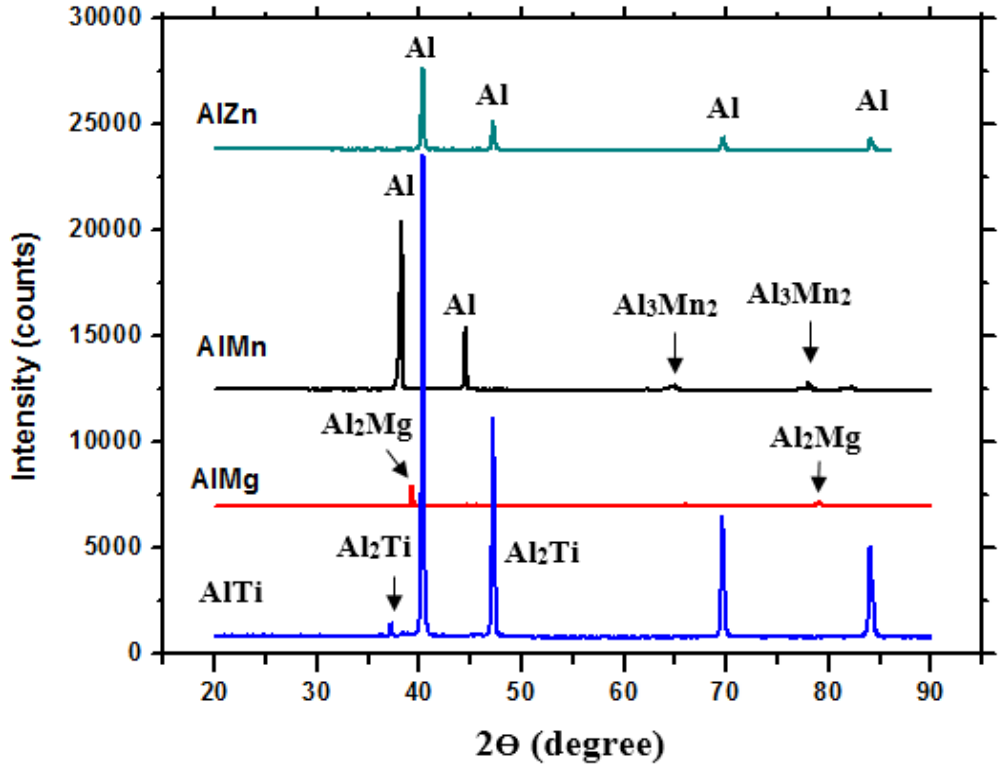

Figure 7.1 XRD pattern of laser surface alloyed samples

Further investigation of laser surface alloyed morphology was made using FESEM as shown in Figure 7.2 (c). The morphology of alloyed region had excellent metallurgical bonding with aluminum substrate. No porosity and micro-cracks were formed during laser surface alloying. As observed in the morphology, the small particles were well bonded together that helped to increase the hardness and corrosion resistance of AlMg alloy formed by laser surface alloying. The advantage of laser surface alloying was to allow the controlled heat input in short duration. Thus, solidification was fast to form fine grained dendritic structure.

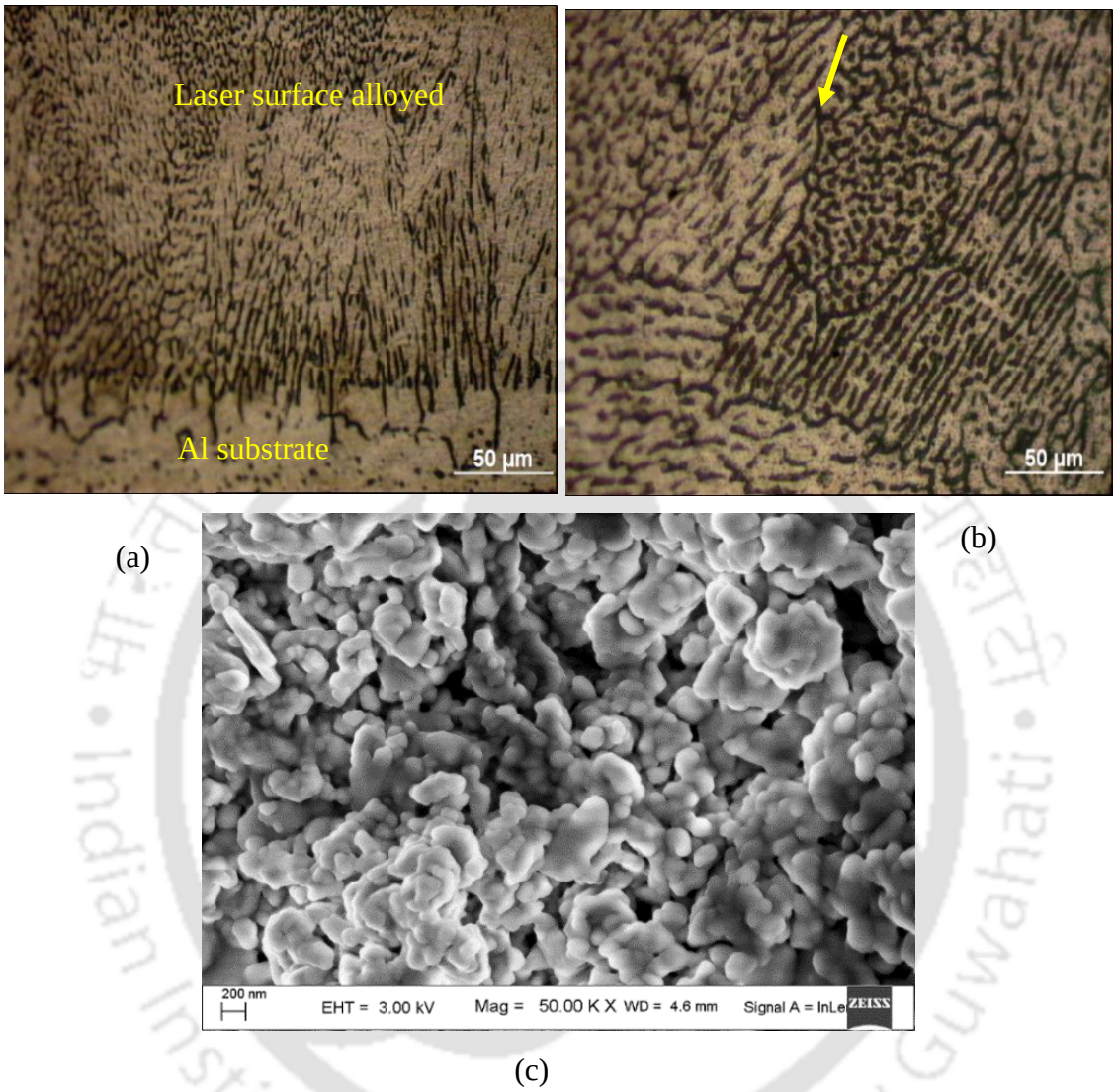

Figure 7.2 Microstructure of AlMg laser surface alloyed sample (a, b) optical images (× 20) and (c) morphology of laser surface alloyed region (×50 k)

The results of microstructure and morphology of laser surface alloyed AlMn sample are shown in Figures 7.3 (a–c). The refinement of grain structure and good metallurgical property were obtained. The optical images shown in Figure 7.3 (a–b) depict the formation of the columnar grain structure. The upper portion had very fine grain structure that was closely clustered without any defects like porosity. This upper portion had a tendency to form the dendritic grain structure above the imaginary line of the arrowhead as shown in Figure 7.3 (b). The upper alloyed portion grains were closely

packed as compared to the grains of the lower portion. The formation of fine grain structure in materials has the advantage for improving its mechanical properties like hardness and strength. The morphology had fine grains and had lateral connections with next grains (arrowhead Fig. 7.3c). No defect in the morphology of the alloy was observed even at high magnification of 150 k. Manganese particles strongly bonded with aluminum particles result in good surface hardness and wear. Since the property of materials depends strongly on its microstructure, laser surface alloying should be applied to maintain a good alloying without defects.

Figures 7.4 (a–c) show the microstructure of laser surface alloyed aluminum with titanium. Figure 7.4 (a) indicates the interface region of the alloyed zone and substrate region. This confirmed that a good metallurgical alloying was done. The dendrite microstructure near the top alloyed region was formed as shown in Figure 7.4 (b). The morphology of AlTi alloyed sample was examined using FESEM as shown in Figure 7.4 (c) confirmed that there was no internal defect in the alloy. The dark portions show dispersion of titanium particles in the morphology of AlTi alloy. Due to good laser surface melting, uniformity of particles was observed. This improves the surface performance of AlTi alloy with respect to wear and corrosion. Abboud and West, (1990) indicated that the columnar grains grow epitaxially from the melt substrate interface towards the top surface during laser surface alloying of titanium with aluminum.

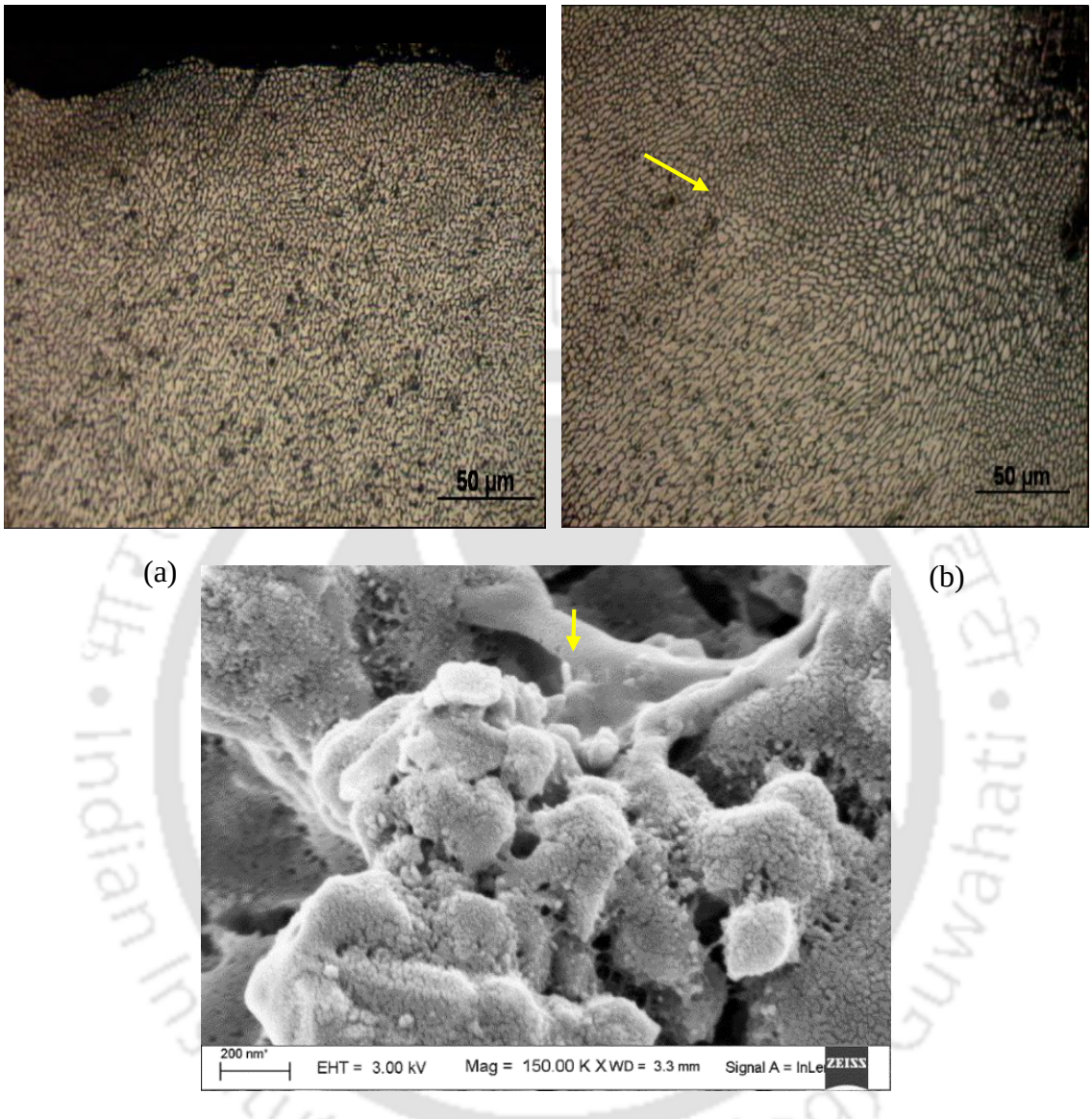

Figure 7.3 Microstructure of AlMn laser surface alloy sample: (a, b) Optical images (× 20) and (c) morphology of laser surface alloyed area (×150 k)

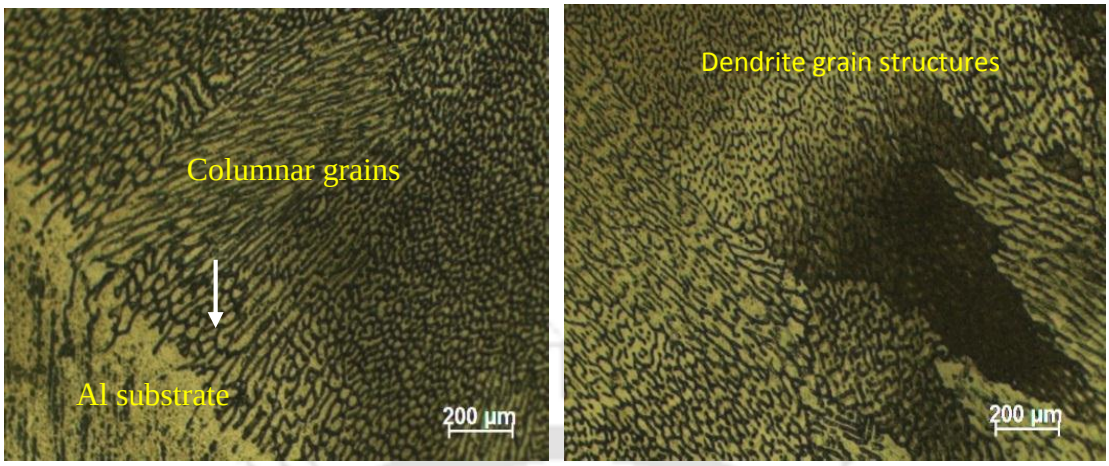

(a) (b)

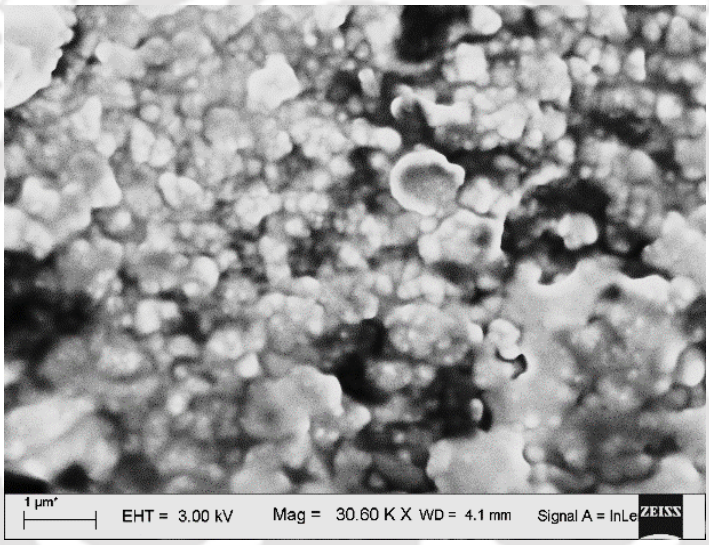

(c)

Figure 7.4 Microstructure of AlTi sample: (a) optical image (×20) at interface region, (b) optical image (×40) at near the top alloyed region and (c) FESEM image (×30 k) near the top

Figures 7.5 (a–c) show the microstructure of AlZn sample. Figure 7.5 (a) shows the interface microstructure where an impurity concentration was observed as a dark region. The interface region was about 356 µm thick, which may affect the corrosion resistance of the interface region. In the center of alloyed region, small dendrite cells were very close, thus improving the corrosion performance of that region (Fig. 7.5 b). At higher magnification of 50 k, the alloyed morphology revealed no internal defects as shown in

Figure 7.5 (c). The uniformity of alloying observed from the morphology of AlZn alloy assured the absence of defects like microcracks and unmelted impurity.

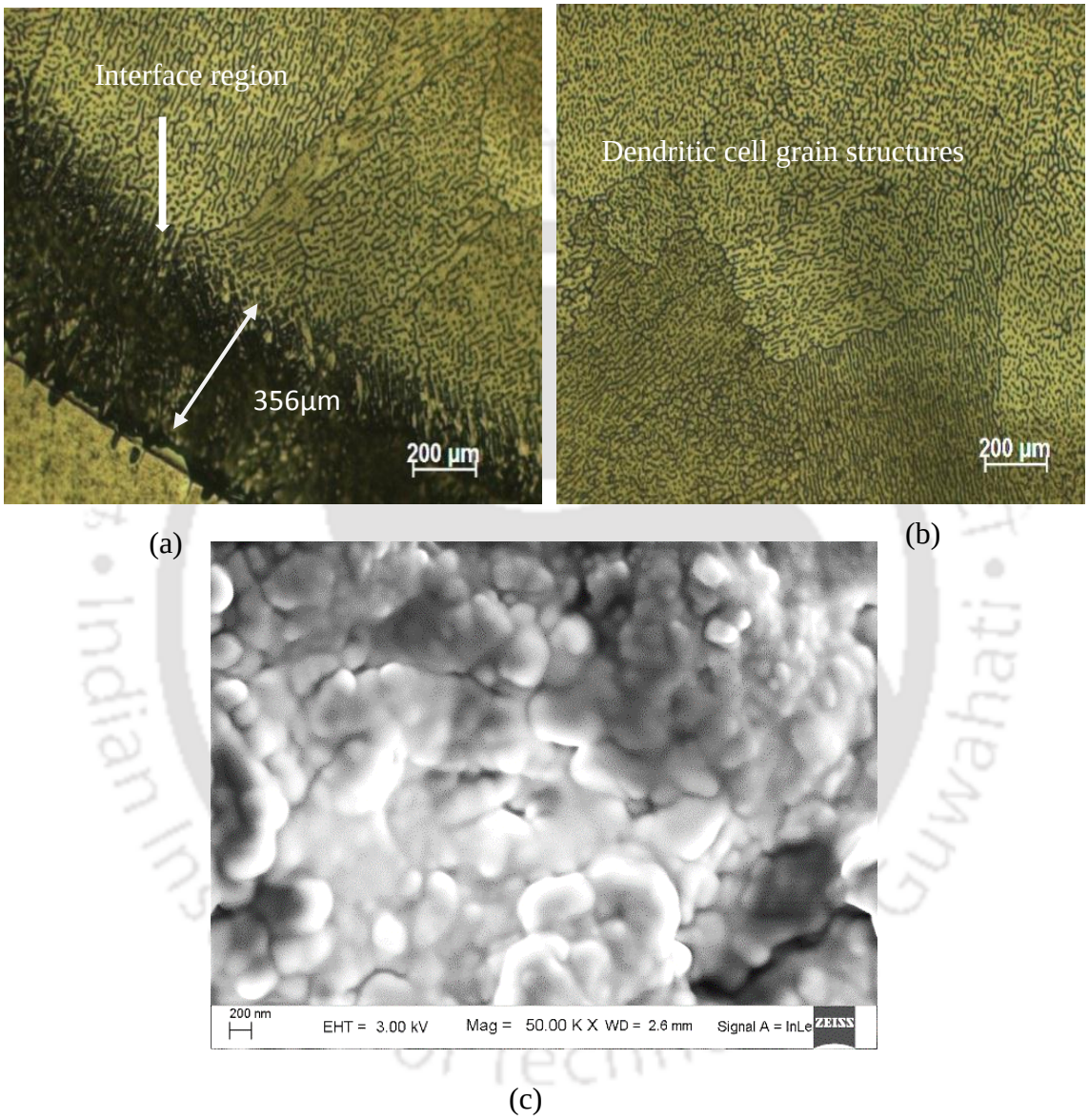

Figure 7.5 Microstructure of AlZn sample: (a) optical image (×20) at interface region, (b) optical image (×40) at near the top alloyed region and (c) FESEM image (×50 K) near the top

7.3.2 Corrosion Analysis

Laser surface alloying with magnesium and manganese had reduced the pitting corrosion damage. The pitting corrosion is difficult to evaluate easily because of the surface damage caused by corrosion. This type of corrosion occurs when passivating oxide formed on the aluminum surface is damaged due to aggressive environments, containing salts and acids. Once pitting or small holes occur, they can easily grow gradually in all directions. For all materials, corrosion pit spreads more in the lateral direction than in the depth direction. It is difficult to quantify corrosion surface damage for aluminum alloys because the corrosion nature is white and it is difficult to identify by naked eye. However, an optical surface profilometer can be used in order to measure corrosion pit depth and width. The optical profilometer was used after corrosion and microhardness tests. Figures 7.6 (a–e) shows the 3D images after the corrosion immersion and microhardness tests. The substrate material had more surface damage as indicated in Figure 7.6(a). Laser surface alloying had two regions: region (I) and region (II), for alloyed and pure aluminum, respectively, as shown in Figures 7.6 (b–c). Figures 7.6 (b) and 7.6 (c) show the topology of AlMg and AlMn alloys, respectively. The corrosion product, aluminum oxide, in the form of white ash is observed in Figure 8(b). For titanium alloyed samples, the indentation mark of microhardness test was observed as holes on the topology of Figure 7.6 (d). While the interface containing both alloyed region (I) and a substrate region (II) is shown for AlZn alloying in Figure 7.6 (e).

The average corrosion pit values for substrate material and laser surface alloyed samples are depicted as a bar chart in Figure 7.7. The maximum and minimum values of corrosion pit depth and width are shown along with error bars. The corrosion damage was the maximum for pure aluminum than laser surface alloyed samples with magnesium and manganese. The average corrosion pit depth and width were found to be 16.1 and 30.5 μm, respectively. The maximum corrosion pit depth and width for pure aluminum were 17.6 and 44.0 μm, respectively. After laser surface alloying with magnesium, there was much reduction in corrosion damage. The average value of corrosion pit depth and width were found to be 10.1 μm and 15.5 μm, respectively.

The maximum corrosion pit depth and width for AlMg were 11.82 and 17.10 μm, respectively. Alloying with magnesium had improved mechanical strengthening due to modified microstructure and the formation of the new Al_2Mg compound. The magnesium itself has good corrosion resistance and further alloying it with aluminum provides the improved performance in the acidic environment. Alloying aluminum with manganese had also improved acid corrosion resistance. Alloying with manganese resulted in corrosion pit depth and width of 14 and 26 μm, respectively. The minimum corrosion pit damage was measured for titanium alloying with aluminum. The average pit depth and width were measured to be 5.2 μm and 33 μm, respectively. While alloying aluminum with zinc, the average corrosion pit depth and width were 9.9 μm and 26.7 μm, respectively.

The weight loss due to corrosion is shown in Figure 7.8. In pure aluminum, 0.06 g was lost due to corrosion attack. However, the weight loss was reduced by 41% and 20 % after laser surface alloying with magnesium and manganese, respectively. Thus AlMg alloys have the better corrosion resistance than AlMn alloys. Arellanes *et al*. (2014) reported the pitting corrosion of AA 6061 alloy in sulfuric acid (1.0 M H_2SO_4), where the corrosion pit depth of 50 μm was formed. Laser surface alloying of aluminum with magnesium and manganese had reduced pitting corrosion damage. Once pitting corrosion was formed, it can easily propagate in a different direction causing gradual failure of components. For aluminum alloy materials, the corrosion pit attacks are more in the lateral direction than in the depth direction. As observed from corrosion morphology, both AlMg and AlMn laser surface alloyed samples showed a less weight loss due to corrosion as compared to pure aluminum. Zhurin *et al.* (1973) reported the corrosion of aluminum during the electrodeposition of zinc and found the dissolution rate of aluminum in 2.5% H_2SO_4 was 0.06 mm/year for 1199 aluminum alloy and 0.20 mm/year for 1100 aluminum alloy. The weight loss due to corrosion for AlTi sample and AlZn sample were 0.027 and 0.038 g, respectively. Titanium alloying improved corrosion resistance more than zinc alloying with aluminum.

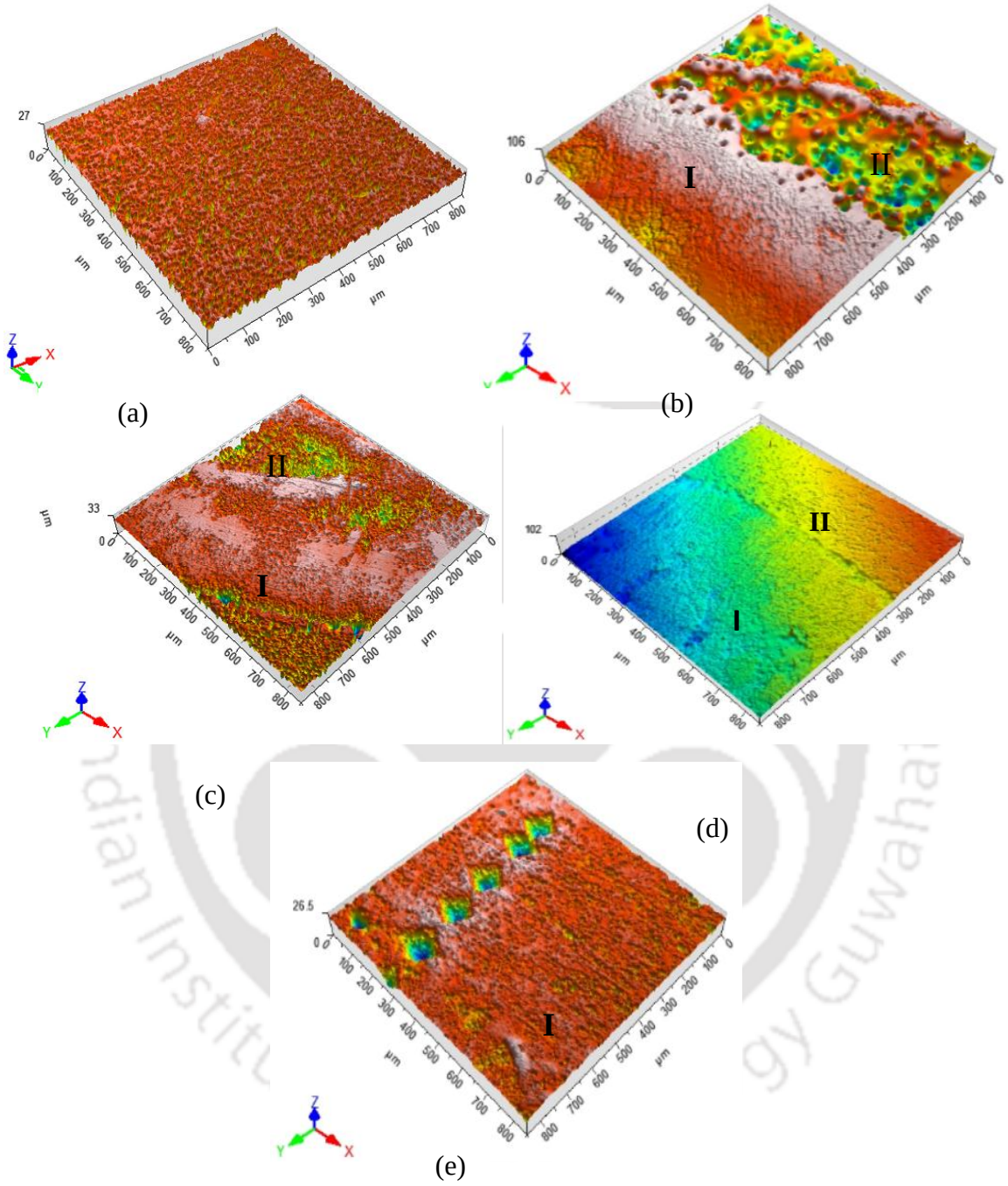

Figure 7.6 3D images after corrosion immersion test in 2.5% H_2SO_4 (a) pure Al sample, (b) AlMg sample (c) AlMn sample (d) AlTi sample and (e) AlZn alloyed sample

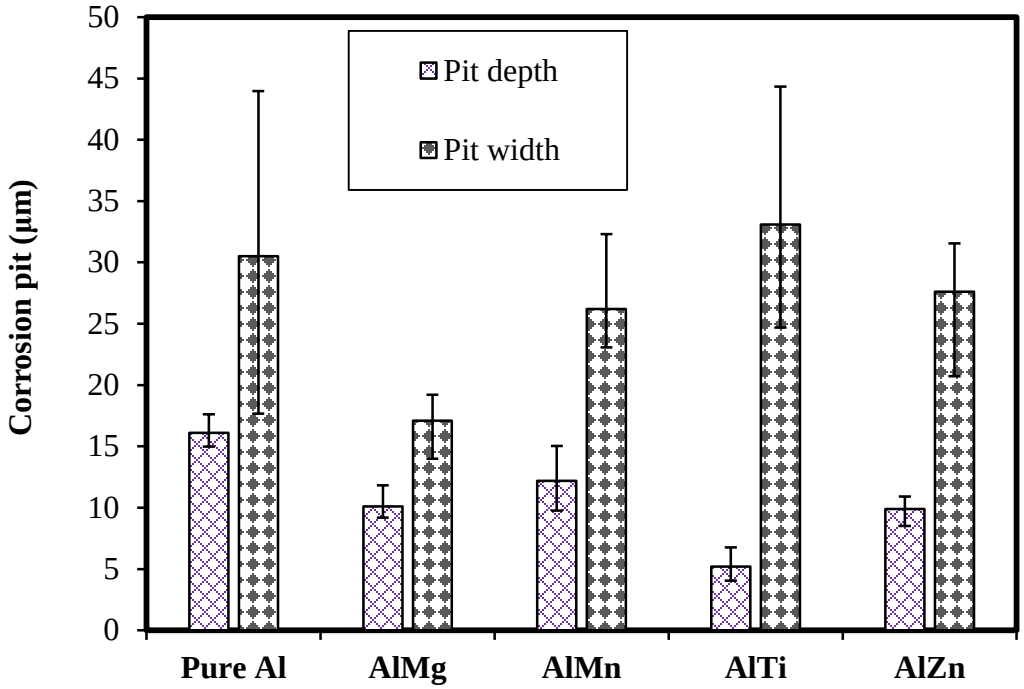

Figure 7.7 Evaluation of corrosion pit in laser surface alloyed samples and pure aluminum

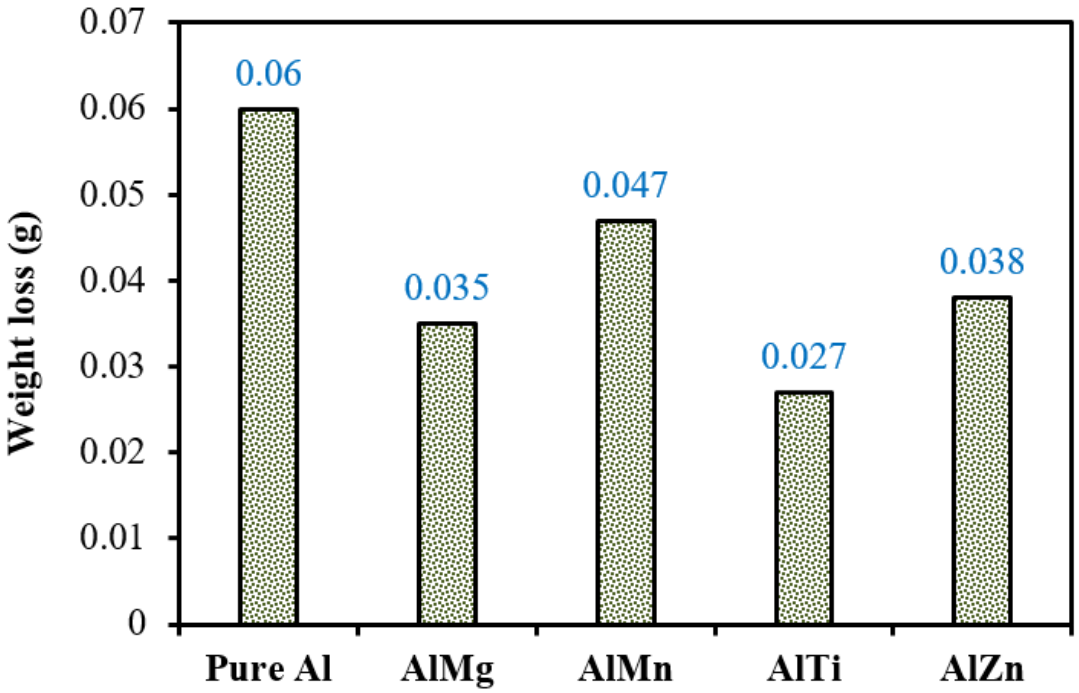

Figure 7.8 Corrosion weight loss after immersion test in 2.5 % H_2SO_4 solution for 200 h

7.3.3 Effect of Corrosion on Hardness

Due to corrosion, the metal becomes soft and its hardness gets reduced. The hardness was measured at the cross-section of the sample from the substrate from point (S) to top (T) laser surface alloyed (LSA) portion (Fig.7.9). The depths of laser surface alloyed zone for magnesium, manganese, titanium and zinc alloyed sample were 1.5, 2.0, 1.2 and 1.14 mm, respectively. The widths of laser surface alloyed portion for magnesium, manganese, titanium and zinc alloyed sample were nearly 5.5, 6.0, 4.3 and 4.2 mm, respectively.

The hardness value of AlMg sample before and after acid corrosion test are shown in Figure 7.10 (a). The hardness (g) and the distance (x) are represented by the linear curve fitted equation. The coefficient of determination R^2 was obtained for both linear and quadratic fitted curves, just to ensure that quadratic fit does not give drastically better results than the linear fit. The R^2 value for linear and quadratic fitted curve for AlMg sample before corrosion was found to be 0.952 and 0.968, respectively. Similarly, the R^2 values after corrosion test for both linear and quadratic fitted curve were found to be 0.930 and 0.984, respectively. This indicates the good correlation with measured data. The initial substrate hardness was 30 $HV_{0.3}$. The hardness increased to 101 $HV_{0.3}$ by alloying with magnesium, but after acid corrosion test, the hardness reduced to 61 $HV_{0.3}$.The reduction in hardness is an indication of corrosion that had removed some depth of the strong alloy region. The hardness values for AlMn sample before and after corrosion are shown in Figure 7.10 (b). The R^2 value for linear and quadratic fitted curve for AlMn sample before corrosion was found to be 0.965 and 0.971, respectively. Similarly, the R^2 values after corrosion test for both linear and quadratic fitted curve were found to be 0.949 and 0.956, respectively. The hardness value before corrosion for newly developed AlMn sample was found to be 262 $HV_{0.3}$, however, the hardness was reduced to 153 $HV_{0.3}$ after the corrosion. This reduction was due to the dissolved metal ions of alloyed material in the corrosive acidic medium. The hardness was reduced because of increased pitting corrosion. The hardness decreased almost linearly from the top surface to the substrates. Due to the corrosion damage, the hardness reduced by 40% and 41.4% for AlMg and AlMn samples, respectively. The hardness of material was highly affected by corrosion.

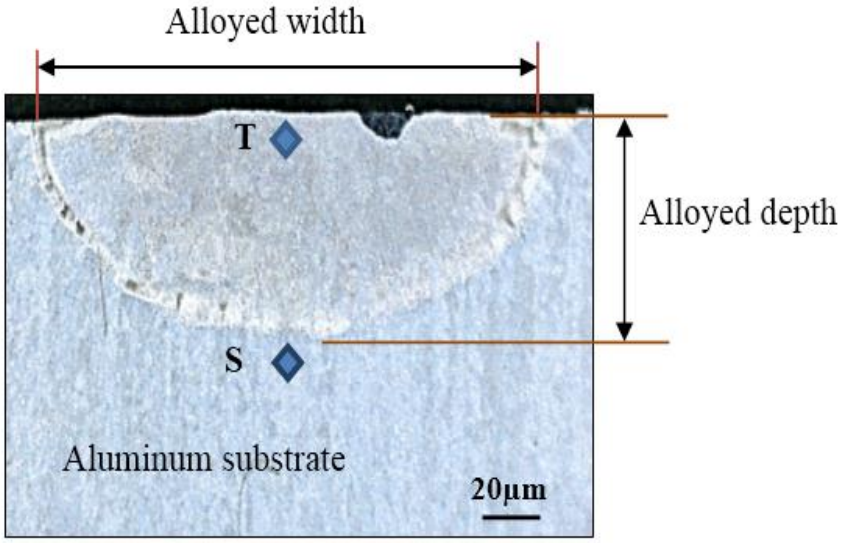

Figigure 7.9 Cross-sectional digital image (×10) of of laser surface alloyed sample

Figure 7.10 (c) shows the effect of corrosion on microhardness for AlTi alloyed surface. The maximum microhardness before corrosion test was 80 $HV_{0.3.}$ However, 51% reduction in microhardness was found due to the removal of hard titanium oxide layer. Similarly, the R^2 values before corrosion test for both linear and quadratic fitted curve were found to be 0.914 and 0.937, respectively. The R^2 values after corrosion test for both linear and quadratic fitted curve were found to be 0.585 and 0.588, respectively. Figure 7.10(d) shows the microhardness of AlZn alloyed sample. The microhardness increased from 30 $HV_{0.3}$ to 60 $HV_{0.3,}$ before corrosion test. However, microhardness reduced by 33% after acid corrosion test. The R^2 values for AlZn alloy were also calculated. Before corrosion R^2 values for linear and quadratic fitted curves were 0.720 and 0.775, respectively. The R^2 values after corrosion test for linear and quadratic fitted curve were found to be 0.849 and 0.854, respectively.

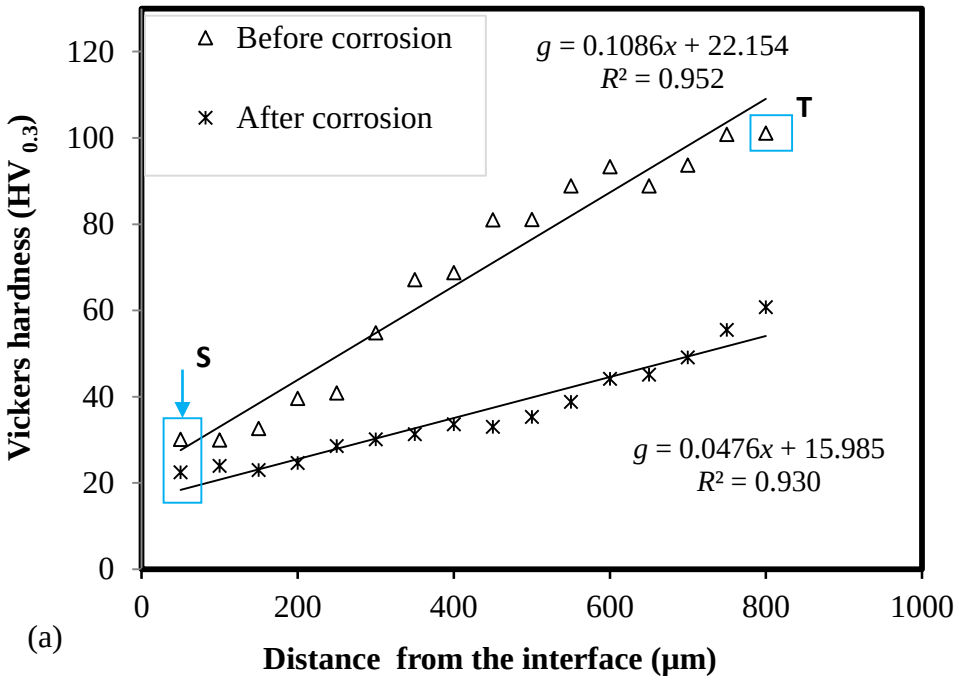
Before corrosion
After corrosion
g = 0.1086x + 22.154
R² = 0.952
g = 0.0476x + 15.985
R² = 0.930
S
T
Vickers hardness (HV 0.3)
Distance from the interface (µm)
0
20
40
60
80
100
120
0
200
400
600
800
1000

(a)

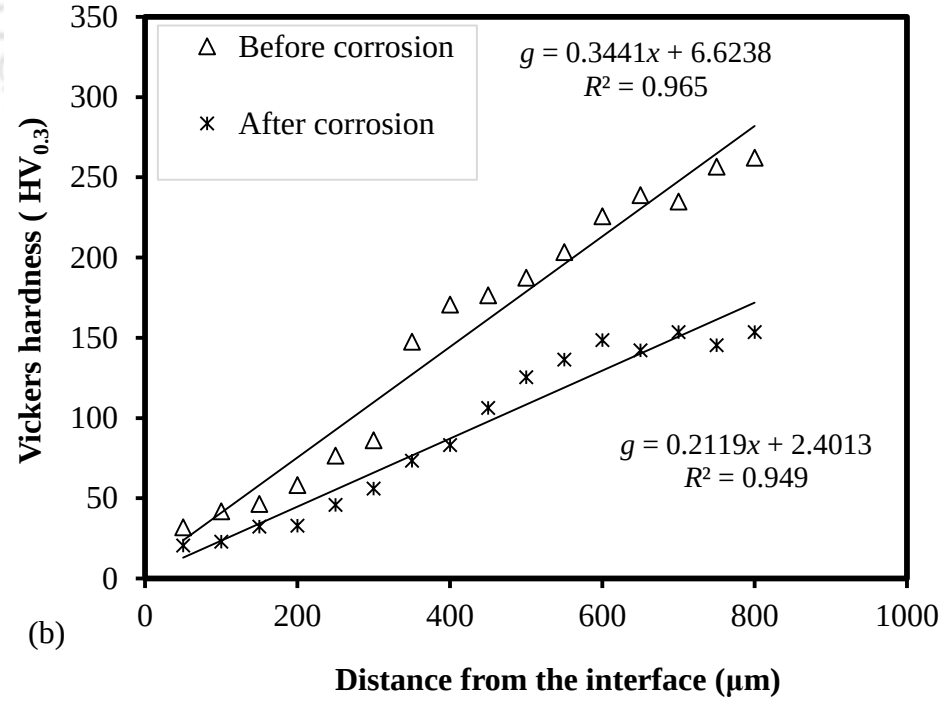
Before corrosion
After corrosion
g = 0.3441x + 6.6238
R² = 0.965
g = 0.2119x + 2.4013
R² = 0.949
Vickers hardness (HV0.3)
Distance from the interface (µm)
0
50
100
150
200
250
300
350
0
200
400
600
800
1000

(b)

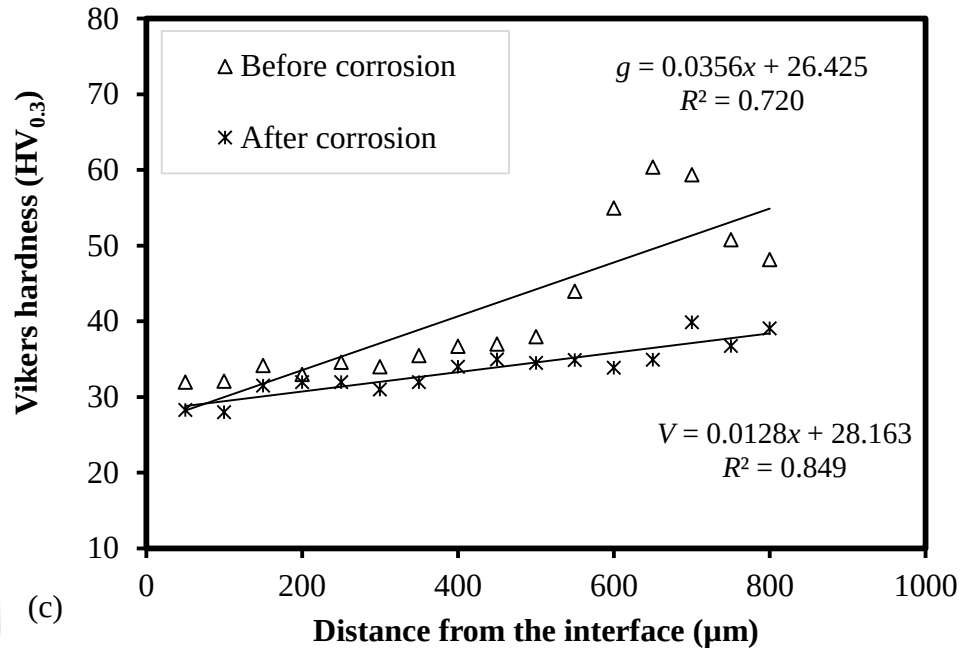

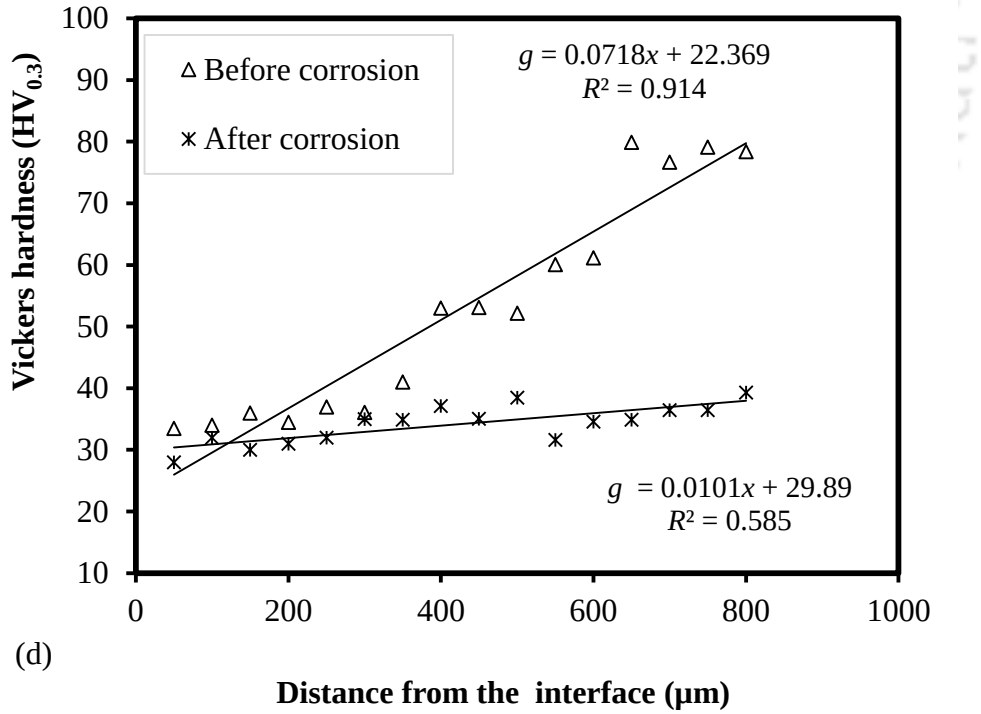

Figure 7. 10 Microhardness before and after acid corrosion test: (a) AlMg sample and (b) AlMn sample, (c) AlTi sample and (d) AlZn sample

7.3.4 Corrosion Mechanism

In order to understand the physics of the corrosion process, the study of corrosion mechanism is very important. Due to the effect of environment and the material properties on corrosion, the mechanism is complex to understand. Vargel, (2004) reported the mechanism of aluminum corrosion in aqueous solution. The mechanism of corrosion of aluminum is depicted in equation (7.1–7.5). The final corrosion product $Al(OH)_3$ is insoluble and precipitated as white gel. The reactions proceed as follows:

$$Al \rightarrow Al^{3+} + 3e^{-} \tag{7.1}$$

$$6H^{+} + 6e^{-} \rightarrow 3H_2 \tag{7.2}$$

$$2Al + 6H_2O \rightarrow 2Al(OH)_3 + 3H_2 \tag{7.3}$$

Arellanes *et al*. (2014) explained aluminum corrosion in sulfuric acid solution, (0.1, 0.3, 0.7 and 1.0 M of H_2SO_4). The reaction during corrosion was similar to present experiments, where the samples were exposed to 2.5 % H_2SO_4 after laser surface alloying. The overall corrosion reaction is as follows:

$$4Al + 2H_2O + 3O_2 \rightarrow 2Al_2O_3(H_2O)_2 \tag{7.4}$$

$$Al_2O_3(H_2O) + 3HSO_4 + 3H^{+} \leftrightarrow Al_2\left[(SO_4)_3(H_2O)\right] + 3H_2O \tag{7.5}$$

Figures 7.11 (a–c) show the corrosion surface morphology of the laser surface alloyed AlMg sample. The cross-section of exposed sample shows both alloyed and substrate region. The interface region is shown in Figure 7.11 (a). It is observed from the morphology of laser surface alloyed region that the damage caused due to corrosion was less as compared to pure aluminum as shown in Figure 7.11 (b) and 7.11(c), depicting unalloyed and alloyed region, respectively.

Figures 7.12 (a–c) show corrosion surface morphology of AlMn sample. The interface region is shown in Figure 7.12 (c). The laser surface alloyed and pure aluminum region are visible from the morphology. Figure 7.12 (a) shows Mn alloyed region where the pitting

corrosion was less as compared to unalloyed aluminum region as shown in Figure 7.12 (b). This was due to the presence of manganese and improved microstructure of the alloy. The pitting corrosion begins with a breakdown of passivation oxide layer at a specific area. Due to the potential difference between anode and cathode, extremely localized corrosion was initiated in the form of pits or small holes. The pits on the surface grow deeper and wider gradually with time. In general, AlMg sample shows more corrosion resistance in sulfuric acid than AlMn sample.

Figures 7.13 (a–c) show the corrosion morphology of the titanium alloyed sample. The corrosion resistance after titanium alloying was confirmed from the FESEM image analysis as shown in Figure 7.13 (c). Titanium alloyed region was less damaged by corrosion. This may be due to the formation of hard titanium oxide layer and dendrite microstructure. Majumdar *et al.* (1990) reported that the formation of Al_2O_3 improves oxidation corrosion resistance after laser surface alloying of Ti with Si, Al and Si+Al. The unalloyed substrate region was highly damaged by acid corrosion effect in 200 hours immersion test (Fig.7.13b). The corrosion mechanism for titanium alloying was in the forms of micro-crack formation that propagated along the grain boundary of the material.

Figures 7.14 (a–c) illustrate the morphology of AlZn alloy after exposure to 2.5% H_2SO_4 for 200 hours in a controlled environment in order to avoid the effect of other gases from the environment. Figure 7.14 (a) illustrates the interface region containing both alloyed and unalloyed region where a clear difference was observed. Laser surface alloying with pure zinc also improved the acid corrosion resistance of aluminum. The refined grain structure and formation of dendrite microstructure played a role to improve corrosion.

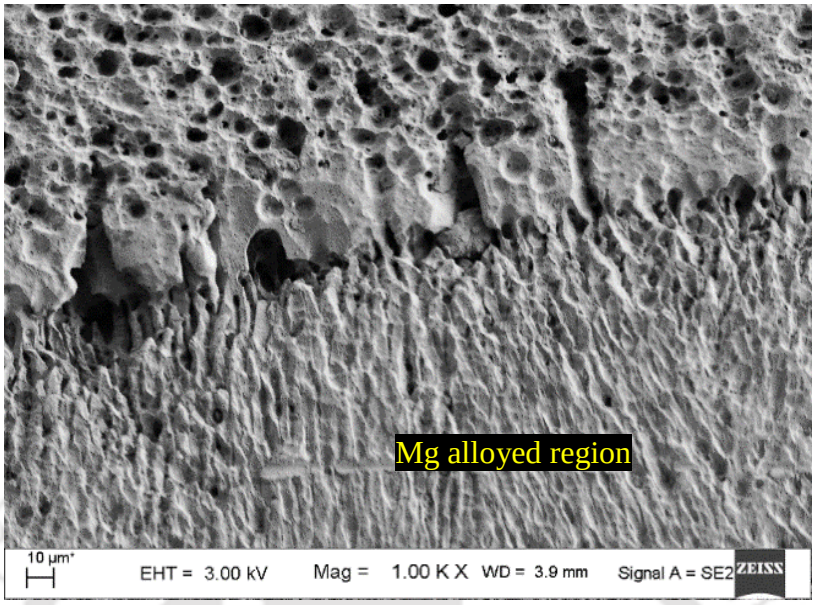

(a)

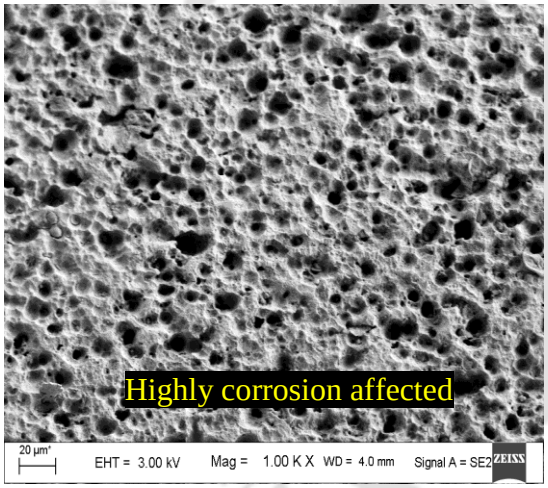

(b)

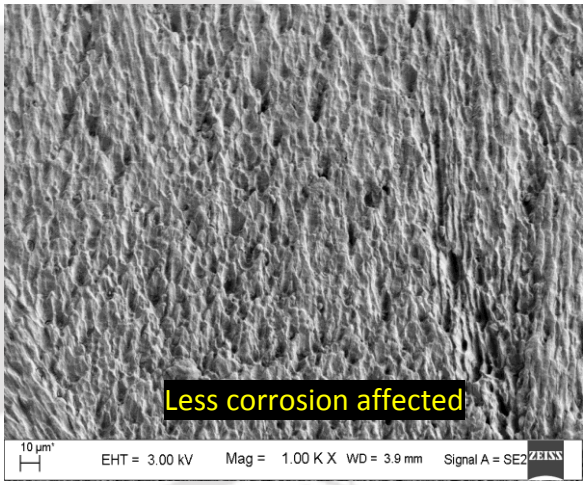

(c)

Figure 7.11 Morphology of AlMg sample after corrosion (×100 k): (a) interface region, (b) unalloyed aluminum region and (c) Mg alloyed region

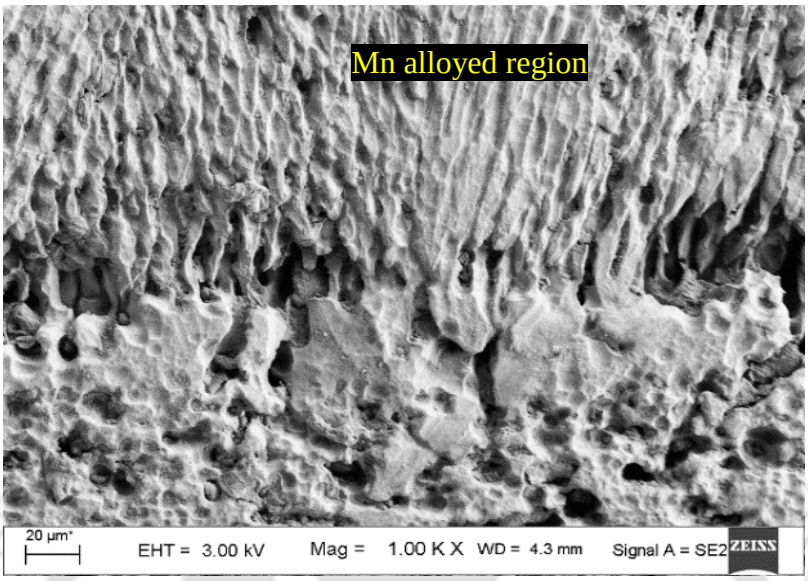

(a)

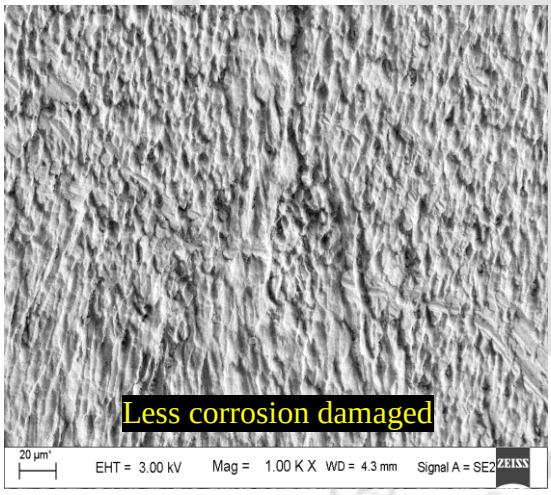

(b)

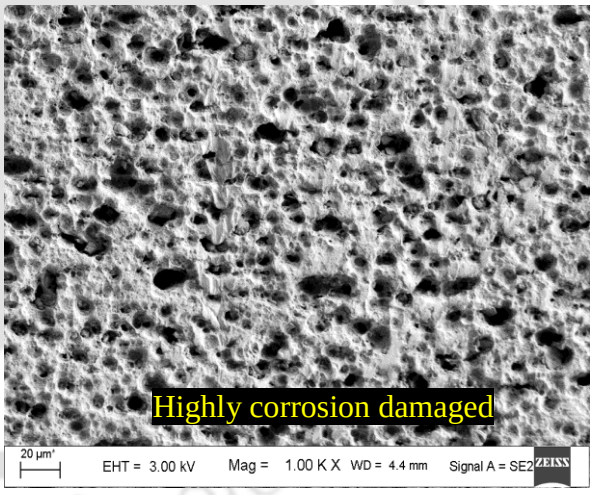

(c)

Figure 7.12 Morphology of AlMn sample after corrosion (×100 k): (a) interface region, (b) Mn alloyed region and (c) unalloyed aluminum region

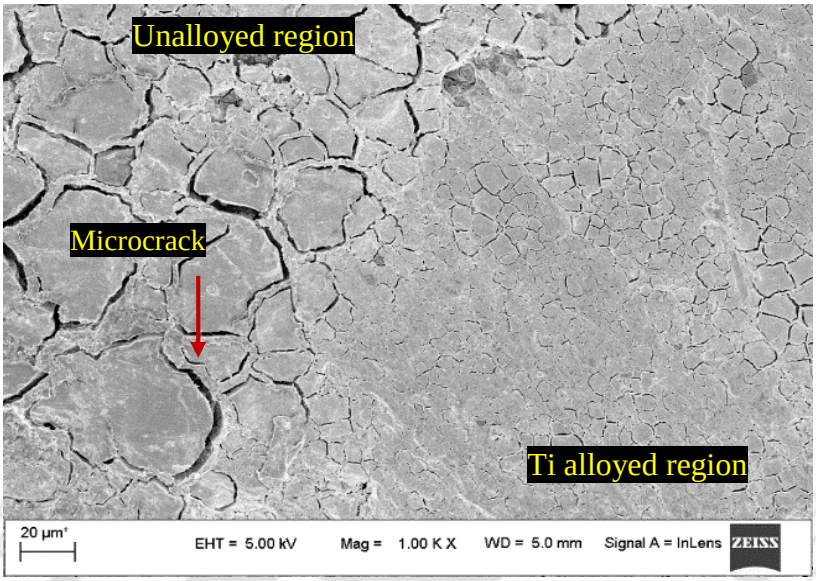

(a)

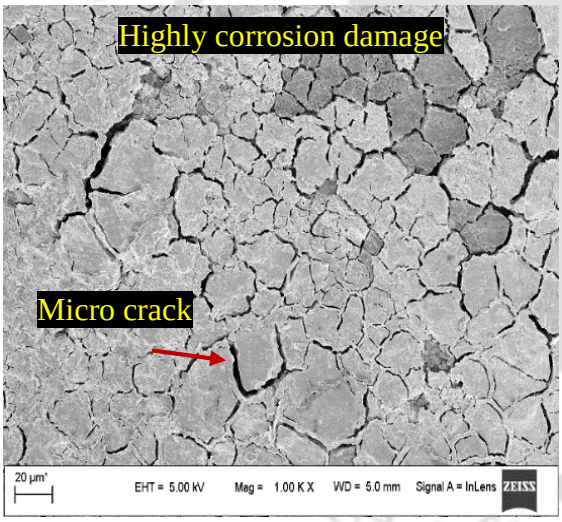

(b)

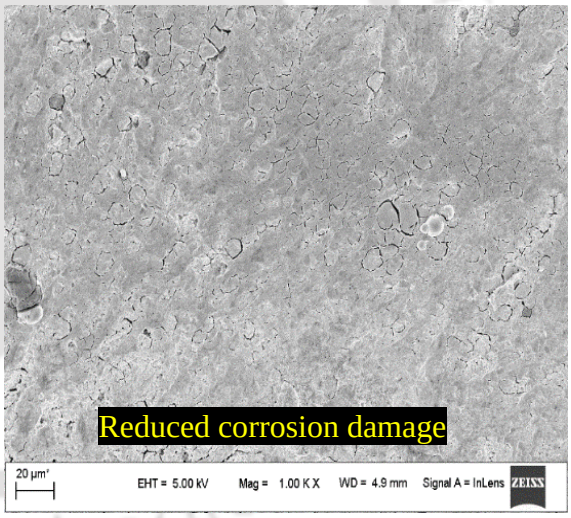

(c)

Figure 7.13 Morphology of AlTi sample after corrosion (×1 k): (a) Interface region, (b) unalloyed aluminum region and Ti alloyed region

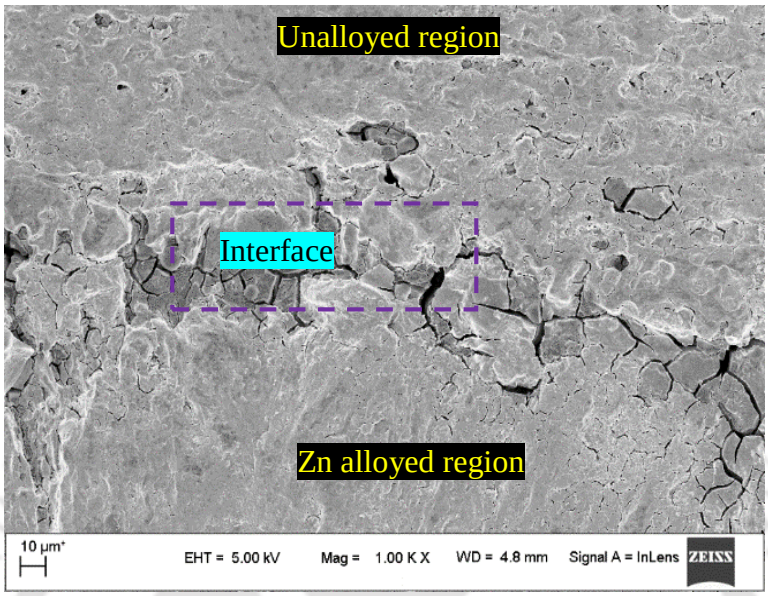

(a)

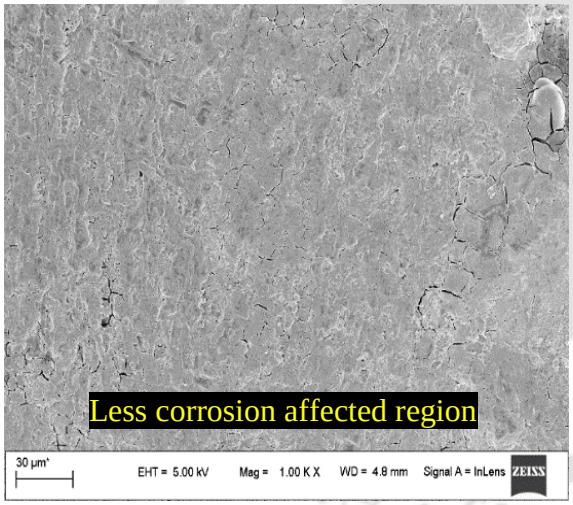

(b)

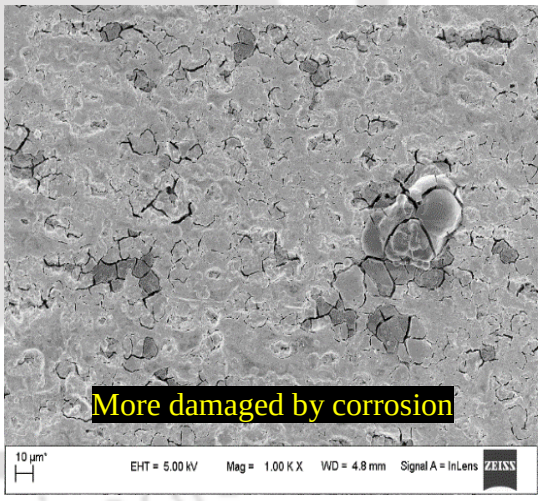

(c)

Figure 7.14 Morphology of AlZn sample after corrosion (×1 k): (a) interface region, (b) Zn alloyed region and (c) unalloyed aluminum region

7.3.5 Acid and Salt Solutions Test

For Al-CuMgMn alloy, the evaluation of corrosion attack after corrosion immersion test in acid solution (2% H_2SO_4) and alkaline solution (5% NaCl) was carried out by percentage weight loss method. The pH of solution are 0.74 and 9.08 for acid and base solutions, respectively. The weight loss was measured in grams. The corrosion weight loss values were caused by corrosion damages in acid solution and salt solution is shown in Figure 7.15. In acidic environment, the substrate material weight loss was 0.64% and for Al-CuMgMn laser surface alloyed material, the percentage weight loss was 0.51%. Thus, laser surface alloying improved corrosion resistance. In corrosion immersion test with 5% NaCl, the substrate material weight loss was 0.41% for substrate material and was 0.25% for Al-CuMgMn alloy. In this case, laser surface alloying had improved the corrosion resistance. It can be stated that percentage weight loss due to acid corrosion attack was higher than salt corrosion attack.

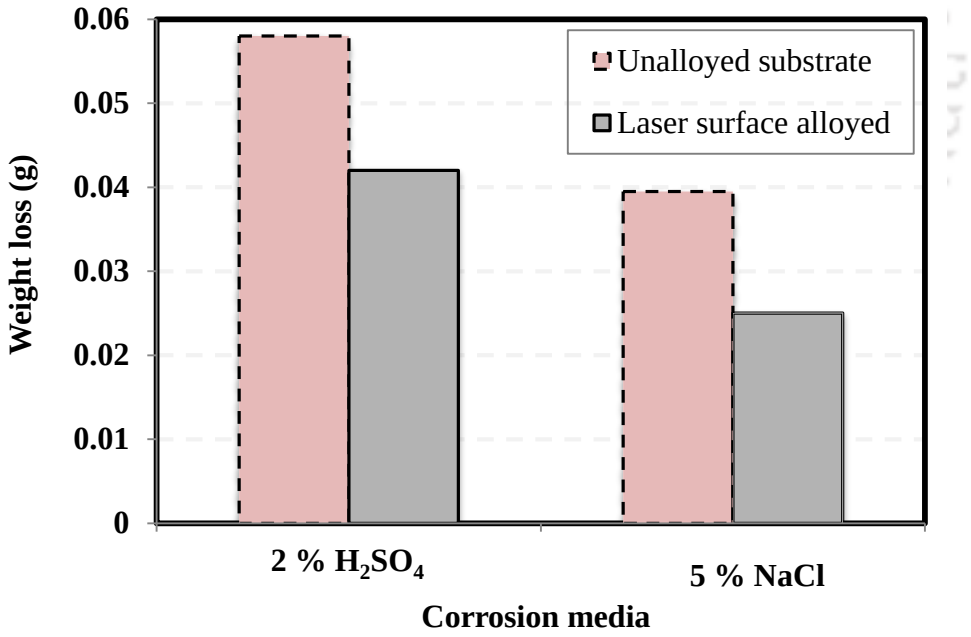

Figure 7.15 Weight loss due to corrosion for substrate and laser surface alloyed Al-CuMgMn alloy

Figures 7.16 (a–d) show the surface morphology after acid and alkaline corrosion immersion tests were carried out for 200 hours. In the alloyed part, the corrosion was in the form of slender cavities that orginated from the edge and propagated into the material shown in Figures 4.24(a) and 7.16 (c). In the substrate material, corrosion was in the form of randomly distributed small holes called pits as shown in Figures7.16 (b) and 7.16 (d). In acidic solution, the size of corrosion pit was larger in the alloyed sample as shown in Figure 7.16 (c). On the other hand, the swelling on the surface of the substrate specimen in the acidic solution was due to internal pressure of corroded materail as shown in Figure 7.16 (d).

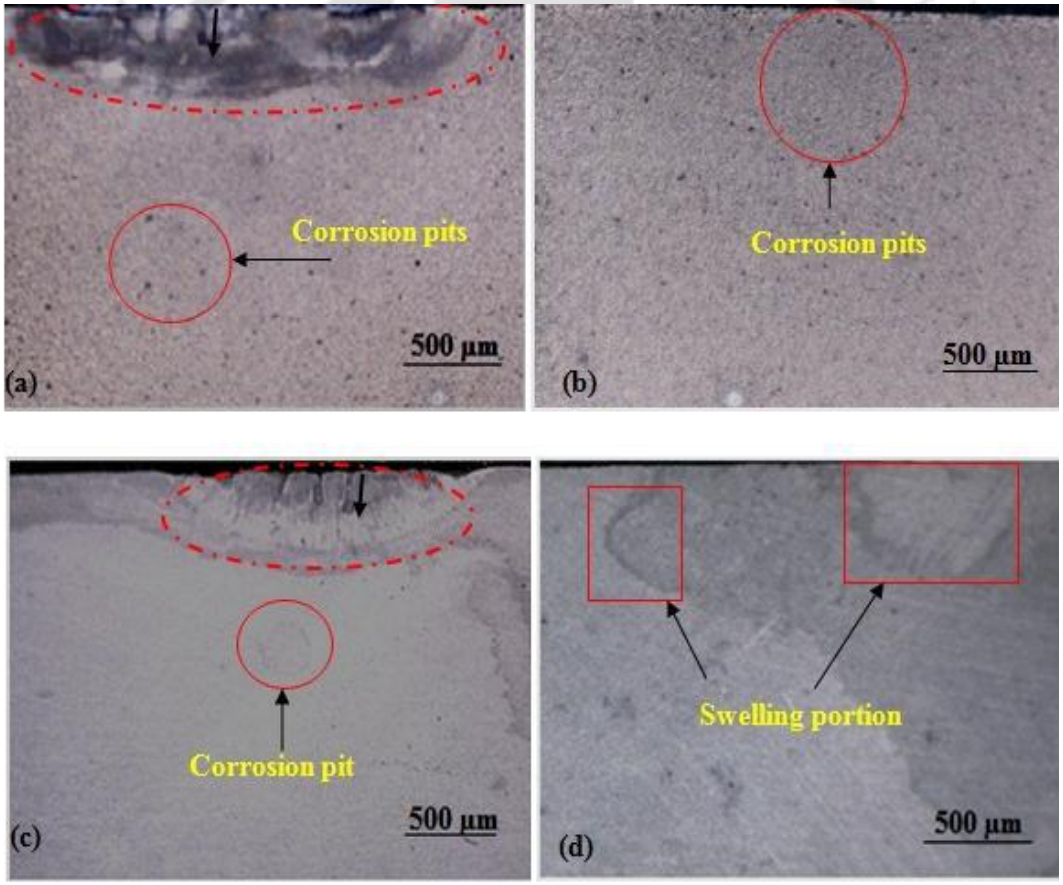

Figure 7.16 Surface morphology of corroded materials after 200 hours corrosion test: (a) laser alloyed in 5% NaCl, (b) substrate material in 5% NaCl, (c) laser alloyed region in 2% H_2SO_4 and (d) substrate material in 2% H_2SO_4

7.4 Conclusion

Corrosion test was carried out after laser surface alloying of commercially pure aluminum with magnesium, manganese, titanium and zinc was successfully done. Corrosion test was also conducted for Al-CuMgMn alloy. The followings are the major findings:

- The weight loss due to acid corrosion attack in 2.5% H_2SO_4 was reduced by 55% for AlTi alloy, 41% for AlMg, 36.6% for AlZn alloy and 22% for AlMn alloy.
- The pitting corrosion was found to be a major cause of damage in the metal. The pitting grows faster in a lateral direction than in the depth direction. However, the shape of pitting was irregular.
- The hardness after laser surface alloying increased by a factor of 8.7, 3.4, 2.7 and 2 by alloying with Mn, Mg, Ti and Zn, respectively. After corrosion test, hardness reduced by 51% for AlTi sample, 40% for AlMg sample and 41.4% for AlMn sample and 33% for AlZn sample.
- Overall, AlTi provided the best corrosion resistance and AlMn the best microhardness after laser surface alloying.

Indian Institute of Technology Guwahati

Chapter 8

Laser Surface Alloying of Aluminum with TiO_2 and SiC powders

8.1 Introduction

Laser surface alloying of aluminum with ceramic materials have many advantages due to the fact that ceramics materials have high hardness, chemical resistance, low density, excellent wear and corrosion resistance. Aerospace and automotive industries require lightweight materials for saving energy. The combination of relative strength to weight ratio of aluminium combined with excellent corrosion resistance and recyclability gives an advantage. After laser beam melting, solidification of the alloy occurs. Draper and Poate (1985) reported that during laser alloying, solidification velocity reached up to 30 m/s. The alloyed area induced extreme heating and cooling at the rate of 10^4–10^{11} K/s and had a thermal gradient of 10^5–10^8 K/m. Laser alloying causes rapid melting, intermixing and solidification in the alloyed region as well as in the part of base material (Razavi and Gordani, 2001). In laser surface alloying, a high cooling rate is always created, which enhances the formation of homogeneous microstructure (Damborenea, 1998).

Ceramic materials possess a low reflectivity to laser beam that enhances absorption of laser energy during laser surface alloying. Vreeling *et al*. (2000) reported injection of SiC particles in to aluminum plates with 99.6 wt.% purity using laser beam melting with 2 kW Nd:YAG laser. Pre-heating the substrate before laser beam processing up to 300 °C enhanced laser beam absorption that created metal matrix composite layer on aluminum. The advantages of alloying SiC with aluminum include enhanced elastic modulus, thermal stability and improved thermal conductivity due to alloying. The effect of adding Mg and Si to aluminum in thermo-mechanical properties was reported by Ren *et al.* (2007). When composition of silicon was less than 6 wt.%, low thermo-physical property was created.

On the other hand, when the composition was more than 12 wt.% Si, bending strength of the aluminium alloy got reduced.

Titanium dioxide is a well-known polycrystalline material. TiO_2 improves the property of the material, which can be used in many fields. Diebold (2003) studied the use of TiO_2 in heterogeneous catalysis, photo catalysis, solar cells and oxygen gas sensors to control the air and fuel mixture in car engines. TiO_2 is also used as a coating for corrosion resistance. Increasing titanium content upto 0.15 wt.% at peritectic composition can cause grain refinement. However, above a certain level, it forms a coarse grain structure that influences grain refinement and causes difficulty in casting (Jaradeh and Carlberg, 2005). The addition of titanium to AlSi eutectic alloy, resulted in the precipitation of the intermetallic compound of Al_3Ti phase. It induced an increased the microhardness of the alloy. Titanium containing alloys increase the wear resistance due to the formation of hard compound phase of Al_3Ti intermetallic (Saheb *et al.,* 2001).

In this chapter, SiC and TiO_2 powders are pre-placed uniformly on commercially pure aluminum substrate. A continuous wave CO_2 laser was used for melting and alloying formation. The effects on microstructure and microhardness after laser alloying are discussed.

The average particle size of SiC powder was 10 µm and it was 45 µm for TiO_2 powder, based on availability. The aim was not to compare SiC and TiO_2 after laser surface alloying rather it was to understand the significance of each ceramic alloying. There is limited data on laser surface alloying of pure aluminum substrate with SiC and there is no study yet conducted using TiO_2 alloying. In this short chapter, it is aimed to illustrate the advantage, especially on improving hardness, after laser surface alloying. However, laser surface alloying SiC with different aluminum alloys was reported by different researchers. Man *et al*. (2002) alloyed SiC with AA6061 aluminum using Nd:YAG laser improved mechanical property. Pantelis *et al*. (1995) improved wear resistance of cast aluminum alloy A-S7G0.3 by SiC particle injection assisted by laser melt process. Mabhali *et al*. (2010) studied laser surface alloying of SiC on AA1200 aluminum alloy using Nd:YAG laser. Majumdar *et al*. (2006) reported improved surface hardness of laser surface alloyed

commercial pure aluminum with SiC powder. Hu and Baker (1995) conducted laser surface alloying on commercially pure aluminum, AA6061 and AA8090 aluminum alloys using CO_2 laser. Their focus was on studying microstructure, phase analysis and effect of laser processing parameters on the quality of alloying. Aluminum reinforced by titanium aluminide alloys exhibited high strength, high fracture toughness, low specific structural weight and good resistance to corrosion, wear and creep (Wagner *et al*., 1999; Gaus *et al*., 2000). Aluminum reinforced by titanium aluminides composite has been manufactured by different methods─ mechanically alloying (Barlow *et al*., 2001); friction stir processing (Zhang *et al*., 2011); reactive squeeze casting (Beyer *et al*., 2000), reactive sintering (Gheorghe *et al*., 2002) and ball milling process (Ying *et al*., 2004). In laser surface alloying, the use of TiO_2 for alloying with pure aluminum material is the novelty of this work. This work is mainly focused to improve hardness on the surface.

The wetting and contact angle of SiC with aluminum has been studied by different researchers. No literature was found on wetting and contact angle reported during laser surface alloying of aluminum with SiC. In this work, the results obtained on improved microstructure and EDS study was related to wetting ability of SiC with molten aluminum during laser beam melting. When the drop of liquid is in contact with solid surface, the interfacial tensions and contact angles are studied by Thomas Young (Young, 1805). There is correlation between contact angle and interfacial tensions between solid, liquid and vapor of three phases at equilibrium condition. The contact angle is the angle formed by the intersections of liquid solid interface and the liquid vapor interface whereas wettability is the ability of a solid surface to be in contact with liquid. The contact angle (θ) < 90º indicates the better wetting property, where θ > 90º indicates the less wetting of the surface (Yuan and Lee, 2013). Nautiya *et al.* (2018) reported the formation of reaction product during plasma spray improves the interfacial wetting and lowers interfacial energy during non-equilibrium wetting of boron nanotubes in molten aluminum.

8.2 Materials and Method

The substrate material used in the present experiment was commercially pure aluminum plate with 70 × 50 × 10 mm dimension. The alloying powders of SiC and TiO_2 were individually mixed with Fevigum binder and were coated on the aluminum substrate. The

coating thickness was 0.5 mm. The average particle size of each powder was about 10 μm. A continuous wave CO_2 laser power of 1.7 kW was used for SiC material and 1.8 kW laser power was used for TiO_2 material. For TiO_2 material, 300 mm/min laser scan speed and 7.4 mm laser beam diameter were used. Laser scan speed of 400 mm/min and laser beam diameter of 5.8 mm were used for SiC material. Figure 8.1 (a) shows photograph of laser surface alloyed samples with SiC powder. From the pattern on the surface, there is a stirring action of laser beam pulling the molten metal. After solidification, the grain structure of the alloyed region was formed. Figure 8.1(b) shows photograph of laser surface alloyed sample with TiO_2 powder. The topology of alloyed region revealed that the fusion bonding was created in the alloyed region.

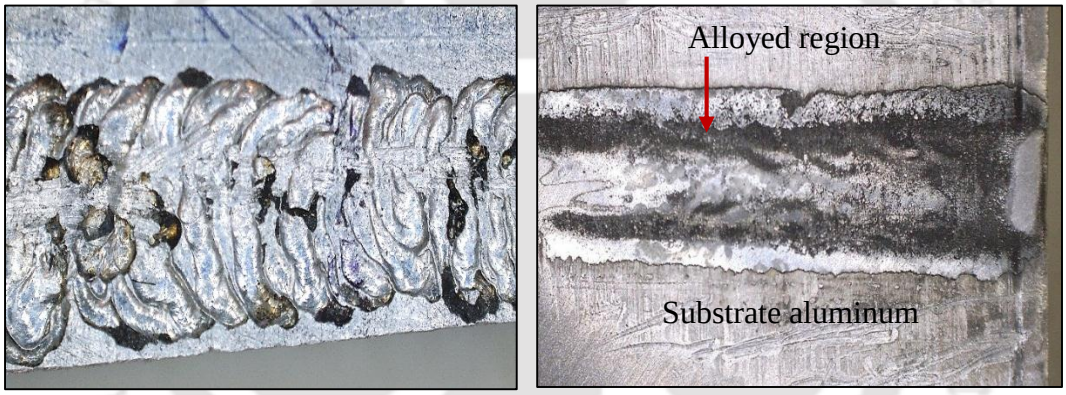

(a) (b)

Figure 8.1 Photographs of laser surface alloyed (a) SiC powder and (b) TiO_2 powder

8.3 Results and Discussion

The results of the experiments are discussed in this section, which includes surface roughness, microstructure, microhardness and chemical composition analysis.

8.3.1 Surface roughness

Figures 8.2 (a–b) show the micrographs of surface roughness after laser surface alloying. The surface topology of laser surface alloyed region was analyzed using non-contact optical surface profilometer. The centerline average roughness was measured. Figure 8.2 (a) shows the surface roughness micrograph of silicon carbide alloyed with aluminium.

The centerline average surface roughness value after laser surface alloying with silicon carbide was 5.94 µm. Figure 8.2 (b) shows the surface roughness micrograph of titanium dioxide alloyed with aluminium. The centerline average surface roughness obtained after laser surface alloying with titanium oxide was 1.01 µm. The alloyed depth formed after alloying with SiC was 126 µm. The alloyed depth formed after alloying with TiO_2 was 1.2 mm. In this case, alloyed depth was more for TiO_2 alloying and less for SiC alloying. When the alloying depth is enough, the surface damage caused by wear and corrosion can be avoided.

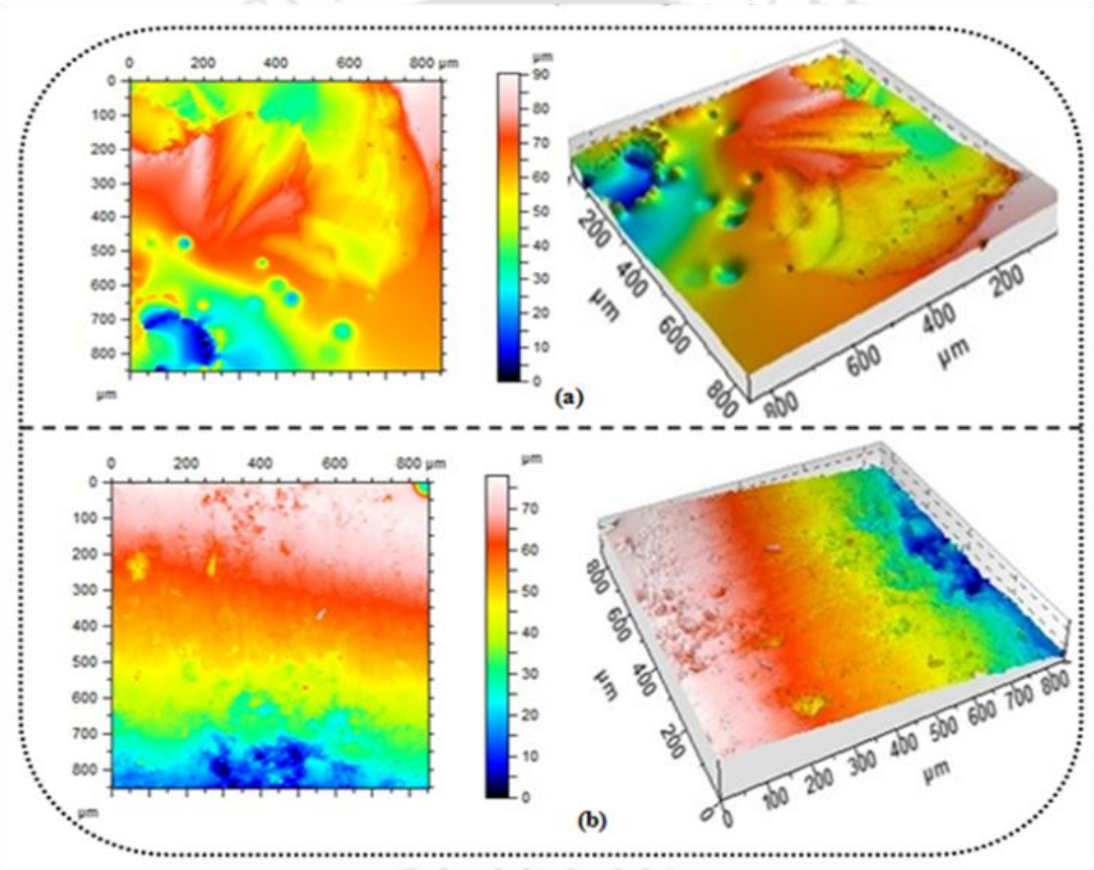

Figure 8.2 3D surface topology after laser surface alloying with: (a) SiC and (b) TiO_2

8.3.2 Microstructure Analysis

Laser alloyed micrograph of Al-SiC material is shown in Figures 8.3(a–b). Figure 8.3(a) shows top alloyed layer where fine granulated structure was created. When the melting temperature reached upto 940 K, Al_4C_3 compound formed while at 1670 K, Al_4SiC_4 ternary

carbide compound formed. The hardness of the two compounds—Al_4C_3 and Al_4SiC_3 – was 1200 HV as reported by Ansndkumsr *et al.* (2007). The average hardness of 250 HV was formed using laser specific energy at 58 MJ/m^2. When laser specific energy was reduced to 26 MJ/m^2, the hardness also got reduced to 120 HV. When silicon content is less than 12.5 wt.%, the microstructure is hypoeutectic. On the other hand, when silicon content is more than 12.5 wt.%, the microstructure is hypereutectic. Figure 8.3(b) shows the microstructure at the end of SiC laser alloyed sample. In this case, laser beam melting created a built up material at one end because the laser beam was pulling the molten metal.

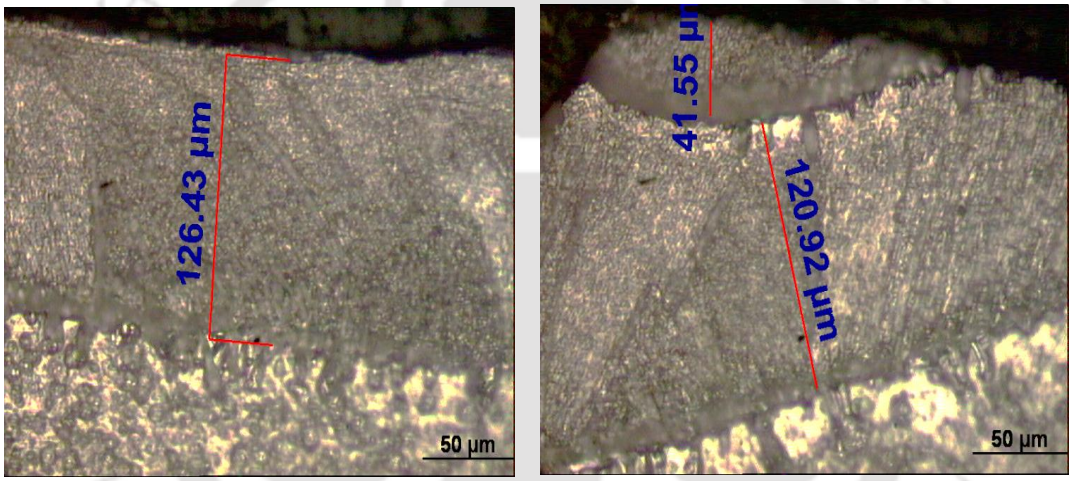

(a) (b)

Figure 8.3 Optical images of laser surface alloyed aluminum with SiC (×20): (a) at the center of alloying and (b) at the edge of alloying

Two layers were formed due to the different temperature in the upper and bottom region of the substrate material. When laser beam was irradiated on the surface, the photon energy was converted into heat that propagated towards the interior of the material. The temperature of upper zone was higher providing more silicon contents in the upper region of the alloy. From AlSi phase diagram, a needle-like primary Si and AlSi eutectics was crystallized from the melted AlSi hypereutectic alloy during the solidification stage. The upper layer of the alloyed region consists of needle-like primary Si, Al–Si eutectics, Al dendrites and less SiC particles as reported in (Sun *et al*., 2008). Due to the less solubility

of silicon in molten aluminium, the alloyed region has more silicon on the top region than the center region.

Luarent *et al*. (1987) reported wettability of SiC by aluminum and Al-Si alloys. Their results show wetting between SiC and aluminum occur at the melting pint of aluminum. When temperature is 973 K, contact angle was very high about 130^{o}. When temperature was in the range 973 to 1073 K, contact angle decreased. In the third temperature over 1073 K, contact angle was about 50^{o}. The factors that improve wettability are surface roughness, grain size and morphology (Ho *et al*. 2015; Indira *et al*. 2016). Xu *et al*. (2007) reported during wetting aluminum penetrate into refractory SiC, resulting in inhabiting both porosity as well as the positions vacated by the diffusing silicon. The wetting is an attributed to composition and microstructure. There is a difference between the base aluminium microstructure and laser alloyed layer. Similar work on a layer-by-layer solidification of SiC particles formed by laser cladding with aluminium was reported by other researchers. Viala *et al*. (1990) and Hu *et al.* (1996) reported the formation of Al_4C_3 compound at 940 K temperature, while at above 1670 K temperature, the ternary Al_4SiC_4 compound formed. Figure 8.4 (a–b) shows the EDS spectrum result of laser alloyed region for Al-SiC where 0.9 wt.% Si was present. Table 8.1 shows chemical composition of Al-SiC material.

Table 8.1 Chemical composition in wt.% of Al-SiC sample

C	Si	Fe	O	Cu	Mg	Al
64.7	0.2	6.2	0	0	0.1	34.9
45.2	0.9	0.4	0	0	0.2	53.3
24.7	0	0.3	15.4	0.1	0.1	59.4
30.0	0.2	0.7	25.2	0	0.1	43.7
16.5	0.2	0.2	6.7	0	0.2	76.2
33.3	0.3	0.5	0	0.1	0.2	65.6

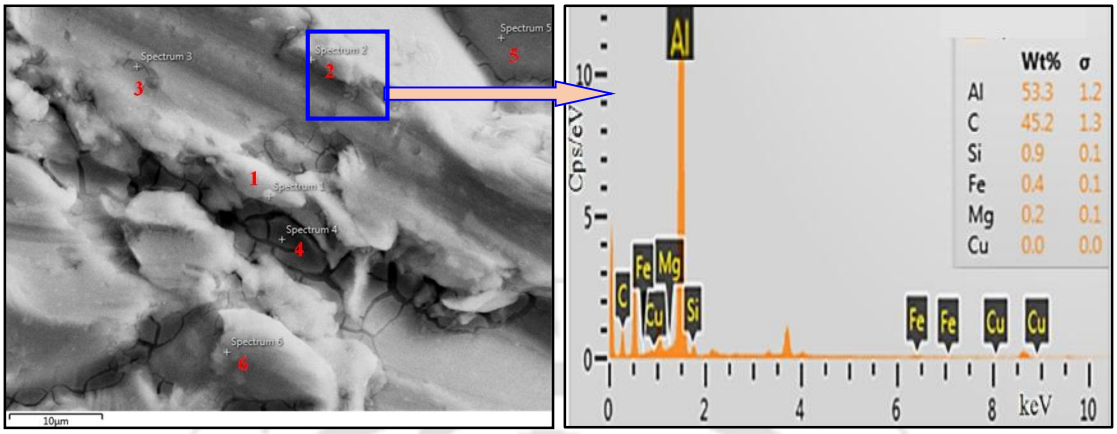

(a) (b)

Figure 8.4 EDS surface topology and spectrum point of laser surface alloyed Al-SiC material: (a) micrograph of surface topology of alloyed region and (b) EDS point spectrum

Figures 8.5 (a–b) represent the surface morphology of laser surface alloyed zone with TiO_2. A strong homogeneity without porosity and micro-segregation was observed confirming good formation of metallurgical alloying with aluminum substrate material. Figure 8.5 (a) is the top layer of alloyed region. Figure 8.5 (b) shows the center of the melt pool with dendrite microstructure. The columnar grains structure between laser alloyed zone and aluminium substrate were formed. The grains are almost perpendicular to the melting surface of the substrate and direction of laser beam energy. The columnar grains grow up to the substrate leading to good metallurgical bonding. Among the columnar spacing, there is segregation of diffused titanium dioxide grains, which makes a strong effect on hardening of the alloy. The grain structures look different in shape and distribution due to variation of solidification rate and diffusion of titanium dioxide in aluminium solution. Table 8.2 shows the chemical composition of Al-TiO_2 material where maximum 30.2 wt.% Ti was observed. Figures 8.6 (a–b) show the EDS micrograph and corresponding point spectrum for Al-TiO_2.

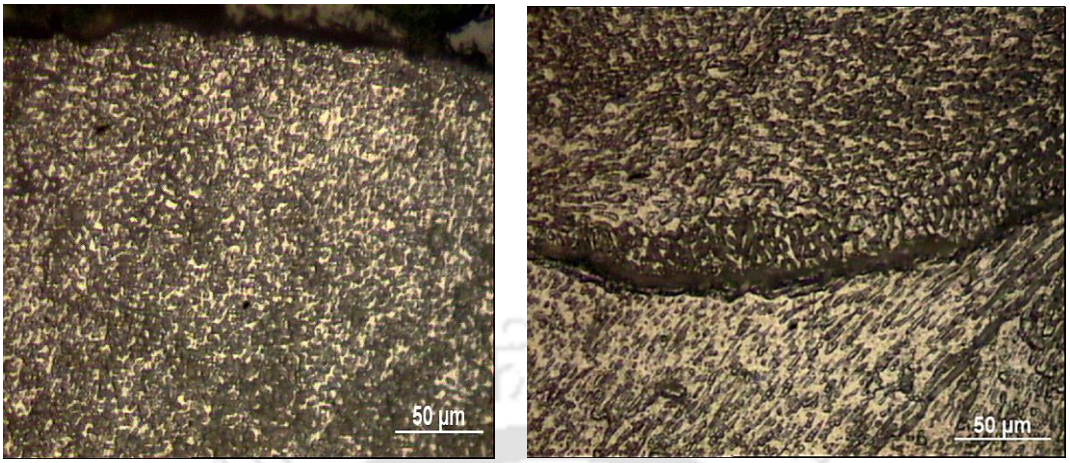

(a) (b)

Figure 8.5 Optical images of laser surface alloyed aluminum with TiO_2 (×20): (a) top alloyed region and (b) interface of alloyed region

The wetting between TO_2 and aluminum substrate was created since alloying was successfully formed after laser melting. There are reasons for this, surface roughness after alloying was reduced and microstructure at the interface zone is free from any defects such as porosity and microcrack. From some literatures works, despite the fact that there is no exact study on laser surface alloying, wettability and contact angle of TO_2 and aluminum were studied by many researchers. Sobczak *et al*. (2004) studied wetting properties of molten aluminum on polycrystalline TiO_2 by sessile drop method in a vacuum at 1173-1373 K. Their results show after application of capillary purification process molten aluminum wets titania at 1173 K and the contact angle was 80^o. Shen *et al*. (2006) reported wettability of polycrystalline rutile TiO_2 by molten aluminum in purified Ar-3% H_2 and vacuum. In argon atmosphere, a strong reaction between TiO_2 and molten aluminum created at high temperature of 1573 K. The contact angle at the interface decreased with increased temperature. However, in a vacuum contact angle decreased with increased temperature of 1473 K. Avraham and Kaplan (2005) reported the wetting kinetics of TiO_2 and molten aluminum spreading of molten aluminum drop on TiO_2 surface was governed by reduction reaction at the solid liquid interface. The contact angle was reported very large about 150^o at 937 k. However, contact angle was decreased with increasing temperature at 1273 K where the contact angle changed from 125 to 85^o.

Table 8.2 Chemical composition in wt.% of Al-TiO_2 sample

Ti	Si	O	Fe	Cu	Mg	Al
4.3	5.3	84.5	1.0	0.9	1.3	2.8
13.4	10.8	63.1	1.0	1.2	2.7	7.9
3.4	8.0	80.7	0.8	0.9	1.9	4.2
6.4	43.0	45.5	0.7	0	1.1	3.4
2.6	2.9	88.0	1.2	0	2.4	3.0
30.2	15.2	40.3	0.9	2.5	2.5	8.3
0.1	44.9	54.8	0.1	0	0	0

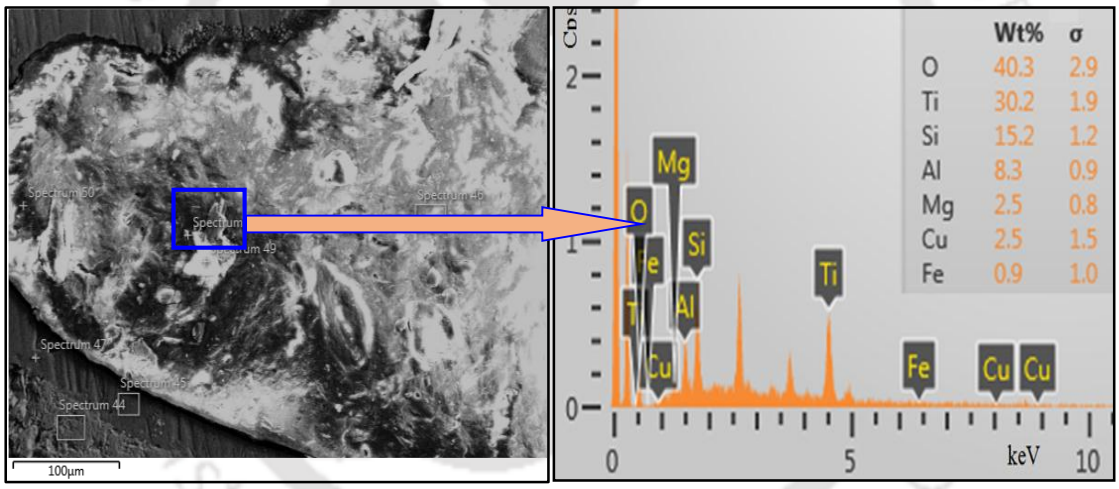

Figure 8.6 EDS surface topology and spectrum point of laser surface alloyed Al-TiO_2 material: (a) micrograph of surface topology of alloyed region and (b) EDS point spectrum

8.3.3 Microhardness of Al-SiC and Al-TiO_2

The micro-hardness of laser alloyed region shows improvement of base material hardness, which is 30 $HV_{0.3}$. Figure 8.7 shows micro-hardness graphs of laser alloyed TiO_2 with alumnium substrate. Figure 8.8 shows the laser alloyed SiC with aluminum substrate. The inset micrograph shows the Vickers hardness indentation in the laser alloyed region. For

both materials, the variation of microhardness got decreased from top-alloyed region to the substrate region for both materials since the alloying elements diffused down the substrate material. Due to SiC laser surface alloying, the microhardness increased up to 180 $HV_{0.3}$. Laser alloying with titanium dioxide increased the micro-hardness up to 220 $HV_{0.3}$ because of the formation of Al_3Ti hard compound. More titanium content had increased the micro-hardness due to the presence of Al_3Ti. The interface microhardness for both materials was less than the laser surface alloyed region. Interface microhardness with Al–TiO_2 laser alloying was found to be less than 90 $HV_{0.3}$ and with Al–SiC laser surface alloying, interface microhardness was less than 60 $HV_{0.3}$. The interface microhardness for both materials was less than the alloyed region because the contribution of alloying elements did not affect the hardness.

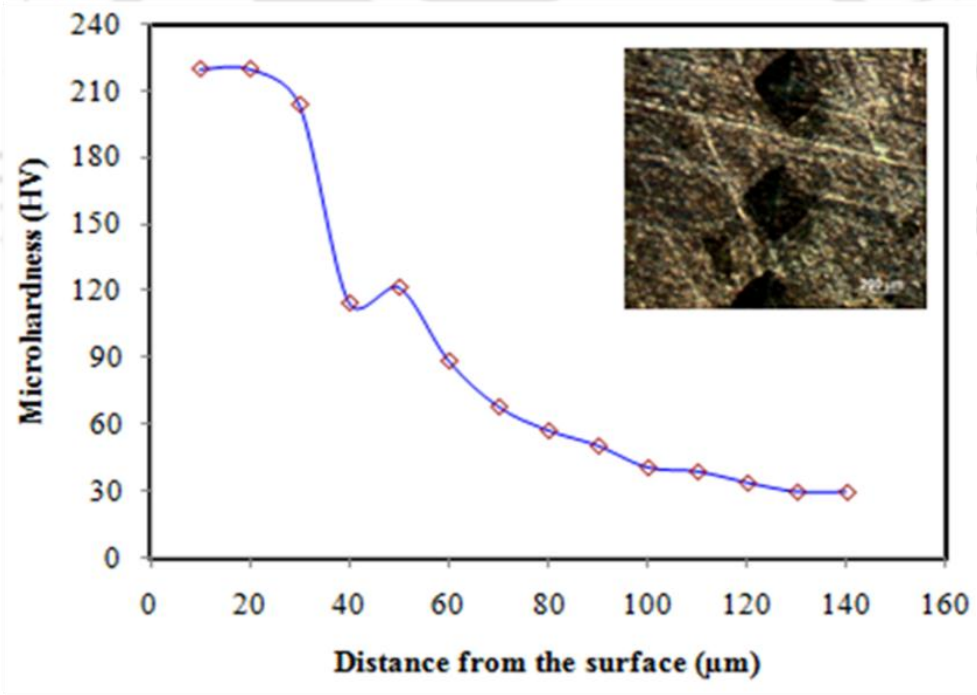

Figure 8.7 Microhardness of TiO_2 deposition on aluminum

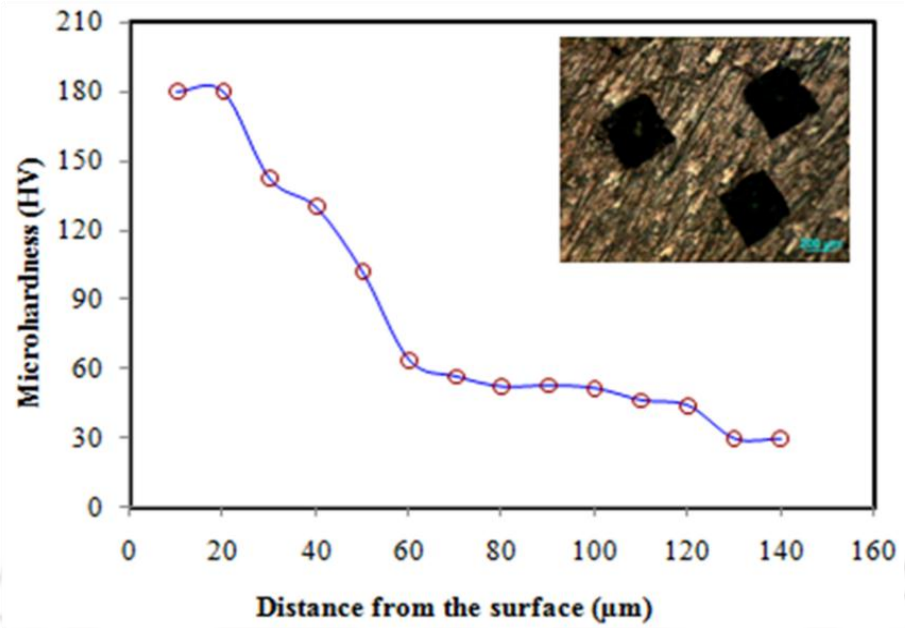

Figure 8.8 Microhardness of SiC deposition on aluminum

8.4 Conclusion

In this chapter, laser surface alloying of commercially pure aluminium with SiC and TiO_2 ceramic powders is discussed. The major findings of this work are as follows:

- In spite of ceramics having higher melting temperature than aluminum, uniform alloying in aluminum was achieved.
- The formation of Al_4SiC_4 and Al_3Ti compounds was observed. For Al-SiC, the maximum microhardness in the alloyed region was 180 $HV_{0.3.}$ For Al-TiO_2 material the maximum microhardness was 220 $HV_{0.3.}$
- The micro-hardness got decreased from the top alloyed region towards the substrate region because of the nature of diffusion mechanism of silicon and titanium in molten aluminium.
- Greater hardness was achieved in alloying aluminum with TiO_2 as it is a very hard polycrystalline oxide material.
- Laser melting and fast solidification refined the grain structure that contributed towards improving its hardness.

भारतीय प्रौद्योगिकी संस्थान गुवाहाटी
Indian Institute of Technology Guwahati

Chapter 9

Laser Surface Melting of Al-12Si-4Cu-1.2Mn Alloy

9.1 Introduction

Al-Si-Cu-Mg alloys are widely used to manufacture cylinder blocks and covers of the engine for small passenger cars because of their good strength at high temperature. Long back, Clarke and Sarkar, (1979) observed that the wear resistance of Al-Si alloys increases with increasing silicon content until the eutectic composition, i.e. 12 wt.%. Hwang *et al*. (2009) observed that addition of 0.45 wt.% Mg to type 319 aluminum alloy (Al-6.7Si-3.75Cu) increased the strength of the alloy, although at the expense of ductility. The addition of manganese further improves the high temperature strength of the aluminum alloys. Manganese addition in Al-7Si-3.8Cu-0.5Fe alloys is usually used to neutralize the detrimental effects of β-Al_5FeSi by transforming it to the α-Al_{13} $(Mn, Fe)_4$ Si_2 phase (Hwang *et al*., 2008). Liao *et al*. (2017) developed high manganese aluminum alloy, Al-12Si-4Cu-1.2Mn by casting route. It displayed high ultimate tensile strength (more than 132 MPa) at 250 °C.

Apart from the high tensile strength for cylinder blocks, a high surface hardness and good tribological behavior is also needed. Laser surface melting (LSM) can be a potential process for improving the surface characteristics. LSM has been applied for improving the hardness of cast alloys as well as fabricating the product from the powder. In this process, cooling rates of the order of 10^5 to 10^8 K/s are obtained that helps in achieving the refined microstructure (Sahoo *et al*., 2015). Pinto *et al.* (2003) carried out LSM of Al-15Cu alloy and observed about 3 times increase in the hardness. Abbas *et al*. (2006) carried out LSM of magnesium alloys, AZ31 and AZ61, using a 1.5 kW high power diode laser (HPDL). A significant improvement in the hardness and wear resistance was observed with a grain size of about 5 μm. Zhang *et al*. (2008) enhanced the tribological

properties of AM50 magnesium alloy by LSM with a 2 kW continuous wave CO_2 laser. A significant improvement in microhardness and wear resistance was observed, although there was no significant effect on the coefficient of friction. Cabeza *et al*. (2012) used LSM to repair the surface of a maraging steel, 14 Ni (200 grade), in different heat treatment conditions using high power solid Nd-YAG laser.

Effect of LSM on corrosion behavior has also been studied. Conde *et al*. (2000) carried out LSM of austenitic, ferritic and martensitic stainless and observed an increase in the corrosion resistance provided the correct processing parameters were used. Majumdar *et al*. (2003) observed that LSM of a commercial Mg alloy, MEZ (Zn 0.5%, Mn 0.1%, Zr 0.1%, rare earth elements 2%, Mg remaining percentage), resulted in an increase of its hardness, wear resistance and corrosion resistance. Osorio *et al*. (2008) investigated the effect of LSM on the corrosion resistance of Al-9Si casting alloys. As-cast samples were remelted using a continuous 1 kW CO_2 laser. However, the corrosion resistance got reduced due to LSM.

Kang *et al*. (2016) carried out selective laser melting of mixtures of Al-12 Si alloy and Si powders to improve the wear performance. Final composition achieved was Al-18Si. Aboulkhair *et al*. (2016) improved the fatigue performance of selectively laser melted Al-Si10Mg alloy. Laorden *et al*. (2017) reported selective laser surface melting of A356 and aluminium matrix composite reinforced with SiC particles (A356/10% SiC particles). Several researchers investigated the polishing of surface using laser irradiation. Ukar *et al*. (2010) reported 90% surface roughness reduction after laser polishing of DIN 1.2379 tool steel using CO_2 and high power diode laser. The mean roughness value obtained was below 0.5 μm. Pfefferkorn *et al*. (2014) reported the advantages of pulsed laser polishing of S7 tool steel. They observed that larger melt pool diameter provided smoother surface than smaller one. Pfefferkorn and Morrow (2017) have presented interesting results on pulsed laser micro-structuring of the surface of Ti-6Al-4V alloy.

In this piece of work, LSM of Al-12Si-4Cu-1.2Mn was carried out to study its influence on microstructure, microhardness, tensile strength and wear resistance. Both as-cast and heat treated by solutionizing samples were remelted using a 2.5 kW CO_2 laser

machine. The samples used for the study were prepared by casting in a graphite crucible. It is the first attempt of improving the surface properties of Al-12Si-4Cu-1.2Mn by LSM. Due to high production speed of LSM, the procedure reported in this work can be conveniently adopted for industrial use, particularly for automobile sectors. As several manufacturing processes can be carried out in the same laser machine, this process can be the part of a rapid manufacturing system.

9.2 Materials and Method

Al-12Si-4Cu-1.2Mn alloy was prepared in a graphite crucible of 3 kg capacity using a melting/vacuum holding furnace with Al-12.5 wt.% Si, Al-10 wt% Sr and Al-10wt.% Mn master alloys, commercial purity Cu (99.8%) ingot and Si (98%) particles. After processing, the melt was poured at 720 °C into a plate-like iron mold (with a cavity of 170 mm × 100 mm × 20 mm, preheated at 250 ^{o}C for 5 hours). The chemical composition of the prepared alloy was measured by MAXx LMF15 spark emission spectrometer as 12.68 wt% Si, 4.07 wt.% Cu, 1.19 wt.% Mn, 0.12 wt.% Fe, 0.023 wt.% Sr and balance aluminum. The prepared samples were divided into two groups. One group was kept for LSM of as-cast samples, whilst the other group was solutionized at 510 °C for 5 h. The solutionized samples were aged at 165°C for 6 h. LSM of solutionized and aged, i.e., heat treated samples, were also carried out. For LSM, samples were solid rectangular parallelpiped of 70 × 35 × 5 mm^3 size, cut from the cast aluminum alloy. On the surface of 70 × 35 mm^2 size, LSM was carried out along the width direction (which was 35 mm long) in a single track without overlapping.

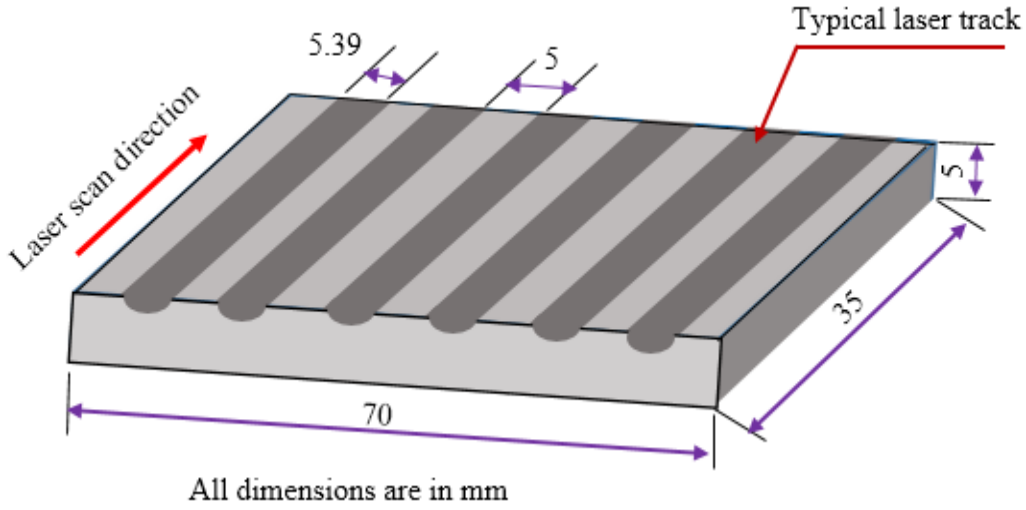

Figure 9.1 Schematic of laser surface melting aluminum alloy

A schematic of LSM is shown in Fig. 9.1. Total six tracks were made with a gap (distance between two track centers) between them as 10.39 mm. This ensured that there was no overlap between the tracks. A 2.5 kW continuous wave CO_2 laser of mode TEM_{00} (Gaussian beam) was used at different laser parameters in the range 1.7–2.2 kW laser power and 300–550 mm/min laser scan speed. Laser standoff distance of 40 mm and laser beam diameter of 5.39 mm were used.

The final mirror polishing was achieved by a velvet cloth impregnated with Silvo chemical. The etching was done for 6–8 s by rubbing with a cotton wool followed by washing with distilled water. The dried samples were observed in an optical microscope as well as in a field emission electron microscopy (FESEM) setup. For studying the chemical composition after laser remelting, both elemental mapping and chemical composition in terms of the weight percentages of various elements were analyzed using EDS. Different mechanical properties were studied after laser remelting was conducted.

The hardnesses variation along thickness in laser remelted region was measured using Vickers microhardness tester with 0.3 kg load. The hardness tester conformed to ASTM E384 standard with a 0.2% load accuracy. Considering the errors in the measurement of diagonals of indentation, it is estimated that the error in the measurement

of microhardness will be less than 2%. The hardness distribution was studied at the middle of the track at two locations along laser scan line. Surface scratch testing was conducted by applying a constant load of 50 N. The load application error was less than 2%. The scratch offset distance of 1 mm and loading speed of 0.2 mm/s were used. The scratch test was conducted starting from substrate portion to laser re-melted region i.e., along orthogonal to melted tracks on the surface. The deformation depth of the scratches formed on the surface was measured using an optical surface profilometer. The tensile tests were conducted at room temperature for as-cast as well as heat treated samples after LSM at 1.9 kW powers and 400 mm/min laser scan speed. The overall laser parameters used are mentioned in Table 9.1. The estimated error in the measurement of ultimate tensile strength was less than 2%. For conducting the tensile test, first the continuous multiple remelting tracks without bead overlapping were carefully prepared on one surface of the sample. Then the tensile specimens were prepared by cutting a portion of the laser treated area using a wire electrical discharge machine. The tensile sample was 5 mm thick with a gauge length of 25 mm. Width at the gauge length portion was 6 mm and the total length of the sample was 100 mm. At least two replicates were carried out in all mechanical tests. Variation between two replicates was less than 5%; hence it was considered appropriate to report the average values of the mechanical properties. In the case of a non-moving laser beam, an important parameter is the power density (irradiance) I given by (Matys *et al*.,2015; Kadhim *et al*., 2013)

$$I = \frac{4P}{\pi d^2}, \tag{9.1}$$

where P is the laser power and d is laser beam diameter at the spot. Usually, the laser beam diameter is taken as the diameter of a circle containing 86% of the beam power with its center at the centroid of the beam profile. Another parameter is energy density (fluency) F given by (Matys *et al*., 2015)

$$F = \frac{4E_t}{\pi d^2}, \tag{9.2}$$

where E_t is the total energy irradiating inside the circle that contains 86% of the beam power. For the moving laser beam, the important parameter is the laser specific energy E given by (Kadhim *et al*., 2013):

$$E = \frac{P}{vd}, \tag{9.3}$$

where v is scan speed. The laser specific energy combines the power density and interaction time (d/v) into one factor; E is proportional to I and interaction time. In this work, the laser parameters were decided based on the pilot experiments.

Table 9.1 Laser process parameters for LSM with laser beam diameter of 5.39 mm

Laser power (kW)	Laser scan speed (mm/min)	Laser specific energy (J/mm^2)
2.2	550	45
2.1	500	47
2.0	450	49
1.9	400	53
1.8	350	57
1.7	300	63

9.3 Results and Discussion

In this section, the results of all experiments are discussed in details. Laser surface melted depth and width for different laser process parameters were studied. The microstructure, grain size, surface morphology and elemental mapping were investigated. Mechanical properties like microhardness, scratch resistance and tensile properties were also studied.

9.3.1 The remelted thickness

Figure 9.2 shows the cross-sectional view of a laser surface melted samples measured by digital microscopy. The laser remelted region is seen as a half-moon shape. The variations of remelted depth and width with laser specific energy is shown in Figure 9.3. In general, the depth and width increase with the laser specific energy. At high laser specific energy,

the depth and width of remelted region are greater for as-cast samples than those for heat treated samples. Also, the effect of laser specific energy on the depth is more pronounced for as-cast than for heat treated. Wong *et al*. (1997) also observed an increase in the depth and width of laser remelted region with laser specific energy. It is expected that the melting point increases with the hardness. This may be the main reason for less remelting of heat treated samples.

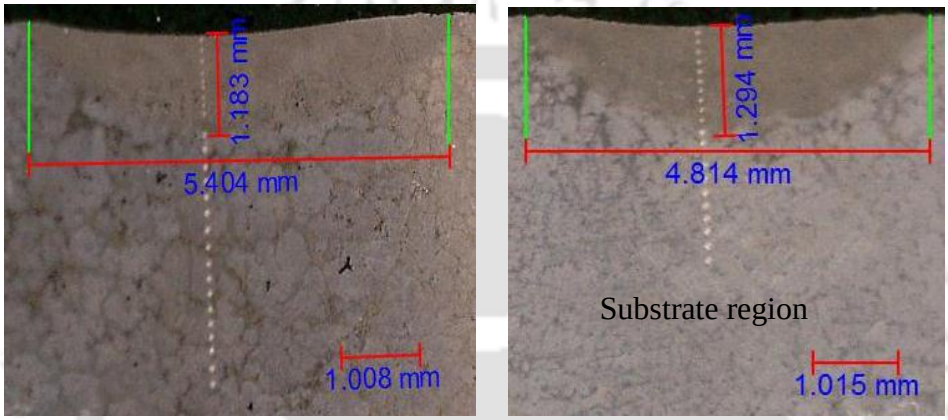

(a) (b)

Figure 9.2 Cross-section view (×20) after laser remelting with laser specific energy of 47 J/mm^2 of (a) as-cast and (b) heat treated samples

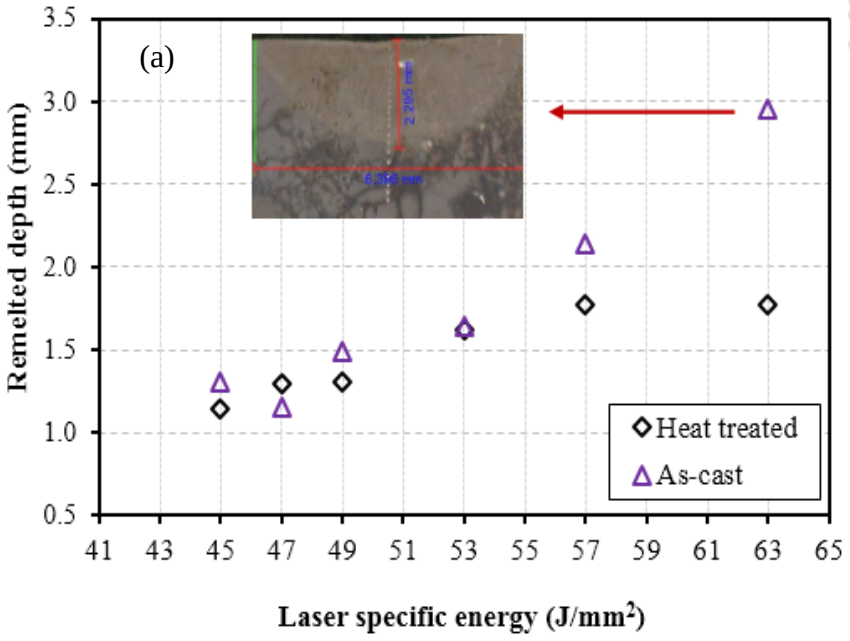

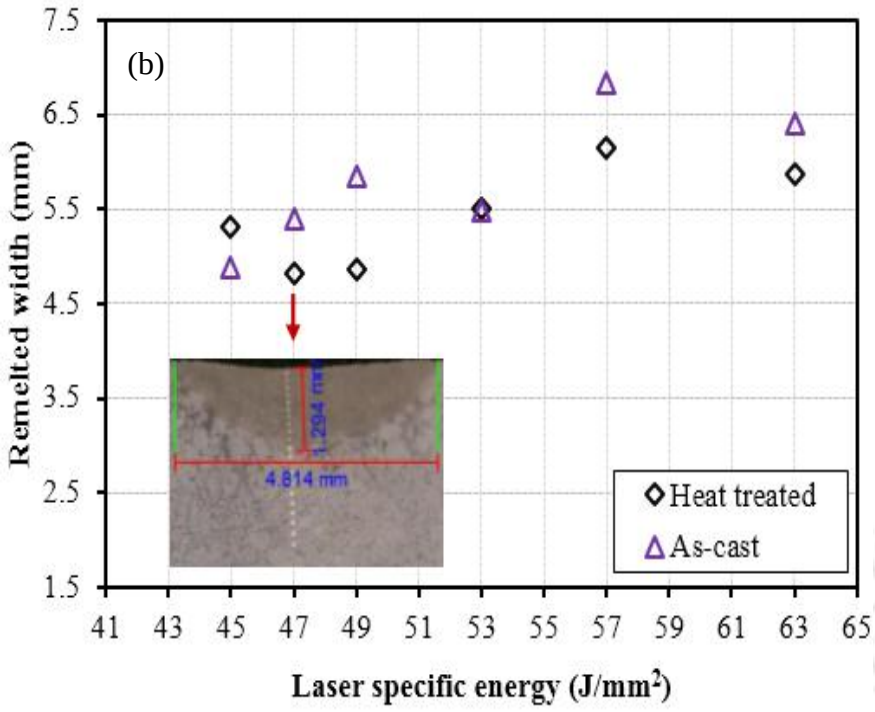

Figure 9.3 The effect of laser specific energy on laser remelted region: (a) depth and (b) width

9.3.2 Microstructure and grain size

Figures 9.4(a–b) show the microstructure of as-cast and heat-treated samples, respectively, prior to LSM. As discussed in detail by Liao *et al.* (2017), for Al-12Si-4Cu-1.2Mn alloy, the as-cast microstructure comprises $Al_{15}Mn_3Si_2$ (Mn-rich), Si, α-Al and θ-$CuAl_2$ phases. The Mn-rich phase is in primary and eutectic forms. The Si phase is in the form of eutectic with α-Al + $Al_{15}Mn_3Si_2$ or added θ-$CuAl_2$ phases. In Fig. 9.4(a), the blue rod-like phase is Mn-rich phase. The heat treatment produced finer Mn-rich phase with grain sized structure (Fig. 9.4b).

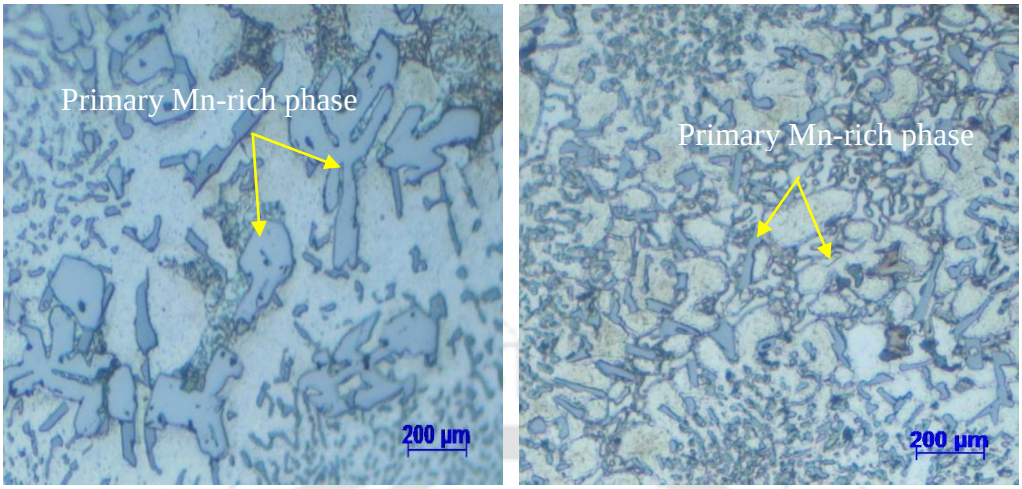

(a) (b)

Figure 9.4 Microstructure (× 40) before LSM of (a) as-cast and (b) heat treated samples

Figures 9.5 (a–f) show the microstructure of as-cast samples after laser remelting. Figures 9.5(a–b) illustrate primary and secondary dendrite formation. The primary Mn-rich phase was observed in these figures as well as in Figures 9.5(c–d). Figure 9.5 (f) shows only small amount of primary Mn-rich phase. When the laser power was applied at the top surface, melting started at the surface and penetrated towards substrate portion. On the other hand, solidification started from the interface between laser remelted region and substrate. It moved towards the top surface. At lower laser energy densities, primary Mn-rich phase survived as observed in Figures 9.5(a–d). Mn-rich phase almost disappeared at high laser specific energy as evident from Figures 9.5(e–f).

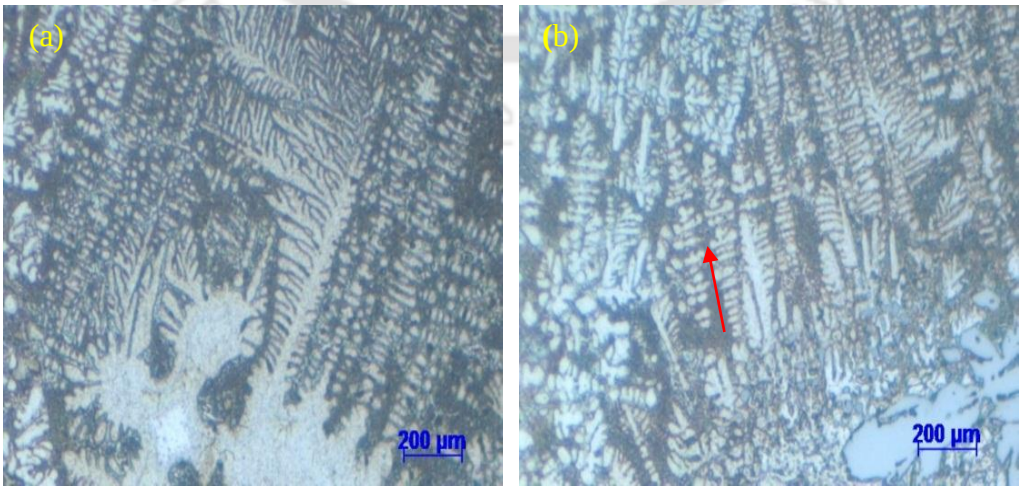

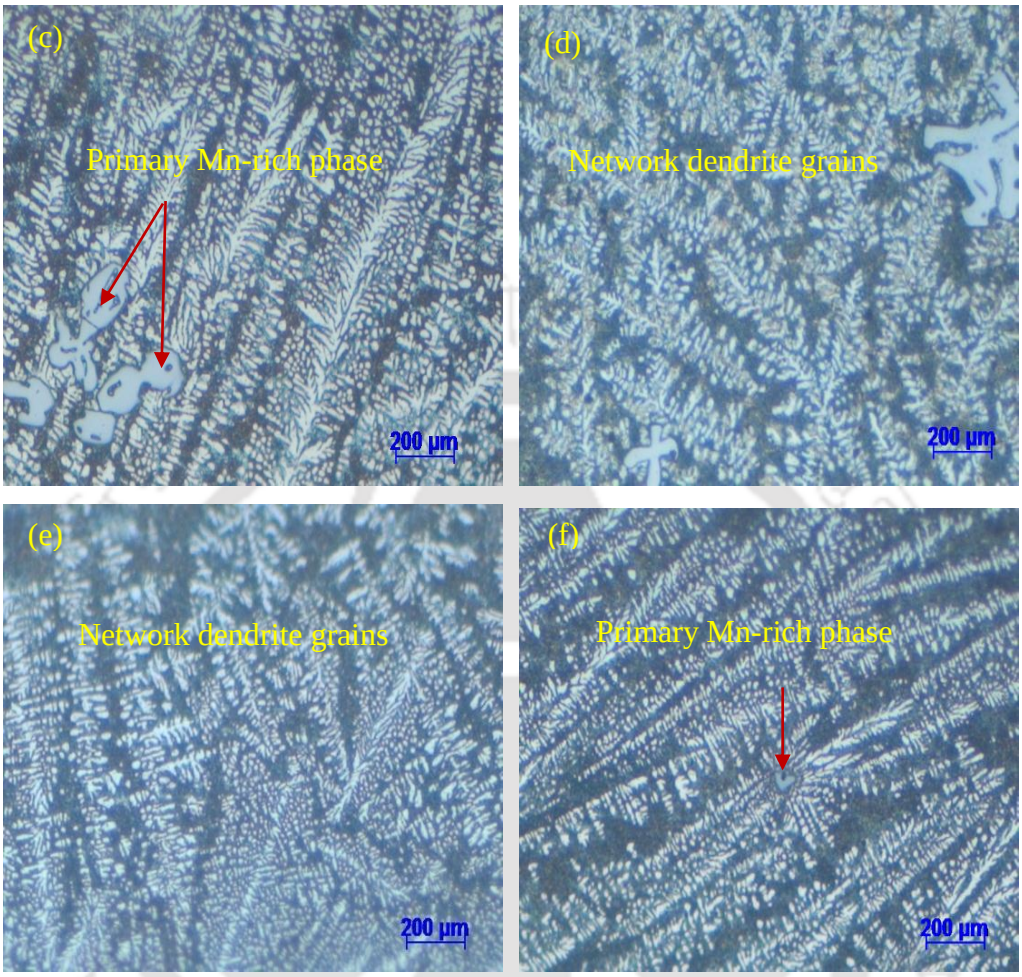

Figure 9.5 Microstructure (×40) of as-cast samples after LSM at laser specific energy of (a) 45 J/mm^2, (b) 47 J/mm^2, (c) 49 J/mm^2, (d) 53 J/mm^2, (e) 57 J/mm^2 and (f) 63 J/mm^2

Figures 9.6 (a–f) show the microstructure of heat-treated samples after laser remelting. The dendrite microstructure was formed like in as-cast samples. The dendrite grains formed at the interface and grew in the direction of melt pool center. For heat treated samples, undissolved silicon and impurity segregation were not found. At high laser specific energy, dendritic arm length is longer and grain size is coarsened as shown in Figures 9.6 (e–f). The high energy used, formed a large remelted region; hence the cooling rate was slower. Because of this effect, the dendrite arm structure got sufficient time to grow. It is also observed in Figures 9.6 (e–f) that the top and center remelted regions have small grain, small dendritic cells and small dendrite arm spacing as compared to interface-

remelted layers. This is as per the investigation of Kaya *et al*. (2007) on dendrite growth process of Al-Si alloy, indicating that microstructure parameters such as primary dendrite arm spacing, secondary dendrite arm spacing, dendrite tip radius and mushy zone depth depend on temperature gradient and growth rate. All these parameters decreased in magnitude when the temperature gradient and dendritic growth rate were increased.

The average grain size was calculated using mean linear intercept method. Figure 9.7 illustrates the average grain size of the laser-remelted samples with respect to laser process parameters. The grain sizes of as-cast and heat treated samples were compared. It was found that the average grain size of as-cast samples was bigger than the heat-treated samples. At the minimum laser specific energy of 44 J/mm^2, an average grain size values were 26 µm and 30 µm, for heat-treated and as-cast samples, respectively. The corresponding values were 30 µm and 43 µm for the laser specific energy of 63 J/mm^2. A high laser specific energy created wider and deeper remelted layer thickness, which increased the cooling time. A large cooling time facilitated the formation of coarser grains. The grain size of the heat-treated sample before laser remelting was 65 µm, while it was 74 µm for as-cast samples. Thus, LSM always refined the grains, which helped in improving the mechanical properties and tribological performance.

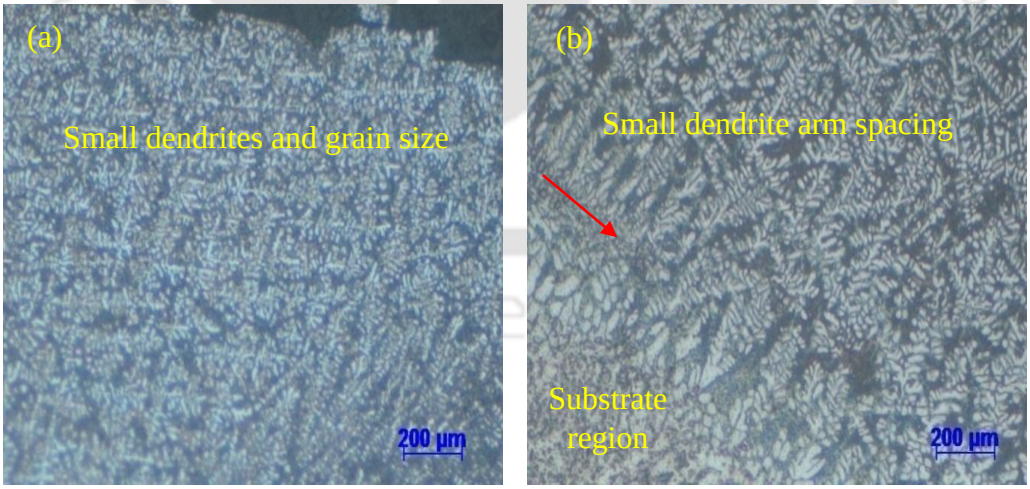

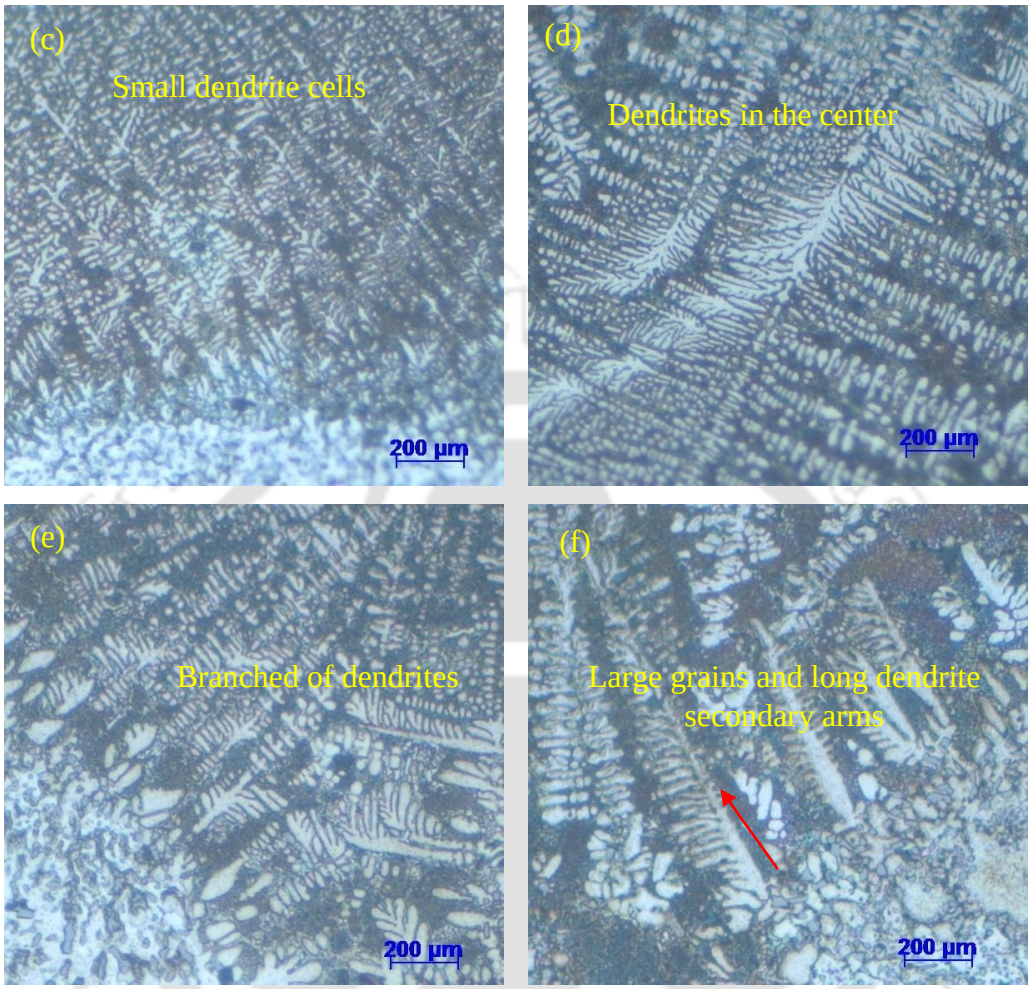

Figure 9.6 Microstructure (×40) of heat treated samples after LSM at laser specific energy of (a) 45 J/mm^2, (b) 47 J/mm^2, (c) 49 J/mm^2, (d) 53 J/mm^2, (e) 57 J/mm^2 and (f) 63 J/mm^2

The samples were observed by field effect scanning electron microscopy (FESEM). Figure 6.8 is the image of as-cast and Figure 9.9 is the image of heat treated samples after LSM. These images were obtained for LSM, carried out at 53 J/mm^2 specific energy. A good metallurgical bonding is observed in both the images.

The energy dispersive X-ray spectroscopy (EDS) was carried out after LSM at 53 J/mm^2. Figures 9.10 (a–b) show element mapping and spectrum for as-cast samples. The composition at the remelted region was 17.6 wt.% Si, 2.9 wt.% Mn and 3.1 wt.% Cu. Figures 9.11 (a–b) show EDS analysis for heat treated samples. Here, the composition of

the remelted region was 13.4 wt.% Si, 3.9 wt.% Mn, 3.6 wt.% Cu and 0.4 wt.% Fe. This composition is nearer to eutectic composition.

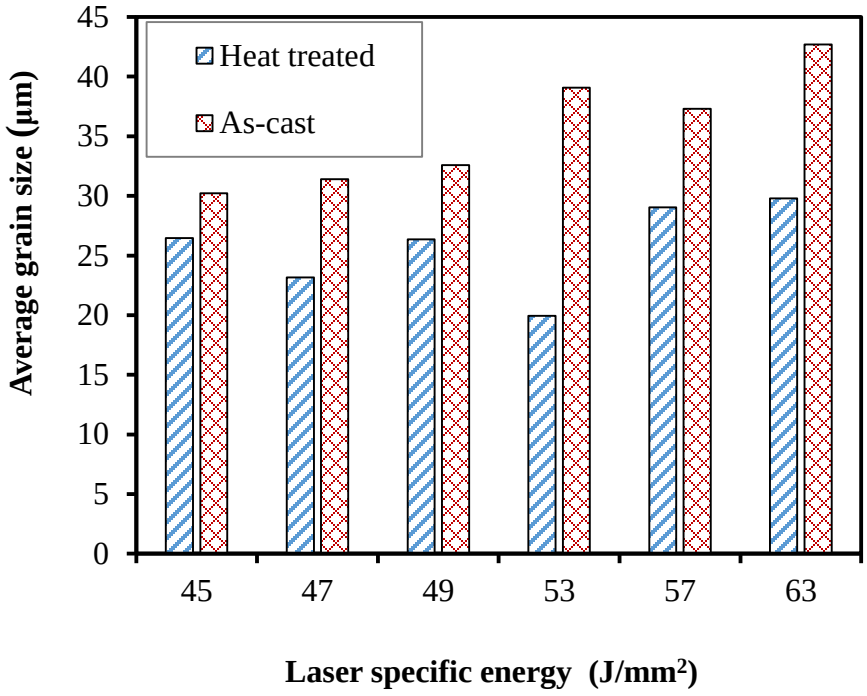

Figure 9.7 The effect of laser specific energy on average grain size after LSM

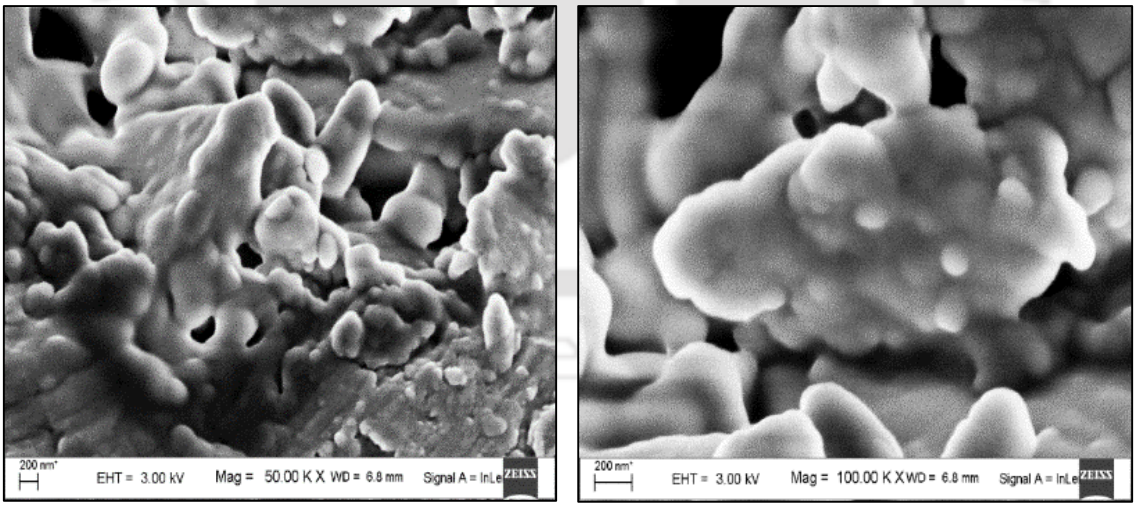

(a) (b)

Figure 9.8 The FESEM image of as-cast sample after LSM at laser specific energy of 53 J/mm^2: (a) × 50000, (b) × 100000

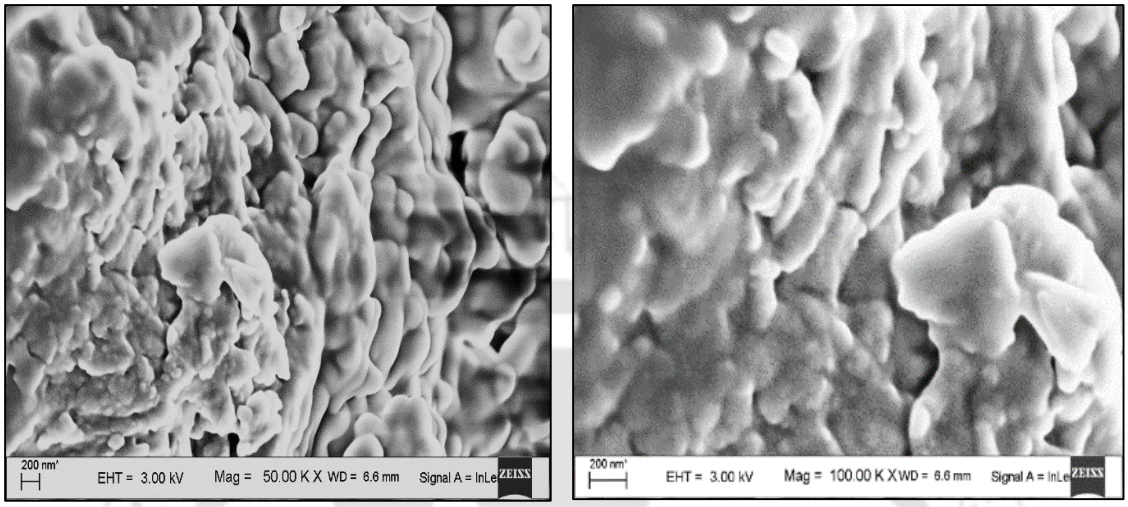

(a) (b)

Figure 9.9 The FESEM image of heat treated sample after LSM at laser specific energy of 53 J/mm^2: (a) ×50000, (b) ×100000

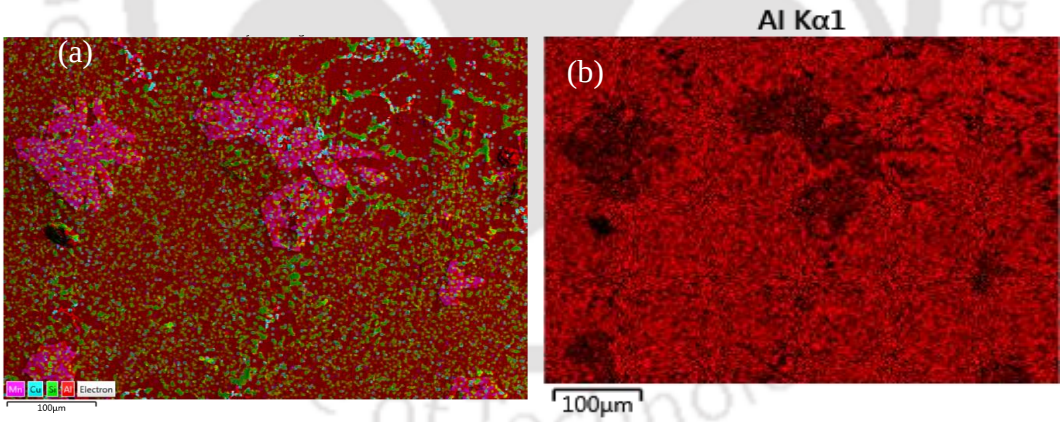

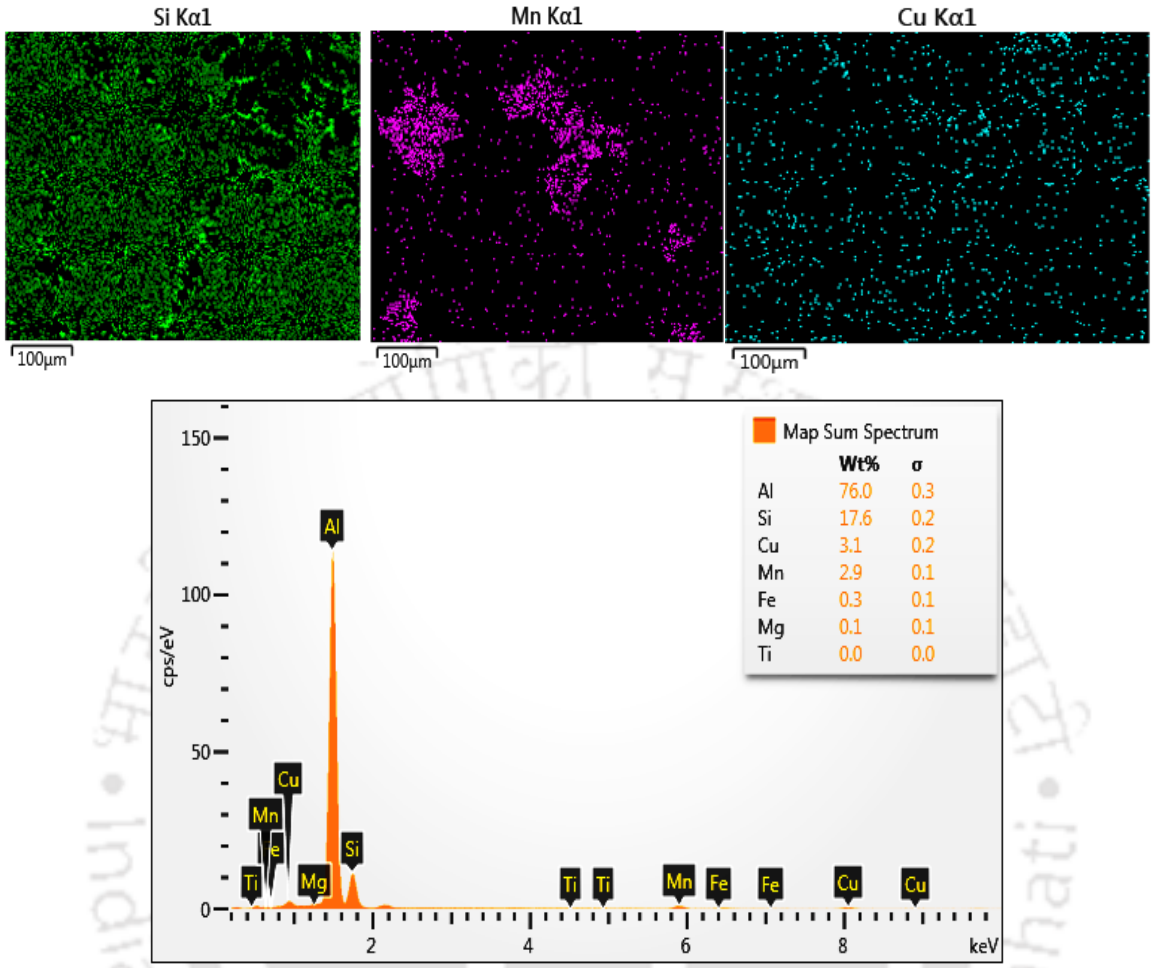

Figure 9.10 EDS analysis of as-cast sample after LSM at laser specific energy of 53 J/mm^2: (a) elemental mapping and (b) spectrum

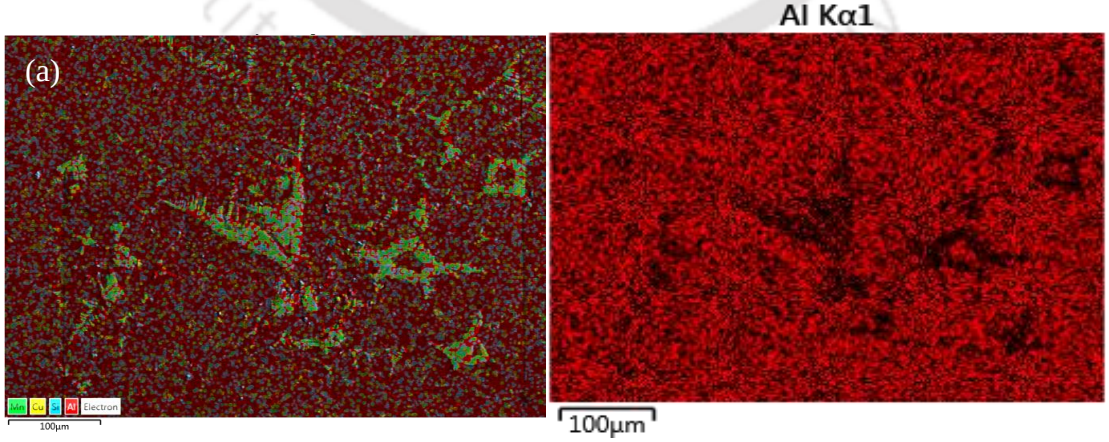

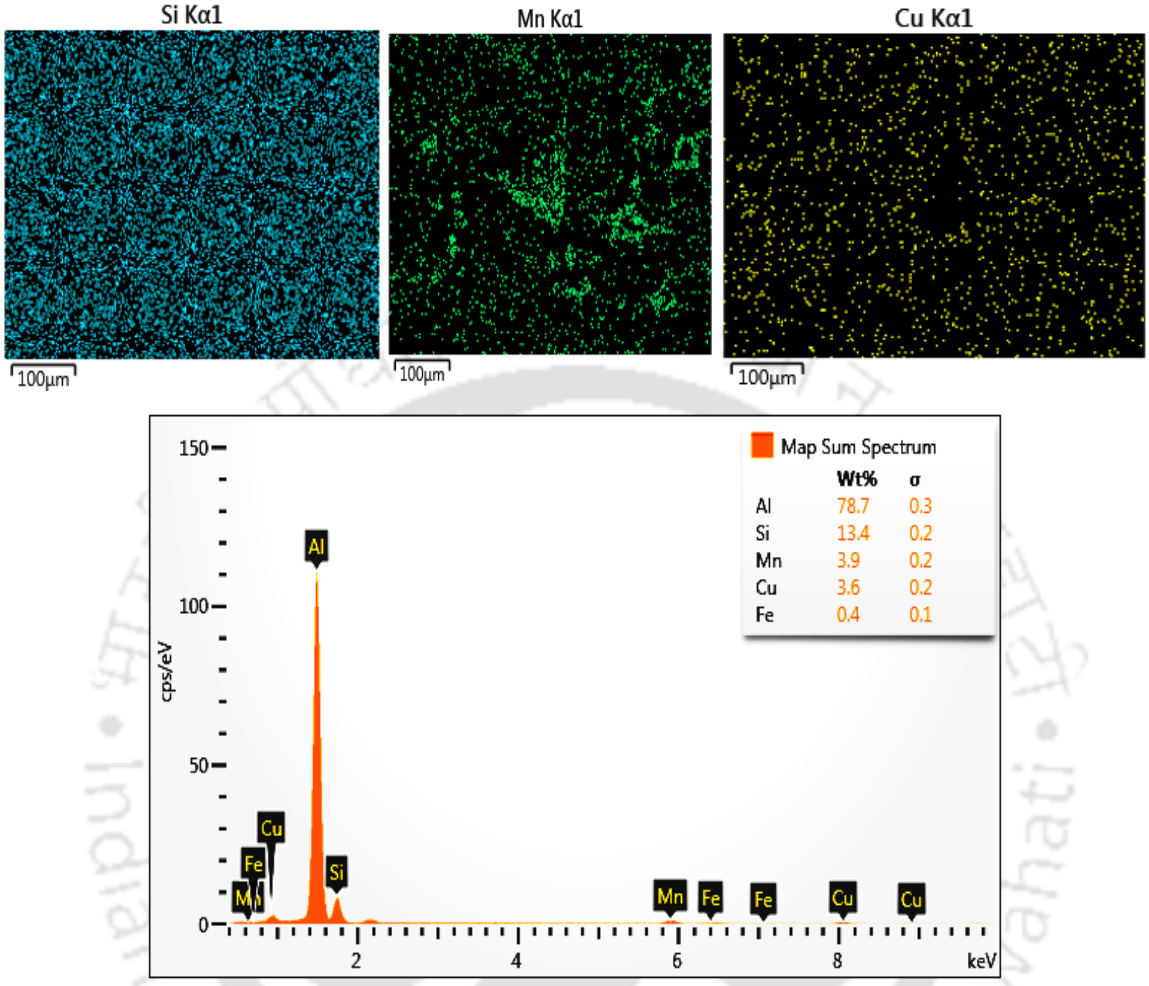

Figure 9.11 EDS analysis of solutionized heat treated sample after LSM at laser specific energy of 53 J/mm^2: (a) elemental mapping and (b) spectrum

9.3.3 Microhardness

The microhardness of laser-remelted layer was measured in cross-section from the top of the laser-remelted region to the substrate region as shown in Figure 9.2. There was a substantial increase in the hardness of the laser-remelted region, although it was not uniform throughout the remelted layer. Figures 9.12 (a–f) show the microhardness values of as-cast and heat treated samples after SLM. The average value of microhardness prior to laser remelting was 82 $HV_{0.3}$ and 79 $HV_{0.3}$ for heat-treated and as-cast samples, respectively. After SLM at 45 J/mm^2, the heat treated sample had the maximum

microhardness of 175 $HV_{0.3}$ near the top remelted region, whilst as-cast sample had the microhardness of 187 $HV_{0.3}$. For the LSM at laser specific energies of 45 J/mm^2 and 47 J/mm^2, the microhardness of as-cast samples was greater than that of heat treated samples. This may be due to over-aging effect in heat treated samples. However, at high laser specific energy, the microhardness of heat treated samples becomes more than that of as-cast samples. Nevertheless for both types of samples, the hardness is more at low laser specific energy rather than at high laser specific energy. For heat treated samples after laser remelting, the maximum hardness of 204 $HV_{0.3}$ was measured for samples processed at 49 J/mm^2 laser specific energy. However, for an as-cast sample processed at 47 J/mm^2 laser specific energy, the maximum microhardness of 206 $HV_{0.3}$ was achieved. This indicates that if the goal is increasing the microhardness, the as-cast samples should be processed at low laser specific energy; there is no need of prior solutionizing heat treatment.

At a laser specific energy of 63 J/mm^2, relatively low microhardness was achieved. This is because a high laser specific energy created deeper remelted thickness of the material with coarse grains. Vaziri *et al*. (2009) also observed that in laser surface alloying of aluminium by Ni, there was an optimum laser power density at which the maximum microhardness was achieved. In all the cases, the microhardness was the highest at slightly beneath the top surface. At the top surface oxidation may cause hindrance in the formation of hard intermetallics. Susnik *et al*. (2012) also observed that in some cases of LSM of Al-Si alloy, the maximum microhardness was achieved at some distance beneath the top surface.

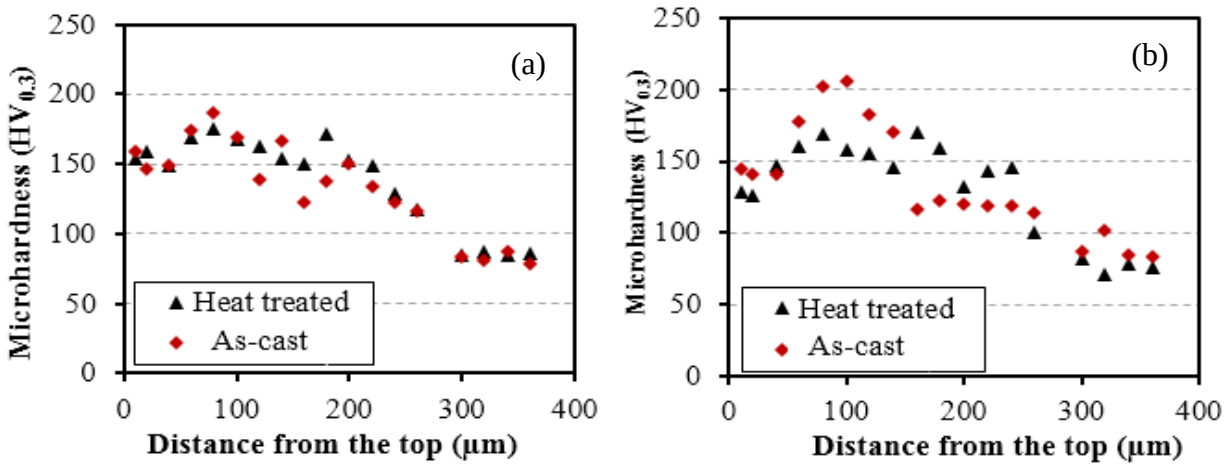

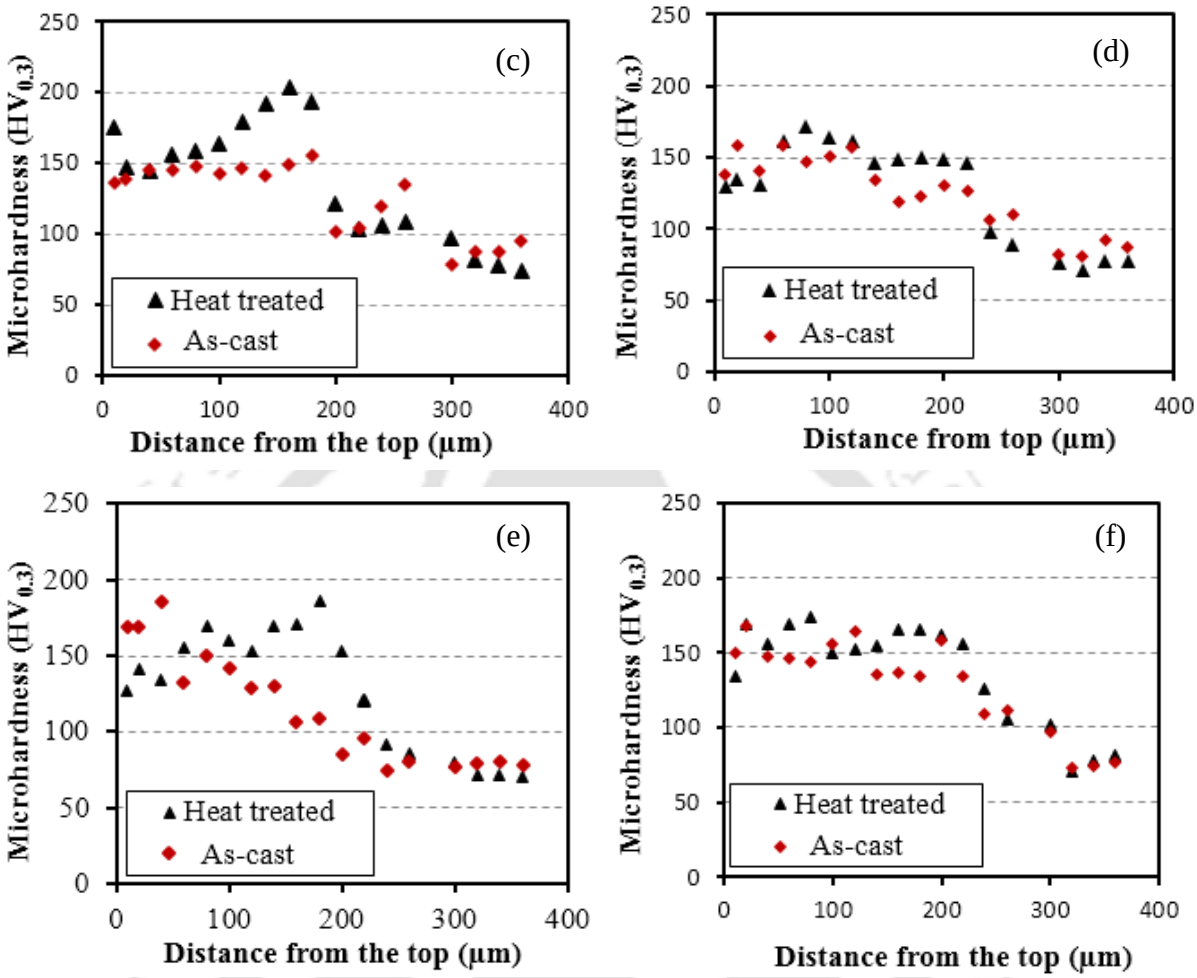

Figure 9.12 Microhardness of samples after LSM at different laser sepecific energies: (a) 45 J/mm^2, (b) 47 J/mm^2, (c) 49 J/mm^2, (d) 53 J/mm^2, (e)57 J/mm^2 and (f) 63 J/mm^2

9.3.4 Surface scratch resistance

The scratch deformation values after LSM are compared in Table 9.2. The scratch test was conducted by applying 50 N load for a sample processed at 49 J/mm^2 laser specific energy. Figures 9.13 (a–d) show the 3-D deformed surface topology and corresponding 2-D profile for each case. Surprisingly, prior to LSM, the scratch resistance of as-cast sample appeared to be more than that of heat treated sample. However, LSM enhanced the scratch resistance for both types of samples.

After laser remelting, the heat treated sample provided less average coefficient of friction of 0.37 than as-cast sample that provided a coefficient of friction of 0.41 as shown in Figure 9.14. In both the cases, the coefficient of friction after LSM was lesser than that before LSM. This is because after LSM, hardness increases significantly. It is well known that harder surface provides less coefficient of friction (Mao *et al*., 2015).

Table 9.2 Scratch deformation at 50 N load

Deformation geometry	**Heat treated (LSM)**	**Substrate for heat treated**	**As-cast (LSM)**	**Substrate for as-cast**
Depth (µm)	29	46	28	33
Width (µm)	325	405	322	370
Area of depth (µm^2)	3836	7825	3546	4557
Areas of built up(µm^2)	3402	5901	3996	7833

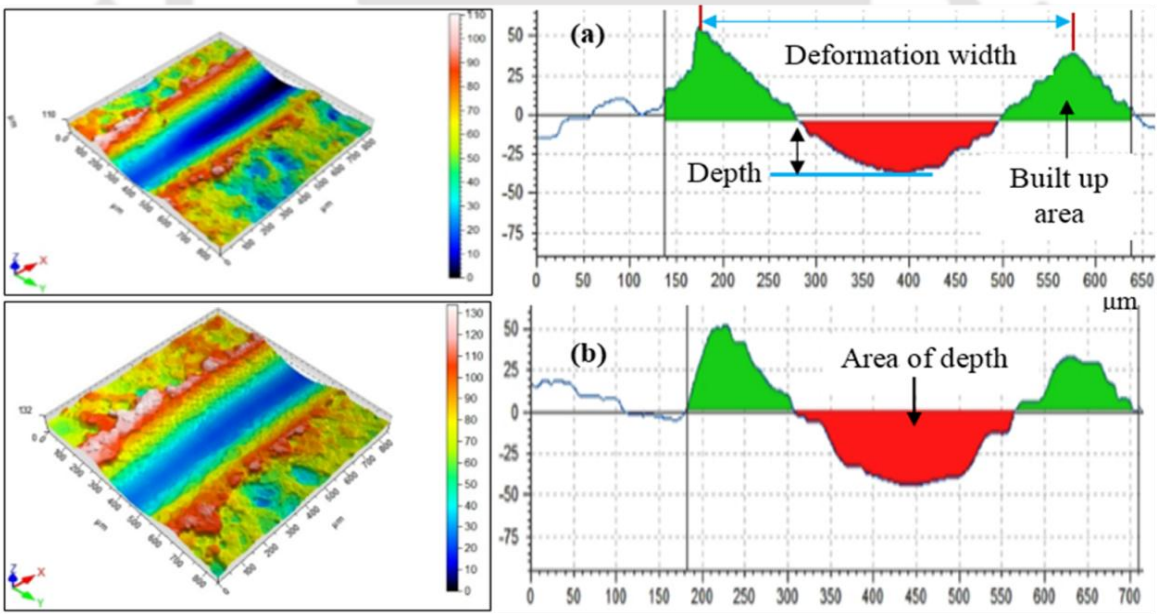

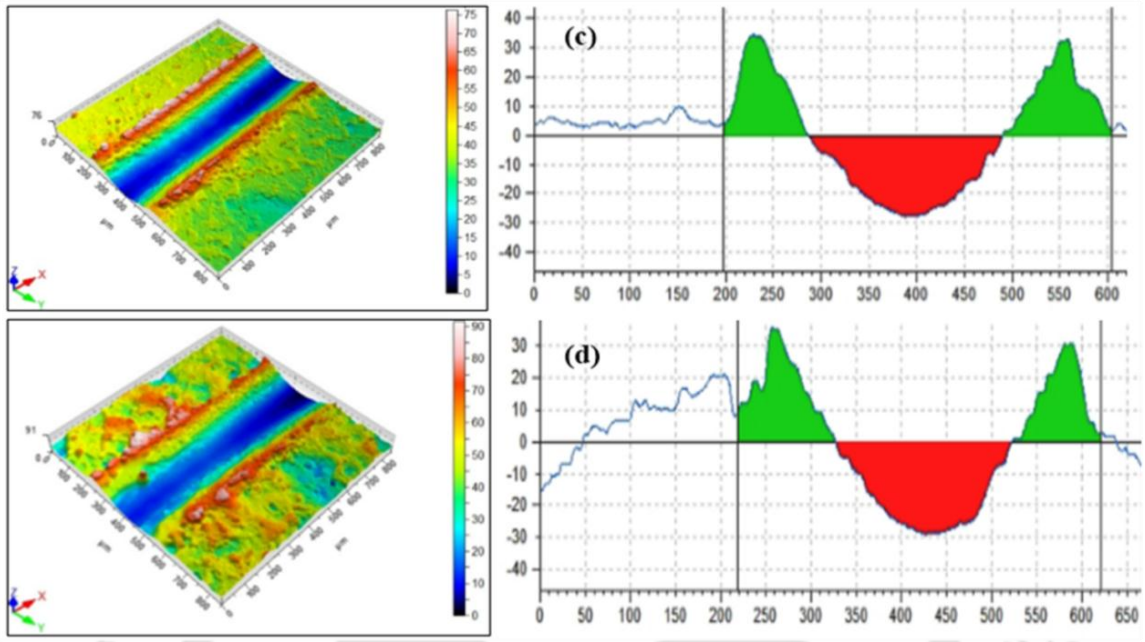

Figure 9.13 3-D and 2-D profile after surface scratch test at 50 N load: (a) substrate of as-cast sample, (b) substrate of heat treated sample, (c) as-cast sample after LSM and (d) heat treated sample after LSM

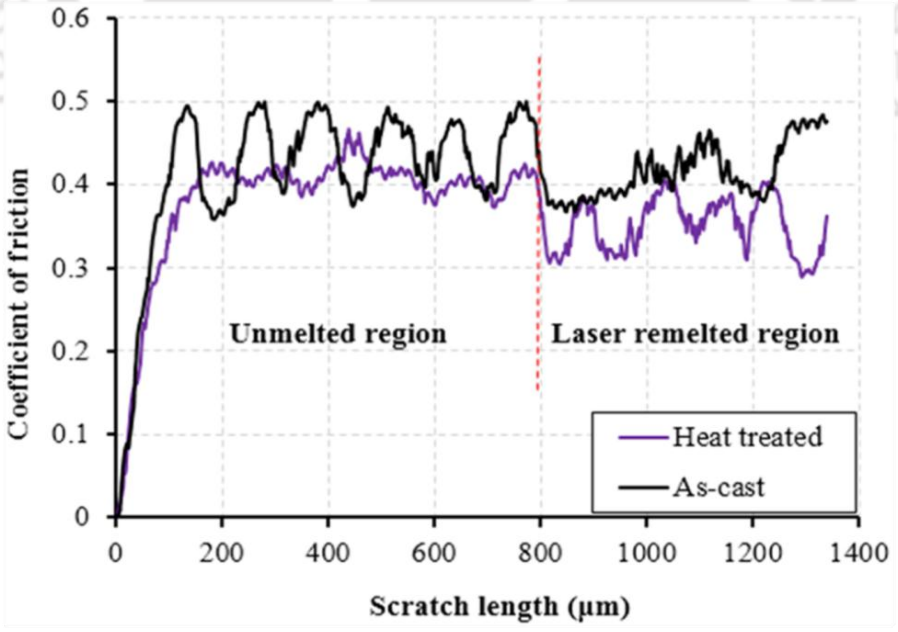

Figure 9.14 The profile of coefficient of friction for laser treated surface and untreated surface of a typical sample processed by 49 J/mm^2 laser energy density under 50 N load

9.3.5 Ultimate Tensile strength

Table 9.3 shows ultimate tensile strength (UTS) values at room temperature. A clear increase in UTS was observed after LSM. As-cast sample has the lowest UTS before LSM, but after LSM its UTS became the highest at 196 MPa. In comparison, the UTS of heat treated samples increased from 143 MPa to 176 MPa after LSM. Thus, in the case of heat treated sample, there was a 23% increase in the UTS after LSM, whilst it was a 70% increase in the case of as-cast sample.

Table 9.3 Ultimate tensile strength (UTS) values

Material Type	**UTS (MPa)**
LSM (heat treated)	176
Substrate (heat treated)	143
LSM (as-cast)	196
Substrate (as-cast)	115

9.4 Conclusion

In this piece of work, laser surface melting of Al-12Si-4Cu-1.2Mn alloy was successfully achieved. The mechanical and metallurgical properties before and after LSM were studied for as-cast and solutionized heat treated samples. The following are main findings of this work:

- The dendrite microstructure and refined grain size provided, improved mechanical properties after laser surface melting.
- There was about 2.5 times increase in the microhardness of heat treated samples after LSM, whilst it was 2.6 times for as-cast samples.
- The UTS increased by 23% and 70% for heat treated and as-cast samples, respectively.
- The scratch resistance also increased after laser surface melting.
- The highest scratch resistance was observed in the case of as-cast sample after LSM. The coefficient of friction also got reduced after laser surface melting.

- Overall, the improvement in mechanical properties of as-cast samples was better at low laser specific energy. Although the heat treated samples also showed the improved mechanical properties, but they could not surpass the improvement of as-cast samples.
- This indicates that the best strategy may be to carry out LSM of as-cast alloy at low laser specific energy. Also, if the goal is only to increase the surface hardness, there is no need to carry out solutionizing heat treatment, thus reducing the cycle time of the process.

Chapter 10

Conclusion and Scope of Future Work

10.1 Conclusion

The objective of this work was to study surface alloying and melting of aluminum. In the pilot study, laser surface alloying of commercially pure aluminum with copper was achieved. The main feature of this work was that a good surface alloying could be obtained by compacting Cu powder on the surface of aluminum alloy. A centerline average surface roughness of 1.9 µm was achieved. After laser surface alloying the microhardness ranged from 60 $HV_{0.5}$ to 156 $HV_{0.5}$ in the alloyed region against the substrate hardness of about 30 $HV_{0.5}$. Hardness was the maximum at the surface. The optimized laser parameters were 1.7 kW laser power, 500 mm/min laser scan speed and 5.39 mm laser beam diameter. The effect of laser processing parameters on microhardness was observed. The micro-hardness distribution varies with laser power, laser scan speed, laser beam diameter and also re-melting parameters. Laser remelting further improved the microhardness after alloying with copper. It was observed that improper placement of alloying powder leads to porosity.

After alloying commercially pure aluminum with Cu, Mg, Mn and their combination in the ratio of 2:1:1, a good surface with refined microstructure was obtained. The microstructure had a refined dendrite structure, free from defects. Laser power, laser scan speed and laser beam diameter greatly influence the height, depth and width of alloying. The hardness was the maximum at the top and kept decreasing along the depth of alloying. A 12% increase in laser power, from 1.7 to 1.9 kW, increased the depth of alloying by about 15.6% for Al-CuMgMn alloy and by about 68.75% for AlMg alloy. Hardness also depended on laser power, e.g., a 12% increase in the laser power, reduced the hardness by 35% for Al-Cu alloy, 38% for Al-CuMgMn alloy, 36% for AlMn alloy and 35% for Al-Mg alloy. Laser surface alloying had no significant effect on the ultimate

tensile strength. The yield strength and the total elongation of laser surface alloyed specimens reduced significantly, because of increased hardness due to laser alloying.

Laser surface alloying increased the wear resistance after alloying with different metals. For all samples processed at 1.7 kW laser power, 500 mm/min scan speed and 5.8 mm laser beam diameter, wear mass loss was reduced by 30–50 % for 10 N normal load at 2 m/s sliding speed in a 20-minute test**.** For all materials, a twofold increase in the normal load increased wear mass loss by 1.4–3.2 times. This affirmed that in a statistical sense, the wear is proportional to normal load**.** The ranking of laser surface alloyed samples in the order of decreasing wear resistance is AlCu, Al-CuMgMn, AlMn and AlMg samples**.** In some cases, as the processing laser power increased, the coefficient of friction reduced due to the reduction in the hardness as evident from an asperity based model. The generation of debris and break down of lubricating oxide layers played their role**.** Study of wear scar morphology showed that different types of wear were adhesive wear, abrasive wear and delamination wear. In a surface scratch, the average coefficient of friction reduced when laser specific energy and scratch load were increased.

Study of corrosion was also conducted. The weight loss due to acid corrosion attack in 2.5% H_2SO_4 was reduced by 55% for AlTi alloy, 41% for AlMg, 36.6% for AlZn alloy and 22% for AlMn alloy. The pitting corrosion was found to be a major cause of damage in the metal. The pitting grows faster in a lateral direction than in the depth direction. However, the shape of pitting was irregular. The hardness after laser surface alloying, increased by a factor of 8.7, 3.4, 2.7 and 2 by alloying with Mn, Mg, Ti and Zn, respectively. After corrosion test, hardness reduced by 51% for AlTi sample, 40% for AlMg sample and 41.4% for AlMn sample and 33% for AlZn sample. Overall, AlTi provided the best corrosion resistance and AlMn the best microhardness after laser surface alloying.

Laser surface melting (LSM) of Al-12Si-4Cu-1.2Mn alloy was successfully achieved. The mechanical and metallurgical properties before and after LSM were studied for as-cast and solutionized heat treated samples. Due to the formation of dendrite microstructure and refined grain size, mechanical properties improved. Atmost, a 2.5 times increase in the microhardness of heat treated samples was observed after LSM, whilst the

microhardness increased by 2.6 times for as-cast samples. The ultimate tensile strength (UTS) increased by 23% and 70% for heat treated and as-cast samples, respectively. The scratch resistance also increased after LSM. The highest scratch resistance was observed in the case of as-cast sample after LSM. The coefficient of friction also reduced after LSM. Overall, the improvement in mechanical properties of as-cast samples is better at low laser specific energy. Although the heat treated samples also showed the improved mechanical properties, yet they could not surpass the improvement of as-cast samples. This indicates that the best strategy may be to carry out LSM of as-cast alloy at low laser specific energy. Also, if the goal is only to increase the surface hardness, there is no need to carry out solutionizing heat treatment, thus reducing the cycle time of the process.

10.2 Scope of Future Work

Here, an experimental study has been conducted on laser surface alloying and melting of aluminum as a part of laser surface modification. The work done till now, confirms that powder pre-placing technique of laser surface alloying is promising. The quality of laser surface alloying can be improved by controlling laser parameters, and other related conditions like the selection of alloying material and coating methods. Laser surface alloying of aluminum improved the properties like hardness, wear and corrosion resistance in salt and acidic environments. Following future research directions are proposed:

- Laser surface alloying of aluminum for high-temperature applications such as in cylinders of internal combustion engines (temperature in the range of 200 to 300 °C)
- Investigation on the diffusion of alloying materials during laser surface alloying using molecular dynamic simulation
- Mathematical modeling for predicting alloy depth, alloy width and studying correlating it with properties
- Conducting laser surface alloying aluminum with other materials like—nano-powders, carbon nanotubes (CNT) and other ceramic powders. Some research works shows that advantage of CNT on improving mechanical property of aluminum alloys— Chen *et al*. (2006) reported laser surface alloying with

hydroxyapatite carbon nanotube and hardness and modulus of elasticity improved. Wu and Kim (2011) reported 42.3 % improvement of hardness after CNT composite made on Al6061 alloy by semisolid powder processing technique. Laha *et al*. (2004) also reported improved hardness after CNT reinforced aluminum matrix composite made by plasma spry coating.

- Comparison of laser surface alloying with other surface modification processes such as thermal barrier coating and vacuum vapor deposition in terms of process efficiency and economics
- Studying machinability, weldability and formability of material after laser surface alloying
- Studying laser surfaces alloying for non-flat geometries such as tubes and other irregular shapes
- Phase diagram study using PANDAT and PanEngine softwares for laser surface alloying is a new research to be conducted. The results will support EDS, XRD results and microstructure as well. In material processing an interesting work has been reported by Hengcheng Liao research groups (Liao *et al*., 2017 and Suo *et al*., 2018); Chen *et al*. (2003) (PANDAT and PanEngine softwares)
- Wettability and contact angle measurement in the field of laser surface alloying is an interesting research area.

References

- Abbas, G., Li, L., Ghazanfar, U. and Liu, Z. (2006), Effect of high power diode laser surface melting on wear resistance of magnesium alloys, Wear, **260(1)**, pp. 175–180.
- Abboud, J.H. and West, D.R.F. (1990), Laser surface alloying of titanium with aluminium, Journal of Materials Science Letters, **9(3)**, pp. 308–310.
- Abe, F., Osakada, K., Shiomi, M., Uematsu, K. and Matsumoto, M. (2001), The manufacturing of hard tools from metallic powders by selective laser melting, Journal of Materials Processing Technology, **111(1)**, pp. 210–213.
- Abolikhina, E.V. and Molyar, A.G. (2003), Corrosion of aircraft structures made of aluminum alloys, Materials Science, **39(6)**, pp. 889–894.
- Aboulkhair, N.T., Maskery, I., Tuck, C., Ashcroft, I. and Everitt, N.M. (2016), Improving the fatigue behaviour of a selectively laser melted aluminium alloy: Influence of heat treatment and surface quality, Materials and Design, **104**, pp. 174–182.
- Agarwala, M., Bourell, D., Beaman, J., Marcus, H. and Barlow, J. (1995), Direct selective laser sintering of metals, Rapid Prototyping Journal, **1(1)**, pp. 26–36.
- Almeida, A., Anjos, M., Vilar, R., Li, R., Ferreira, M.G.S., Steen, W.M. and Watkins, K.G. (1995), Laser alloying of aluminium alloys with chromium, Surface and Coatings Technology, **70(2-3)**, pp. 221–229.
- Almeida, A., Petrov, P., Nogueira, I. and Vilar, R. (2001), Structure and properties of Al–Nb alloys produced by laser surface alloying, Materials Science and Engineering: A, **303(1)**, pp. 273–280.
- Almeida, A. and Vilar, R. (2008), Alloy formation in laser surface alloying of Al with transition metals, Lasers in Engineering, **18(1)**, pp. 49–60.
- Almeida, A. and Vilar, R. (2010), Al-Al 7 Cr eutectic in Al-Cr alloys synthesized by laser alloying, Scripta Materialia, **63(8)**, pp. 811–814.

- Aluminum Association (1998), Aluminum Alloy Selection and Applications, The Aluminum Association, Inc. New York.
- Aluminum Association (2017), Comments on Section 232 National Security Investigation of Imports of Aluminum, Inc. New York, http://www.aluminum.org/sites/default/files/Aluminum%20Association%20232%20Submission_0.pdf , accessed on November 3, 2017.
- Agarwal, A. and Dahotre, N.B. (1999), Laser surface engineering of steel for hard refractory ceramic composite coating, International Journal of Refractory Metals and Hard Materials, **17(4)**, pp. 283—293.
- Agarwal, A., Katipelli, L.R. and Dahotre, N.B. (2000), Elevated temperature oxidation of laser surface engineered composite boride coating on steel, Metallurgical and Materials Transactions A, **31(2)**, pp. 461—473.
- Agarwal, A. and Dahotre, N.B. (2001), Mechanical characterisation of interface in laser surface engineered composite TiB_2 coating on steel, Surface engineering, **17(1)**, pp. 66—70.
- Alwafi, Y. Ab., Bidin, N., Bin Hussin, R., Hussain, M. S. and Gustiono, D. (2011), Microhardness evaluation of pure aluminum substrate after laser surface alloying with iron and copper, Journal of Materials Science and Engineering, B, **1(2)**, pp. 200–205.
- Anandkumar, R., Almeida, A., Colaço, R., Vilar, R., Ocelik, V. and De Hosson, J.T.M. (2007), Microstructure and wear studies of laser clad Al-Si/SiC (p) composite coatings. Surface and Coatings Technology, **201(24)**, pp. 9497–9505.
- Anthony, T.R. and Cline, H.E. (1977), Surface rippling induced by surface-tension gradients during laser surface melting and alloying, Journal of Applied Physics, **48(9)**, pp. 3888–3894.
- Archard, J.F. and Hirst, W. (1956), The wear of metals under unlubricated conditions, Proceedings of The Royal Society, Mathematical, Physical and Engineering Sciences, A, **236(1206)**, pp.397—410.
- Arellanes-Lozada, P., Olivares-Xometl, O., Guzmán-Lucero, D., Likhanova, N.V., Domínguez-Aguilar, M.A., Lijanova, I.V. and Arce-Estrada, E. (2014), The inhibition

of aluminum corrosion in sulfuric acid by poly (1-vinyl-3-alkyl-imidazolium hexafluorophosphate), Materials, **7(8)**, pp. 5711–5734.

- Ares, A.E., Gassa, L.M., Gueijman, S.F. and Schvezov, C.E. (2008), Correlation between thermal parameters, structures, dendritic spacing and corrosion behavior of Zn–Al alloys with columnar to equiaxed transition, Journal of Crystal Growth, **310(7)**, pp. 1355–1361.
- Ares, A.E. and Gassa, L.M. (2012), Corrosion susceptibility of Zn-Al alloys with different grains and dendritic microstructures in NaCl solutions, Corrosion Science, **59**, pp. 290–306.
- ASTM Standard G99, (1995), Test method for wear testing using a pin on disk apparatus, ASTM.
- Avraham, S. and Kaplan, W.D. (2005), Reactive wetting of rutile by liquid aluminium, Journal of Materials Science, **40(5)**, pp. 1093―1100.
- Balla, V.K., Bose, S. and Bandyopadhyay, A. (2009), Laser surface modification of Al–4Cu–1Mg alloy for enhanced thermal conductivity, Optics and Lasers in Engineering, **47(6)**, pp. 651–655.
- Bardal, E. (2007), Corrosion and Protection, Springer Science and Business Media, Germany.
- Barlow, I.C., Jones, H. and Rainforth, W.M. (2001), Evolution of microstructure and hardening, and the role of Al_3Ti coarsening, during extended thermal treatment in mechanically alloyed Al-Ti-O based materials, Acta Materialia, **49(7)**, pp. 1209―1224.
- Bartkowiak, K., Ullrich, S., Frick, T. and Schmidt, M. (2011), New developments of laser processing aluminium alloys via additive manufacturing technique, Physics Procedia, **12**, pp. 393–401.
- Bergsdal, H., Stromman, A.H. and Hertwich, E.G. (2004), The Aluminium Industry: Environment, Technology and Production, Industrial Ecology Program (IndEcol), Norway, www.indecol.ntnu.no .
- Bermann, H.W and Mordike, B.L. (1986), Laser surface melting, NASA STI/Recon Technical Report N., **88**, 21435

- Beyer, P., Janssen, R. and Claussen, N. (2000), Synthesis of Aluminide–Alumina Composites by Reactive Squeeze Casting, Advanced Engineering Materials, **2(11)**, pp. 734─737.
- Bhat, K.D. and Majumdar, P. (2003), Transport phenomena in surface alloying of metals irradiated by a high-energy laser beam (Doctoral dissertation, Northern Illinois University).
- Bhushan, B., and Gupta, B.K. (1991), Handbook of Tribology: Materials, Coatings, and Surface Treatments, United States.
- Biswas, A., Siegel, D.J., Wolverton, C. and Seidman, D.N. (2011), Precipitates in Al–Cu alloys revisited: Atom-probe tomographic experiments and first-principles calculations of compositional evolution and interfacial segregation, Acta Materialia, **59(15)**,pp. 6187—6204.
- Branzoi, V., Golgovici, F. and Branzoi, F. (2003), Aluminium corrosion in hydrochloric acid solutions and the effect of some organic inhibitors, Materials Chemistry and Physics, **78(1)**, pp. 122–131.
- Brochu, M., Portillo, J.G., Milligan, J. and Heard, D.W. (2011), Development of metastable solidification structures using the electrospark deposition process, Open Surface Science Journal**, 3**, pp. 105—114.
- Cabeza, M., Castro, G., Merino, P., Pena, G. and Román, M. (2012), Laser surface melting: A suitable technique to repair damaged surfaces made in 14 Ni (200 grade) maraging steel, Surface and Coatings Technology, **212**, pp. 159–168.
- Campbell Jr, F.C. (2011), Manufacturing Technology for Aerospace Structural Materials, Elsevier, Netherlands.
- Campbell, F.C. (2012), Phase Diagram Applications. Phase Diagrams: Understanding the Basics, Materials Park, Ohio: ASM International, pp. 290—291.
- Chan, C.P., Yue, T.M. and Man, H.C. (2002), Effect of excimer laser surface treatment on corrosion behaviour of aluminium alloy 6013, Materials Science and Technology, **18(5)**, pp. 575–580.

- Chen, S.W. and Huang, C.C. (1996), Solidification curves of AlCu, AlMg and AlCuMg alloys, Acta Materialia, **44(5)**, pp. 1955–1965.
- Chen, S.W. and Huang, C.C. (1996), Solidification curves of AlCu, AlMg and AlCuMg alloys, Acta Materialia, **44(5)**, pp. 1955—1965.
- Chen, Y., Zhang, Y.Q., Zhang, T.H., Gan, C.H., Zheng, C.Y. and Yu, G. (2006), Carbon nanotube reinforced hydroxyapatite composite coatings produced through laser surface alloying, Carbon, **44(1)**, pp. 37—45.
- Chen, S.L., Zhang, F., Xie, F.Y., Daniel, S., Yan, X.Y., Chang, Y.A., Schmid-Fetzer, R. and Oates, W.A., (2003), Calculating phase diagrams using PANDAT and PanEngine, Jom, 55(12), pp.48-51.
- Chi, Y., Gu, G., Yu, H. and Chen, C. (2018), Laser surface alloying on aluminum and its alloys: a review, Optics and Lasers in Engineering, 100, pp. 23–37.
- Chong, P.H., Man, H.C. and Yue, T.M. (2001), Microstructure and wear properties of laser surface-cladded Mo–WC MMC on AA6061 aluminum alloy, Surface and Coatings Technology, **145(1-3)**, pp.51–59.
- Chong, P.H., Liu, Z., Skeldon, P. and Thompson, G.E. (2003), Large area laser surface treatment of aluminium alloys for pitting corrosion protection, Applied Surface Science, **208**, pp. 399–404.
- Chryssolouris, G., Zannis, S., Tsirbas, K. and Lalas, C. (2002), An experimental investigation of laser cladding, CIRP Annals-Manufacturing Technology, **51(1)**, pp.145–148.
- Chuang, Y.C., Lee, S.C. and Lin, H.C. (2006), Microstructure and characteristic of laser surface alloyed Ni and Ni–Cr–B–Si on Al-MgSi alloy, Materials Transactions, **47(1)**, pp. 106–111.
- Chryssolouris, G., (2013), Manufacturing Systems: Theory and Practice, Springer Science and Business Media, Germany.
- Chryssolouris, E.L.K.E. (2013), Laser Machining: Theory and Practice, Springer, New York.
- Clarke, J. and Sarkar, A.D. (1979), Wear characteristics of as-cast binary aluminium-silicon alloys, Wear, **54(1)**, pp. 7–16.

- Conde, A., Colaço, R., Vilar, R. and de Damborenea, J. (2000), Corrosion behaviour of steels after laser surface melting, Materials and Design, **21(5)**, pp. 441–445.
- Czeppe, T., Zakulski, W. and Bielańska, E. (2003), Study of the thermal stability of phases in the Mg-Al system, Journal of Phase Equilibria, **24(3)**, pp. 249**—**254.
- Dahotre, N. B. (Ed.), (1998). Lasers in Surface Engineering (Vol. 1). USA: ASM International.
- Dahotre, N.B. and Harimkar, S. (2008), Laser based rapid prototyping process, in Laser Fabrication and Machining of Materials, Springer, Boston, MA, pp. 353–411.
- Das, D.K. (1994), Surface roughness created by laser surface alloying of aluminium with nickel, Surface and Coatings Technology, **64(1)**, pp. 11–15.
- Das, S. (2003), Physical aspects of process control in selective laser sintering of metals, Advanced Engineering Materials, **5(10)**, pp. 701–711.
- Davis, J.R. ed., (1999), Corrosion of Aluminum and Aluminum alloys, ASM International
- Davis, J.R. (1993), ASM Specialty Hand book: Aluminum and Aluminum Alloys, ASM International, Materials Park, OH.
- Davis, J.R. (2001), Alloying Understanding The Basics: Aluminum and Aluminum Alloys, ASM International, pp. 351–416, Materials Park, OH, https://materialsdata.nist.gov/bitstream/handle/11115/173/Aluminum%20and%20Aluminum%20Alloys%20Davis.pdf, accessed on November 3, 2017.
- De Damborenea, J. (1998), Surface modification of metals by high power lasers, Surface and Coatings Technology, **100**, pp. 377–382.
- Diebold, U. (2003), The surface science of titanium dioxide, Surface science reports, **48(5)**, pp.53–229.
- Dubey, A.K. and Yadava, V. (2008), Laser beam machining—A review, International Journal of Machine Tools and Manufacture, **48(6)**, pp. 609–628.
- Dong, S., Xu, B., Wang, Z., Ma, Y. and Liu, W. (2008), Laser remanufacturing technology and its applications, Lasers in Material Processing and Manufacturing III, International Society for Optics and Photonics, **6825**, pp. 68251.

- Draper, C.W. and Poate, J. M. (1985), Laser surface alloying, International Metals Reviews, **30 (1)**, pp.85–108.
- Dubourg, L., Hlawka, F. and Cornet, A. (2002), Study of aluminium-copper-iron alloys: application for laser cladding, Surface and Coatings Technology, **151**, pp. 329–332.
- Dubourg, L., Pelletier, H., Vaissiere, D., Hlawka, F. and Cornet, A. (2002), Mechanical characterisation of laser surface alloyed aluminium–copper systems, Wear, **253(9)**, pp. 1077–1085.
- Du, Y., Chang, Y.A., Huang, B., Gong, W., Jin, Z., Xu, H., Yuan, Z., Liu, Y., He, Y. and Xie, F.Y. (2003), Diffusion coefficients of some solutes in FCC and liquid Al: critical evaluation and correlation. Materials Science and Engineering: A, **363(1-2)**, pp. 140—151.
- Eideh, A., Dixit, U.S. and Echempati, R. (2015), A simple analytical model of laser bending process, In Lasers Based Manufacturing, Springer India.
- Einstein, A. (1917), The quantum theory of radiation, PhysikalischeZeitschrift, **18**, pp. 121–128.
- El-Sherbini, E.F., Abd-El-Wahab, S.M. and Deyab, M. A. (2003), Studies on corrosion inhibition of aluminum in 1.0 M HCl and 1.0 M H_2SO_4 solutions by ethoxylated fatty acids, Materials Chemistry and Physics, **82(3)**, pp. 631–637.
- Epstein, S.G., Kaufman, J.G. and Pollak, P. (1994), Aluminum and Its Alloys, Washington, DC: Aluminum Association.
- Farnia, A., Ghaini, F.M. and Sabbaghzadeh, J. (2013), Effects of pulse duration and overlapping factor on melting ratio in preplaced pulsed Nd: YAG laser cladding, Optics and Lasers in Engineering, **51(1)**, pp. 69–76.
- Forget, P., Jeandin, M., Lechervy, P. and Varela, D. (1988), Laser drilling of a superalloy coated with ceramic, The metallurgical society, pp. 553–562.
- Fouad, M.A., Zewail, T.M., Amine, N.A. and El-Tawail, Y.A. (2017), Comparison Between Corrosion Behavior of Copper and Stainless Steel 90° Elbow and Failure Investigation of 90° Copper Elbow, Journal of The Institution of Engineers (India): Series C, **98(2)**, pp. 141–145.

- Fu, Y. and Batchelor, A.W. (1998), Laser alloying of aluminum alloy AA 6061 with Ni and Cr, Part II, The effect of laser alloying on the fretting wear resistance, Surface and Coatings Technology, **102(1)**, pp. 119–126.
- Gaus, S.P., Harmer, M.P., Chan, H.M., Caram, H.S. and Claussen, N. (2000), Alumina–Aluminide Alloys (3A) Technology: I, Model Development, Journal of the American Ceramic Society, **83(7)**, pp.1599─1605.
- Gheorghe, I. and Rack, H.J. (2002), Reactive infiltration of 25 vol pct TiO_2/Al composites, Metallurgical and Materials Transactions A, **33(7)**, pp. 2155─2162.
- Ghosh, K., McCay, M.H. and Dahotre, N.B. (1999), Formation of a wear resistant surface on Al by laser aided in-situ synthesis of $MoSi_2$, Journal of Materials Processing Technology, **88(1-3)**, pp. 169**—**179.
- Gnanamuthu, D.S. (1980), Laser surface treatment, Optical Engineering, **19(5)**, pp.195–783.
- Gordani, G.R., ShojaRazavi, R., Hashemi, S.H. and Isfahani, A.R.N. (2008), Laser surface alloying of an electroless Ni–P coating with Al-356 substrate. Optics and Lasers in Engineering, **46(7)**, pp. 550–557.
- Guo, Y., Liu, G., Jin, H., Shi, Z. and Qiao, G. (2011), Intermetallic phase formation in diffusion-bonded Cu/Al laminates, Journal of Materials Science, **46(8)**, pp. 2467**—**2473.
- Hatch, E. (1984), Aluminum Properties and Physical Metallurgy, America Society for Metals, Metals Park, Ohio.
- Hecht, J. (2011), Understanding Lasers: An Entry-Level Guide (Vol. 21). New York: Wiley.
- Hinton, B.R. (1995), Corrosion Prevention and Control, Handbook on the Physics and Chemistry of Rare Earths, North Holland.
- Huang, Y., Gao, L., Yi, Z., Tai, K., Kalita, P., Prapainainar, P. and Garg, A. (2018), An application of evolutionary system identification algorithm in modelling of energy production system, Measurement, **114**, pp. 122–131.

- Hutchings, I. and Shipway, P. (2017), Tribology: Friction and Wear of Engineering Materials, Butterworth-Heinemann, United Kingdom.
- Hu, C., Xin, H. and Baker, T.N. (1996), Formation of continuous surface Al–SiCp metal matrix composite by overlapping laser tracks on AA6061 alloy, Materials Science and Technology, **12 (3)**, pp. 227–232.
- Hu, C. and Baker, T.N. (1995), Laser processing to createin-situ Al-SiCp surface metal matrix composites, Journal of Materials Science, **30(4)**, pp.891─897.
- Hwang, J.Y., Doty, H.W. and Kaufman, M.J. (2008), The effects of Mn additions on the microstructure and mechanical properties of Al–Si–Cu casting alloys, Materials Science and Engineering: A, **488(1)**, pp. 496–504.
- Hwang, J.Y., Banerjee, R., Doty, H.W. and Kaufman, M.J. (2009), The effect of Mg on the structure and properties of Type 319 aluminum casting alloys, Acta Materialia, **57(4)**, pp. 1308–1317.
- Ignat, S., Sallam, P., Grevey, D. and Lambertin, M. (2004), Magnesium alloys laser (Nd: YAG) cladding and alloying with side injection of aluminium powder, Applied Surface Science, **225(1)**, pp. 124–134.
- Indira, K., Sylvie, C., Zhongke, W. and Hongyu, Z. (2016), Investigation of wettability properties of laser surface modified rare earth Mg alloy, Procedia Engineering, **141**, pp. 63―69.
- Ion, J. (2005), Laser Processing of Engineering Materials: Principles, Procedure and Industrial Application, Butterworth-Heinemann, pp.1–837, United Kingdom.
- Iwatani, S., Ogata, Y., Uenishi, K., Kobayashi, K.F. and Tsuboi, A. (2005), Laser cladding of Fe–Cr–C alloys on A5052 aluminum alloy using diode laser, Materials Transactions, **46(6)**, pp.1341–1347.
- Janotová, I., Švec Sr, P., Švec, P., Mat'ko, I., Janičkovič, D., Zigo, J., Mihalkovič, M., Marcin, J. and Škorvánek, I. (2017), Phase analysis and structure of rapidly quenched Al-Mn systems, Journal of Alloys and Compounds, **707**, pp. 137―141.
- Jaradeh, M. and Carlberg, T. (2005), Effect of titanium additions on the microstructure of DC-cast aluminium alloys, Materials Science and Engineering: A, **413**, pp. 277–282.

- Kadhim, M.J., Ibrahim Al-Rubaiey, S. and Sabea, H. A. (2013), The influence of laser specific energy on laser sealing of plasma sprayed yttria partially stabilized zirconia coating. Optics and Lasers in Engineering, **51(2)**, pp. 159–166.
- Kadolkar, P. and Dahotre, N.B. (2003), Effect of processing parameters on the cohesive strength of laser surface engineered ceramic coatings on aluminum alloys, Materials Science and Engineering: A, **342(1)**, pp. 183–191.
- Kadolkar, P.B., Watkins, T.R., De Hosson, J.T.M., Kooi, B.J. and Dahotre, N.B. (2007), State of residual stress in laser-deposited ceramic composite coatings on aluminum alloys, Acta Materialia, **55(4)**, pp. 1203–1214.
- Kaesche, H. (2012), Corrosion of Metals: Physicochemical Principles and Current problems, Springer Science and Business Media, Germany.
- Kamoutsi, H., Haidemenopoulos, G. N., Bontozoglou, V. and Pantelakis, S. (2006), Corrosion-induced hydrogen embrittlement in aluminum alloy 2024, Corrosion Science, **48(5)**, pp. 1209–1224.
- Kannatey-Asibu Jr, E. (2009), Principles of Laser Materials Processing, John Wiley and Sons, Canada.
- Kang, N., Coddet, P., Liao, H., Baur, T. and Coddet, C. (2016), Wear behavior and microstructure of hypereutectic Al-Si alloys prepared by selective laser melting, Applied Surface Science, **378**, pp. 142–149.
- Kant, R., Joshi, S.N. and Dixit, U.S. (2015), An integrated FEM-ANN model for laser bending process with inverse estimation of absorptivity, Mechanics of Advanced Materials and Modern Processes, **1(1)**, pp. 1–12
- Katipelli, L.R., Agarwal, A. and Dahotre, N.B. (2000), Laser surface engineered TiC coating on 6061 Al alloy: microstructure and wear, Applied Surface Science, **153(2)**, pp. 65–78.
- Kaya, H., Çadırlı, E. and Gündüz, M. (2007), Dendritic Growth in an Aluminum-Silicon Alloy, Journal of Materials Engineering and Performance, **16(1)**, pp. 12–21.
- Kaufman, J.G. and Rooy, E.L. (2004), Aluminum Alloy Castings: Properties, Processes and Applications, ASM International, Materials Park, OH

- Kim, J.D. and Peng, Y. (2000), Melt pool shape and dilution of laser cladding with wire feeding, Journal of Materials Processing Technology, **104(3)**, pp. 284–293.
- Kooi, B.J., Pei, Y.T. and De Hosson, J.T.M. (2003), The evolution of microstructure in a laser clad TiB–Ti composite coating, Acta Materialia, **51(3)**, pp. 831–845.
- Kwok, C.T. and Wong, P.K. (2010), Laser surface alloying of various engineering alloys for sliding wear and corrosion resistance, Journal of Laser Micro/Nanoengineering, **5**, pp.90–96.
- Kwok, C.T., Man, H.C., Cheng, F.T. and Lo, K.H. (2016), Developments in laser-based surface engineering processes: with particular reference to protection against cavitation erosion, Surface and Coatings Technology, **291**, pp. 189—204.
- Labisz, K. (2014), Microstructure and mechanical properties of high power diode laser (HPDL) treated cast aluminium alloys, Materialwissenschaft und Werkstofftechnik, **45(4)**, pp. 314–324.
- Laha, T., Agarwal, A., McKechnie, T. and Seal, S. (2004), Synthesis and characterization of plasma spray formed carbon nanotube reinforced aluminum composite, Materials Science and Engineering: A, **381(1-2)**, pp. 249—258.
- Lalas, C., Tsirbas, K., Salonitis, K. and Chryssolouris, G. (2007), An analytical model of the laser clad geometry, The International Journal of Advanced Manufacturing Technology, **32(1)**, pp. 34–41.
- Lancaster, J.K. (1967), The influence of substrate hardness on the formation and endurance of molybdenum disulphide films, Wear, **10(2)**, pp. 103–117.
- Laorden, L.M., Rodrigo, P., Torres, B. and Rams, J. (2017), Modification of microstructure and superficial properties of A356 and A356/10% SiC by Selective Laser Surface Melting (SLSM), Surface and Coatings Technology, **309**, pp. 1001–1009.
- Laurent, V., Chatain, D. and Eustathopoulos, N. (1987), Wettability of SiC by aluminium and Al-Si alloys, Journal of Materials Science, **22(1)**, pp. 244—250.
- Lepper, K., James, M., Chashechkina, J. and Rigney, D.A. (1997), Sliding behavior of selected aluminum alloys, Wear, **203**, pp. 46–56.

- Liao, H., Tang, Y., Suo, X., Li, G., Hu, Y., Dixit, U.S. and Petrov, P. (2017), Dispersoid particles precipitated during the solutionizing course of Al-12 wt% Si-4 wt% Cu-1.2 wt% Mn alloy and their influence on high temperature strength, Materials Science and Engineering: A, **699**, pp. 201—209.
- Li, H.T., Wang, Y. and Fan, Z. (2012), Mechanisms of enhanced heterogeneous nucleation during solidification in binary Al–Mg alloys, Acta Materialia, **60(4)**, pp. 1528—1537.
- Liang, G.Y., Wong, T.T., MacAlpine, J.M.K. and Su, J.Y. (2000), A study of wear resistance of plasma-sprayed and laser-remelted coatings on aluminium alloy, Surface and Coatings Technology, **127(2)**, pp. 232–237.
- Liao, H., Tang, Y., Suo, X., Li, G., Hu, Y., Dixit, U.S. and Petrov, P. (2017), Dispersoid particles precipitated during the solutionizing course of Al-12wt% Si-4wt% Cu-1.2wt% Mn alloy and their influence on high temperature strength, Materials Science and Engineering: A, **699**, pp. 201–209.
- Li, L. (2000), The advances and characteristics of high-power diode laser materials processing, Optics and Laser in Engineering, **34**, pp. 231–253.
- Li, R., Ferreira, M.G.S., Almeida, A., Vilar, R.,Watkins, K.G., McMahon, M.A. and Steen, W.M. (1996), Localized corrosion of laser surface melted 2024-T351 aluminium alloy, Surface and Coatings Technology, **81(2-3)**, pp. 290–296.
- Li, J.X., Zhai, T., Garratt, M.D. and Bray, G.H. (2005), Four-point-bend fatigue of AA 2026 aluminum alloys, Metallurgical and Materials Transactions A, **36(9)**, p. 2529—2539.
- Liu, X.J., Ohnuma, I., Kainuma, R. and Ishida, K. (1999), Thermodynamic assessment of the aluminum-manganese (Al-Mn) binary phase diagram, Journal of phase equilibria, **20(1)**, p.45—56
- Liu, Z., Chong, P.H., Skeldon, P., Hilton, P.A., Spencer, J.T. and Quayle, B. (2006), Fundamental understanding of the corrosion performance of laser-melted metallic alloys, Surface and coatings technology, **200(18)**, pp. 5514–5525.

- Li, Y., Zhang, P., Bai, P., Wu, L., Liu, B. and Zhao, Z. (2018) Microstructure and properties of Ti/TiBCN coating on 7075 aluminum alloy by laser cladding, Surface and Coatings Technology, **334**, pp. 142–149.
- Liu, Z., Chong, P.H., Butt, A.N., Skeldon, P. and Thompson, G.E. (2005), Corrosion mechanism of laser-melted AA 2014 and AA 2024 alloys, Applied Surface Science, **247(1)**, pp. 294–299.
- Louvis, E., Fox, P. and Sutcliffe, C.J. (2011), Selective laser melting of aluminum components, Journal of Materials Processing Technology, **211(2)**, pp. 275–284.
- Luo, Z. and Soria, A. (2007), Prospective Study of the World Aluminium Industry, JRC Scientific and Technical Reports, EUR, 22951, Spain.
- Luo, Z. and Soria, A. (2007), Prospective study of the world aluminium industry, Institute for Prospective Technological Studies, European Commission Joint Research Centre, pp. 1–79.
- Luyckx, S. and Love, A. (2004), The relationship between the abrasion resistance and the hardness of WC-Co alloys, Journal of the South African Institute of Mining and Metallurgy, **104(10)**, pp. 579—582.
- Mabhali, L.A., Pityana, S.L. and Sacks, N. (2010), Laser surface alloying of aluminum (AA1200) with Ni and SiC powders. Materials and Manufacturing Processes, **25(12)**, pp.1397─1403.
- Mabhali, L., Sacks, N. and Pityana, S. (2012), Three body abrasion of laser surface alloyed aluminium AA1200, Wear, **290**, pp.1–9.
- Maiman, T.H. (1960), Stimulated optical radiation in ruby, Nature, **187(4736**), pp. 493–494.
- Majumdar, J.D., Weisheit, A., Mordike, B.L. and Manna, I. (1999), Laser surface alloying of Ti with Si, Al and Si+ Al for an improved oxidation resistance, Materials Science and Engineering: A, **266(1-2)**, pp. 123–134.
- Majumdar, J.D. and Manna, I. (2003), Laser processing of materials, Sadhana, **28(3-4)**, pp. 495–562.

- Majumdar, J., Galun, R., Mordike, B.L. and Manna, I. (2003), Effect of laser surface melting on corrosion and wear resistance of a commercial magnesium alloy, Materials Science and Engineering: A, **361(1)**, pp. 119–129.
- Majumdar, J.D., Chandra, B.R., Nath, A.K. and Manna, I. (2006), Compositionally graded SiC dispersed metal matrix composite coating on Al by laser surface engineering, Materials Science and Engineering: A, **433(1-2)**, pp. 241–250.
- Man, H.C., Kwok, C.T. and Yue, T.M. (2000), Cavitation erosion and corrosion behaviour of laser surface alloyed MMC of SiC and Si3N4 on Al alloy AA6061, Surface and Coatings Technology, **132(1)**, pp. 11─20.
- Man, H.C., Zhang, S., Yue, T.M. and Cheng, F.T. (2001), Laser surface alloying of NiCrSiB on Al6061 aluminium alloy, Surface and Coatings Technology, **148(2-3)**, pp.136–142.
- Man, H.C., Zhang, S. and Cheng, F.T. (2007), Improving the wear resistance of AA 6061 by laser surface alloying with NiTi, Materials Letters, **61(19-20),** pp. 4058–4061.
- Mao, M., Peng, L., Yi, P. and Lai, X. (2015), Modeling of the Friction Behavior in Metal Forming Process Considering Material Hardening and Junction Growth, Journal of Tribology, **138(1)**, pp. 012202–18.
- Mao, M., Peng, L., Yi, P. and Lai, X. (2016), Modeling of the friction behavior in metal forming process considering material hardening and junction growth, Journal of Tribology, **138(1)**, pp. 012202–18.
- Matys, J., Dominiak, M. and Flieger, R. (2015), Energy and Power Density: A Key Factor in Lasers Studies, Journal of Clinical and Diagnostic Research : JCDR, **9(12)**, pp. ZL01–ZL02.
- Meijer, J. (2004), Laser beam machining, state of the art and new opportunities. Journal of Materials Processing Technology, **149(1)**, pp. 2–17.
- Moreno, D., Garrett, J. and Embury, J.D. (1999), A technique for rapid characterization of intermetallics and interfaces, Intermetallics, **7(9)**, pp.1001—1009.
- Moore, M.A., (1974), The relationship between the abrasive wear resistance, hardness and microstructure of ferritic materials, Wear, 28(1), pp. 59—68.

- Nath, S., Pityana, S. and Majumdar, J.D. (2012), Laser surface alloying of aluminium with WC+ Co+ NiCr for improved wear resistance, Surface and Coatings Technology, **206(15)**, pp. 3333–3341.
- Nautiyal, P., Zhang, C., Boesl, B. and Agarwal, A. (2018), Non-equilibrium wetting and capture of boron nitride nanotubes in molten aluminum during plasma spray, Scripta Materialia, **151**, pp. 71—75.
- Noordhuis, J. and De Hosson, J.T. M. (1993), Microstructure and mechanical properties of a laser treated Al alloy, Acta Metallurgica et Materialia, **41(7)**, pp. 1989–1998.
- Nowotny, S., Richter, A. and Tangermann, K. (1999), Surface protection of light metals by one-step laser cladding with oxide ceramics, Journal of Thermal Spray Technology, **8(2)**, pp. 258–262.
- Obadele, B.A., Lepule, M.L., Andrews, A. and Olubambi, P.A. (2014), Tribocorrosion characteristics of laser deposited Ti–Ni–ZrO_2 composite coatings on AISI 316 stainless steel, Tribology International, **78**, pp. 160–167.
- Osório, W.R., Cheung, N., Spinelli, J.E., Cruz, K.S. and Garcia, A. (2008), Microstructural modification by laser surface remelting and its effect on the corrosion resistance of an Al–9wt% Si casting alloy, Applied Surface Science, **254(9)**, pp. 2763–2770.
- Ouyang, J.H., Nowotny, S., Richter, A. and Beyer, E. (2001), Laser cladding of yttria partially stabilized ZrO_2 (YPSZ) ceramic coatings on aluminum alloys, Ceramics International, **27(1)**, pp. 15–24.
- Pagano, N., Angelini, V., Ceschini, L. and Campana, G. (2016), Laser remelting for enhancing tribological performances of a ductile iron, Procedia CIRP, **41**, pp. 987–991.
- Pantelis, D., Tissandier, A., Manolatos, P. and Ponthiaux, P. (1995), Formation of wear resistant Al–SiC surface composite by laser melt–particle injection process, Materials Science and Technology, **11(3)**, pp. 299—303.
- Pariona, M.M., Teleginski, V., dos Santos, K., de Lima, A.A., Zara, A.J., Micene, K. T. and Riva, R. (2013), Influence of laser surface treated on the characterization and corrosion behavior of Al–Fe aerospace alloys, Applied surface science, **276**, pp.76–85.

- Pelletier, J.M., Issa, A. and Fouquet, F. (1991), Possibilities and limitations of laser surface alloying by melting of predeposited layers, Le Journal de Physique IV, **1(C7)**, pp.C7—87.
- Phanikumar, G., Dutta, P., Galun, R. and Chattopadhyay, K. (2004), Microstructural evolution during remelting of laser surface alloyed hyper-monotectic AlBi alloy, Materials Science and Engineering: A, **371(1)**, pp. 91–102.
- Pelleg, J. (2012), Mechanical Properties of Materials (Vol. 190), Springer Science and Business Media, Germany.
- Pfefferkorn, F.E., Duffie, N.A., Morrow, J.D. and Wang, Q. (2014), Effect of beam diameter on pulsed laser polishing of S7 tool steel, CIRP Annals, **63(1)**, pp. 237–240.
- Pfefferkorn, F.E. and Morrow, J.D. (2017), Controlling surface topography using pulsed laser micro structuring, CIRP Annals, **66(1)**, pp. 241–244.
- Pinto, M.A., Cheung, N., Ierardi, M.C.F. and Garcia, A. (2003), Microstructural and hardness investigation of an aluminum–copper alloy processed by laser surface melting, Materials Characterization, **50(2)**, pp. 249–253.
- Pirso, J., Viljus, M. and Letunovits, S. (2004), Sliding wear of TiC–NiMo cermets, Tribology International, **37(10)**, pp. 817–824.
- Pirso, J., Viljus, M., Juhani, K. and Letunovitš, S. (2009), Two-body dry abrasive wear of cermets, Wear, **266(1-2)**, pp. 21–29.
- Popoola, A.P.I., Pityana, S.L. and Popoola, O.M. (2011), Laser deposition of (Cu+ Mo) alloying reinforcements on AA1200 substrate for corrosion improvement. Int. J. Electrochemical Science, **(6)**, pp. 5038 –5051.
- Rajamure, R.S., Vora, H.D., Gupta, N., Karewar, S., Srinivasan, S.G. and Dahotre, N. B. (2014), Laser surface alloying of molybdenum on aluminum for enhanced wear resistance, Surface and Coatings Technology, **258**, pp. 337–342.
- Rambabu, P.P.N.K.V., Prasad, N.E., Kutumbarao, V.V. and Wanhill, R.J.H. (2017), Aluminium alloys for aerospace applications, In Aerospace Materials and Material Technologies (pp. 29—52). Springer, Singapore.

- Ravnikar, D., Dahotre, N.B. and Grum, J. (2013), Laser coating of aluminum alloy EN AW 6082-T651 with TiB_2 and TiC: microstructure and mechanical properties, Applied Surface Science, **282**, pp. 914–922.
- Razavi, R.S. and Gordani, G.R. (2011), Laser surface treatments of aluminum alloys, In Recent Trends in Processing and Degradation of Aluminium Alloys, INTECH, pp.116–154.
- Read, N., Wang, W., Essa, K. and Attallah, M.M. (2015), Selective laser melting of AlSi10Mg alloy: Process optimization and mechanical properties development, Materials and Design, **65**, pp. 417– 424.
- Ren, S., He, X., Qu, X., Humail, I.S. and Li, Y. (2007), Effect of Mg and Si in the aluminum on the thermo-mechanical properties of pressureless infiltrated SiCp/Al composites, Composites science and Technology, **67 (10)**, pp. 2103–2113.
- Rosliza, R., Nik, W.W. and Senin, H.B. (2008), The effect of inhibitor on the corrosion of aluminum alloys in acidic solutions, Materials Chemistry and Physics, **107(2-3)**, pp. 281–288.
- Saheb, N., Laoui, T., Daud, A.R., Harun, M., Radiman, S. and Yahaya, R. (2001), Influence of Ti addition on wear properties of Al–Si eutectic alloys, Wear, **249 (8)**, pp. 656–662.
- Sahoo, C.K., Sahu, J.K. and Masanta, M. (2015), Effect of pulsed Nd: YAG laser parameters in preplaced TiC coating on aluminium substrate, in Lasers Based Manufacturing: 5^{th} International and 26^{th} All India Manufacturing Technology, Design and Research Conference, AIMTDR 2014, edited by S.N. Joshi and U.S. Dixit, Springer, New Delhi, pp. 117–137.
- Salim, A.A., Bidin, N. and Islam, S. (2017), Low power CO_2 laser modified iron/nickel alloyed pure aluminum surface: Evaluation of structural and mechanical properties, Surface and Coatings Technology, **315**, pp. 24–31.
- Samant, A.N. and Dahotre, N.B. (2009), Laser machining of structural ceramics-a review, Journal of the European Ceramic Society, **29(6)**, pp. 969–993.

- Sarkar, S., Raj, P.M., Chakraborty, S. and Dutta, P. (2002), Three-dimensional computational modeling of momentum, heat and mass transfer in a laser surface alloying process, Numerical Heat Transfer: Part A: Applications, **42(3)**, pp. 307–326.
- Sato, N. (1990), An overview on the passivity of metals, Corrosion Science, **31**, pp.1–19.
- Schubert, E., Klassen, M., Zerner, I., Walz, C. and Sepold, G. (2001), Lightweight structures produced by laser beam joining for future applications in automobile and aerospace industry, Journal of Materials Processing Technology, **115(1)**, pp. 2–8.
- Selvan, J.S., Soundararajan, G. and Subramanian, K. (2000), Laser alloying of aluminium with electrodeposited nickel: Optimization of plating thickness and processing parameters, Surface and Coatings Technology, **124(2)**, pp.117–127.
- Selvan, J.S., Soundararajan, G. and Subramanian, K. (2000), Laser alloying of aluminium with electrodeposited nickel: optimization of plating thickness and processing parameters, Surface and Coatings Technology, **124(2-3)**, pp. 117–127.
- Serbiński, W., Olive, J.M., Frayret, J. P. and Desjardins, D. (2002), Morphology and corrosion characteristics of laser surface remelted Al-Si alloy at cryogenic conditions, Materials and Corrosion, **53(5)**, pp. 335–340.
- Serbiński, W., Łubiński, J.I. and Druet, K. (2003), Microstructure and wear of cast aluminium alloy with laser modified surface layer, Advances in Materials Science, **3(2-4)**, pp. 71–80.
- Serlin, R.A. and Serlin, R.A. (1980), Surface alloying method and apparatus using high energy beam, U.S. Patent 4, **212**, 900.
- Sexton, L., Lavin, S., Byrne, G. and Kennedy, A. (2002), Laser cladding of aerospace materials, Journal of Materials Processing Technology, **122(1)**, pp. 63–68.
- Shen, P., Fujii, H. and Nogi, K. (2006), Wettability of polycrystalline rutile TiO_2 by molten Al in different atmospheres, Acta Materialia, **54(6)**, pp. 1559**—**1569.
- Shepeleva, L., Medres, B., Kaplan, W. D., Bamberger, M. and Weisheit, A. (2000), Laser cladding of turbine blades, Surface and Coatings Technology, **125(1)**, pp. 45–48.

- Shichun, W. and Jinsong, Z. (2001), An experimental study of laser bending for sheet metals, Journal of Materials Processing Technology, **110(2)**, pp. 160–163.
- Singh, A. and Harimkar, S.P. (2012), Laser surface engineering of magnesium alloys: A Review, Journal of Minerals, Metals and Materials Society, **64(6)**, pp.716–733.
- Sigworth, G.K. (2014), Fundamentals of solidification in aluminum castings, International Journal of Metalcasting, **8(1)**, pp.7—20.
- Smith, B., 2003. The Boeing 777, Advanced Materials and Processes, **161(9)**, pp. 41—44.
- Singh, R. and Dahotre, N.B. (2007), Corrosion degradation and prevention by surface modification of biometallic materials, Journal of Materials Science, Materials in Medicine, **18(5)**, pp. 725—751.
- Staia, M.H., Cruz, M. and Dahotre, N.B. (2000), Microstructural and tribological characterization of A-356 aluminum alloy superficially modified by laser alloying, Thin Solid Films, **377**, pp. 665–674.
- Sušnik, J., Šturm, R. and Grum, J. (2012), Influence of laser surface remelting on Al-Si alloy properties, Strojniški vestnik-Journal of Mechanical Engineering, **58(10)**, pp. 614–620.
- Su, H.L., Harmelin, M., Donnadieu, P., Baetzner, C., Seifert, H.J., Lukas, H.L., Effenberg, G. and Aldinger, F. (1997), Experimental investigation of the Mg-Al phase diagram from 47 to 63 at.% Al, Journal of Alloys and Compounds, **247(1-2)**, pp. 57—65.
- Suo, X., Liao, H., Hu, Y., Dixit, U.S. and Petrov, P., (2018), Formation of Al 15 Mn 3 Si 2 Phase During Solidification of a Novel Al-12% Si-4% Cu-1.2% Mn Heat-Resistant Alloy and Its Thermal Stability, Journal of Materials Engineering and Performance, pp. 1—11.
- Sobczak, N., Stobierski, L., Radziwill, W., Ksiazek, M. and Warmuzek, M. (2004), Wettability and interfacial reactions in Al/TiO_2 Surface and Interface Analysis: An International Journal devoted to the development and application of techniques for the analysis of surfaces, Interfaces and Thin Films, **36(8)**, pp. 1067—1070.

- Song, L., Bagavath-Singh, V., Dutta, B. and Mazumder, J. (2012), Control of melt pool temperature and deposition height during direct metal deposition process, The International Journal of Advanced Manufacturing Technology, **58(1)**, pp. 247–256.
- Staia, M.H., Cruz, M. and Dahotre, N.B. (2000), Microstructural and tribological characterization of A-356 aluminum alloy superficially modified by laser alloying, Thin Solid Films, **377**, pp. 665–674.
- Syed, W.U.H. and Li, L. (2005), Effects of wire feeding direction and location in multiple layer diode laser direct metal deposition, Applied Surface Science, **248(1)**, pp. 518–524.
- Szklarska. S, Z. (1999), Pitting corrosion of aluminum, Corrosion Science, **41(9)**, pp. 1743–1767.
- Suh, N.P. (1986), Tribophysics, Pretice-Hall, Englewood Cliffs, New Jersey 07632, USA.
- Srinivas, V. and Moorthy, C.V. (2014), Corrosion and Heat Transfer Characteristics of Water Dispersed with Carboxylate Additives & Multi-walled Carbon Nano Tubes. Nano-Science and Nano Engineering, **2(3)**, pp. 59–69.
- Sun, R. and Lei, Y. (2008), Microstructure and hardness of laser clad SiC Al composite coatings on Al alloys, Materials Letters, **62(17)**, pp. 3272–3275.
- Sun, H. (1998), Thin lens equation for a real laser beam with weak lens aperture truncation. Optical Engineering, **37(11)**, pp. 2906–2914.
- Sušnik, J., Šturm, R. and Grum, J. (2012), Influence of Laser Surface Remelting on Al-Si Alloy Properties, Strojniški vestnik - Journal of Mechanical Engineering, **58(10)**, pp. 614–620.
- Tomida, S., Nakata, K., Saji, S. and Kubo, T. (2001), Formation of metal matrix composite layer on aluminum alloy with TiC-Cu powder by laser surface alloying process, Surface and Coatings Technology, **142**, pp. 585–589.
- Tomida, S., Nakata, K., Shibata, S., Zenkouji, I. and Saji, S. (2003), Improvement in wear resistance of hyper-eutectic Al_2Si cast alloy by laser surface remelting, Surface and Coatings Technology, **169**, pp. 468–471.

- Tomida, S. and Nakata, K. (2003), Fe–Al composite layers on aluminum alloy formed by laser surface alloying with iron powder, Surface and Coatings Technology, **174**, pp. 559–563.
- Tomlinson, W.J. and Bransden, A.S. (1995), Cavitation erosion of laser surface alloyed coatings on Al-12% Si, Wear, **185(1-2)**, pp. 59–65.
- Toyserkani, E., Khajepour, A. and Corbin, S.F. (2004), Laser Cladding, CRC, New York.
- Ukar, E., Lamikiz, A., López de Lacalle, L.N., del Pozo, D. and Arana, J.L. (2010), Laser polishing of tool steel with CO_2 laser and high-power diode laser, International Journal of Machine Tools and Manufacture, **50(1)**, pp. 115–125.
- Van Otterloo, J.D.M., Bagnoli, D. and De Hosson, J.T.M. (1995), Enhanced mechanical properties of laser treated Al-Cu alloys: A microstructural analysis, Acta Metallurgica et Materialia, 43(7), pp. 2649–2656.
- Vargel, C.(2004), Corrosion of Aluminium , Elsevier, London.
- Vaziri, S.A., Shahverdi, H.R., Torkamany, M.J. and Shabestari, S.G. (2009), Effect of laser parameters on properties of surface-alloyed Al substrate with Ni, Optics and Lasers in Engineering, **47(9)**, pp. 971–975.
- Viala, J.C., Fortier, P. and Bouix, J. (1990), Stable and metastable phase equilibrium in the chemical interaction between aluminium and silicon carbide, Journal of Materials Science, **25 (3)**, pp.1842–1850.
- Vilar, R. (1999), Laser alloying and laser cladding, Materials Science Forum, Trans Tech Publications, **301**, pp. 229–252.
- Vreeling, J.A., Ocelık, V., Pei, Y.T., van Agterveld, D.T.L. and De Hosson, J.T.M. (2000), Laser melt injection in aluminum alloys: on the role of the oxide skin, Acta Materialia, 48(17), pp. 4225–4233.
- Vora, H.D., Rajamure, R.S., Soundarapandian, S., Srinivasan, S.G. and Dahotre, N.B. (2013), Dilution of molybdenum on aluminum during laser surface alloying, Journal of Alloys and Compounds, **570**, pp. 133–143.

- Wagner, F., Garcia, D.E., Krupp, A. and Claussen, N.(1999), Interpenetrating Al_2O_3-$TiAl_3$ alloys produced by reactive infiltration, Journal of the European Ceramic Society, **19(13-14)**, pp. 2449─2453.
- Wang, W., Liu, Y.X., Xing, F. and Xie, H.L. (2010), Laser Remanufacturing Technology and its Applications, Advanced Materials Research Trans Tech Publications, **139**, pp. 1424–1427.
- Wang, D., Tian, Z., Shen, L., Liu, Z. and Huang, Y. (2014), Effects of laser remelting on microstructure and solid particle erosion characteristics of ZrO_2–7wt% Y_2O_3 thermal barrier coating prepared by plasma spraying, Ceramics International, **40(6)**, pp. 8791–8799.
- Watkins, K.G., Liu, Z., McMahon, M., Vilar, R. and Ferreira, M.G.S. (1998), Influence of the overlapped area on the corrosion behaviour of laser treated aluminium alloys, Materials Science and Engineering: A, **252(2)**, pp. 292–300.
- Wendt, U., Settegast, S. and Grodrian, I.U. (2003), Laser alloying of aluminum with titanium wire, Journal of materials science letters, **22(19)**, pp. 1319–1322.
- Williamson, G. K. and Hall, W. H. (1953). X-ray line broadening from filed aluminium and wolfram. Acta Metallurgica, **1(1)**, pp. 22–31.
- Wong, T.T., Liang, G.Y. and Tang, C.Y. (1997), The surface character and substructure of aluminium alloys by laser-melting treatment', Journal of Materials Processing Technology, **66(1)**, pp. 172–178.
- Wu, Y. and Kim, G.Y. (2011), Carbon nanotube reinforced aluminum composite fabricated by semi-solid powder processing, Journal of Materials Processing Technology, **211(8)**, pp.1341―1347.
- Xu, J., Liu, X., Barbero, E., Hemrick, J.G. and Peters, M. (2007), Wetting and reaction characteristics of Al_2O_3/SiC composite refractories by molten aluminum and aluminum alloy, International Journal of Applied Ceramic Technology, **4(6)**, pp. 514―523.
- Yang, Y. and Wu, H. (2012), Microstructure and Microhardness of Tempered Ni–Al Alloyed Layer, Journal of Materials Science and Technology, **28(10)**, pp. 937–940.

- Yang, L., Zhang, Y., Zeng, X. and Song, Z. (2012) Corrosion behaviour of superplastic Zn–Al alloys in simulated acid rain. Corrosion Science, **59**, pp. 229–237.
- Yevko, V., Park, C.B., Zak, G., Coyle, T.W. and Benhabib, B. (1998), Cladding formation in laser-beam fusion of metal powder, Rapid Prototyping Journal, **4(4)**, pp. 168–184.
- Yilbas, B.S., Khaled, M. and Karatas, C. (2009), Corrosion properties and morphology of laser melted aluminum alloy 8022 surface, Journal of materials engineering and performance, **18(1)**, pp. 1–7.
- Ying, D.Y., Zhang, D.L. and Newby, M. (2004), Solid-state reactions during heating mechanically milled Al/TiO_2 composite powders, Metallurgical and Materials Transactions A, **35(7)**, pp. 2115─2125.
- Yue, T.M., Yan, L.J., Chan, C.P., Dong, C.F., Man, H.C. and Pang, G.K.H. (2004), Excimer laser surface treatment of aluminum alloy AA7075 to improve corrosion resistance, Surface and Coatings Technology, **179(2)**, pp. 158–164.
- Yunlian, Q., Ju, D., Quan, H. and Liying, Z. (2000), Electron beam welding, laser beam welding and gas tungsten arc welding of titanium sheet, Materials Science and Engineering: A, **280(1)**, pp.177–181.
- Yunshan, Y.X.L.H.W., Ronglu, L.L.U.Y.T.Y.S.U. and Jichen, L.J.X. (2003), Laser refabricating technology for repairing expensive and important equipment, Laser and Optronics Progress, **5629**, pp. 23–31
- Zimmermann, M., Carrard, M. and Kurz, W. (1989), Rapid solidification of Al-Cu eutectic alloy by laser remelting, Acta Metallurgica, **37(12)**, pp. 3305–3313.
- Zinth, W., Laubereau, A. and Kaiser, W. (2011), The long journey to the laser and its rapid development after 1960, The European Physical Journal H, **36(2)**, pp. 153–181.
- Zhang, Y., Chen, J., Lei, W. and Xv, R. (2008), Effect of laser surface melting on friction and wear behavior of AM50 magnesium alloy, Surface and Coatings Technology, **202(14)**, pp. 3175–3179.
- Zhang, Q., Xiao, B.L., Wang, Q.Z. and Ma, Z.Y. (2011), In situ Al_3Ti and Al_2O_3 nanoparticles reinforced Al composites produced by friction stir processing in an Al-TiO_2 system, Materials Letters, **65(13)**, pp. 2070─2072.

- Zhao, L.Z., Zhao, M.J., Li, D.Y., Zhang, J. and Xiong, G.Y. (2012), Study on Fe–Al–Si in situ composite coating fabricated by laser cladding, Applied Surface Science, **258(8)**, pp. 3368–3372.
- Zhao, Z., Wang, C., Li, M., Wang, L. and Kong, L. (2006), The effects of pulsed Nd: YAG laser irradiation on surface energy of copper, Applied Surface Science, **252(12)**, pp. 4257—4263.
- Zhong, M. and Liu, W. (2010), Laser surface cladding: the state of the art and challenges, Proceedings of the Institution of Mechanical Engineers, Part C: Journal of Mechanical Engineering Science, **224(5)**, pp. 1041–1060.
- Zhurin, A.I., Kosmynin, A.I., Vlasenko, O.B. (1973), Corrosion of aluminum cathodes during the electrodeposition of zinc, Izv. Vyssh. Ucheb, Zaved. Tsvet. Metall, **5**, pp. 71–75.
- Zuo, Y. and Chang, Y.A. (1993), Thermodynamic calculation of the Al_2Mg phase diagram, Calphad, **17(2)**, pp. 161—174.

Appendix

Appendix A

Important specification of CO_2 laser cutting machine

Make	Orion 3015 from LVD
Type	GE FANUC HF excited CO_2 laser
Capacity	2.5 kW
Wave length	10.6 μm
Sheet size	3000 mm ×1500 mm
Maximum sheet weight	570 kg
X-axis travel	3080 mm
Y-axis travel	1555 mm
Z-axis travel	290 mm
Machine dimension	7975 mm × 2825 mm × 2200 mm
Total weight installation	11500 kg

Maximum position speed

X-Y axis	100 m/min
Z-axis	15 m/min
Repetitive accuracy	$\pm$ 0.02 mm
Position accuracy	$\pm$ 0.05 mm/min

Controlling parameters

CNC control	GE FANUC 16 iLB with Pentium processor
Software	CADMAN-L3D
Laser power	50 – 2500 W
Output stability	$\pm$ 1% – 2%
Focal lens	5 to 7.5 inches focal length

Duty cycle	5 to 100%
Frequency	Continuous wave, pulsed 1 to 2000
Laser gas composition	He (60%), N_2 (35%) and CO_2 (5%) with 99%
purity	
Laser gas flow rate	10 liter/hour (for maximum power)
Assist gas (for cutting)	Oxygen and nitrogen

Appendix B

Important specification of Field effect scanning electron microscope (FESEM)

Make	Zeiss
Model	Sigma
Specific Chamber	330 mm inner diameter, 270 mm height
Specimen weight	up to 500 g titled, up to 200g not tilted
Movement	X = 125 mm, Y = 125 mm, Z = 50 mm
	T = -10^{O} to + 90^{O}, R = 360^{O}
Specific stage	5-axis motorized Cartesian
Chamber detector	Inlense, SE-2, NEBSD
Magnification range	300 X to 1000 kX

Appendix C

Important specification of universal testing machine (UTS)

Make	INSTRON
Model	8801
Capacity	±100 kN
Actuator stroke	±75 mm (±3 in)
Load cell height	97 mm (3.8 in)
Actuator fully retracted	63 mm (22.1in)
Maximum day light	1480 mm (58.3 in)
Column spacing	652 mm (22.1 in)
Column diameter	70 mm (2.1 in)
Table height	890 mm (35 in)
Overall width	920 mm (36.2 in)
Overall depth	546 mm (21.5 in)
Overall height (maximum)	2778 mm (109.4 in)
Weight	625 kg (1375 lb)

Appendix D

Important specification of optical microscope

Make	Carl Zeiss
Model	Axiotech-100HD, 3D
Table movement	3 axis measuring system, reflect light measuring Stage 75 mm X 5 mm x 50 mm
Tubes	Binocular photo tube (siedentopf principle) 20^{O}/23, 100 vis/100 doc
Camera	Axio-Cam and Axiovision 4.8.2 software in built
Magnification range	500X to 5kX

Appendix E

Important specification of microhardness tester

Make	Buehler
Model	Micromet-2101
Indentation force	1, 10,50,100,300,500,2000 g force
Dwell time	5 to 60 s at interval of 5 s
Microscope magnification range	100x to 400x
Measurement of indentation	Manual Filler eyepiece
Maximum measurement height	175 microns
Maximum height of specimen	65 mm
Maximum depth of specimen	85 mm
Stage dimension	100 mm × 100 mm
Video port	For photography and computerization
Power supply	AC 230 V

Appendix F

Important specification of non-contact profilometer

Make	Taylor Hobson
Model	CCI-Lite
Magnification	20X
Precision (megapixel)	1
Power supply	220 V
Focal distance	4.7 mm
Field of view	0.825 mm × 0.825 mm

Publications from the Present Thesis

Journals

1. **Jiru, W.G**., Sankar, M.R., Dixit, U.S. (2016), Laser surface alloying of copper, manganese, and magnesium with pure aluminum substrate, Journal of Materials Engineering and Performance, 25 (3), pp. 1172–1181.

2. **Jiru, W.G**., Sankar, M.R., Dixit, U.S. (2017), Investigation of microstructure and microhardness in laser surface alloyed aluminum with TiO_2 and SiC powders, Materials Today: Proceedings, 4 (2), pp. 717–724.

3. **Jiru, W.G**., Sankar, M.R., Dixit, U.S. (2018), Laser surface alloying of aluminum for improving acid corrosion resistance, Journal of Institute of Engineers, Series C, India. https://doi.org/10.1007/s40032-018-0452-8

4. **Jiru, W.G**., Sankar, M.R., Dixit, U.S. (2018), Laser surface Melting of Al-12%Si-4%Cu-1.2%Mn, International Journal of Mechatronics and Manufacturing Systems,11 (2-3), pp. 230–249.

5. Book chapter

1. **Jiru, W.G**., Sankar, M.R. and Dixit, U.S. (2015), Laser surface alloying aluminum with Copper Using CO_2 Laser, In Lasers Based Manufacturing, pp. 107–116. Springer India

Conferences

1. **Jiru, W.G**., Sankar, M.R. and Dixit, U.S. (2014), Laser surface alloying aluminum with copper using CO_2 laser, 5th International & 26th All Indian Manufacturing Technology, Design and Research Conference (AIMTDR 2014), December 12th–14th, 2014, IIT Guwahati, India. (Enhenced version of this paper was published as a book chapter material above).

2. **Jiru, W.G**., Sankar, M.R. and Dixit, U.S. (2016). Investigation of microstructure and microhardness in laser surface alloyed aluminum with TiO_2 and SiC powders. 5th International Conference of Materials Processing and Characterization, (ICMPC 2016), March 12th – 13th, 2016, Hyderabad, India. (Enhenced version of this paper was published as a Journal paper number 2 material above).

3. **Jiru, W.G**., Sankar, M.R. and Dixit, U.S., (2016), Improving acid corrosion resistance of pure aluminum by laser surface alloying with magnesium and manganese, IVth International Conference on Production and Industrial Engineering (CPIE-2016), December 19th–21th, (2016), DRB R Ambedkar NIT, Jalandhar, India. (Enhenced version of this paper was published as a Journal paper number 3 material above).